PERFORMANCE AND CAPACITY OF ISOLATED STEEL REINFORCED CONCRETE COLUMNS AND DESIGN APPROACHES

ENGINEERING CONSULTING & DESIGN INSTITUTE:

CHINA ACADEMY OF BUILDING RESEARCH (CABR) TECHNOLOGY CO., LTD.

T: +86 10 84280389 | F: +86 10 84279246 | Email: chentao@cabrtech.com | www.cabr-ec.com

Address: No. 30 Beisanhuandonglu, Beijing 100013, China

Drafted by: DENG Fei

Checked by: CHEN Tao

Approved by: XIAO Congzhen

RESEARCH PROPONENT & SPONSOR:

ARCELORMITTAL (AM)

RESEARCH COORDINATOR:

COUNCIL ON TALL BUILDINGS AND URBAN HABITAT (CTBUH)

ENGINEERING PARTNER:

MAGNUSSON KLEMENCIC ASSOCIATES (MKA)

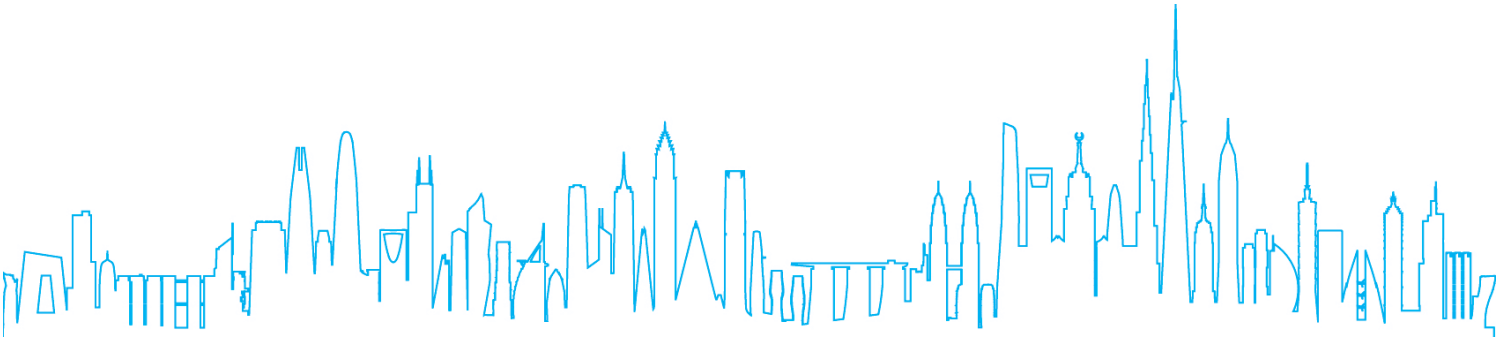

Abstract

Steel reinforced concrete (SRC) columns are widely used in super high-rise buildings, since they can provide larger bearing capacity and better ductility than traditional reinforced concrete (RC) columns. As the height of the building increases, the dimensions of mega-columns have to be enlarged to carry the increasing gravity load. However, with the increase of section dimensions, weld work will increase incredibly at the construction site at the same time, thus violating the integrity of the steel sections, increasing the labor cost, and leading to safety issues as well. This report investigates a new configuration of mega-columns – isolated steel reinforced concrete (ISRC) columns. The ISRC columns adopt multiple separate steel sections without any connections with each other, making the construction process more convenient and increasing the return on investment of the projects. This program examines the performance of ISRC columns under static and quasi-static loads.

Current standards/codes have incorporated various ways to calculate the ultimate strength of SRC columns. Relative studies and different approaches to the design of SRC columns were reviewed, including Eurocode4 (2004), AISC-LRFD (1999), ACI 318 (2008), AIJ-SRC (2002) and Chinese codes YB 9082 (2006) and JGJ 138 (2001). An evaluation of the code predictions on the capacities of ISRC columns was conducted.

A two-phase test was conducted on scaled ISRC columns designed based on a typical mega-column of a super high-rise building to be constructed within China. Phase 1 of the study includes six 1/4-scaled ISRC columns under static loads: every two of the specimens were loaded statically with the eccentricity ratio of 0, 10%, and 15%, respectively. Phase 2 of the study includes four 1/6-scaled ISRC columns under quasi-static loads: every two of the specimens were loaded under simulated seismic loads with the equivalent eccentricity ratios of 10% and 15%, respectively. A finite element analysis (FEA) was conducted as a supplement to the physical tests to provide a deeper insight into the behavior of ISRC columns. Both the static and quasi-static tests have yielded stable test results, suggesting a desirable performance of ISRC columns under static and simulated seismic loads. It is concluded from these experiments that sufficient composite action exists between the concrete and the steel sections for the tested ISRC specimens, and that the current code provisions are applicable in predicting the flexural capacity of ISRC columns when the eccentricity ratio is less than or equal to 15%.

Table of Contents

List of Tables

List of Figures

1 Introduction

This report provides an investigation on the performance of isolated steel reinforce composite (ISRC) columns under static and simulated seismic loads. Composite columns, which consist of the reinforced concrete and encased steel sections, make advantages of these two materials, so that the strength of the concrete and the steel sections can be fully utilized. Steel sections, usually with high yield strength and good ductility, contribute to the bearing capacity and ductility of the column. On the other hand, the reinforced concrete protects the steel sections from buckling and fire. By using the composite action between the concrete and the steel sections, the bearing capacity of the composite column is larger than the summation of the bearing capacities of the concrete and the steel sections.

For ISRC columns, however, whether the composite action can be realized, and how the concrete and the steel sections interact with each other need to be studied. In addition, the design approaches of ISRC columns are not included in current codes yet. Limited studies have been conducted to investigate this kind of composite columns.

This chapter of the report presents an overview of the state-of-art researches of typical SRC columns, the concept of ISRC columns, and the scope of this research program.

1.1 Overview of typical SRC columns

The reinforced concrete (RC) is an effective material because it makes the use of the strength of the concrete and the reinforcing bars. However, the use of RC columns is limited in high-rise buildings, because the gravity of the building itself induces a very large axial load in the columns, reducing the ductility of RC columns. In order to sustain the axial loads, the dimensions of RC columns have to be enlarged a lot, which in turn further increases the axial load, not to mention the considerably large dimensions are often unacceptable in the architecture point of view. The SRC columns turn out to be a solution to this problem, since the SRC can increase the bearing capacity of the columns and maintain a good sense of ductility without significantly enlarging the dimensions of the columns. Typical configurations of the SRC columns are presented in Figure 1-1.

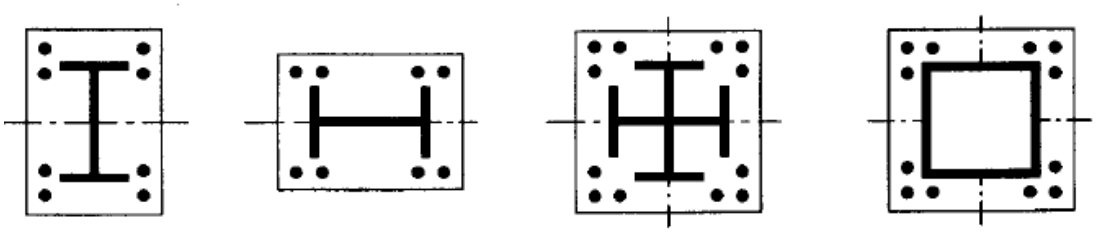

Figure 1-1 Typical configurations of the SRC column

The interaction between the concrete and the steel section is a critical issue in the design of SRC columns. Since the capacity of the column under combined compression and bending is dependent on the axial force, the connection between the concrete and the steel section is a key factor in determining the ultimate strength of SRC columns. If the concrete and the steel section are fully connected, there will be no relative slip on the concrete-steel interfaces, and the normal strain of these two materials on the interface will be compatible (Figure 1-2(a)). The transfer of axial force between the concrete and the steel section is realized by shear force on the concrete-steel interfaces. If the concrete and steel section are partially connected (or without connection), the shear force on the concrete-steel interfaces will not be large enough to ensure zero relative slip on that interface, and the strain distribution of the concrete and the steel section will not be in the same plane (Figure 1-2(b)). Namely, the plane sections do not remain plane.

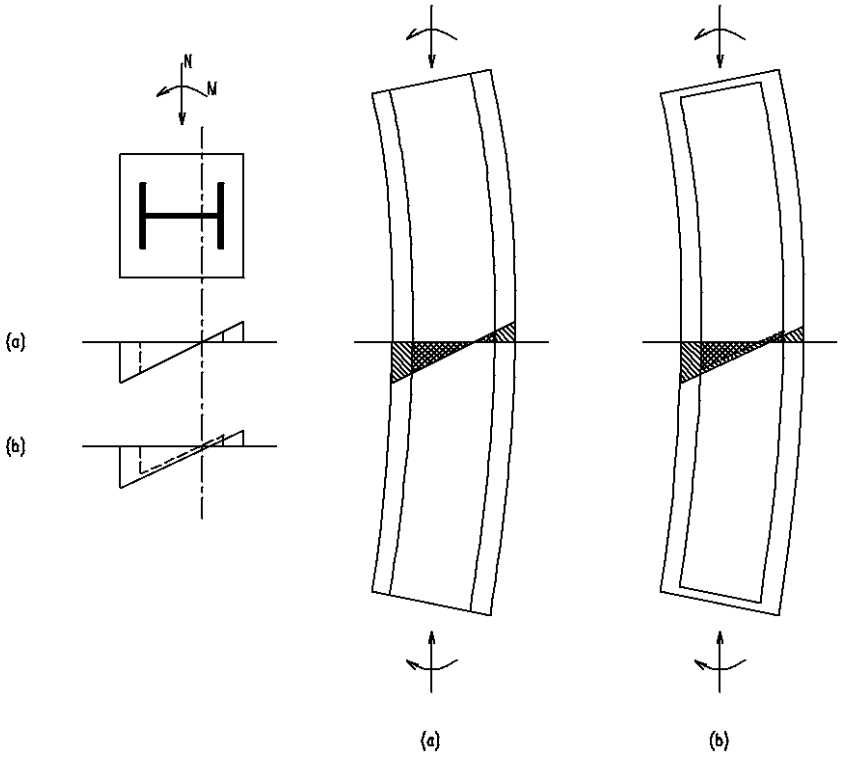

Figure 1-2 Section strain distribution: (a) fully connected composite column; (b) partially connected composite column

The shear resistance on the concrete-steel interfaces is provided by the bond stress and shear connectors, such as studs, deformed rebar, steel shapes, etc. Japanese researchers found that the bond stress between concrete and steel section is less than 45% of the bond stress between concrete and smooth rebar (AIJ-SRC 2002). Therefore, if no particular measures have been taken to increase the roughness of the steel section, it is reasonable to neglect the bond stress if shear connectors are applied. However, the bond stress can be very large when the surfaces of the steel sections are made rough, or ribs are employed on the surfaces of the steel sections.

In practice, shear connecters are usually provided in composite columns. The major purpose of shear connectors is to transfer the axial force between the concrete and the steel section. It is convinced that the existence of shear connectors will increase the bearing capacity of composite members (Macking, 1927). Studs are the most commonly used shear connectors nowadays, since the production and fabrication of shear studs is relatively easy. Furthermore, shear studs are isotropic and ductile components, which may mitigate the stress concentration within the adjacent concrete. Ollgaard (1977) proposed the following constitutive curve for shear studs:

$$V = V_u \left(1 - e^{-ns}\right)^m \tag{1.1}$$

where: V_u – the ultimate strength of the shear stud

s – the relative slip [mm]

m, n – parameters calibrated by experiments, m=0.558, n=1

R.P. Johnson proposed that m=0.989, n=1.535; Aribert proposed that m=0.8, n=0.7. The proposed constitutive curves are presented in Figure 1-3.

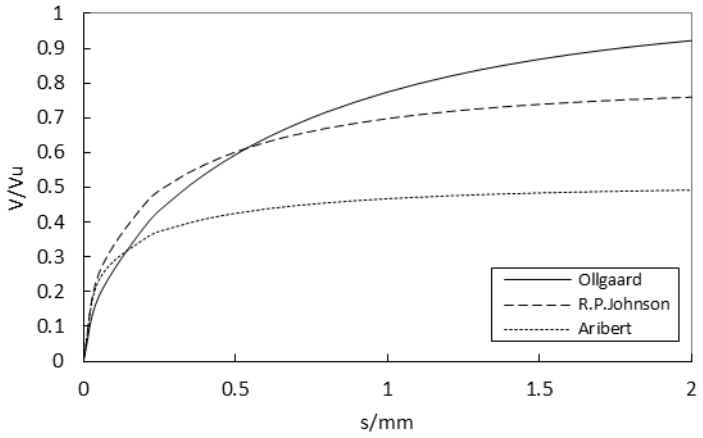

Figure 1-3 Constitutive curves for shear studs

1.2 Introduction of ISRC columns

Since the axial load of the column grows as the height of the building increases, the dimensions of the column have to be enlarged accordingly. As a result, the steel sections in mega SRC columns are often welded on site, since it is impractical to produce such a huge steel section in the factory and transport it to where it will be installed. A typical SRC section made from welded steel plates is presented in Figure 1-4 (a).

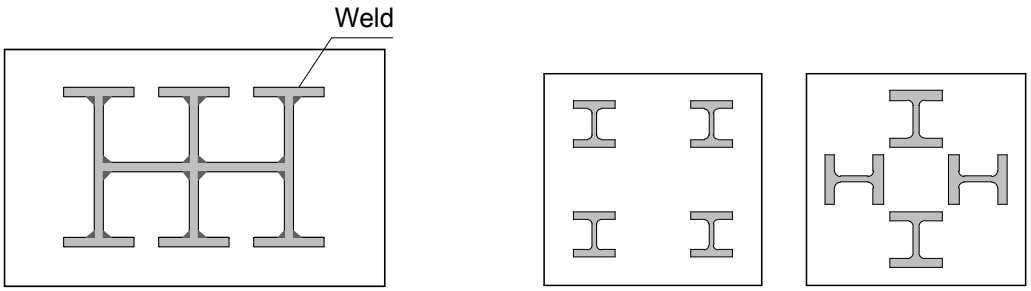

(a) SRC cross section with welded steel plates (b) ISRC cross sections

Figure 1-4 Typical sections of SRC and ISRC columns

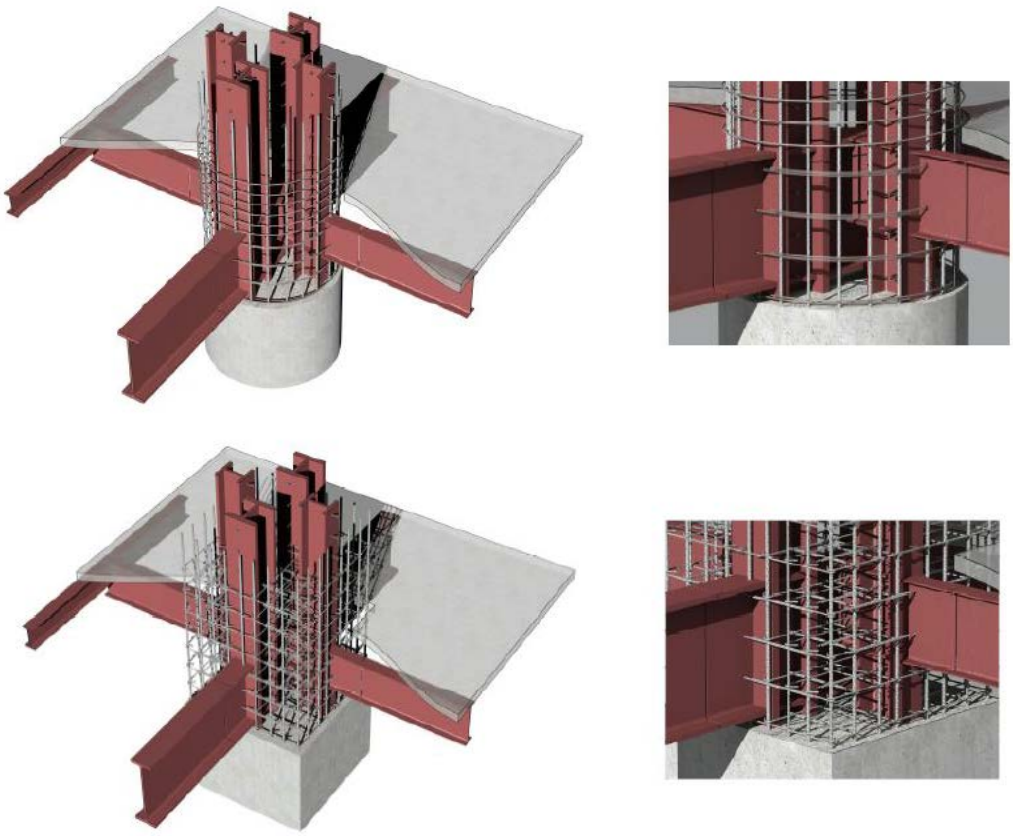

Figure 1-5 Layout of ISRC columns with round and square cross sections (provided by MKA)

Contrary to traditional SRC columns, multiple separate steel sections are encased in ISRC columns without connection with each other. The steel sections are often placed in the position that fits the connection to the beams or other structural elements (Figure 1-4 (b) and Figure 1-5).

If the results of this research program are able to validate the reliance of ISRC columns (with eccentricity ratios no more than 15%), then it is an alternate approach to use ISRC columns in the design of super high-rise buildings. The adoption of ISRC columns can produce the following benefits:

1) **Reduce the construction cost**

   Welding work at the construction site will be reduced by either adopting hot-rolled steel sections or steel sections welded in the factory, reducing the labor cost significantly. Besides, duration of the project may also be shortened because of the easy construction.

2) **Improve the construction safety**

   The reduction of welding work reduces the risk of fire. An easy installation is also beneficial to safety issues.

3) **Avoid the adverse effect of residual stress and weld imperfection**

   Steel structures are sensitive to residual stress and the quality of welds, especially for large and thick steel plates. Adopting ISRC columns may reduce the adverse effect of these two problems.

1.3 Research objectives

Although current codes have accommodated design provisions for SRC columns, provisions for ISRC columns are not included. With the considerable benefits ISRC columns may bring, it is urgent to validate the reliance of this kind of composite columns, and explore simplified design approaches. This research hopes to present an insight into the mechanism of ISRC columns. Objectives of this research include:

1) Perform a literature survey of past researches on the study of SRC/ISRC columns, collect related data and projects for the research;
2) Design and carry out the tests. Record the behavior of the ISRC columns during the test, and examine the failure modes of the concrete, rebar and steel sections. Record the test data, and evaluate the performance of ISRC columns based on the analysis of the collected data;
3) Carry out the finite element analysis (FEA) as an supplement to the physical tests;

4) Present suggestions and simplified approaches to the design and construction of ISRC columns.

1.4 Project overview

This research project is a two-phase test program investigating the performance of ISRC columns. Phase 1 of the study consists of static tests on six 1/4-scaled ISRC columns: every two of the specimens will be loaded statically with eccentricity ratio of 0, 10% and 15% respectively. Only an axial load will be applied to the columns with different eccentricities to examine the performance of ISRC columns under static loads, and the test results will serve as a guide to the subsequent phase. Phase 2 of the study consists of quasi-static tests on four 1/6-scaled ISRC columns: every two of the specimens with be loaded under simulated seismic loads with an equivalent eccentricity ratio of 10% and 15% respectively. The capacity, ductility, failure mode and crack distribution of the specimens will be examined.

1.5 Notation

A_c	=	area of concrete [mm^2]
A_p	=	area of steel section [mm^2]
A_s	=	gross area of longitudinal rebar [mm^2]
A_{st}	=	cross area of a shear stud [mm^2]
δ	=	steel contribution ratio
e	=	eccentricity [mm]
e_b	=	balanced eccentricity [mm] (Compressive concrete fiber fails and tensile steel fiber yields at the same time.)
E_c	=	secant modulus of concrete [MPa]
E_s	=	modulus of elasticity of longitudinal bar [MPa]
E_p	=	modulus of elasticity of steel section [MPa]
ε	=	normal strain of the cross section
f_c	=	axial compressive strength of concrete [MPa]
f_u	=	shear strength of stud [MPa]
f_p	=	yield strength of steel section [MPa]
f_s	=	yield strength of longitudinal rebar [MPa]
ϕ	=	curvature of the cross section [mm^{-1}]
h	=	height of the cross section [mm]

I_c	=	moment of inertia of concrete [mm^4]
I_s	=	moment of inertia of concrete [mm^4]
I_p	=	moment of inertia of concrete [mm^4]
l_u	=	unsupported length of the ISRC column [mm]
M_u	=	flexural resistance under combined compression and bending [kN·m]
M_{u0}	=	plastic resistance under pure bending (Nominal strength) [kN·m]
N_u	=	axial resistance under combined compression and bending [kN]
N_{u0}	=	axial resistance under pure compression [kN]
P	=	applied axial load [kN]
r	=	radius of gyration of the cross section [mm]
R_k^c	=	stiffness reduction factor for compression
R_k^b	=	stiffness reduction factor for bending
ρ_a	=	reinforcement ratio of steel sections
ρ_s	=	reinforcement ratio of longitudinal bars
ρ_{sv}	=	volume ratio of transverse reinforcement
V_u	=	shear capacity of a shear stud [kN]
ϕ_c	=	resistance factor for compression in AISC
ϕ_b	=	resistance factor for bending in AISC

2 Previous research

The SRC column concept was first introduced to the design of steel structures as a method to enhance the durability and fire resistance of the structural steel. The structural steel can be either hot-rolled steel sections or welded steel plates. Compared to steel columns, the reinforced concrete can prevent the steel section from local buckling, increase the rigidity of the column, and improve the durability and fire resistance of the structural steel. On the other hand, the steel section helps increase the bearing capacity, especially shear capacity, of the column, thus improving the seismic behavior of the column. The composite action between the concrete and the steel section makes the bearing capacity of SRC columns higher than the summation of the bearing capacities of the concrete and the steel section. Therefore, neglecting the interaction between the concrete and the steel section will lead to a more conservative design result. The mechanism of load transfer between the concrete and the steel section has to be explored before a reliable design method can be developed.

2.1 Composite action

The study of composite action begins with the study of composite beams. A methodology was presented by J. Nei and J. Shen (Nie and Shen 1997) to explain how the slip effect on the concrete-steel surface would influence the strength and stiffness of the composite beam. When relative slip exists, the plane section assumption fails. However, the curvature of the concrete and the structural steel is the same since the deflection curves of these two parts are identical. Figure 2-1 shows the strain distribution of the cross-section. The actual strain (Figure 2-1 (b)) could be regarded as the superposition of the ‘plane section’ and the ‘curved section’. Then, the elastic bending capacity contributed by the ‘plane section’ and the ‘curved section’ could be obtained respectively, and the total elastic bending capacity was the summation of the two. Theoretical analysis showed that the elastic bending capacity would decrease when the relative slip grows.

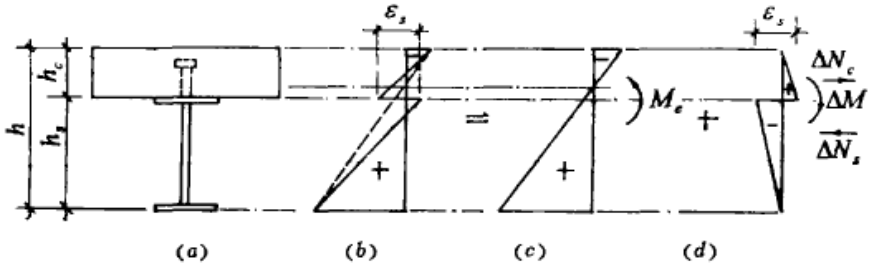

Figure 2-1 Strain distribution of the cross-section

It could be proved that the plastic flexural capacity and the stiffness of the composite beam were also reduced because of the slip effect. However, only the reduction in elastic bending capacity was validated by the experiment – the plastic flexural capacity of the composite beam did not drop. This was because the strengthening of the steel after yielding offset the adverse effect of slip. Therefore, for fully connected composite beams, slip effect can be neglected if one is only interested in the ultimate flexural strength.

2.2 Bond stress and shear connectors

The bond stress and the shear stud are two ways to provide the shear resistance on the concrete-steel interface. The mechanism of bond stress is usually studied by push-out tests as shown in Figure 2-2 (Yang et al 2005). Studies (Fercuson and Thompson 1956; Bro 1966; Mohamed et al 1998) have shown that the bond stress is mainly consisted of three parts: the chemical bond, the friction, and the mechanical bond. Before the concrete and the steel section begin to slip, the bond stress is mainly contributed by the chemical bond. After that, the friction and the mechanical bond mainly contribute to the bond stress.

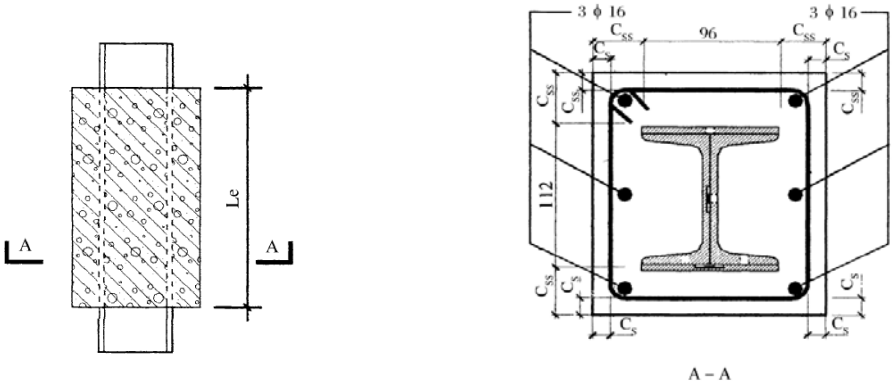

Figure 2-2 Push-out test for bond stress

The magnitude of bond stress is not only dependent on the surface conditions of the concrete-steel interfaces, but also dependent on the embedded length of the steel sections, the thickness of the concrete cover, the volume ratio of the transverse reinforcing bars, etc. Therefore, accurately predicting the value of bond stress can be challenging.

The strength of shear connectors, on the other hand, is relatively easy to be determined. The commonly used types of shear connectors are shear studs, perfo-bond ribs, and T-connectors (Valente and Cruz 2003).

Shear stud | Perfo-bond connector | T connector

Figure 2-3 Connector types

According to Eurocode4, the push-out tests should be conducted to study the behavior of shear connectors. A standard push-out test specified in Eurocode4 consists of a steel section held vertically in the middle by two identical reinforced concrete slabs. Each of the concrete is connected with the steel section via two rows of shear connectors. The axial load is applied to the steel section, and the behavior of the shear connectors can be obtained.

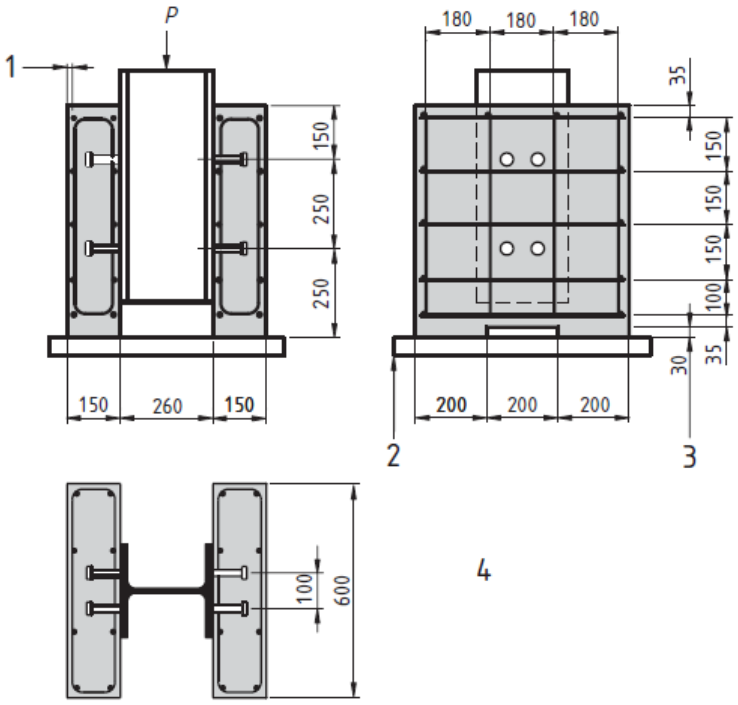

Figure 2-4 Push-out test for shear connectors

It is found that (Ollgaard et al 1971) the behavior of shear studs in a composite structure is similar to an elastic beam foundation (Figure 2-5 (a)). Suppose the concrete serves as the

'ground', and the shear stud is an elastic beam lying on the 'ground'. The movement of the steel section applies a shear force at end 'A' of the stud and imposes a potential to move downward at this end, which in turn causes the stud to rotate counter clockwise. In addition, the concrete imposes a restriction to end 'B' to counteract the potential of the rotation. The elastic stress distribution of the concrete is presented in Figure 2-5 (b). A part of the concrete is in compression, while the other part of the concrete is in tension. As the load increases, the stress of the concrete develops. The plastic stress first occurs near end 'A', and then develops toward end 'B'. Finally, the plastic stress distribution of the concrete is presented in Figure 2-5(c).

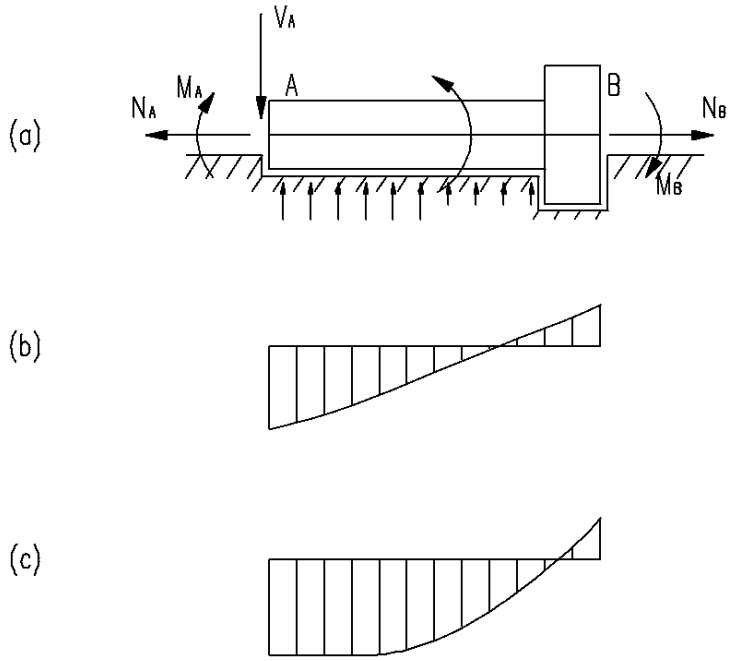

Figure 2-5 Behavior of the shear stud

Ollgaard (Ollgaard et al 1971) found that the shear strength of stud connectors is influenced by the compressive strength and the modulus of elasticity of the concrete. Although the density of the concrete also influences the shear strength of shear studs, but the influence is not significant. By running a regression, the following equation was proposed to predict the strength of shear studs:

$$V_u = 1.106 A_{st} f_c^{0.3} E_c^{0.44} \tag{2.1}$$

A simplified equation was proposed for design purposes:

$$V_u = 0.5 A_s \sqrt{f_c E_c} \tag{2.2}$$

Table 2-1 lists different methods and specifications for the design of shear studs.

Table 2-1 Approaches for determining the strength of shear studs

Code	Strength of shear studs	Specifications
Eurocode4	$V_u = \min\{\frac{0.8 f_u \pi d^2 / 4}{\gamma_V}, \frac{0.29 \alpha d^2 \sqrt{f_c E_c}}{\gamma_V}\}$ where: $\alpha = 0.2\left(\frac{h}{d}+1\right)$, *for* $3 \le \frac{h}{d} \le 4$ $\alpha = 1$ *for* $\frac{h}{d} > 4$	• $f_u \le 500$ MPa • $16\text{mm} \le d \le 25\text{mm}$ • concrete density not less than 1750kg/m^3
Chinese GB50017	$V_u = \min\{0.7\gamma \frac{f_u \pi d^2}{4}, \frac{0.43 \pi d^2}{4}\sqrt{f_c E_c}\}$ where γ – ratio of tensile to yield strength of the stud	• $h/d \ge 4$ • when the stud is not positioned right over the web: (1) $d \le 1.5t_f$ if the flange is designed to be in tension; (2) $d \le 2.5t_f$ if not.
AISC-LRFD	$V_u = \min\{\frac{f_u \pi d^2}{4}, \frac{0.5 \pi d^2}{4}\sqrt{f_c E_c}\}$	• $h/d \ge 4$ • concrete density not less than 1440kg/m^3 • $d \le 2.5t_f$ if the stud is not positioned right over the web

2.3 Behavior of SRC columns

Considerable amounts of experimental tests have been done to study the behavior of SRC columns subjected to static and simulated seismic loads. A series of tests were conducted by Ricles (Ricles and Paboojian 1994) to study several parameters that may influence the seismic behavior of SRC columns, including the degree of concrete confinement, effectiveness of flange shear studs, and concrete compressive strength. This research tested four configurations of the cross-section (Figure 2-6), and concrete strength ranged from 31MPa to 68.9MPa.

Test results show that the capacity and ductility of the tested SRC columns were desirable if adequate confinement of the concrete core was provided. Longitudinal bars should be prevented from buckling to ensure the core concrete remain uncrushed. The bearing capacity of the specimen under combined axial and flexural loading exceeded the ACI and AISC-LRFD provisions, indicating these two codes are conservative in strength design. It was

also concluded that shear studs installed on the flange of the steel sections did not have significant effect on the flexural strength and stiffness of the SRC columns. However, shear studs are still necessary to transfer gravity load from steel beams to the composite columns.

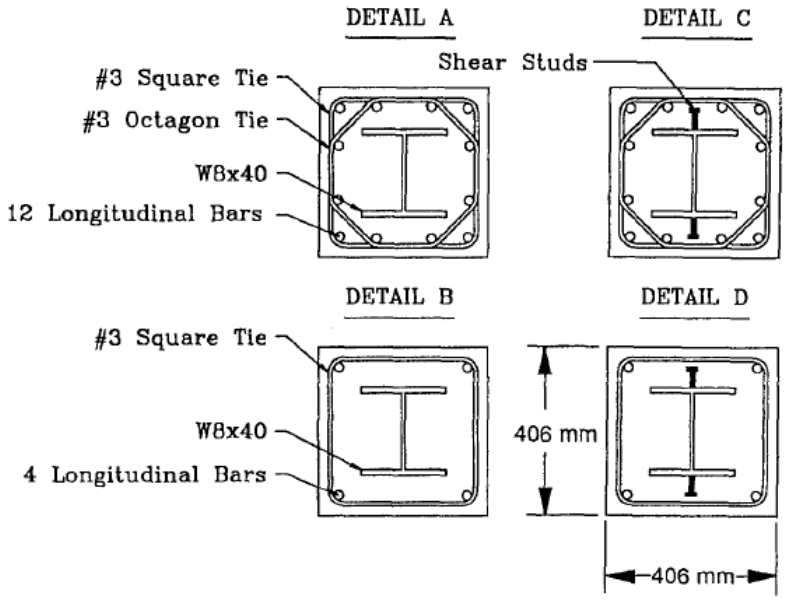

Figure 2-6 Test specimen details

Bond stress and shear connector requirements in SRC structures were examined (Roeder et al 1999). Eighteen specimens with different interface length, concrete configuration, and most importantly, degree of confinement, were tested.

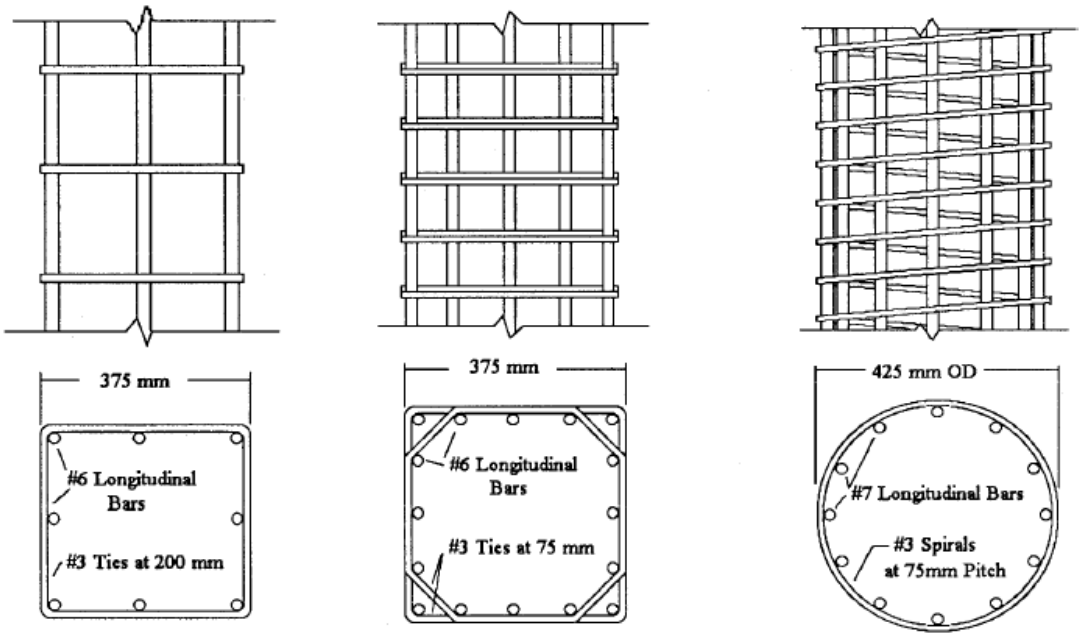

Figure 2-7 Reinforcement details for the test specimens

Test results showed that the confinement had little impact on the maximum bond stress on the interface, but a larger confinement increased the post slip resistance. The results validated the theory that bond stress was exponentially distributed along the embedded length under service load, and was approximately uniformly distributed when the loads were approaching the ultimate capacity. Cyclic test results showed that when the load was under 40% of the maximum capacity, there was no significant deterioration on the interface; interface deterioration was significant after that load.

Two specimens with shear studs were tested. The results suggested that the existence of shear connectors might damage the adjacent concrete by inducing location deformation and stress concentration. Therefore, it was recommended that shear connectors would not be used if the shear requirement were less than the shear capacity provided by the bond stress. That is, design the load to be transferred either by bond stress or by shear connectors, but not by the combination of the two.

SRC columns using high strength steel was also tested (Wakabayashi 1992). Test results suggested that the SRC members were more ductile when the steel had a higher ultimate strength. Biaxial loaded SRC columns also show desirable performance (Munoz et al 1997; Dundar et al 2007)

3 Experimental study – phase 1

The first phase of the research was completed in March 2015 at the structural laboratory of Tsinghua University, China. The objective of this phase of the experiment was to study the behavior of ISRC columns under combined compression and bending conditions. Six reduced scaled specimens were tested. This chapter presents a detailed description of the experiment program.

3.1 Test overview

The loading conditions of the specimens are presented in Figure 3-1. The axial load would be applied to the end of the column with certain eccentricity ratios, and the rate of loading will be slow enough to prevent any dynamic effects during the test. The axial load would be increased gradually until failure of the column occurred (Figure 3-2).

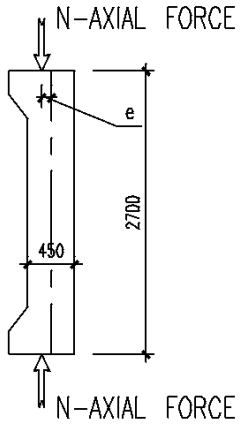

Figure 3-1 Loading diagram

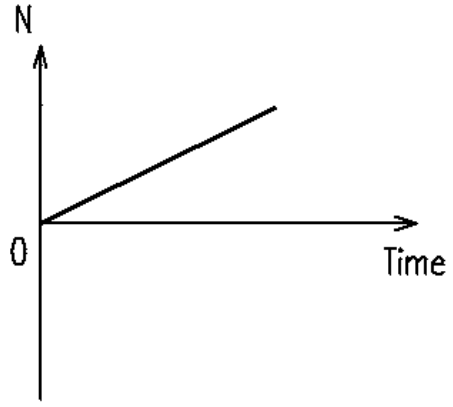

Figure 3-2 Loading history

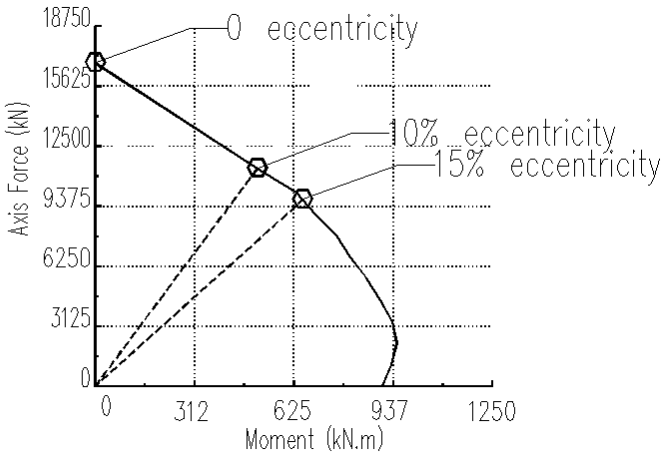

Figure 3-3 Estimated capacity

Figure 3-3 shows the planned loading paths and the estimated capacities of the specimens. Since mega columns are primarily designed in high-rise buildings, columns at the bottom of the buildings are often carried with very large gravity loads. Therefore, the eccentricities in mega columns are usually less than balanced eccentricity (e_b), which is defined as the eccentricity corresponding to the balanced strain condition. Therefore, the maximum eccentricity in this test program was set to 15% - a reasonable limit based on project experience. However, the real eccentricity at failure could exceed the initial eccentricity because of the second order effect. The horizontal deflection in the middle of the column was measured to account for the second order effect during the test.

3.2 Materials

Strength grades of the materials were selected based on both the design in real projects and the limits of the loading machines. Table 3-1 presents the material strength designed for phase 1.

Table 3-1 Designed material strengths

Material	Strength
Concrete	C60 ($f_{cu,k} = 60$MPa) maximum aggregate size no more than 5mm.
Steel sections	S355 $f_{yk} \geq 355$MPa produced by ArcelorMittal, shipped to China
Longitudinal bars	HRB 400 $f_{yk} \geq 400$MPa
Ties	HRB 500 $f_{yk} \geq 500$MPa To be adjusted according to available bars.
Studs	6mm × 25mm or 5mm × 20mm headed studs or Grade 4.8 bolts

Since concrete strength was sensitive to its age, concrete cubes for each specimen were tested right before or after the specimen was tested. Figure 3-4 shows the concrete strength development for phase 1. The first specimen was tested 42 days after the concrete had been placed. By then, the average concrete cubic strength was $f_{cu,m} = 61.17$ MPa, which met the expected strength (60 MPa).

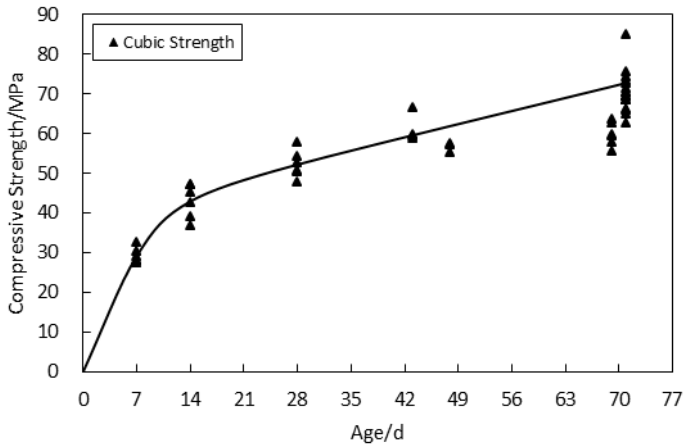

Figure 3-4 Concrete strength development for static tests

Table 3-2 Material strengths for static tests (Units: MPa)

Specimen ID	Concrete cubic strength	Concrete axial strength	Yield strength of steel section flange*	Yield strength of steel section web*	Yield strength of longitudinal bar	Yield strength of transverse bar
E00-1	61.2	61.2	408	523	438	$f_{3.25}$ = 597MPa $f_{4.80}$ = 438MPa
E00-2	56.6	55.0	398	411		
E10-1	60.9	56.4	423	435		
E10-2	72.8	59.2	383	415		
E15-1	66.1	57.2	377	404		
E15-2	67.6	56.3	389	405		
Average	64.8	57.6	396	432	-	-

where:

$f_{3.25}$ – yield strength for bars of 3.25mm diameter

$f_{4.80}$ – yield strength for bars of 4.80mm diameter

* Material strength for steel sections are provided by ArcelorMittal

3.3 Specimen design and fabrication

Six identical specimens were designed in phase 1, and each set of two were loaded under the same eccentricity ratio: 0, 10%, and 15%, respectively (Table 3-3). Figure 3-5 shows the dimensions and details of these specimens. The specimen was 2700 mm in length, and the typical section size was 450 mm x 450 mm. There was a bracket at each end of the column to

allow for eccentric loading. To ensure safety during the test, 8-mm thick Q235 steel plates surrounded the ends of the columns. In addition, there were more ties within the bracket zones. Since the critical section was located in the mid-height of the specimen, extra confinement at the ends would not affect the test results. Note that an 8-mm thick piece of polystyrene was placed under each of the endplates, whose purpose was to release the constraint between the endplates and the concrete, thus allowing for relative displacement between concrete-steel interfaces to represent the boundary conditions in real projects as accurately as possible. Two I-shaped steel beams were welded to the ends of the column to simulate beam-column joints.

Table 3-3 Specimen ID – phase 1

Specimen ID	Load type	Scale factor	Eccentricity
E00-1	Static	1/4	0
E00-2			
E10-1			10%
E10-2			
E15-1			15%
E15-2			

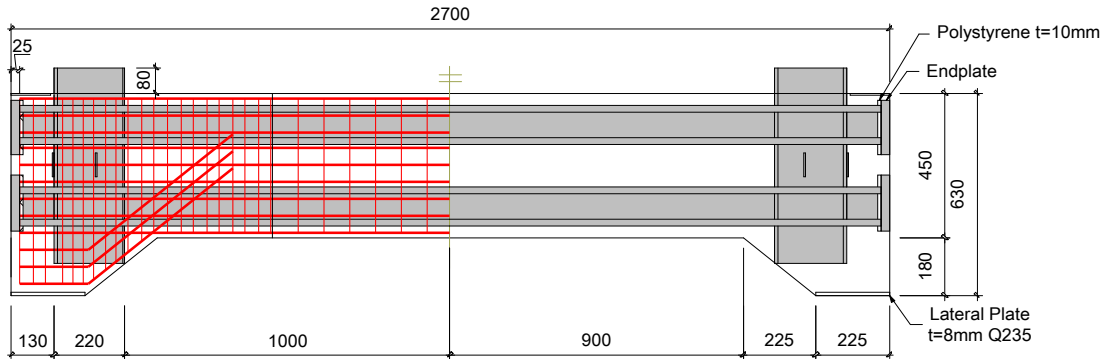

Figure 3-5 Details of the specimens for phase 1

Figure 3-6 shows the layout of steel sections and ties of a typical cross section. There were four S355 encased 120 mm x 106 mm x 12 mm x 20 mm hot-rolled steel sections, located at each side of the column without any connections with each other. The distance between centers of the steel sections and the center of the cross section was 137.5mm. Ties were welded on the web of the steel sections if they intersected with each other. Concrete cover was 10mm. Figure 3-7 shows the layout of the shear studs. Two rows of studs were installed on the outside flange of the steel sections, and one row on the inside flange as well as on the web. The outside shear studs were shortened to allow for enough concrete cover thickness.

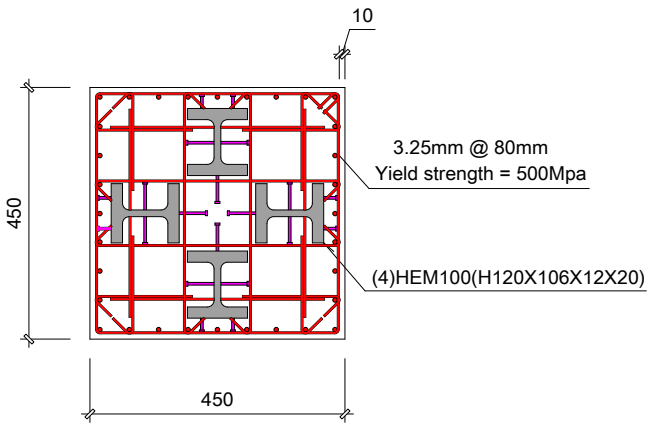

Figure 3-6 Details of the cross section

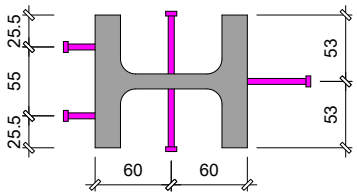

Figure 3-7 Layout of the shear studs

A summary of the dimension of the specimens of phase 1 is listed in Table 3-4.

Table 3-4 Summary of specimens for static test

Dimension		Steel sections and rebar	
Length l/ mm	2700	Steel Section /mm	120 x 106 x 12 x 20
Unsupported Length l_u/mm	3590	ρ_a	10%
Section dimension /mm	450 x 450	ρ_s	0.8%
l_u/h or kl_u/r	7.98 or 27.6	ρ_{sv}	0.26% / 1.15%

Where:

l_u – Unsupported length, distance between the centroid of the hinges

l_u/h – length to section height ratio according to Chinese Code

kl_u/r – slenderness ratio according to ACI 318

ρ_a – reinforcement ratio of the steel sections

ρ_s – reinforcement ratio of the longitudinal bars

ρ_{sv} – volume ratio of the ties in non-enhancement zone or enhancement zone

Figure 3-8 shows the fabrication of the specimens.

(a) Overview

(b) Bracket details

(c) Longitudinal bar details

(d) Concrete mold

Figure 3-8 Specimen fabrication – phase 1

3.4 Test setup

Phase 1 of the test was completed by a 2000-ton servo system in Tsinghua University. Figure 3-9 shows the test setup of phase 1 in details. A bottom hinge was placed on the ground and was fixed by two blocks, while the upper one was connected to a transition beam, which connected to the vertical and horizontal actuators. The column was placed between the hinges, confined by steel caps at each ends. Horizontal actuators served as a stabilizer when the column was being loaded. One of the horizontal actuator pulled the transition beam at a constant force, and the other one was displacement-controlled at the original point. Thus, the displacement of the transition beam could be restricted to avoid lateral drift of the top of the column. A steel frame was provided to restrict out-of-plane displacement of the specimen, connecting to both the transition beam and the steel cap at the top of the column. Connectors between the frame and the transition beam/steel cap allowed for vertical displacement but restricted horizontal displacement by using two long slotted holes within each joint (Figure 3-9 (b)).

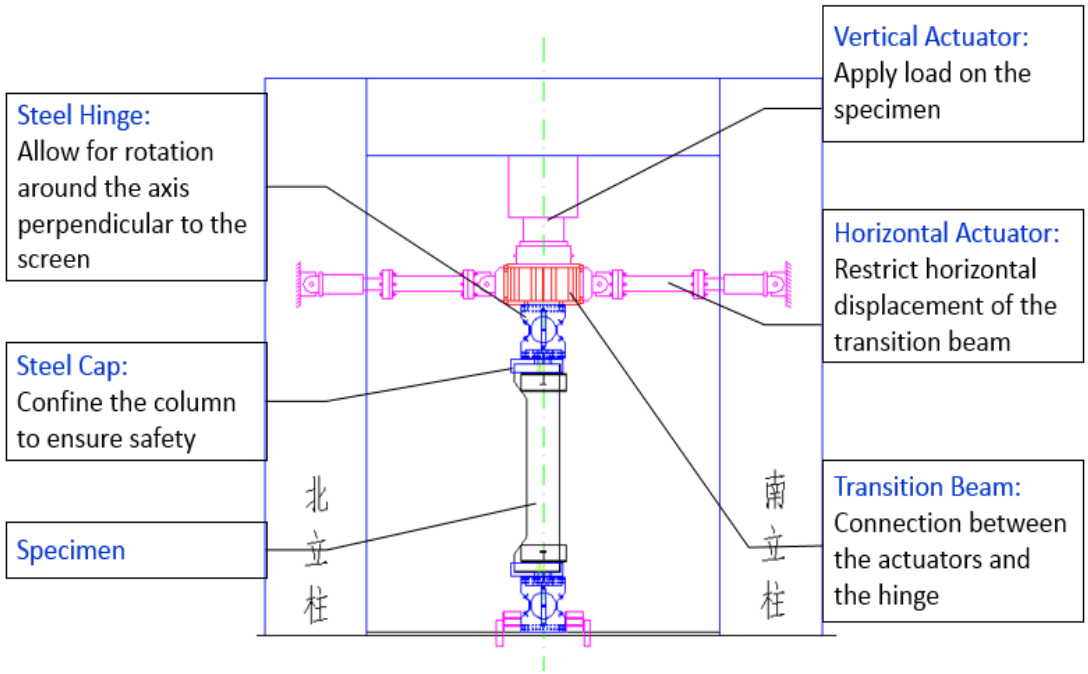

(a) Front face

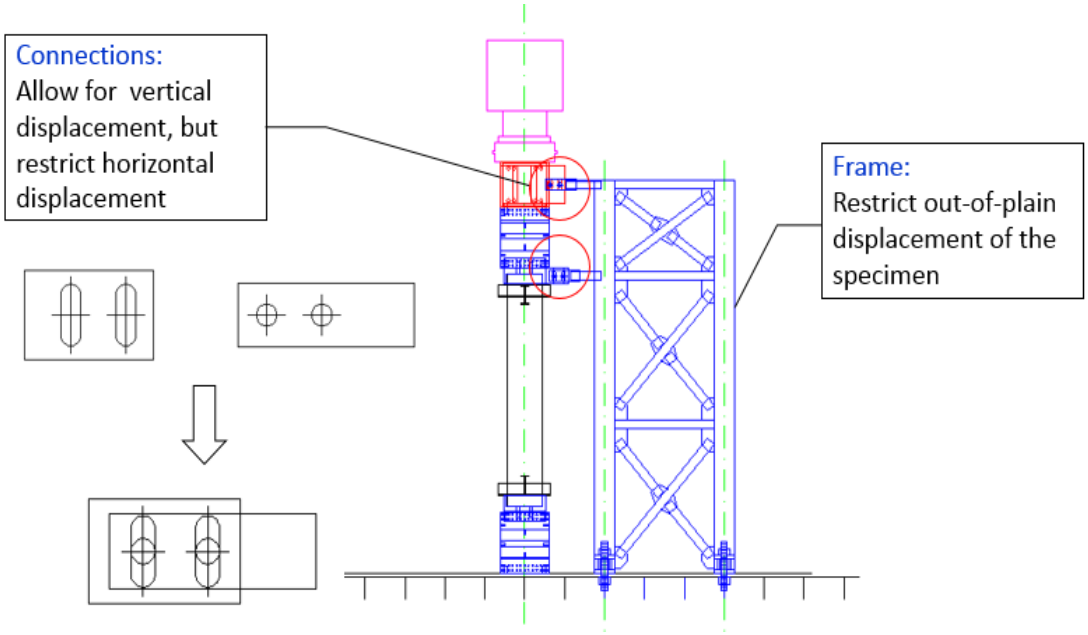

(b) Lateral face

Figure 3-9 Test setup – phase 1

Figure 3-10 Test setup in real site – phase 1

3.5 Test measurement

The measured data in this test program included strain on the steel sections, longitudinal bars, ties, concrete surfaces, and the relative displacement between concrete-steel interfaces. Strain sensors were installed at four elevations (Figure 3-11 (a)). Most of the data would be collected on section A, B and C. Section D served as a backup in case sensors on the previous three sections were damaged severely. Take section A as an example. Five strain gauges were installed on the longitudinal bars on one side of the column; fourteen strain gauges on the steel sections (four gauges on the in-plane direction steel section, three gauges on the out-of-plane direction steel section); four strain gauges on each direction of the ties; and four displacement sensors. Strain gauges on other sections were presented in Figure 3-11 (b) ~ (d).

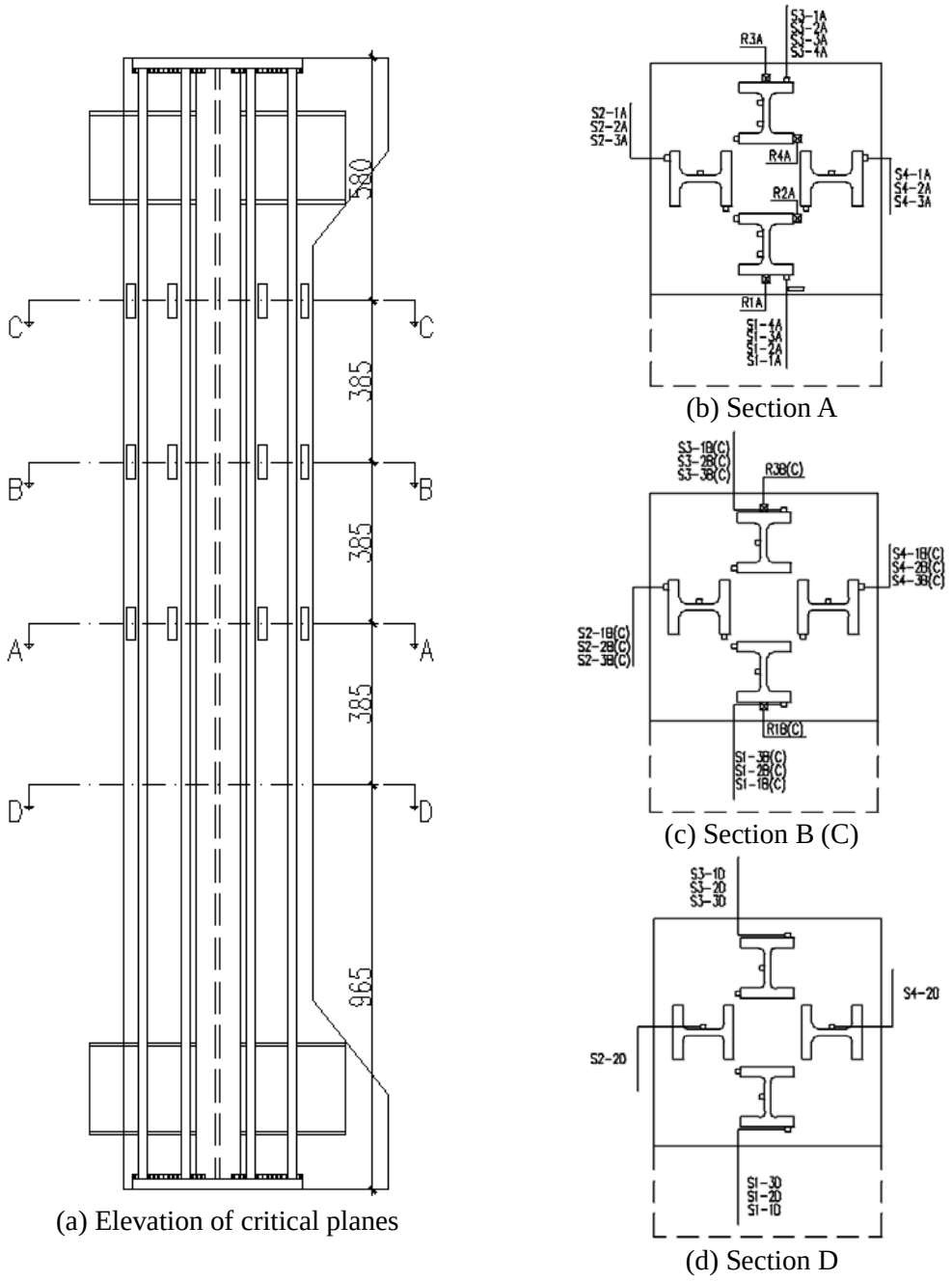

(a) Elevation of critical planes

(b) Section A

(c) Section B (C)

(d) Section D

Figure 3-11 Sensors layout - phase 1

3.6 General behavior of static specimens

3.6.1 Pure axial specimens (E00-1/E00-2)

The two pure axial loaded specimens failed in a same pattern, and the phenomena of these two specimens were very similar to each other. Therefore, take E00-1 as an example:

(a) Vertical cracks occurred on the front face of the column when axial load reached 9000kN (53% of the ultimate capacity). The crack was located in the middle of the front face, where concrete cover was relative small because a longitudinal bar was placed right inside the concrete at this location. No visible horizontal deflection was detected.

Figure 3-12 Specimen E00-1 at 9000kN

(b) The length of the crack increased with the axial load, but no other cracks developed besides the first one. At axial load level 12000kN, the crack stopped growing. Similar phenomena could be observed on other faces of the column.

Figure 3-13 Specimen E00-1 at 12000kN

(c) The appearance of the column remained the same until the axial force reached maximum load. When the axial force reached 17000kN, corners of both the ends of the specimen cracked, and concrete at those corners was damaged. Therefore, the top hinge rotated clockwise, and the bottom hinge rotated counter clockwise, which led to the column bent toward left. Bending moment developed on the mid-height cross section of the column, and the axial capacity reduced significantly from 17000kN to 13500kN because the loading condition had changed from pure compression to combined compression and bending. In the end, the column failed due to crush of concrete near the mid-height cross section.

Figure 3-14 Specimen E00-1 at failure

Loading curves of E00-1 and E00-2 are shown in Figure 3-15. There were two drops of the axial load. The first drop took place right after the maximum load, but no significant deformation or concrete damage was detected. Then the columns survived for a long time when the actuators kept pushing down at a residual load, which was about 70% of the maximum load. As the vertical deflection developed, the residual load decreased gradually. Finally, the column failed accompanied by the second drop of the load. It was at the second drop that significant horizontal deflection and concrete damage was observed.

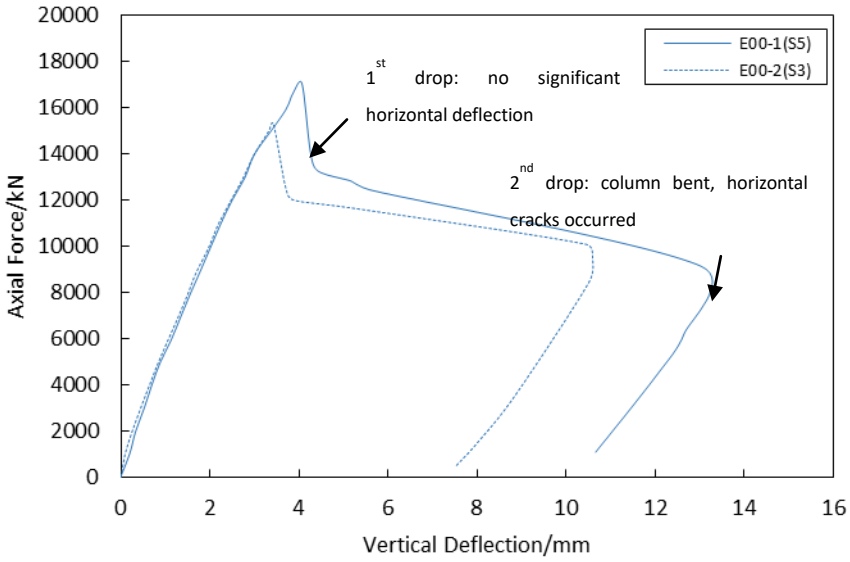

Figure 3-15 Load vs. Vertical deflection (e/h=0)

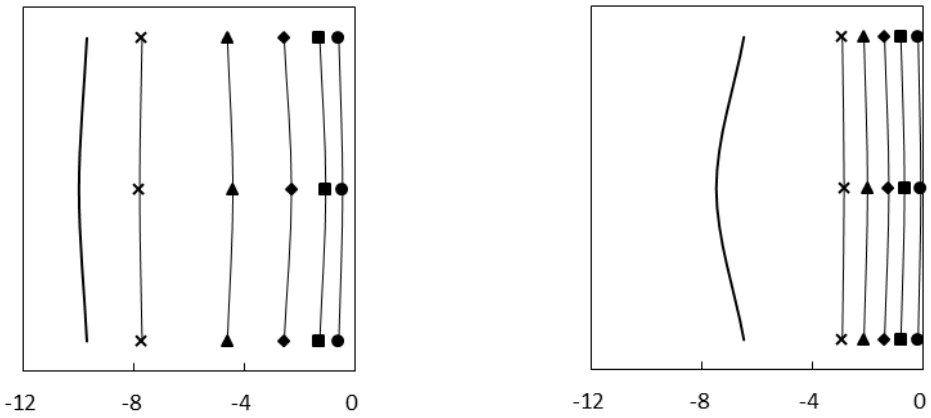

(a) E00-1 (b) E00-2

Figure 3-16 Horizontal deflection of pure axial specimens

Legend for lateral deflection:

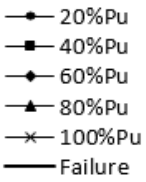

As is shown in Figure 3-16, the deflection curve of the pure axial column is a straight line at load level 20%~100% P_u, suggesting that the specimen did not convex at those load levels. Instead, the column drifted horizontally due to the rotation of the hinges. Deflection curves at failure level convex leftward, and the deflection at mid-height cross section of the column was much larger than the deflection at maximum load level, which was observed after the second drop of the axial load.

3.6.2 Eccentric specimens (E10-1/E10-2/E15-1/E15-2)

Specimens with 10% and 15% eccentricity experienced similar phenomena, so a typical specimen E15-1 was selected to demonstrate the behavior of eccentric specimens.

(a) At load level 5000kN (40% of ultimate capacity), the first crack also appeared in the middle of the front face where the concrete cover was small, similar to pure axial specimens.

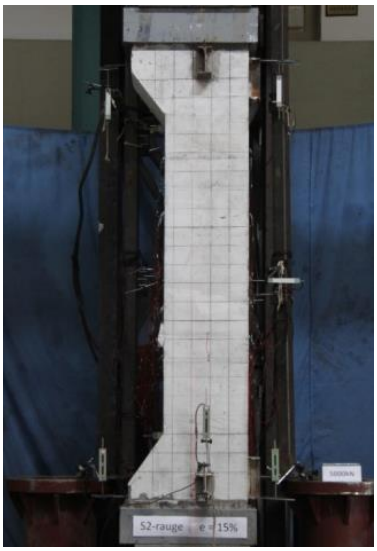

Figure 3-17 Specimen E15-1 at 5000kN

(b) As the load increased, horizontal cracks appeared at the tensile side of the column at load level 10000kN. The mid-section of the column deflected rightward due to bending moment.

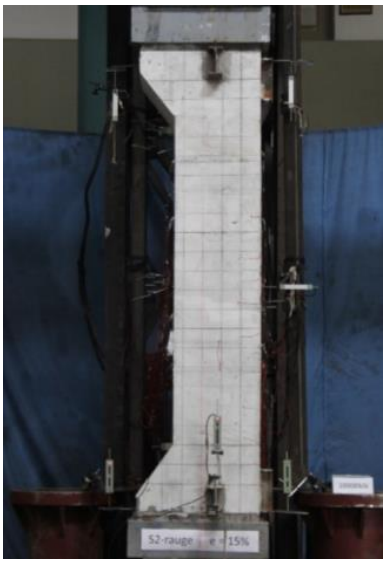

Figure 3-18 Specimen E15-1 at 10000kN

(c) Concrete in the compressive zone began to crush after peak load (12759kN), and more horizontal cracks appeared on the tensile zone of the concrete. Both vertical and horizontal deflection developed fast. Axial load decreased as the vertical deflection developed. The test stopped when the horizontal deflection of the mid-section was considerably large.

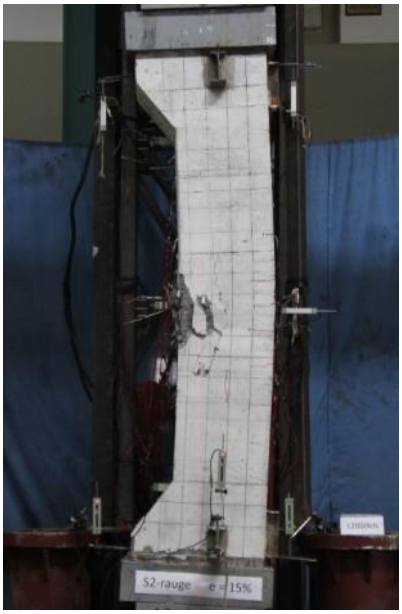

Figure 3-19 Specimen E15-1 at failure

Contrary to pure axial specimens, eccentric specimens did not experience sudden drop of the applied load – the axial load decreased gradually after peak point. Meanwhile, horizontal deflection and concrete damage continuously developed as the actuators kept pushing down (Figure 3-20).

For e/h=10% specimens, the deflection of mid-height cross section at peak load level is 9.89mm, which is 22% of the original eccentricity (45mm). For e/h=15% specimens, the average deflection of mid-height cross section at peak load level is 12.94mm, which is 19% of the original eccentricity (67.5mm) (Figure 3-21).

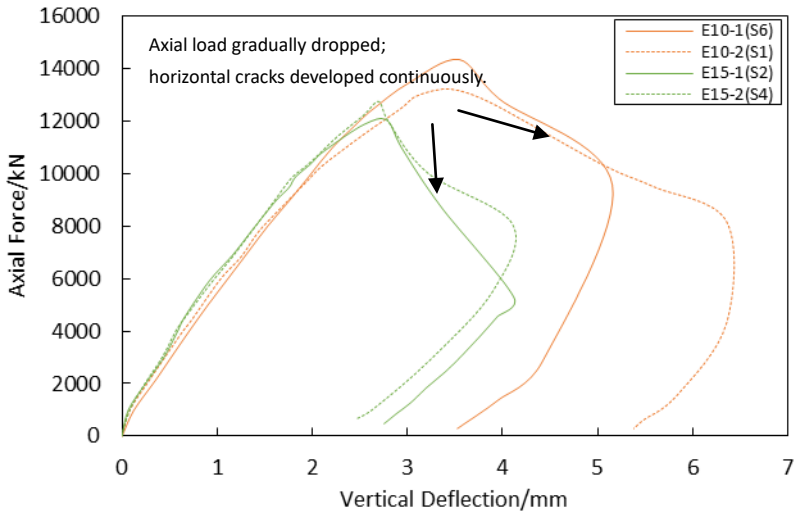

Figure 3-20 Load vs. Vertical deflection (e/h=10% and 15%)

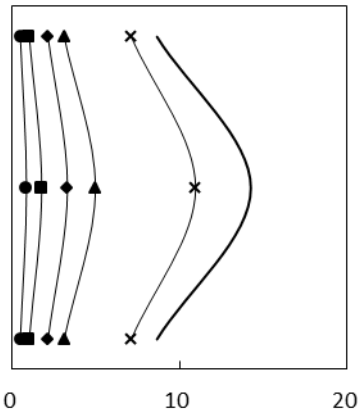

(a) E10-1

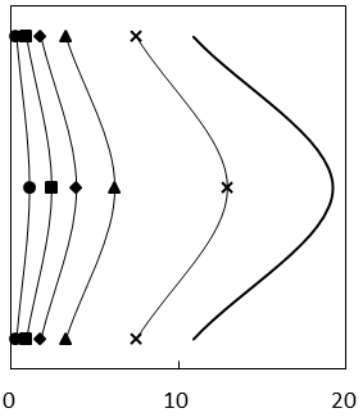

(b) E10-2

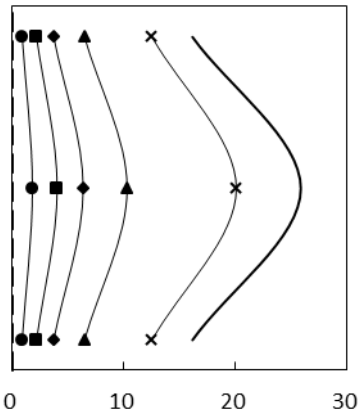

(c) E15-1

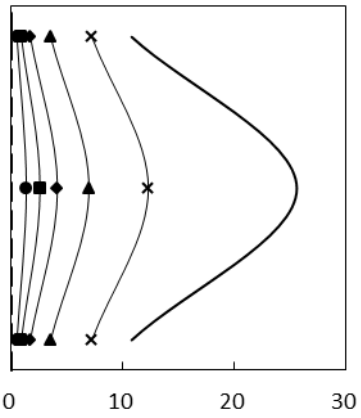

(d) E15-2

Figure 3-21 Horizontal deflection of eccentric specimens

3.6.3 Summary of failure modes and capacities

Table 3-5 and Table 3-6 summarize the capacities and horizontal deflections of the specimens in phase 1. The percentiles in the brackets are the ratios of measured horizontal deflections to the initial eccentricities of the column. It is clear that the actual eccentricities became larger because of the second order effect.

Table 3-5 Capacities for phase 1 test

Specimen ID	Capacity P_u/kN	Vertical deflection at P_u /mm
E00-1	17082	4.07
E00-2	15325	3.43
E10-1	14360	3.55
E10-2	13231	3.46
E15-1	12041	2.79
E15-2	12759	2.70

Table 3-6 Horizontal deflections for phase 1 test

Specimen	Deflection at peak load		Deflection at failure	
		Average		Average
E00-1	-7.78(-)	-5.31(-)	-9.98 (-)	-8.73(-)
E00-2	-2.84(-)		-7.47(-)	
E10-1	10.97(24.38%)	11.96(26.58%)	14.26(31.69%)	16.76(37.24%)
E10-2	12.95(28.78%)		19.25(42.78%)	
E15-1	20.15(31.29%)	16.21(24.01%)	25.82(38.25%)	25.73 (38.11%)
E15-2	12.30(18.22%)		25.63(37.97%)	

The failure patterns of all of the six specimens were combined compression and bending. The pure axial specimens bent toward the bracket direction, while the eccentric specimens bent toward the other direction. Both compressive cracks and tensile cracks could be detected on the concrete surfaces. In the end, the specimens failed due to concrete crush in the middle of the specimens (Figure 3-22).

(a) Specimen E00-1

(b) Specimen E00-2

(c) Specimen E10-1

(d) Specimen E10-2

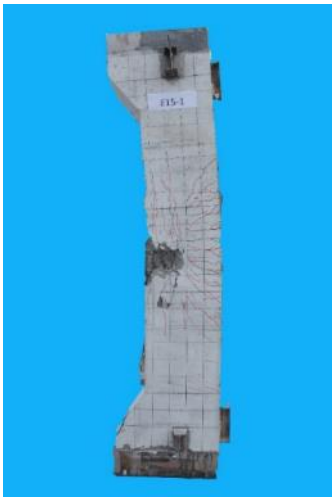

(e) Specimen E15-1

(f) Specimen E15-2

Figure 3-22 Failure mode phase 1 specimens

The crack distributions are presented Figure 3-23. Crack distributions in E00-1 and E00-2 were opposite to that in eccentric specimens. So did the horizontal deflection. It can be explained in two ways:

(a) With the existence of the bracket, the column stiffness center at the bracket zone slightly drifted toward left. But the load was applied in the middle of the column, result in an bending moment that caused the column to deflect;

(b) Since pressure was unevenly distributed at the end of the column, corners at the right side of the end bore more pressure than the left corners did. This caused the right corners crushed ahead of the left corners. Therefore, the ends will rotate and lead to the observed failure modes.

(c)

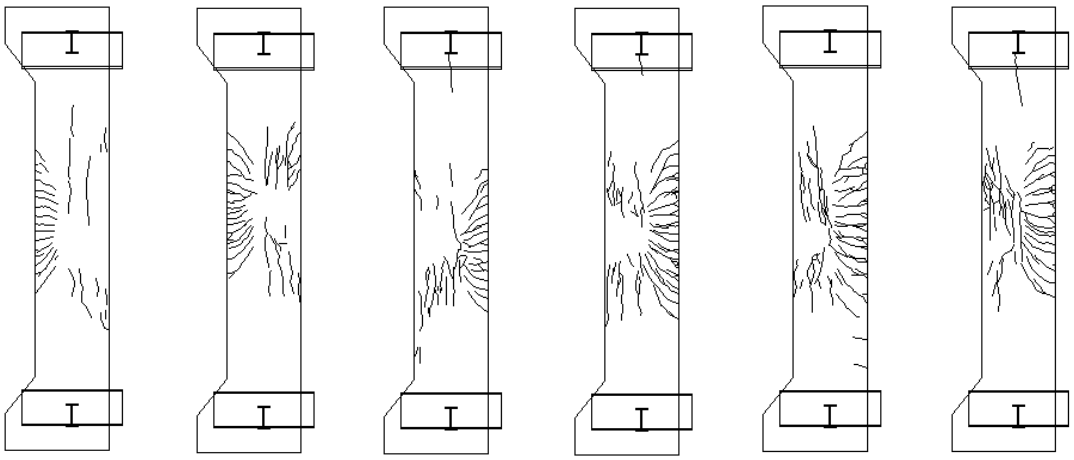

Figure 3-23 Crack distribution of phase 1 test

Figure 3-24 (a) (b) shows the deformed bars in E00-1 and E10-1. Ties were broken in E00-1/E00-2, so the longitudinal bars were no longer confined in the middle of the column. Therefore, buckling of longitudinal bars was very common in E00-1/E00-2. On the other hand, ties were not broken in E10-1/E10-2/E15-1/E15-2. Although longitudinal bars also buckled in these columns, but the buckling length was shorter than that in E00-1 and E00-2. On the other hand, buckling failure of the steel sections was not detected after the test had been completed (Figure 3-24(c)).

(a) Specimen E00-1

(b) Specimen E10-1

(c) Steel sections

Figure 3-24 Failure of bars and steel sections

3.7 Moment – curvature behaviors

Loading curves in Figure 3-15 and Figure 3-20 may reflect the capacity and ability of deformation of the ISRC columns to some degree. However, one can hardly extract the axial deformation from the total vertical deflection if the column is eccentrically loaded, since vertical deflection is contributed by both axial deformation and flexural deformation, thus confusing the analysis. On the other hand, the curvature of a cross section is a pure reflection of its flexural behavior. Therefore, the moment - curvature curves are used for analyzing eccentrically loaded columns.

Figure 3-25 shows the deformed shape of the column, neglecting the vertical deflection. Assume the deformation pattern was symmetric during the test. Since no shear force was applied to the specimen, the curvature of the specimen is the same throughout the entire length of the column.

Figure 3-25 Sketch of deformation and rotation

Figure 3-26 presents the moment –curvature curves of section 'A' (middle section) of the columns. Before the moment capacity was reached, the bending moment of section 'A' grew with the increase of the curvature. The slope of the curves became smaller with the increase of the curvature, suggesting that the bending stiffness decreased as load increased.

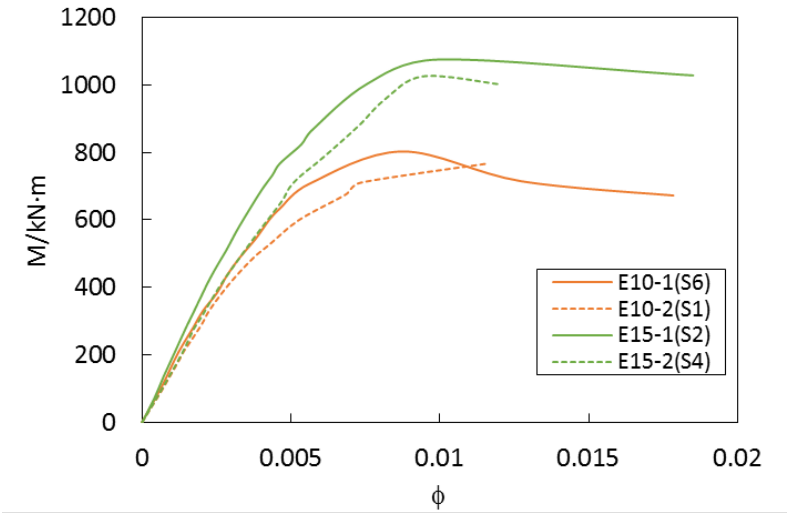

Figure 3-26 Moment vs. rotation of mid-section

It can be concluded that the ductility of the column, in the perspective of moment versus curvature, was good for ISRC columns with eccentricity ratio no more than 15%. Axial load dropped rapidly as the vertical deflection increased, but the bending moment on the mid-height cross section barely dropped. This is because the axial load and the lateral deflection contribute to the bending moment on the mid-height cross section ($M = P(e + \delta)$). When the axial load began to drop after the maximum capacity, the horizontal deflection grew rapidly, which counteracts with the decrease of the axial load.

3.8 Interaction curve

The interaction curves of phase 1 specimens are shown in Figure 3-27; results given by Plumier *et al* are also shown in the figure (Simple Model). Confinement effect had been considered when calculating the interaction curves, but it still underestimated the capacity of the columns when the eccentricity ratio was more than 10%, which demonstrated that the confinement effect was beyond expectation. In fact, the middle part of the concrete was confined, not only by ties, but also by four steel sections. Limited studies have been conducted to investigate the confinement effect provided by the steel sections.

Because of the second order effect, the actual eccentricity ratios got larger as load level increased. The actual eccentricities of the four specimens are listed in Table 3-7. The maximum eccentricity ratio of specimen E15-1 almost reached 20% due to the slenderness effect.

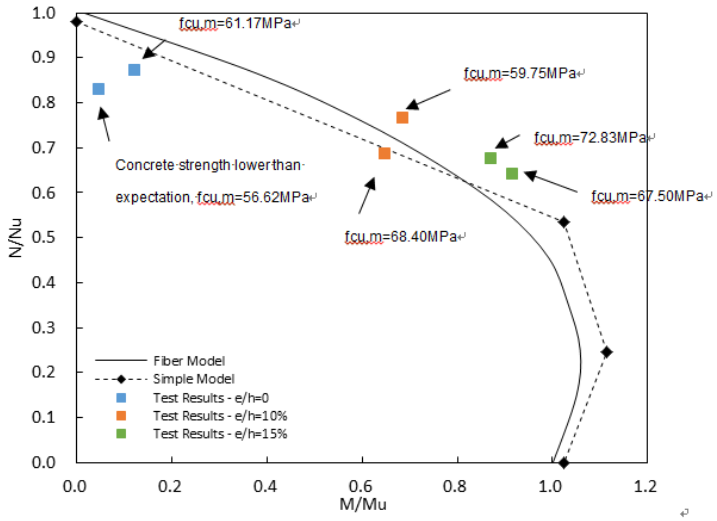

Figure 3-27 Interactive curve of phase 1 specimens

Table 3-7 Actual eccentricities of phase 1specimens

Specimen ID	Original eccentricity	Actual eccentricity
E10-1	10%	12.4%
E10-2		12.9%
E15-1	15%	19.9%
E15-2		17.9%

3.9 Cross-section strain distribution

The mid-height cross section was selected to be the critical section to study strain development of the specimens.

Note that the horizontal axis of the strain curve in Figure 3-29~Figure 3-31 is defined as follows. Assume the bracket is on the left, the distance between a strain sensor and the left bound of the column is defined as 'relative position', regardless of the position in the perpendicular direction (Figure 3-28).

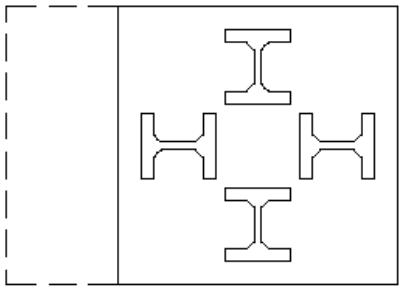

Figure 3-28 Relative position of the strain curve

3.9.1 Specimen E00-1/E00-2

Figure 3-29 shows the strain distribution of longitudinal reinforcing bars, steel sections, and the concrete of specimen E00-2, respectively. At each load level, strains at different relative positions were nearly the same. Strains of the three materials agreed with each other very well. The strains of longitudinal bars and steel sections at load level $100\%P_u$ were less than $2000\mu\varepsilon$, suggesting that longitudinal bars and steel sections remained elastic when the column reached its maximum capacity.

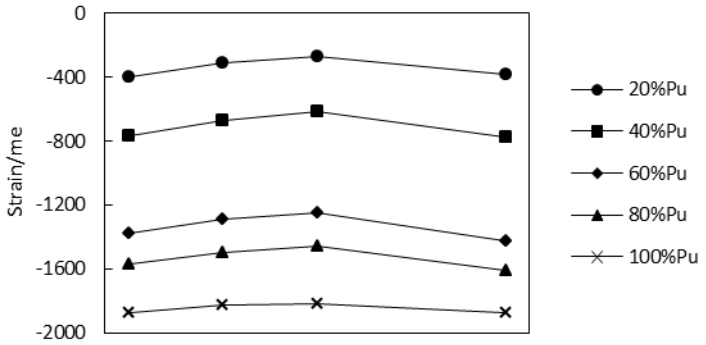

(a) Strain of Longitudinal bars

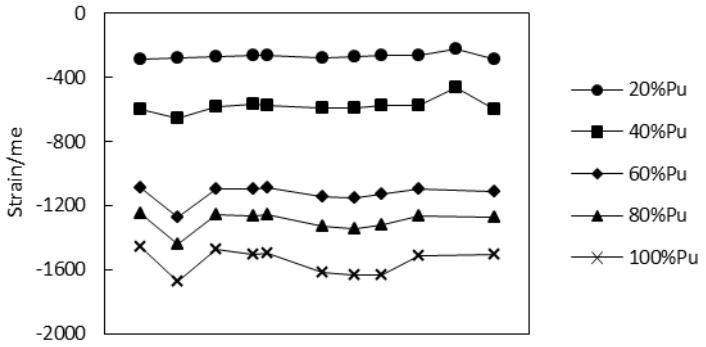

(b) Strain of steel sections

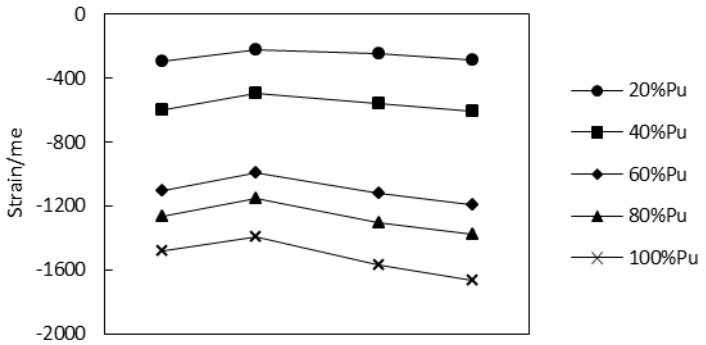

(c) Strain of concrete

Figure 3-29 Strain distribution of section A of E00-2

3.9.2 Specimen E10-1/E10-2

Figure 3-30 shows the strain distribution of specimen E10-2. The strain developed as the load increased, and the longitudinal bars and steel sections on the tensile side began to yield somewhere between 40%~60% of the maximum capacity. The whole cross section was under compression at load level $100\%\ P_u$, since no positive strain was detected by then.

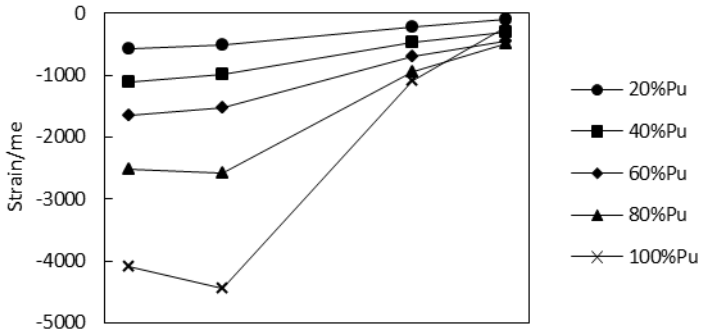

(a) Strain of Longitudinal rebar

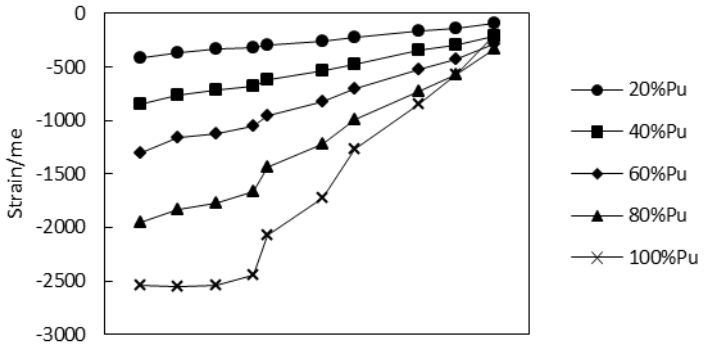

(b) Strain of steel sections

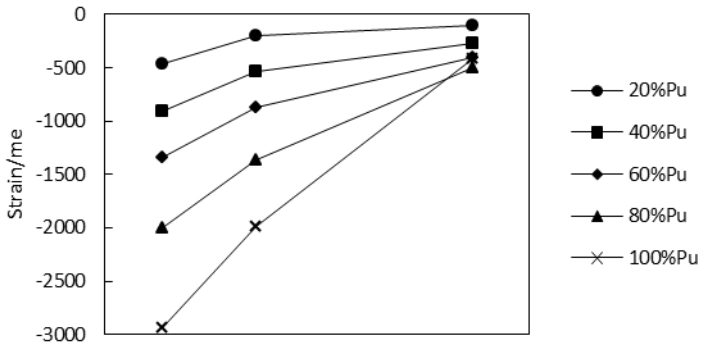

(c) Strain of concrete

Figure 3-30 Strain distribution of section A of E10-2

3.9.3 Specimen E15-1/E15-2

Figure 3-31 shows the strain distribution of specimen E15-2. It shows that the tensile side of longitudinal bars and steel sections yielded earlier than that of specimen E10-2 did. At the 100% P_u load level, positive strain was detected on the right side of the section, which means that a part of the section was in tension.

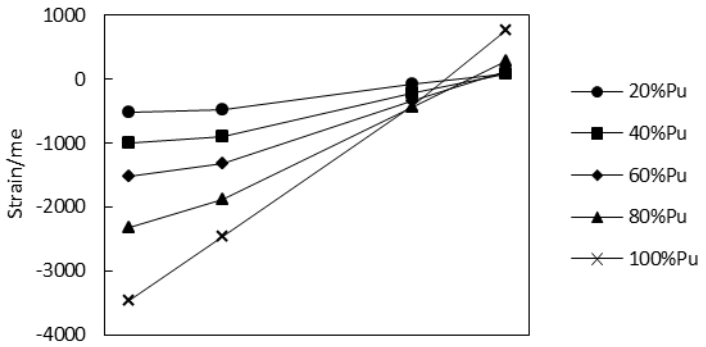

(a) Strain of Longitudinal rebar

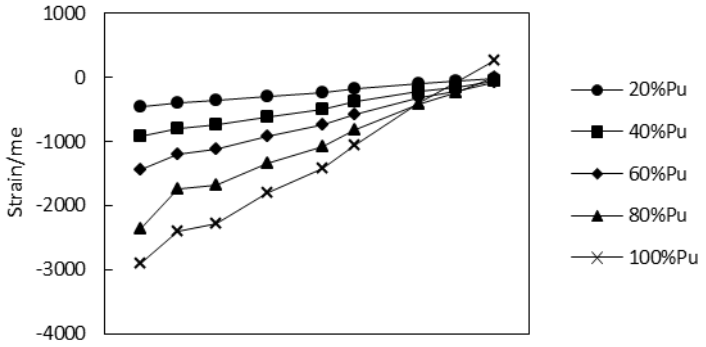

(b) Strain of steel sections

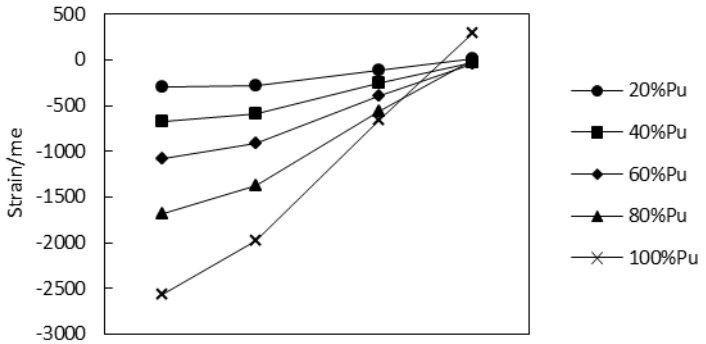

(c) Strain of concrete

Figure 3-31 Strain distribution of section A of E15-2

The strain distribution of section ‘A’ may validate the ‘Plane Section Assumption’ in this phase of the test.

3.10 Stiffness reduction

Both axial and flexural stiffness will decrease as load level increases. In the US codes (ACI318) and Eurocode4 (2004), the first order analysis of a structure should be calculated based on the reduced stiffness where sway frame or non-sway frame is to be designed. This section of the report studies the rules of stiffness reduction for both pure axial and eccentrically loaded columns.

3.10.1 Pure axial specimens (E00-1/E00-2)

The axial rigidity EA of pure axial columns was reduced due to the concrete cracking, leading to the reduction of stiffness of the entire column. There are two ways of calculating the reduction factor (R_k^c): (a) ratio of reduced axial stiffness to the original axial stiffness of the **whole section**, which is also called the ACI 318 method; and (b) ratio of reduced axial stiffness to the original axial stiffness of **the concrete**, which is called the EC 4 method.

In method (a), R_k can be defined as:

$$P = R_k^c \left(E_c A_c + E_s A_s + E_p A_p \right) \varepsilon \tag{3.1}$$

In method (b), R_k can be defined as:

$$P = \left(R_k^c E_c A_c + E_s A_s + E_p A_p \right) \varepsilon \tag{3.2}$$

where:

P – Axial load

ε – Equivalent average axial stain of the column

E_cA_c – Original axial stiffness of concrete

E_sA_s – Original axial stiffness of longitudinal rebar

E_pA_p – Original axial stiffness of steel sections

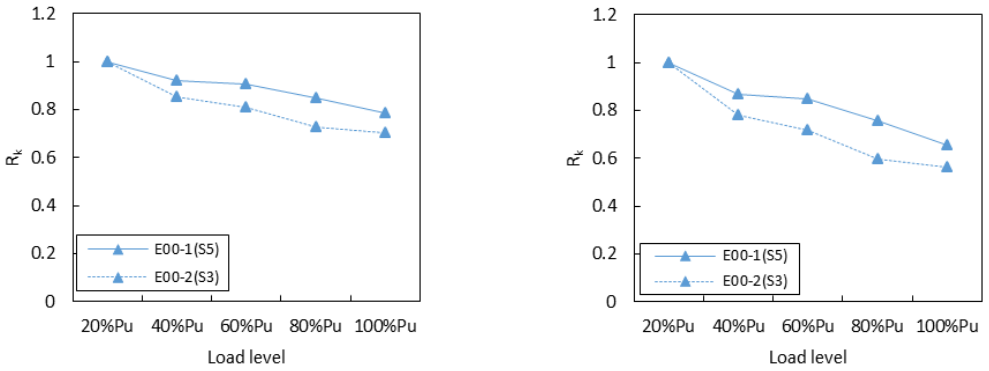

(a) ACI 318 method (b) EC 4 method

Figure 3-32 Axial stiffness reduction R_k^c

As already mentioned in the last section, the normal strain of concrete, longitudinal bars, and steel sections were almost the same, so it is reasonable to assume the normal strain of each material was equal, which was the vertical deflection of the column divided by the length between the two measured points.

Figure 3-32 shows the axial rigidity degradation of the column with two methods. The reduction factor calculated by EC 4 method is smaller than that calculated by ACI 318 method. At maximum load level, the reduction factor R_k^c for ACI 318 method is 0.787 and 0.704, while for EC 4 method is 0.654 and 0.562. Therefore, it is reasonable to take R_k^c as 0.7 and 0.6 for ACI 318 method and EC 4 method, respectively.

3.10.2 Eccentric specimens (E10-1/E10-2/E15-1/E15-2)

Likewise, the reduction factor for flexural rigidity may be defined in the following two ways:

ACI 318 method:

$$M = R_k^b \left(E_c I_c + E_s I_s + E_p I_p \right) \phi \tag{3.3}$$

EC 4 method:

$$M = \left(R_k^b E_c I_c + E_s I_s + E_p I_p \right) \phi \tag{3.4}$$

where:

M – Bending moment

ϕ – Equivalent average curvature of the column

E_cI_c – Original bending stiffness of concrete

E_sI_s – Original bending stiffness of longitudinal rebar

E_pI_p – Original bending stiffness of steel sections

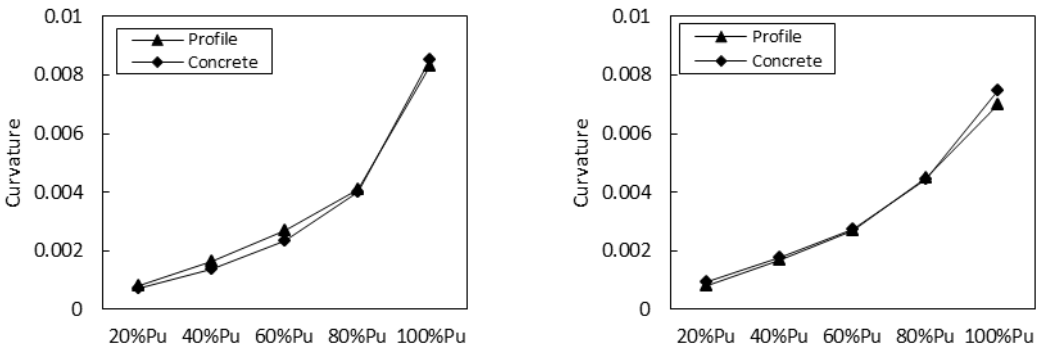

(a) Specimen E10-1 (b) Specimen E10-2

Figure 3-33 Curvature development of section A of specimens E10-1~E15-2

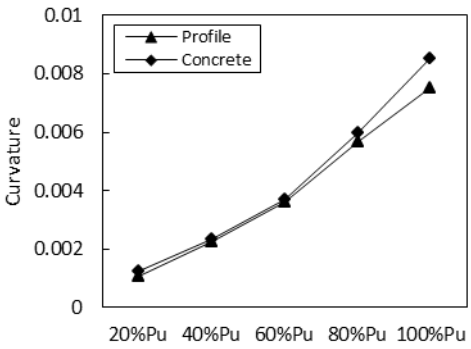

(c) Specimen E15-1

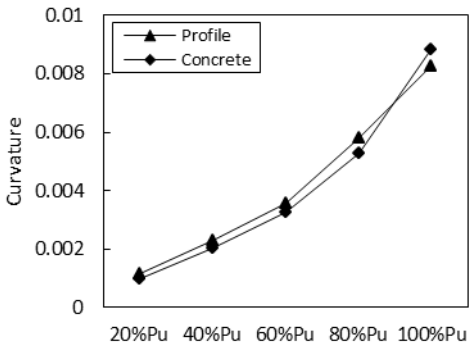

(d) Specimen E15-2

Figure 3-33 Curvature development of section A of specimens E10-1~E15-2 (Continued)

Figure 3-33 shows the development of curvature of section 'A' of specimens E10-1~E15-2. A linear regression is created using points of normal stain versus relative position under a certain load level. Then, the slope of the regressed straight line is taken as the curvature. Curvatures of the concrete correlate with that of the steel sections very well. Together with the validation of 'Plane Section Assumption', it is reliable to assume the curvatures of different materials on a particular section are the same.

Strain gauges that were on the steel sections were more reliable than that were on the longitudinal rebar or concrete, so the column curvature was calculated by normal strain of the steel sections. In addition, it can be observed that the curvature developed more rapidly when the load level was beyond 60%, indicating the reduction of bending stiffness.

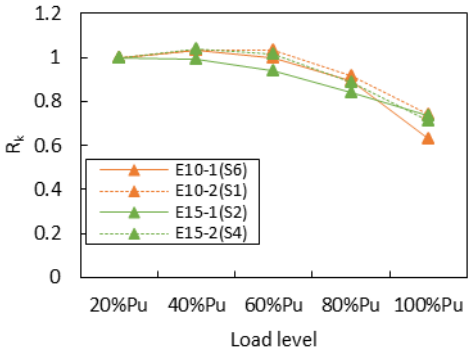

(a) ACI 318 method

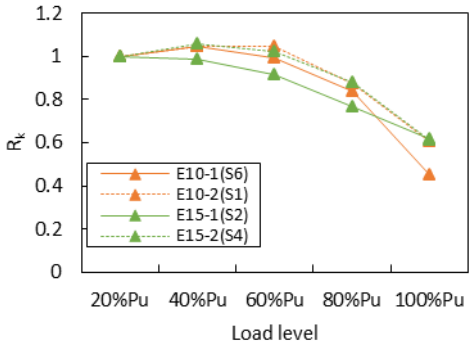

(b) EC 4 method

Figure 3-34 Flexural rigidity degradation of two methods

Figure 3-34 shows the development of flexural stiffness reduction of the column using these two methods. The rigidity barely reduces before load level 60%P_u. While after 60%P_u, rigidity of the concrete reduces more rapidly than rigidity of the whole section. The reduction factors at maximum capacity level of each specimen are listed in Table 3-8.

Table 3-8 Stiffness reduction R_k^b factor of E10-1~E15-2

Specimen ID	ACI 318 method	EC 4 method
E10-1	0.629	0.448
E10-2	0.738	0.607
E15-1	0.736	0.619
E15-2	0.709	0.614

In conclusion, for both axial and flexural behavior, the reduction factor (R_k) can always be taken as 0.7 for the ACI 318 method, and 0.6 for the EC 4 method.

3.11 Interface slip

3.11.1 Pure axial specimens (E00-1/E00-2)

Figure 3-35 presents the slip on concrete-steel interface of specimen E00-1. A negative slip means the concrete is compressed more than the steel section is. As concrete damage grew with the increase of load level, the strain at some local points on the concrete was larger than that on the steel sections. Therefore, the cumulated strain difference resulted in relative slips on the interface. Under pure compression, the slip was very small. In this test, the maximum slip was less than 0.04mm.

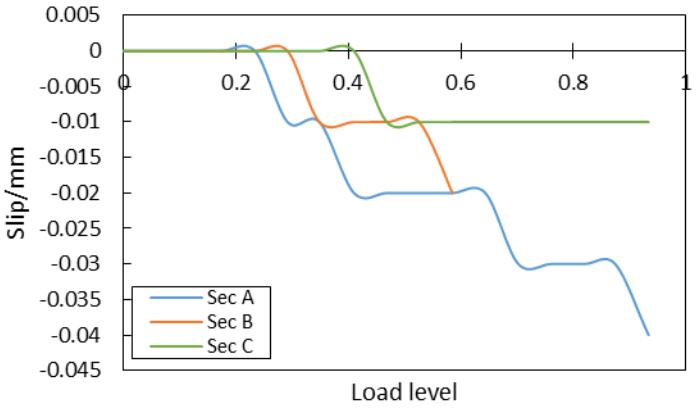

Figure 3-35 Interface slip of E00-1

3.11.2 Eccentric specimens (E10-1/E10-2/E15-1/E15-2)

Figure 3-36 and Figure 3-37 shows the interface slip of E10-1 and E15-1. It is shown that the concrete-steel interface began to slip at load level 0.1~0.4, and the maximum slip increased as the eccentricities. For e/h=10%, the maximum slip was 2.22mm and 1.19mm for section B and section C respectively; for e/h=15%, the maximum slip was 5.22mm and 4.43mm for section A and section B respectively (Note: for e/h=15%, the actual slip may exceed the rage of the displacement sensors).

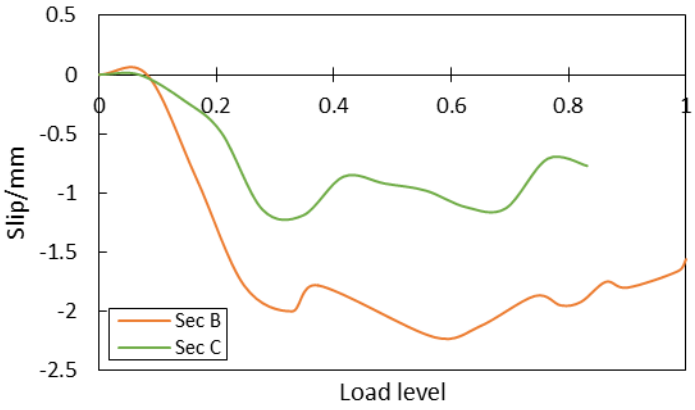

Figure 3-36 Interface slip of E10-1

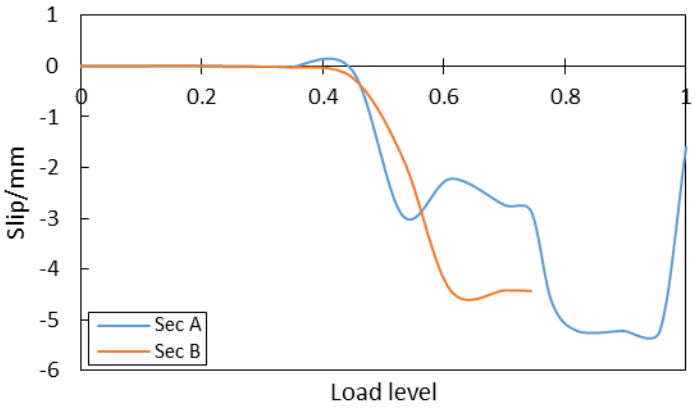

Figure 3-37 Interface slip of E15-1

Results show that although there was no shear force on the cross-section, the slip (or the potential of slip) created a demand for shear resistance on the concrete-steel interface. Theoretically, the slip effect will weaken the assumption that plane sections remain plane. However, the test results support the conclusion that the plane section assumption can be used when determining the flexural capacity of the ISRC columns with the eccentricity ratio less than or equals to 15%.

3.12 Summary of phase1 test

1) The maximum applied load of the ISRC column decreases as eccentricity increases. The pure axial column experiences drops of axial load twice: one right after the peak load, and the other right before failure. For eccentric specimens, the axial loads decrease gradually after they reach peak loads.
2) The moment - curvature curves of the mid-height cross section shows a good sense of ductility.
3) The 'Plane Section Assumption' can be verified in the test when the column is subjected to combined compression and bending with eccentricity ratio less than or equal to 15%. Curvatures of the concrete and the steel section are nearly the same during the loading process.
4) The capacity of the ISRC columns corresponds with the theoretical interaction curve well, which is calculated by fiber model based on 'Plane Section Assumption'.
5) Both axial and flexural rigidity decreases as load increases. The stiffness reduction factor R_k at failure level may be taken as 0.7 for both axial and flexural rigidity if the ACI 318 method (method 'a') is applied or 0.6 if the EC4 method (method 'b') is applied.
6) Although slip is detected on the concrete-steel interfaces, it does not affect the ultimate capacity of the specimens.

4 Experimental study – phase 2

The second phase of the research contains four 1/6-scaled specimens that were loaded under axial loads and quasi-static cyclic loads. The tests were conducted in the CABR structure laboratory in July 2015. The behavior, including the capacity, deformation capacity, and hysteretic performance, of the specimens under simulated seismic loads were examined.

4.1 Test Design

Four 1/6-scaled specimens, designated D10-1, D10-2, D15-1, and D15-2, were tested under cyclic loads. All of the four specimens were identical in dimensions and configurations. A typical cross section of the specimen is presented in Figure 4-1 (a). The dimension of the gross cross-section was $b_c \times h_c = 300 \times 300(\text{mm})$. Four I-shaped steel sections were embedded in the concrete, and the dimension of the steel section was $h \times b \times t_w \times t_f = 80 \times 70 \times 12 \times 12(\text{mm})$. The distance between the centers of the steel sections and the center of the cross section was 85mm. To provide shear resistance on the concrete-steel interface, shear studs were welded on the surface of the steel sections Figure 4-1 (b). The length and diameter of a typical shear stud was 25mm and 5mm respectively. Since the edge of the steel section was very close to the boundary of the cross-section, shear studs that were located on the outside flange of the steel section were cut to 15-mm long to allow for enough thickness of concrete cover. Note that some of the transverse bars were intersecting with the web of the steel sections. Instead of passing through the web, the bar was cut into two segments, and each of them were welded on the web of the steel section to guarantee the integrity of the steel sections. The dimensions and extra information of the cross-section are summarized in Table 4-1.

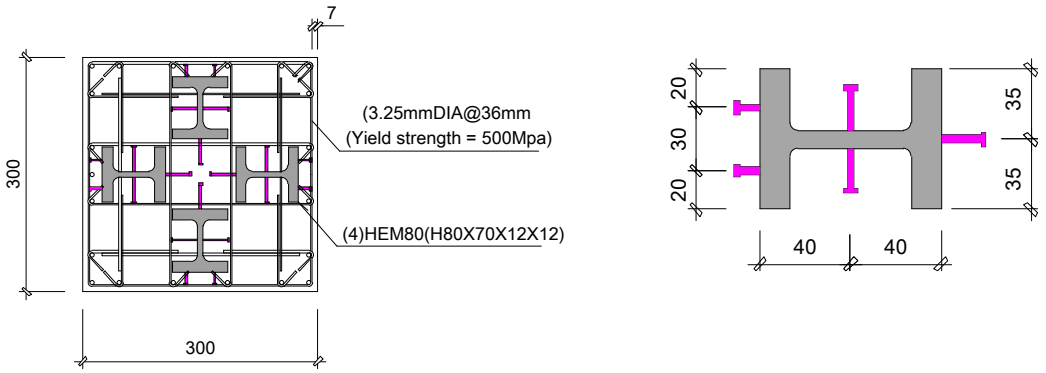

(a) Cross section details (b) Layout of shear studs

Figure 4-1 The dimension of the cross section

Table 4-1 Details of steel sections and reinforcement

Item	Dimensions/mm
Gross cross section	$b_c \times h_c = 300 \times 300$, concrete cover=7mm
Steel section	$h \times b \times t_w \times t_f = 80 \times 70 \times 12 \times 12$
Shear stud	LEN × DIA = 25 × 5, interval=150mm
Longitudinal reinforcement	$\mathrm{DIA} = 6\mathrm{mm}/8\mathrm{mm}, \rho_s = 0.8\%$
Transverse reinforcement	$3.25@36, \rho_{sv} = 0.85\%$

In a typical experiment where the specimen is to be tested under combined compression and lateral cyclic loads, the axial load is usually applied by a vertical actuator which connects to a girder with slides, so that the actuator may move horizontally with the specimen when the specimen was subjected to lateral loads. However, friction may exist on the surfaces of the slide, and the coefficient of friction gets considerably large when the slides deform due to the increasingly growing vertical load. Usually, the magnitude of the friction is hard to measure. Therefore, the accuracy of the test results will be affected because of the friction on the surfaces of the slides. To eliminate the effect of friction, a symmetric specimen was designed in this test program as shown in Figure 4-2. A traditional specimen usually contains a column and a ground beam. The symmetric specimen is a duplicate of the traditional specimen from top to bottom. The height of the specimen was 1900 mm. Two I-shaped steel beams $(140 \times 73 \times 4.7 \times 6.9(\mathrm{mm}))$ were welded to the steel sections to simulate the beam-column joint.

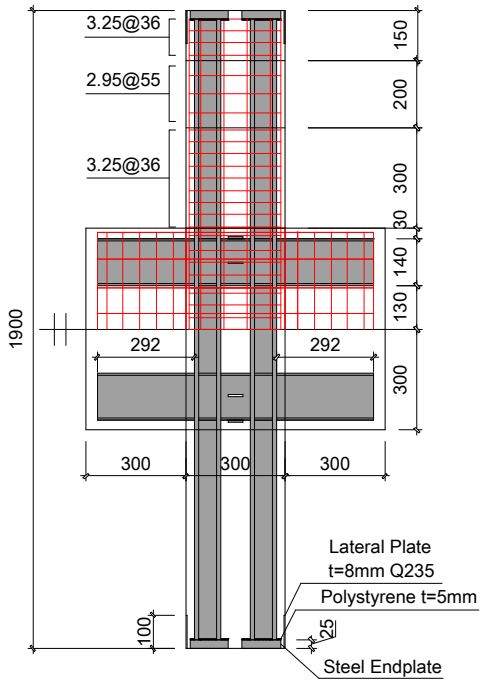

Figure 4-2 The dimension of the specimen

Figure 4-3 presents the installation of the specimen. Each end of the specimen was embedded into a hinge so that it may rotate under lateral loads. One of the hinges was placed on the ground, and the other hinge was installed on the top of the specimen to connect to the vertical actuator. Both of the two hinges were fixed by braces to restrict horizontal displacement as well as out-of-plane displacement. In this way, the hinges and the specimen could form a static-determinate system to eliminate the effect of the friction. Suppose the force applied by the horizontal actuator was 2V, then the shear force carried by each half of the specimen was V. Therefore, the bending moment of the critical section could be determined regardless of the friction.

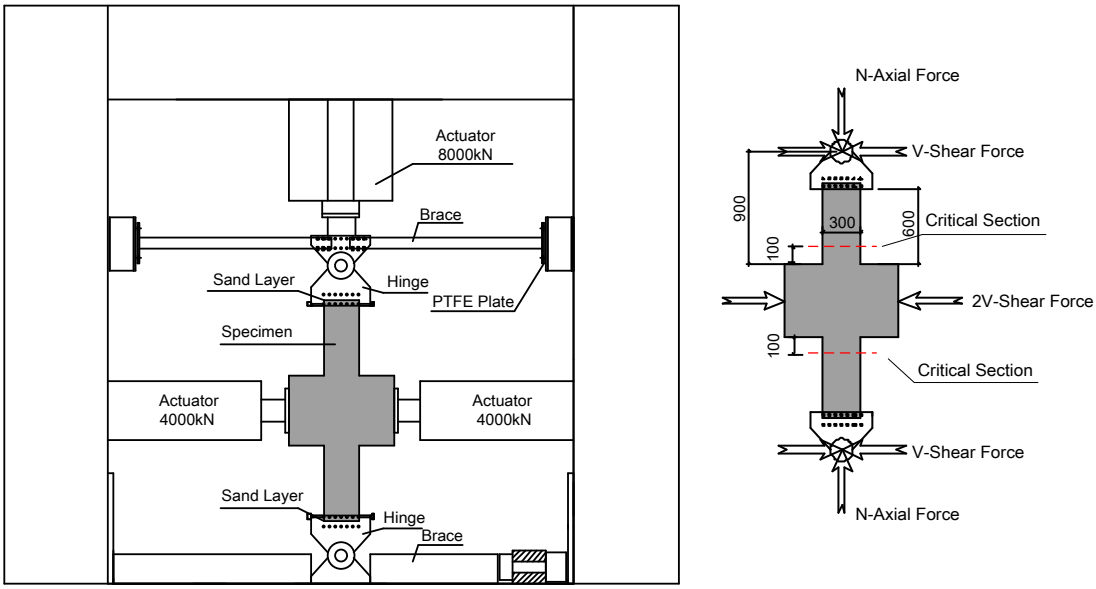

Figure 4-3 Specimen setup

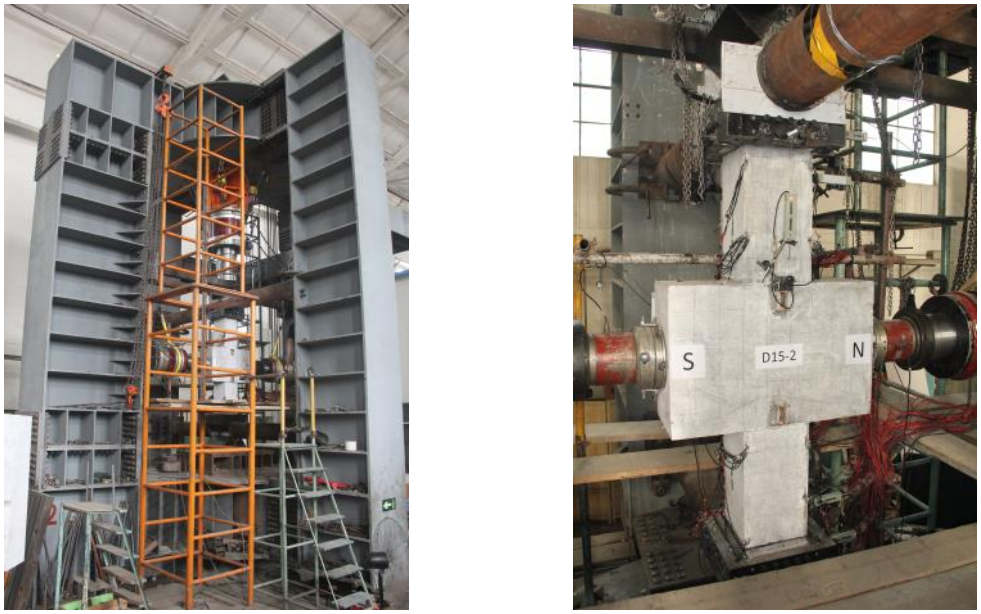

Figure 4-4 The specimen and the loading machine

Note that there was a 5-mm thick sand layer at each end of the specimen between the surface of the specimen and the hinge, whose purpose was similar to that in the static tests. If the sand layer was not provided, the surface of the steel sections and the concrete would be forced into a same plane. Namely, an extra constraint would be applied to the end of the specimen, which did not represent the real boundary conditions in real structures. Since the sand was soft, it released the constraint to best simulate the boundary conditions in real structures.

4.2 Materials

The specimens were made of C60 concrete. The maximum size of the aggregate was 5 mm, and gradation of the size of the aggregate was strictly controlled. The steel sections and beams were made of Q460 and S235 steel (The steel beams were provided by ArcelorMittal). Table 4-2 and Table 4-3 present the tested material strength. It should be noted that the compressive strength of the concrete was obtained by testing $150 \times 150 \times 150(\text{mm})$ cubes according to Chinese standards.

Table 4-2 Strength of the concrete

Specimen ID	Block ID	Ultimate load/kN	Compressive strength/MPa	Average strength/MPa
D10-1	1	1506	67	70
	2	1609	72	
	3	1614	72	
D10-2	1	1643	73	70
	2	1609	72	
	3	1489	67	
D15-1	1	1686	75	76
	2	1769	79	
	3	1687	75	
D15-2	1	1490	66	67
	2	1559	69	
	3	1506	67	

Table 4-3 Strength of steel sections, reinforcement, and shear stud

Material	Yield strength/MPa	Ultimate strength/MPa
Steel section	457	603
Longitudinal reinforcement (d=8mm)	459	689
Longitudinal reinforcement (d=6mm)	367	584
Transverse reinforcement	572	638
Shear stud	320	400

Shown in Figure 4-5 are the fabrications of the specimen. The concrete was placed in June 2015 when the temperature was about 25℃~30℃.

Figure 4-5 Fabrication of the specimen

4.3 Loading protocol

In real structures, the axial force and shear force in a column may vary with the intensity of the earthquake, so a constant vertical load is not appropriate in quasi-static tests. Therefore, a two-phase loading protocol was proposed to simulate the seismic reaction of a column under earthquakes. During stop 1, only axial load was applied to the specimen. The target axial load N_0 in step 1 represented the gravity load in a structure, and it was determined as follows:

$$\mu_N = \frac{1.25N_0}{A_c f_c + A_p f_p} = 0.7 \tag{4.1}$$

where μ_N is the axial compression ratio of the specimen, defined as the axial force divided by the axial capacity of the column; A_c and A_p are the area of the concrete and steel sections respectively; f_c is the specified design axial compressive strength of C60 concrete

and is taken as 27.5 MPa; f_p is the design yield strength of Q460 steel and is taken as 415 MPa; and the value of 0.7 is the maximum allowable design axial compression ratio for composite columns specified in Chinese code JGJ 3. In this test program, N_0 was taken as 3500 kN.

During step 2, the axial load and the transverse load increased in proportion to reach the target eccentricity ratio as shown in Figure 4-6 (a). Within each level during this phase, the axial load increased by 500 kN first, and then the lateral load was applied cyclically, holding the axial load constant. Before the extreme compressive fiber of the steel sections yielded, the lateral load was applied by one cycle in each level, and its maximum value within this level was determined according to the loading path in Figure 4-6 (a). When the extreme compressive fiber of the steel sections had yielded, the lateral load was applied by three cycles in each load level. When the maximum lateral load had been reached, the axial load stopped increasing and remained constant for the rest of this step. In the meantime, the lateral load was changed to displacement control by a 2-mm increase in lateral displacement for each load level.

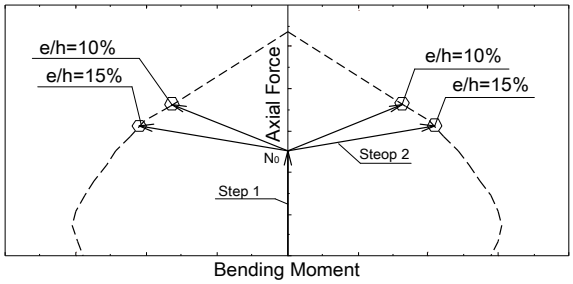

(a) Target loading path

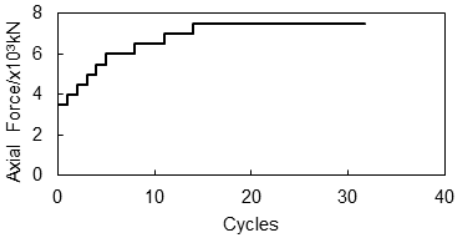

(b) Axial load (e/h=10%)

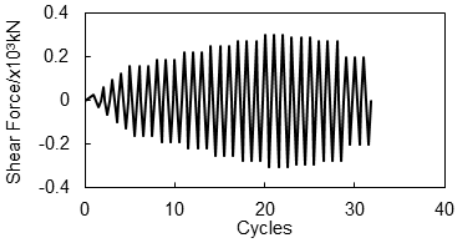

(c) Horizontal load (e/h=10%)

Figure 4-6 Loading protocol of quasi-static tests

Every two of the specimens were loaded under a same eccentricity ratio to account for diversity in materials and the fabrication – D10-1 and D10-2 with e/h=10%, and D15-1 and D15-2 with e/h=15%.

Table 4-4 Details of the loading protocol

Loading Phase	e/h=10%			e/h=15%		
	Axial Load /kN	Lateral Load /kN	Cycles	Axial Load /kN	Lateral Load /kN	Cycles
Phase 1	0	0	-	0	0	-
	3500	0	-	3500	0	-
Phase 2	4000	30	1	4000	55	1
	4500	60	1	4500	105	1
	5000	95	1	5000	150	1
	5500	125	1	5500	200	1
	6000	160	3	6000	250	3
	6500	190	3	6500	$\Delta_m + 2mm$	3
	7000	220	3	6500	$\Delta_m + 4mm$	3
	7500	250	3	6500	$\Delta_m + 6mm$	3
	7500	$\Delta_m + 2mm$	3			
	7500	$\Delta_m + 4mm$	3			
	7500	$\Delta_m + 6mm$	3			

4.4 Test measurement

During the test, the magnitude of the vertical and horizontal loads was recorded directly by the actuator system. Displacement and strain sensors were installed, and the layout is presented in Figure 4-7. Critical section 1 was near the conjunction of the column and the beam, located 100 mm from the corner of the column, while critical section 2 was near the end of the column, 300 mm away from critical section 1. The sensors were installed on both the upper and lower columns.

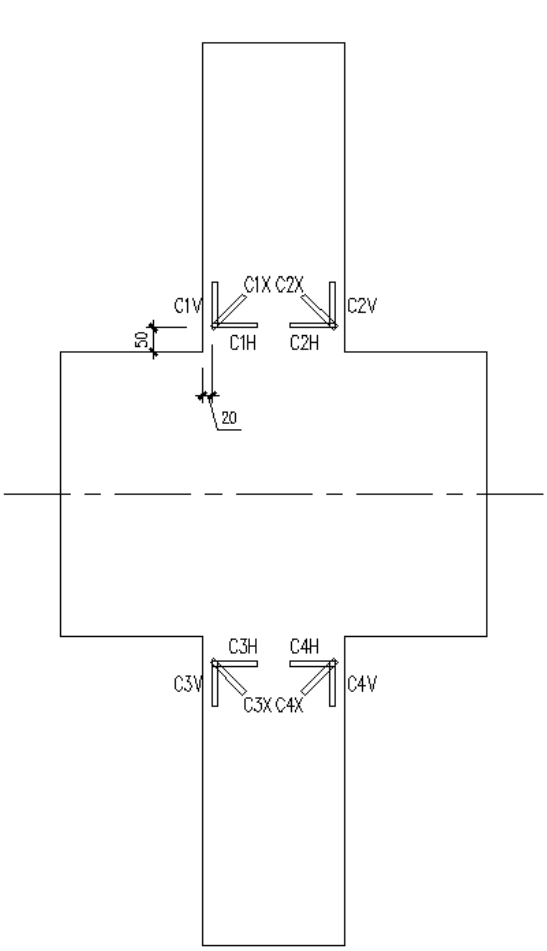

(a) Strain sensors on the concrete

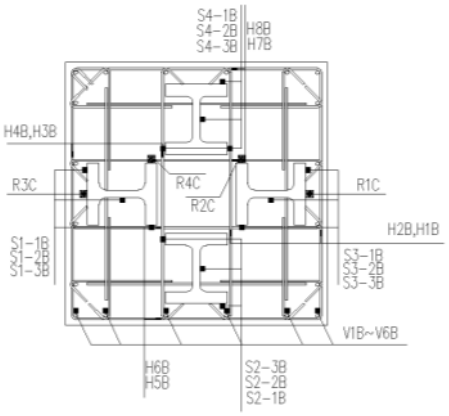

(b) Strain sensors on critical section 1

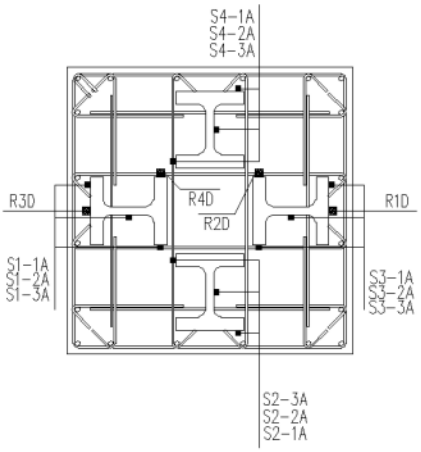

(c) Strain sensors on critical section 2

Figure 4-7 Layout of the strain sensors

4.5 General behavior of the specimens

The sign of horizontal loads and displacements during the test is defined as follows: the lateral loads and displacements are positive when the left actuator pushes the specimen and the specimen moves right, and vice versa.

Like the static tests, initial vertical cracks occurred first on the face of the column. Then, the cracks and the damage of the concrete developed as the load increased. All of the specimens failed in compression-controlled flexural patterns with severe damage at the corners of the concrete. At the end of the test, a large amount of vertical cracks and crush of the concrete were registered. Details of the behavior of the specimens were discussed in the following sections.

4.5.1 Specimen D10-1/D10-2

Specimen D10-1 and D10-2 were loaded with 10% eccentricity ratio. The planned and actual loading paths of the specimens are shown in Figure 4-8. The actual eccentricity ratios were relatively larger than 10% because of the second order effect. The capacities of specimen E10-1~E15-2 are also presented in this figure for comparisons. Note that results of the static tests have been adjusted according to the scaling factors. Since the material strength were different for the 1/4-scaled specimens and the 1/6-scaled specimens, results obtained from these two series of tests need not to be well agreed. The static tests just serve as references.

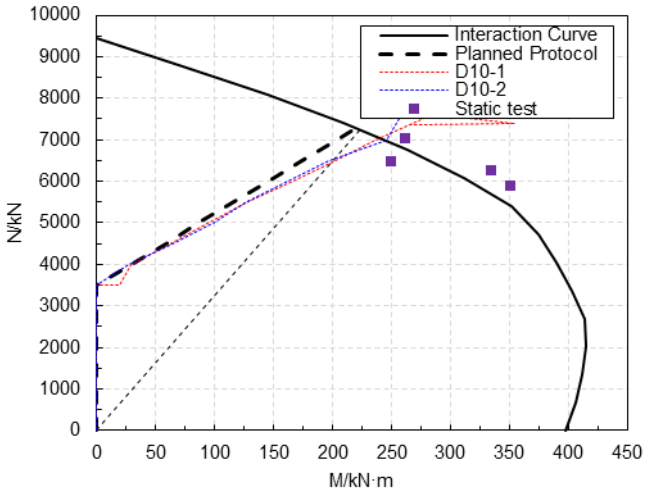

Figure 4-8 Actual loading path of D10-1 and D10-2

(a) When the vertical load increased to gravity load level, there was no significant deformation and cracks on the specimen. As the test went on, a few vertical cracks occurred on the column as well as on the beam. The vertical cracks developed in the middle of the column, where the concrete was relatively weaker due to the very small thickness of concrete cover. Although cracks were registered on the beams, but these cracks did not develop a lot. Therefore, cracks on the beams were of no interest because the authors believed that they had little influence on the behavior of the specimen.

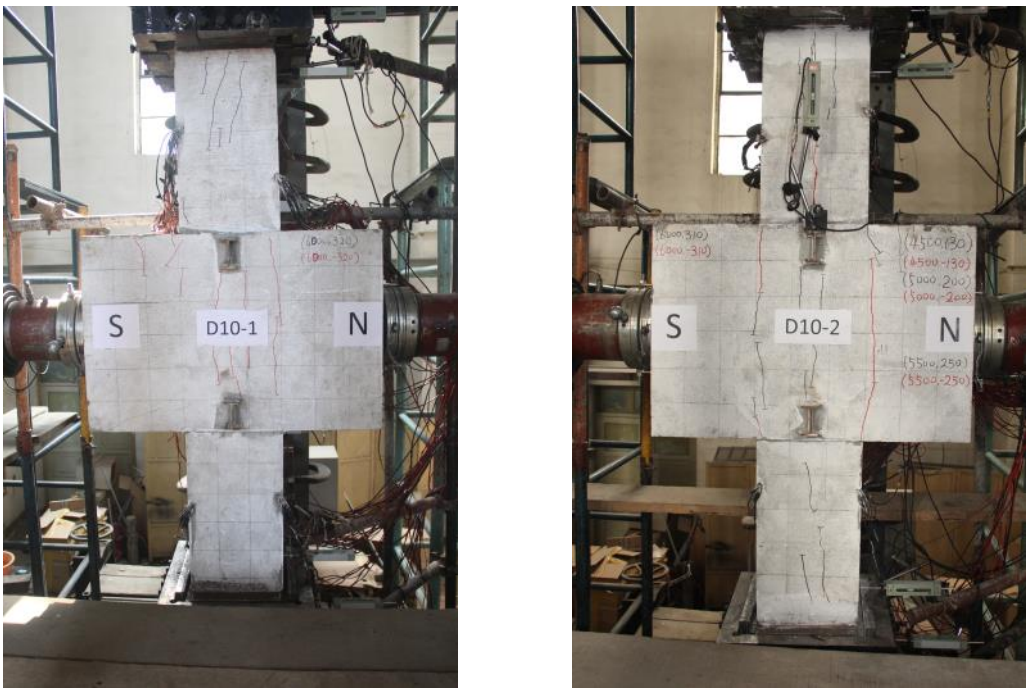

Figure 4-9 Specimen D10-1/D10-2 at (6000kN,160kN)

(b) As the vertical and lateral loads increased, the width of the initial cracks increased. More cracks occurred on the corners of the column. Concrete was falling off the column on specimen D10-2 at this load level. The concrete had already been crushed in the mid-height of the column of specimen D10-2. However, little damage of specimen D10-1 was observed.

Figure 4-10 Specimen D10-1/D10-2 at (7000kN,220kN)

(c) The failure of specimen D10-1 and D10-2 was attributed to the crush of the concrete corners. Apart from the cracks, the concrete near the bottom of the column was also damaged, resulting in a horizontal stripe area of the concrete falling off the specimen. Based on the loading conditions, we believe that the horizontal cracks were not caused by tensile stress in the specimen, but the shortening of the specimen due to vertical load.

Figure 4-11 Specimen D10-1/D10-2 at failure level

4.5.2 Specimen D15-1/D15-2

Specimen D15-1 and D15-2 were loaded with equivalent eccentricity ratio of 15%. During the loading, we purposely controlled the magnitude of transverse load to account for the second order effect. Therefore, the actual and planned loading protocols of D15-1 and D15-2 were very close.

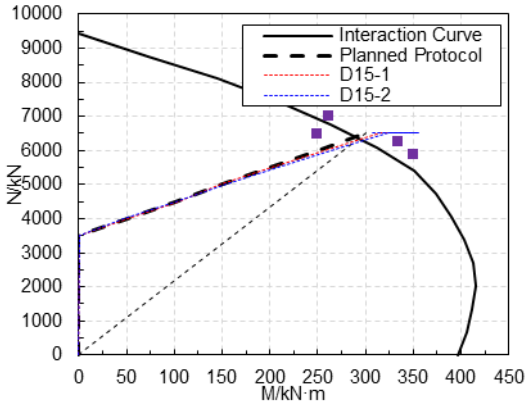

Figure 4-12 Actual loading path of D15-1 and D15-2

(a) For specimen D15-1 and D15-2, the vertical cracks also occurred in the first place. Because the eccentricity was larger, the initial cracks occurred earlier than that in specimen D10-1 and D10-2 when the vertical and lateral loads reached 5000 kN and 150 kN, respectively.

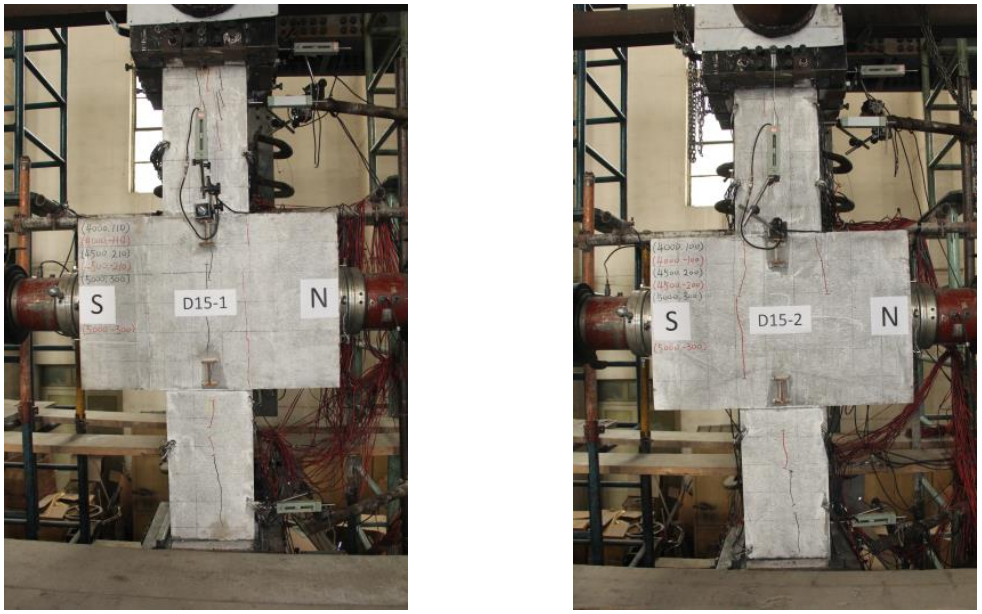

Figure 4-13 Specimen D15-1/D15-2 at (5000kN,150kN)

(b) As the load increased, the damage of the concrete developed to the corners of the columns. Compared to D10-1 and D10-2, less inclined cracks were observed in D15-1 and D15-2, suggesting that the loading condition was prone to bending moment rather than shear.

Figure 4-14 Specimen D15-1/D15-2 at (6500kN,9mm)

(c) The corners of the column were crushed in the end, causing the specimen to fail. In addition, some of the concrete fell off the faces of the column.

Figure 4-15 Specimen D15-1/D15-2 at failure level

4.5.3 Summary of failure mode

All of the four specimens failed in combined compression and bending – the specimen failed because the corners of the concrete were crushed – which met the purpose of the experiment program. The final crack distributions of the specimens are presented in Figure 4-16. The specimens held integrity during the whole loading process. Despite the surrounding concrete was damaged due to lack of confinement, the core concrete remain intact because of the confinement effect provided by the steel sections. In turn, the core concrete helped ensure that the steel sections would not buckle when the vertical load was very large.

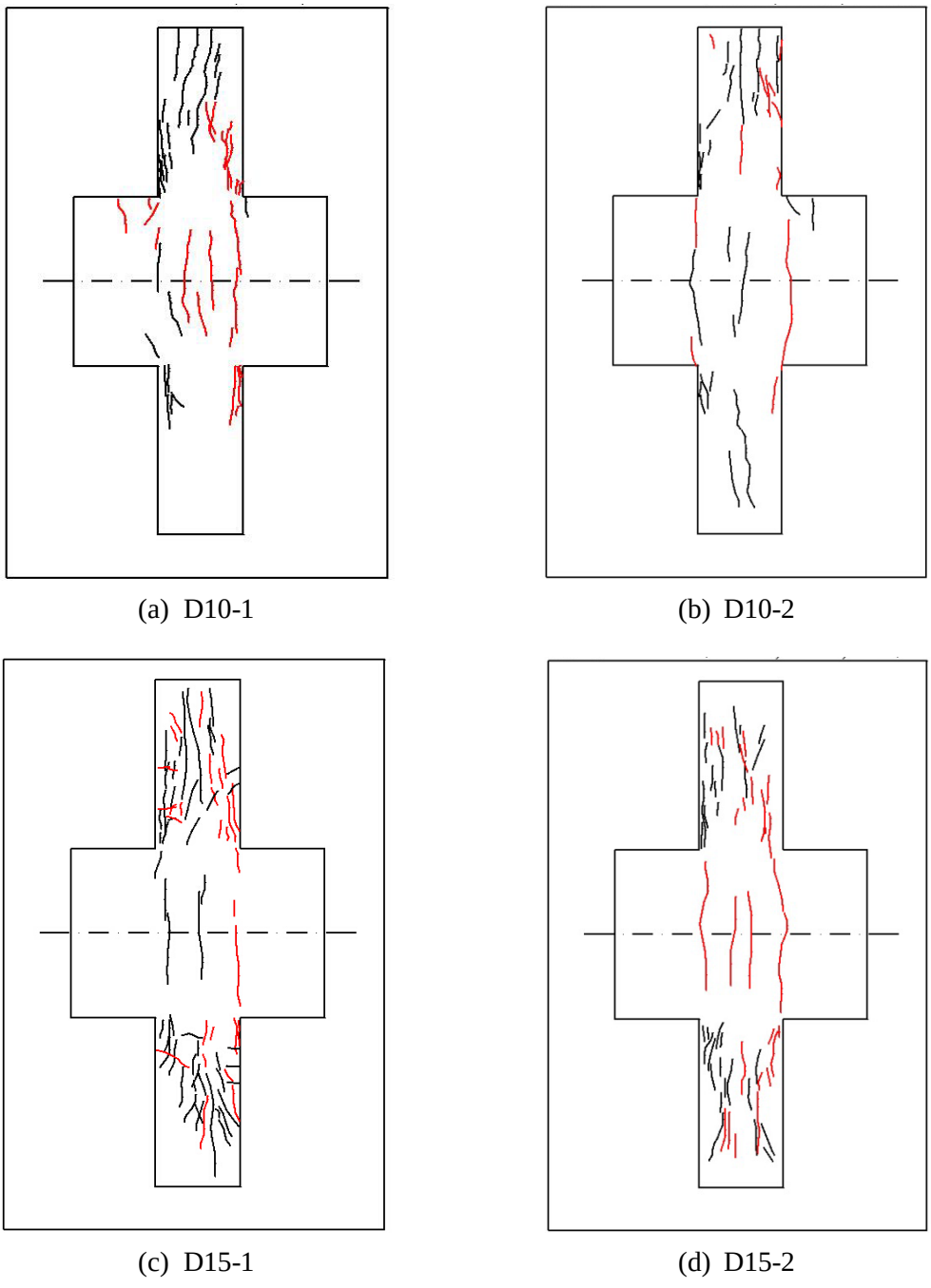

(a) D10-1 (b) D10-2

(c) D15-1 (d) D15-2

Figure 4-16 Crack distribution of the specimens

After the specimen was severely damaged, locale buckling of the longitudinal reinforcement and break of the transverse reinforcement was detected at places where the concrete fell off. Most of the buckling areas lay where the volume ratio of the transverse reinforcement changed from 0.85% to 0.25%.

Figure 4-17 Locale failure of the specimen

Figure 4-18 shows the conditions of the steel sections of specimen D15-2 after the test has been completed. Features of the steel sections suggest that the integrity of the steel sections can be guaranteed even if no connections exist between them. The curvatures of the four steel sections are compatible with each other, indicating no separation of these steel sections exists. In addition, little damage of the shear studs can be observed.

(a) Overview of the steel sections

Figure 4-18 Deformation of steel sections of D15-2

(b) Feature of the upper column

(c) Feature of the lower column

(e) Feature of the shear studs

(f)

Figure 4-18 Deformation of steel sections of D15-2 (Continued)

Rotation of the beams was recorded during the test. Despite the specimens were symmetric in geometric dimensions, the behaviors of the upper and lower columns of the specimen were not identical due to diversities in material properties and fabrication errors, especially at failure load levels. For these reasons, the degree of damage for the upper and lower column was not the same. Moreover, since the damage reduce the rigidity of the adjacent area, the deformation was more likely to develop at these areas, which in turn intensify the damage. Therefore, the stiffness of the specimen was not symmetrically distributed due to the difference in damage degree, result in the rotation of the beams.

4.6 Hysteretic behavior

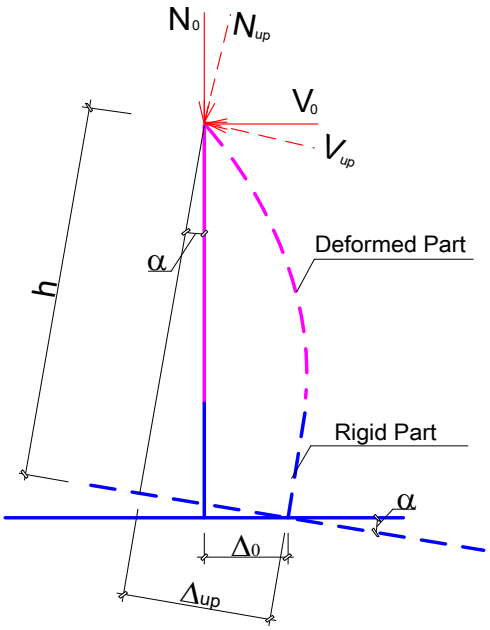

Figure 4-19 Deformation of the specimen

As mentioned above, the rotation of the beam leads to different loading conditions for the upper and lower column. Therefore, the measured axial load, lateral load, and lateral displacement have to be modified to account for the rotation. Shown in Figure 4-19 is the deformation pattern of the upper half of the specimen. Suppose the rotation of the 'ground beam' is α – positive in clockwise direction, and negative in counter-clockwise direction. In addition, assume the 'ground beam' of the specimen is a rigid body, which does not have any deformation during the test. This assumption is reasonable because no significant deformation was observed within the 'ground beam' during the test. N_0, V_0, and Δ_0 are the recorded data

of axial load, lateral load, and lateral displacement, where N_0 was directly recorded by the system; Δ_0 was recorded by a displacement sensor installed in the middle of the specimen; and V_0 is one-half of the load applied by the lateral actuator. N_{up}, V_{up}, and Δ_{up} are the equivalent axial load, lateral load, and lateral displacement of the upper column. 'h' is the height of one-half of the specimen, 1200 mm. According to the geometric relationships, the modified test data can be expressed as follows:

$$\begin{cases} N_{up} = N_0 \cos\alpha + V_0 \sin\alpha \\ V_{up} = -N_0 \sin\alpha + V_0 \cos\alpha \\ \Delta_{up} = \Delta_0 / \cos\alpha + h \tan\alpha \end{cases} \tag{4.2}$$

Similarly, the modified test data for the lower column is:

$$\begin{cases} N_{low} = N_0 \cos\alpha - V_0 \sin\alpha \\ V_{low} = N_0 \sin\alpha + V_0 \cos\alpha \\ \Delta_{low} = \Delta_0 / \cos\alpha - h \tan\alpha \end{cases} \tag{4.3}$$

The modified hysteretic curves of the specimens were presented in Figure 4-20. Except for specimen D10-1, other specimens have all been affected by the rotation of the beam. The beam of specimen D15-1, for example, rotated counter-clockwise during the test. When the specimen moved toward right, the rotation made the equivalent lateral displacement of the upper column smaller, and that of the lower column larger. Therefore, the hysteretic curve of specimen D15-1(up) is more spread out in the negative part, while the curve of specimen D15-1(low) is more spread out in the positive part.

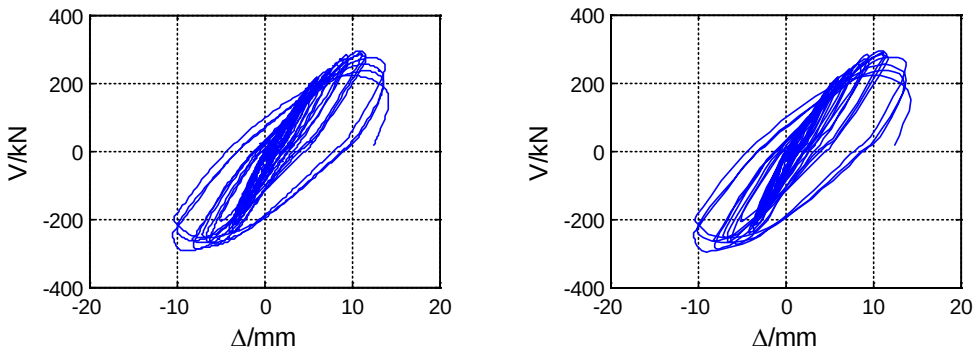

(a) D10-1(up) (b) D10-1(low)

Figure 4-20 Hysteretic curves of the specimens

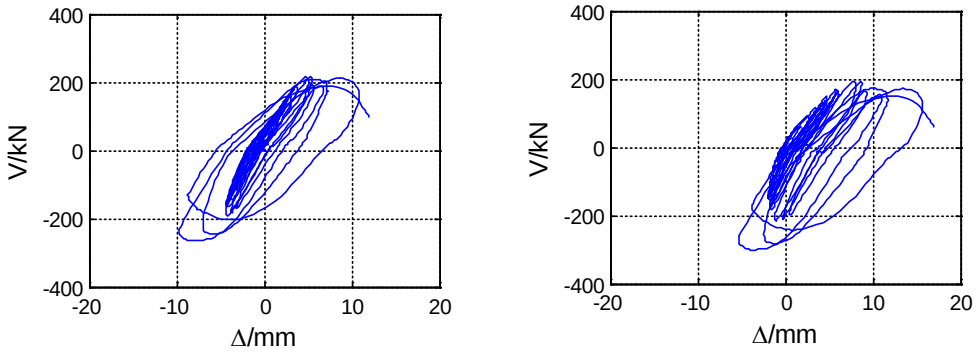

(c) D10-2(up)

(d) D10-2(low)

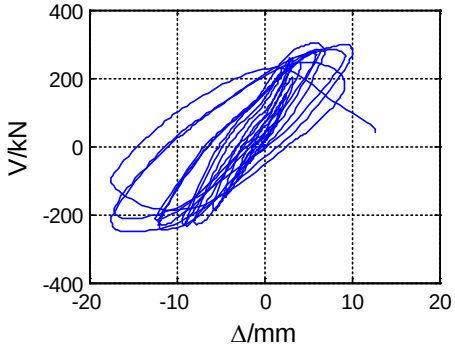

(e) D15-1(up)

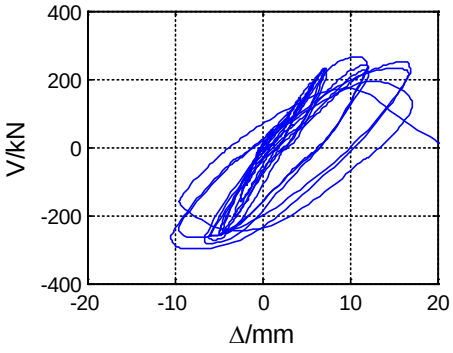

(f) D15-1(low)

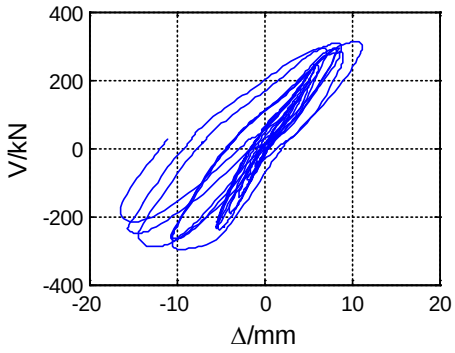

(g) D15-2(up)

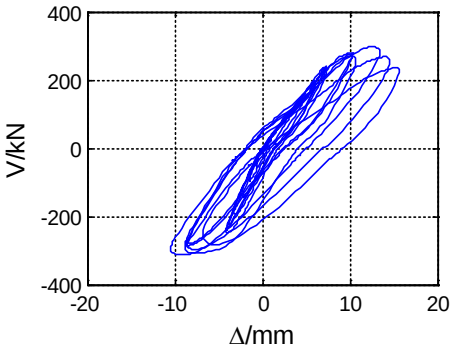

(h) D15-2(low)

Figure 4-20 Hysteretic curves of the specimens (Continued)

Although the behaviors of the specimens were affected by the rotation of the beams, the hysteretic curves are still stable. The specimens showed some pinching at the beginning of the test, but the degree of pinching was mitigated as the lateral displacement was increasing. For the last several circles of the loading, the hysteretic curves are round and stable, suggesting a good ability of energy dissipation.

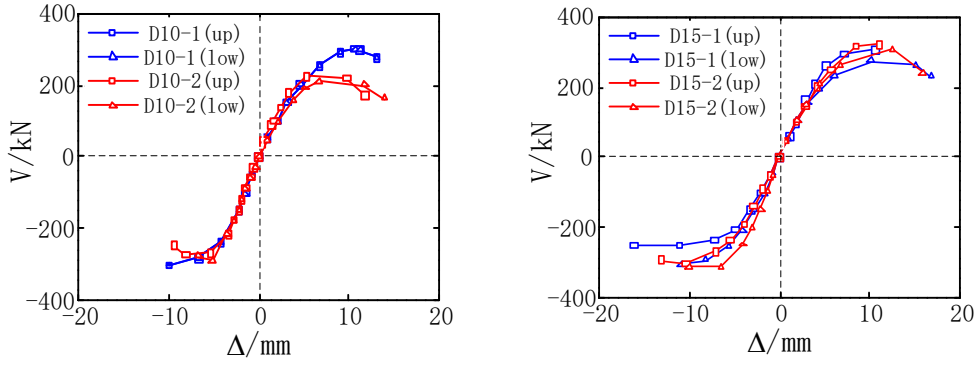

(a) D10-1/D10-2 (b) D15-1/D15-2

Figure 4-21 Envelop curves of the specimens

4.7 Capacities and deformations

Shown in Table 4-5 are the test results of the specimen under three different load stages – yield stage, peak stage, and ultimate stage. The yield point of a specimen is determined based on reduced stiffness method (Figure 4-22). The equivalent secant modulus of a specimen is determined by the original point and the $0.6V_p$ point on the ascending branch of the envelop curve, and the yield point is determined accordingly. The ultimate point is defined as the $0.85V_p$ point on the descending branch of the envelop curve, or the point where the test stops, whichever is larger.

According to the test data or the envelop curves, the initial lateral stiffness of the specimens are almost the same, regardless of the eccentricity ratio. When the maximum lateral load is reached, the lateral load barely descends afterwards until the specimen fails. This phenomenon is caused by the unique loading protocol employed in this test program. During step 2 in the quasi-static test, the vertical load keeps increasing as the test going on. When the lateral load reaches its peak, the combination of axial load and bending moment on the critical section of the column has already reached the interaction curve, which means the specimen is just about to fail. At the same time, the axial compression ratio for design was 1.50 and 1.14 for e/h=10% specimens and e/h=15% specimens respectively. The extremely high axial load causes the specimen to fail right after the maximum lateral load is reached.

Table 4-5 Test results under different load stages

Specimen		Direction	Yield			Peak			Ultimate		
			V_y/kN	Δ_y/mm	θ_y	V_p/kN	Δ_p/mm	θ_p	V_u/kN	Δ_u/mm	θ_u
D10-1	Up	+	248	6.73	1/134	300	10.60	1/85	255	13.49	1/67
		-	252	4.84	1/186	300	9.87	1/91	258	10.78	1/83
		Average	250	5.79	1/156	300	10.24	1/88	257	12.14	1/74*
	Low	+	246	6.71	1/134	303	10.56	1/85	258	13.55	1/66
		-	256	4.88	1/184	299	9.90	1/91	254	10.76	1/84
		Average	251	5.80	1/155	301	10.22	1/88	256	12.16	1/74*
D10-2	Up	+	187	3.81	1/236	220	5.43	1/166	187	11.04	1/82
		-	241	4.25	1/212	275	8.06	1/112	250	9.31	1/97
		Average	214	4.03	1/223	248	6.75	1/133	219	10.18	1/88*
	Low	+	187	5.08	1/177	208	6.63	1/136	177	13.11	1/69
		-	257	4.45	1/202	287	5.20	1/173	260	7.30	1/123
		Average	222	4.77	1/189	248	5.92	1/152	218	10.21	1/88
D15-1	Up	+	265	5.79	1/155	302	10.67	1/84	302	10.67	1/84
		-	214	5.39	1/167	252	16.00	1/56	214	16.63	1/54
		Average	240	5.59	1/161	277	13.34	1/67	258	13.65	1/66*
	Low	+	228	5.96	1/151	270	10.20	1/88	230	16.57	1/54
		-	256	5.64	1/160	300	10.80	1/83	272	11.30	1/80
		Average	242	5.80	1/155	285	10.50	1/86	251	13.94	1/65*
D15-2	Up	+	271	6.79	1/133	317	11.00	1/82	317	11.00	1/82
		-	240	4.60	1/196	300	9.35	1/96	255	14.09	1/64
		Average	255	5.70	1/158	309	10.18	1/88	286	12.55	1/72*
	Low	+	252	6.46	1/143	301	12.56	1/72	256	14.84	1/61
		-	261	4.46	1/182	312	10.00	1/90	284	11.49	1/78
		Average	257	5.46	1/165	307	11.28	1/80	270	13.17	1/68*

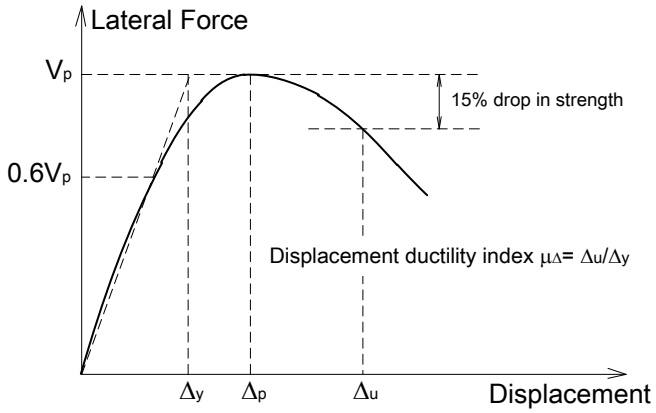

Figure 4-22 Definition of ductility

Shown in Figure 4-23 is the capacities of the specimens with a comparison between the test results and the calculated interaction curves. When calculating the interaction curves, the confinement effect provided by the transverse reinforcement is taken into account. Results obtained from the static tests are also presented in this figure. Note that the static test results have been rescaled according the following equations:

$$N'_{static} = 1.1 \times \frac{4^2}{6^2} N_{static}$$
$$M'_{static} = 1.1 \times \frac{4^3}{6^3} M_{static} \quad (4.4)$$

where the coefficient of 1.1 is used to account for the difference in material strength of the static tests and quasi-static tests. The results indicate that the quasi-static tests correspond well with the static tests and the current code provisions. Even though the confinement effect has been taken into account, the calculation still yields a more conservative result compared to physical tests. In conclusion, the composite action between concrete and steel sections is realized in ISRC columns under simulated seismic loads, and the current code provisions can effectively predict the flexural capacity of ISRC columns if the eccentricity ratio is NOT greater than 15%.

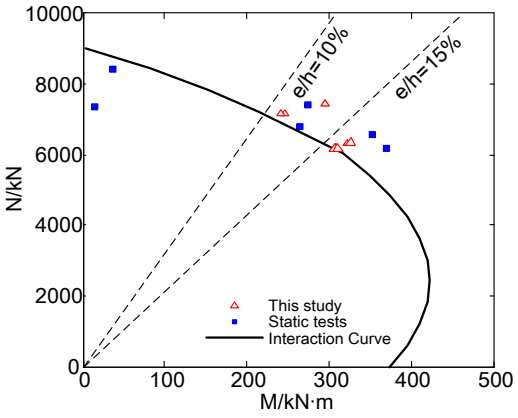

Figure 4-23 Capacities of the specimen

The drift ratio is defined as $\theta = \Delta/H$, where Δ is the equivalent lateral displacement of the specimen, and H is the effective length of the column. Table 4-5 shows the drift ratio of the specimens under different load stages. In fact, some of the tested ultimate drift ratios do not reflect the real deformation capacity of the specimens. The lower column of specimen D10-2, for example, did not show significant damage on the negative side of the column during the test, but the test had to stop because the upper column of the specimen had already failed and the specimen could not hold the axial load any longer. Therefore, the measured ultimate drift ratio 1/123(-) is not the actual deformation capacity of the column. In other words, this column could have shown a better deformation capacity if the upper column was not badly damaged. For these reasons, the authors believe that the lower part of specimen D10-2 can be removed from the database when analyzing the deformation properties of the specimens because of the asymmetric distribution of the damage. For the other three specimens, the

damage distributions were almost symmetric although the 'foundation beam' rotated during the test. Except for D10-2(lower), the average ultimate drift ratios of the specimens (market with '*' in Table 4-5) all exceed 1/100, which is the specified limit in Chinese codes JGJ 3 (2010), suggesting sufficient deformation capacities under simulated seismic loads.

4.8 Strain distribution

Figure 4-24 shows the strain distribution of the specimens under different load stages. The horizontal axis in these figures indicates the distance between the strain gauges and the left side of the cross section. Because the steel sections are separate from each other, the strain values are not on the same steel section in Figure 4-24 (a) (c) (e) (f). Specifically, the left steel section lies within [0mm, 110mm]; the two middle steel sections lie within [110mm, 190mm], and average values of the strain of these two steel sections are presented in the figure; the right steel section lies within [190mm, 300mm].

For specimen D10-1 and D10-2, the plane section assumption (almost) holds effective from the beginning to the end of the loading process for both the steel sections and the longitudinal reinforcement. For specimen D15-1 and D15-2, the plane section assumption is effective under gravity and yield load level. However, under peak and ultimate load level, the strain distribution of the longitudinal reinforcement clearly violates the plane section assumption because of the buckling of the bars.

In addition, the strain distribution of steel sections is more complex. Although the plane section assumption roughly remains effective, the three steel sections actually form three different planes, especially for specimen D15-1/D15-2 under peak and ultimate load level. Actually, the violation of plane section assumption is attributed to the slip effect of concrete-steel interface. Test results indicate that the slip effect gets larger as the load increases, and it is more evident for D15-1/D15-2 than D10-1/D10-2. Theoretically, the flexural capacity of composite columns will decrease if slip effect exists. However, the decrease in capacity can be offset by the strengthening of the steel sections. Therefore, the capacity of the specimen does not decrease in practices.

To summary, the plane section assumption is more likely to fail when the eccentricity ratio gets larger. Within 15% eccentricity ratio, the plane section assumption is, broadly speaking,

effect for ISRC columns. Current code provisions can provide a good and conservative prediction on the flexural capacity of ISRC columns.

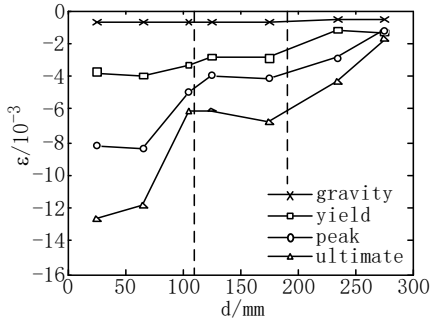

(a) Steel sections of D10-1

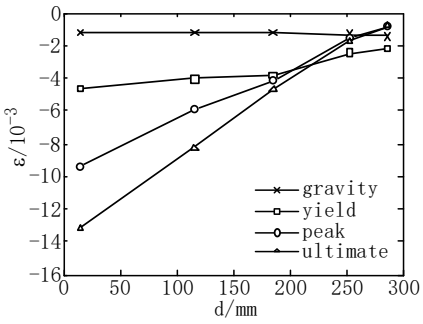

(b) Longitudinal reinforcement of D10-1

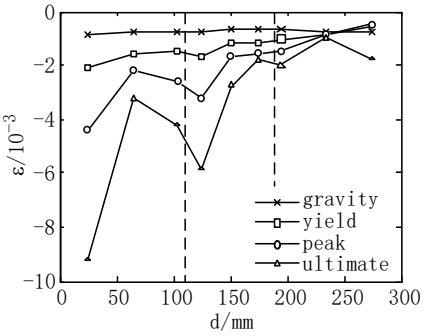

(c) Steel sections of D10-2

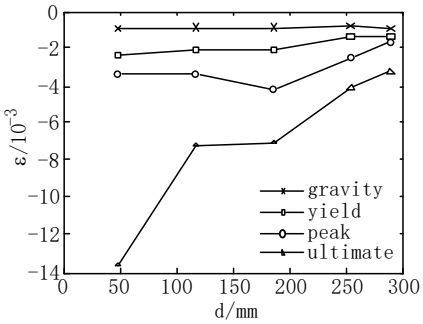

(d) Longitudinal reinforcement of D10-2

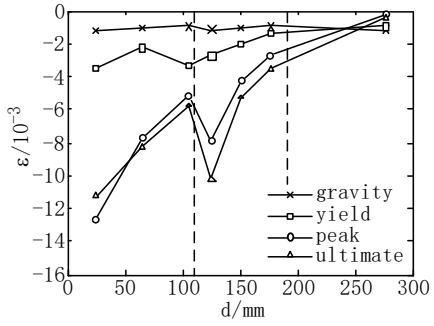

(e) Steel sections of D15-1

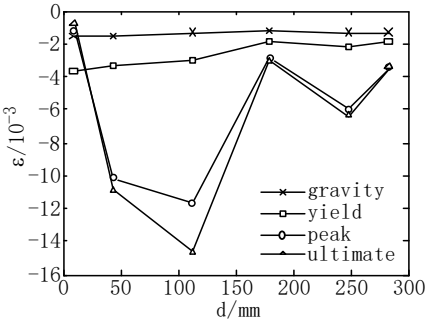

(f) Longitudinal reinforcement of D15-1

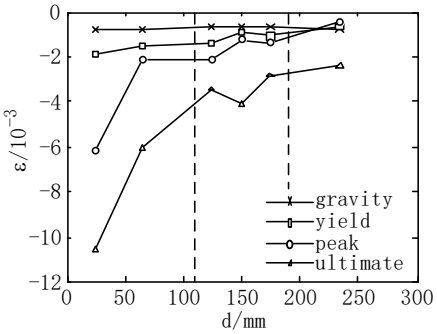

(g) Steel sections of D15-2

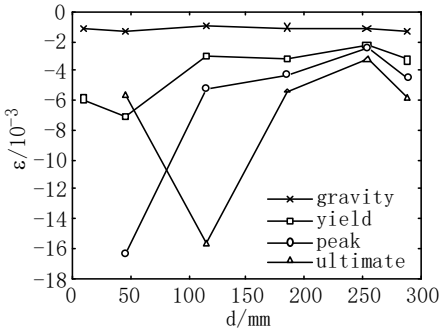

(h) Longitudinal reinforcement of D15-2

Figure 4-24 Strain distribution

4.9 Lateral stiffness

The lateral stiffness of a column is defined as the lateral load divided by the lateral displacement. Shown in Table 4-6 is the lateral stiffness of the columns under different load stages. Test results suggest that the lateral stiffness decreases as the loading increases, but the eccentricity ratio has little influence on the lateral stiffness.

Table 4-6 Lateral stiffness under different load stages

Specimen		$K/kN \cdot mm^{-1}$		
		Yield	Peak	Ultimate
D10-1	Up	44.47	29.35	21.42
	Low	44.56	29.49	21.32
D10-2	Up	52.85	37.33	21.90
	Low	47.24	43.28	24.55
D15-1	Up	42.75	22.03	20.59
	Low	41.88	27.12	18.96
D15-2	Up	46.03	30.45	23.46
	Low	48.78	27.59	20.98

Figure 4-25 shows the reduction of lateral stiffness in terms of lateral displacement. The vertical axis in these figures indicates the ratio of lateral stiffness to the initial lateral stiffness of the column, and the unit is in percentile. Results show that the lateral stiffness decreases linearly as the displacement grows. Under yield load stage, the lateral stiffness is 60%~80% of the initial ones; under peak load stage, this ratio is 40%~60%; and under ultimate load stage, this ratio is 20%~40%.

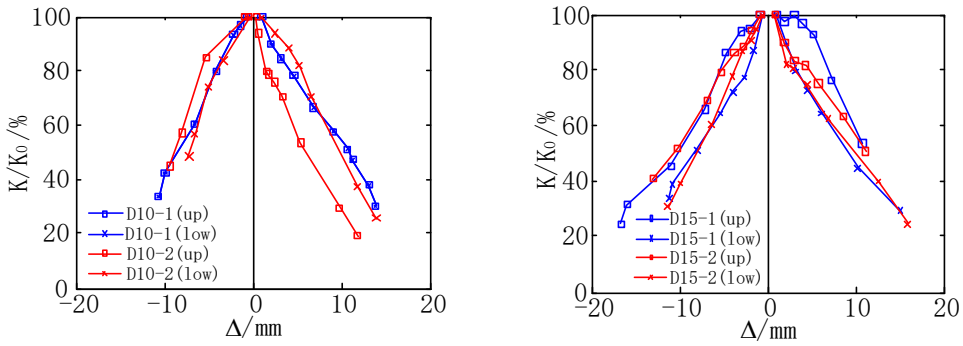

(a) Specimen D10-1/D10-2 (b) Specimen D15-1/D15-2

Figure 4-25 Reduction of lateral stiffness

4.10 Energy dissipation

The ability of energy consumption is a very important aspect when evaluating the seismic performance of a composite column. A good energy consumption ability means the element may dissipate more energy from the earthquake, and be less damaged. Since the hysteretic curve reflects the relationship between the lateral load and lateral top displacement of the specimen, the area surround by the curves indicates the energy dissipated by the specimen during the loading. By integrating the product of lateral load and displacement, one can get the dissipated energy under different load levels, as shown in Figure 4-26. When the lateral displacement is small, the specimen does not yield yet, so the energy consumption is very small. When the lateral displacement grows, the materials yield, and friction between the materials also consumes energy. Therefore, the energy consumption becomes larger and larger as the lateral displacement increases. Figure 4-26(c) compares the ability of energy dissipation between specimen D10-1/D10-2 and specimen D15-1/D15-2. The ability of energy dissipation does not change much as the eccentricity ratio grows. This is probably because the increase in eccentricity ratio is not large enough to provide a significant change in the ability of energy dissipation.

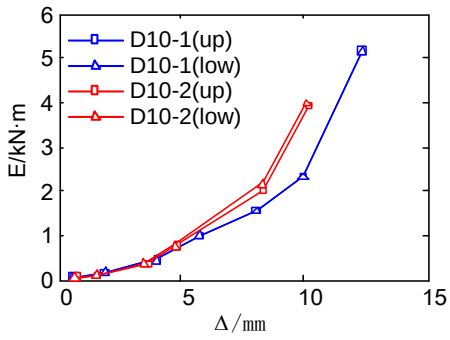

(a) Specimen D10-1/D10-2

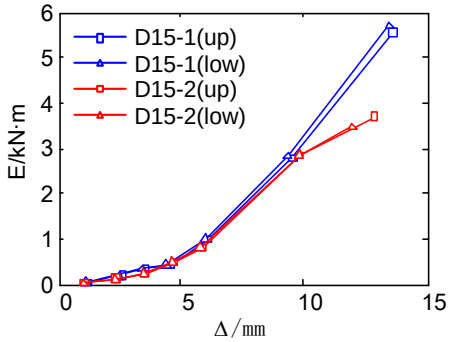

(b) Specimen D15-1/D15-2

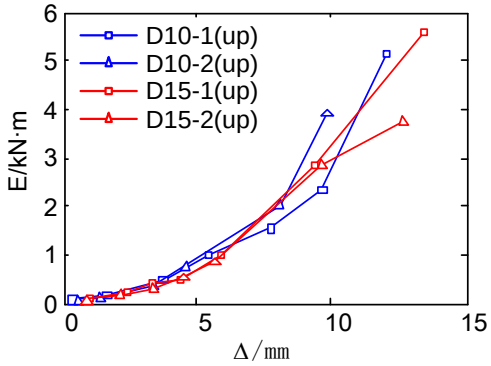

(c) Comparison of energy consumption

Figure 4-26 Energy consumption of the specimens

Another index used to evaluate the ability of energy consumption is equivalent damping ratio. The equivalent-damping ratio h_e is defined in Figure 4-27:

$$h_e = \frac{1}{2\pi}\frac{S_{loop}}{S_{AOB} + S_{COD}} \tag{4.5}$$

where S_{loop} is the area surround by the hysteretic curve; S_{AOB} and S_{COD} is the area of the shaded triangles. The larger the equivalent damping ratio, the stronger the ability of energy consumption the specimen has.

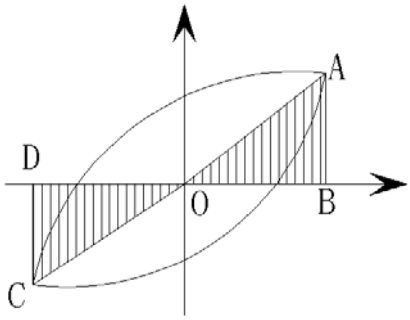

Figure 4-27 Definition of equivalent damping ratio

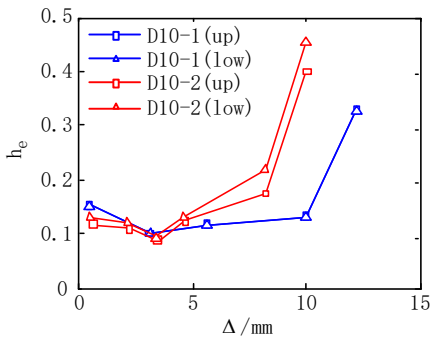

(a) Specimen D10-1/D10-2

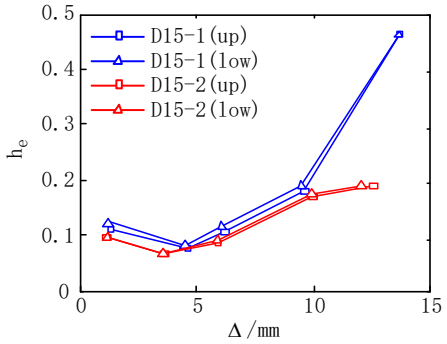

(b) Specimen D15-1/D15-2

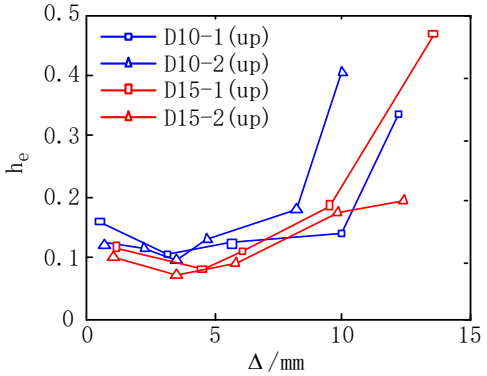

(c) Comparison of equivalent damping ratio

Figure 4-28 Equivalent damping ratio of the specimens

Figure 4-28 shows the relationships between the equivalent damping ratio and the lateral displacement. For all of the specimens, the equivalent damping ratio decreases as the lateral displacement grows before yield displacement, and increases as the lateral displacement grows afterwards. Test results show that the hysteretic curves 'pinch' when the specimen is being unloaded. Caused by slip effect and cracking of the concrete, this phenomenon is unfavorable for dissipating energy since it reduces the area surrounded by the hysteretic curves. The pinch effect is more evident when the lateral displacement is small and most of the materials remain elastic. When the lateral displacement gets larger, more and more parts of the steel sections and longitudinal reinforcement develop into plastic state, improving the specimen's ability to consume energy. Therefore, the equivalent-damping ratio gets larger as the load increases.

4.11 Summary of phase 2 test

1) The four specimens fail in combined compression and bending. Shear failure is not evident during the test. Although there is no connection between the steel sections, the composite action still works during the test. The specimens fail due to crush of the concrete corners. Buckling of the longitudinal reinforcement and breaking of the transverse reinforcement is detected. The steel sections are well confined by the concrete, hence no buckling or separations of the steel sections are found.
2) The flexural capacities of the specimens agree with the static tests as well as the calculated interaction curves based on ACI 318, Eurocode4, and YB 9082 with the confinement effect of the concrete included. The current code provisions can provide a good and conservative prediction on the capacity of ISRC columns.
3) The plane section assumption weakens as the eccentricity ratio grows. However, within 15% eccentricity ratio, the plane section assumption is effective in general.
4) The drift ratios of the specimens under ultimate loads levels suggest sufficient deformation capacities of ISRC columns.
5) The specimens show a desirable ability in energy dissipation. The energy dissipation does not show significant change as the eccentricity ratio grows.

5 FEA – phase 1

Finite element (FE) analysis was carried out to verify the test results and provide a more detailed stress distribution of the inner part of the column. ABAQUS was chosen to do the analysis due to its ability of complex calculation and friendly interactive interface.

5.1 FE model development

There are three material models for concrete in ABAQUS: smeared crack model, damaged plasticity model, and brittle cracking model. In ABAQUS standard modules, the damaged plasticity model is preferred in analyzing the behavior of concrete.

The uni-axial constitutive curve for concrete is obtained by using Mander model (Mander et al 1988) with confinement effect taken into account. The confined compressive strength and corresponding compressive strain are:

$$f_{cc}^{'} = f_{c0}^{'} + k_1 f_l \tag{5.1a}$$

$$\varepsilon_{cc} = \varepsilon_{c0}\left[1 + k_2\left(\frac{f_{cc}^{'}}{f_{c0}^{'}} - 1\right)\right] \tag{5.1b}$$

where f'_{c0} and ε_{c0} are the compressive strength and the corresponding strain for unconfined concrete; f'_{cc} and ε_{cc} is the compressive strength and the corresponding strain for confined concrete; f_l is the confining pressure applied to the concrete; k_1 and k_2 are two coefficients. Richart (Richart et al 1928) conducted a series of tests and concluded that $k_1 = 4.1$ and $k_2 = 5$. Mander [proposed] a theoretical model in which the constitutive curve for the compressive concrete is given by the following equations:

$$f_c = \frac{f_{cc}^{'} xr}{r - 1 + x^r} \tag{5.2a}$$

$$x = \frac{\varepsilon_c}{\varepsilon_{cc}} \tag{5.2b}$$

$$r = \frac{E_c}{E_c - E_{\sec}} \tag{5.2c}$$

$$\varepsilon_{cc} = \varepsilon_{c0}\left[1 + 5\left(\frac{f_{cc}^{'}}{f_{c0}^{'}} - 1\right)\right] \tag{5.2d}$$

where E_c is the modulus of elasticity of the concrete and E_{sec} is defined as follows:

$$E_{\sec} = \frac{f_{cc}^{'}}{\varepsilon_{cc}} \tag{5.3}$$

An equation was proposed to calculate the compressive strength of the confined concrete:

$$f_{cc}^{'} = f_{c0}^{'}\left(-1.254 + 2.254\sqrt{1+\frac{7.94\,f_l^{'}}{f_{c0}^{'}}} - 2\frac{f_l^{'}}{f_{c0}^{'}}\right) \tag{5.4}$$

where f_l' is the effective confining pressure of the concrete, which is assumed to be uniformly distributed on the lateral surface of the concrete. f_l' can be calculated based on the layout of the transverse reinforcement. The detailed calculation procedures are omitted.

Since the damage of the concrete leads to a reduction of confinement to the longitudinal bars, researchers (Chen et al 2006) proposed that the stress of compressive longitudinal bars should be reduced when damages occur in the compressive concrete. However, for ISRC columns, the steel sections are often located far from the neutral axis, so the longitudinal bars contribute little to the bending moment compared to steel sections. Therefore, the tri-linear constitutive model is adopted for longitudinal bars as well as for steel sections. f_y and f_u are determined from the test. The strain corresponding to f_u is $5\varepsilon_y$. When the tensile strength is reached, the stress begins to drop, and the stiffness is the same as modulus of elasticity. The constitutive curves for concrete and steel are presented in Figure 5-1.

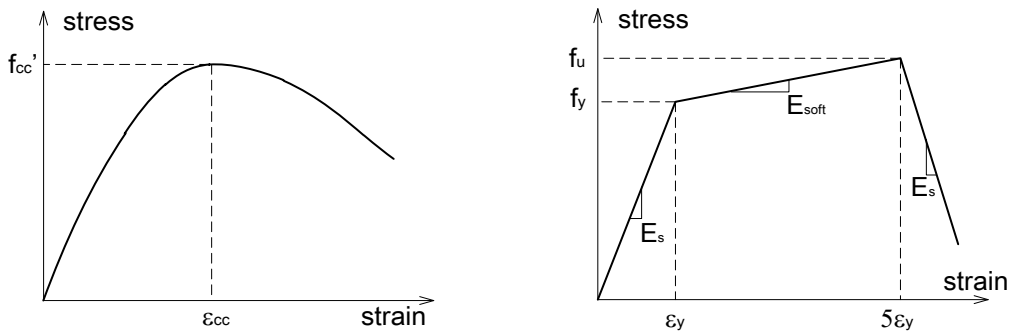

(a) Concrete (b) Steel

Figure 5-1 Constitutive curves

Only half of the ISRC column was built in the program due to the symmetry. An overview of the FE model and the mesh of concrete and steel sections are presented in Figure 5-2. An elastic 'cap' was positioned above the model to simulate the sand layer. Four materials were used in the FE model: concrete, Q460 steel for the sections, S235 steel for the beams and corresponding steel for the bars. Axial load was applied to the reference point (RP), whose position was the same as the center of the hinge. The load was first transferred to the elastic cap through constrains between the RP and cap top surface, then to the column itself.

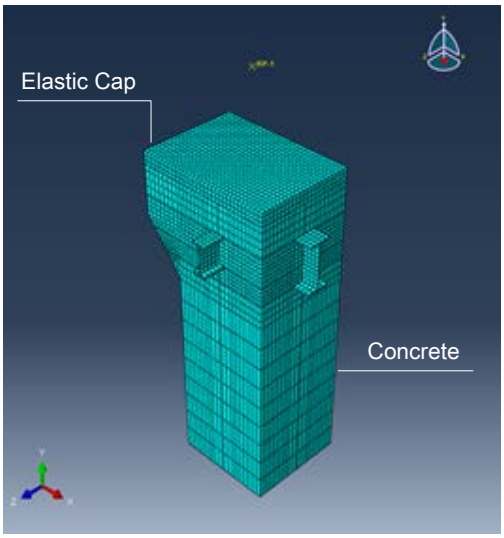

(a) Mesh of concrete

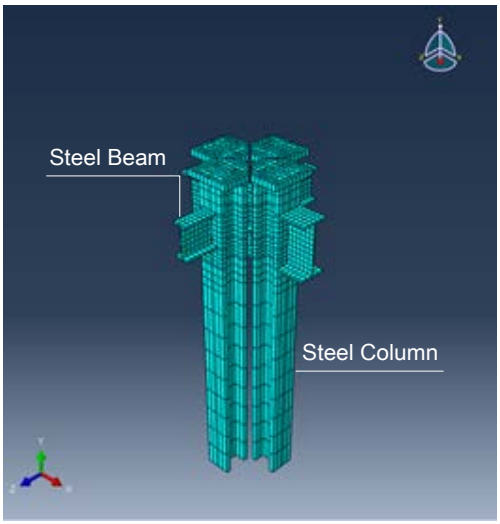

(b) Mesh of steel sections

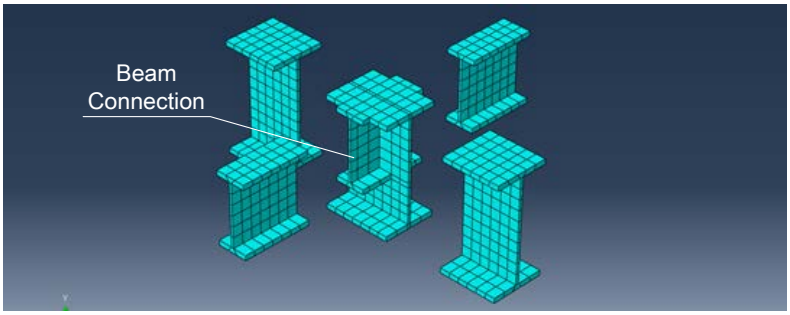

(c) Parts of steel beam

Figure 5-2 FE model in ABAQUS

The concrete and steel sections were simulated by three dimensional eight-node solid elements, and bars are simulated by two dimensional three-node truss elements. To simplify the model, bars and steel beams were TIE connected to the concrete – no relative displacement and strain difference. The interaction of concrete and steel section interface was simulated by nonlinear springs along each dimension (Figure 5-3). There were three spring connectors at each node pair, one in the normal direction and two in the tangential direction.

In fact, the node of concrete and steel of each node pair overlapped in space, the initial length of the spring elements were zero.

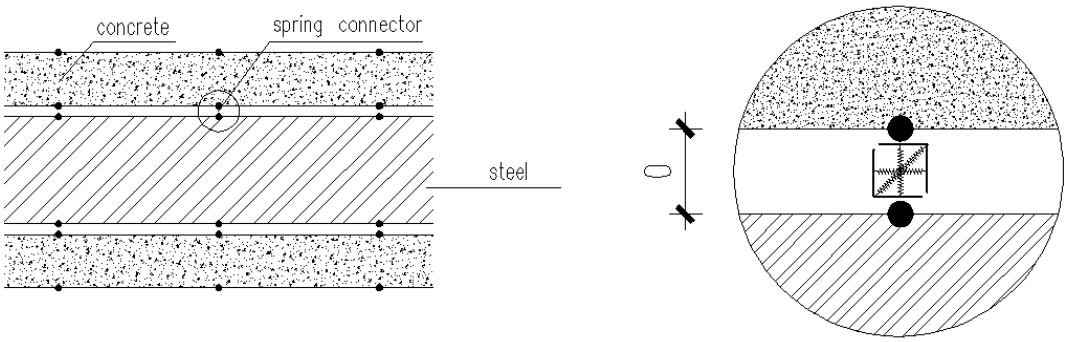

Figure 5-3 Spring connector

The constitutive curve of spring elements along the tangential direction is nonlinear (Figure 5-4), which follows the equation below:

$$V = V_u \left(1 - e^{-1.535s}\right)^{0.989} \tag{5.5}$$

While elastic spring elements are used to simulate normal behavior of concrete-steel interface. The modulus of elasticity is very large so that it approximately simulates 'hard contact' of the two materials.

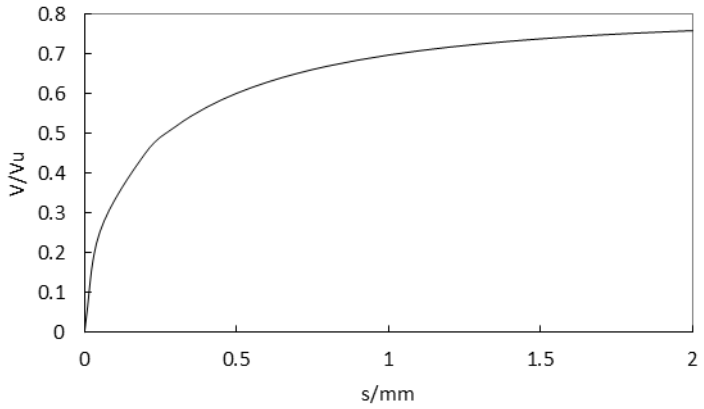

Figure 5-4 Constitutive curve for shear studs

5.2 Capacity

The calculated axial capacity is listed in Table 5-1. FEM results correspond with experimental results very well.

Table 5-1 FEA results of ISRC columns - phase 1

Specimen ID	Calculated capacity /kN	Experimental capacity /kN	Ratio of calculated capacity to experimental capacity
E00-1	17392	17082	1.018
E00-2		15325	1.135
E10-1	14227	14360	0.991
E10-2		13231	1.075
E15-1	11924	12041	0.990
E15-2		12759	0.935

5.3 Loading curve

The calculated curves of the six columns are presented in Figure 5-5~Figure 5-7. Before peak point, the calculated curve corresponds with the experimental curve very well; the difference is enlarged after peak point. The reduction of axial capacity is contributed by degradation of material strength, cracks in the concrete, spill and damage of the concrete and buckling of the longitudinal bars. The FE model fails to simulate the situation where concrete are smashed and falls from the column. However, the inaccuracy after peak point, the calculated results present a good reference of the capacity of the column.

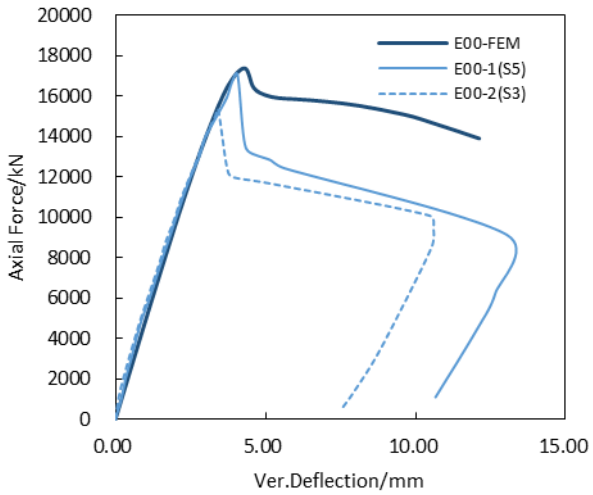

Figure 5-5 Calculated curve (E00-1 & E00-2)

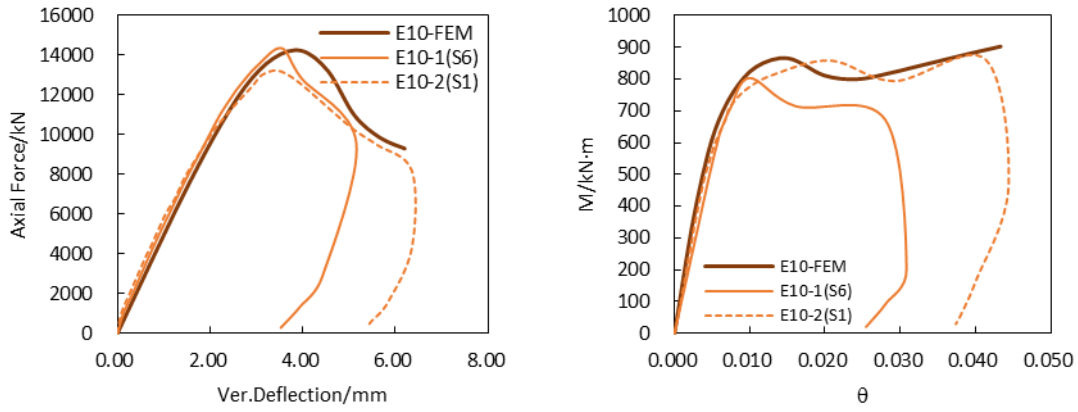

(a) Axial force vs. vertical deflection (b) Bending moment vs. rotation

Figure 5-6 Calculated curve (E10-1 & E10-2)

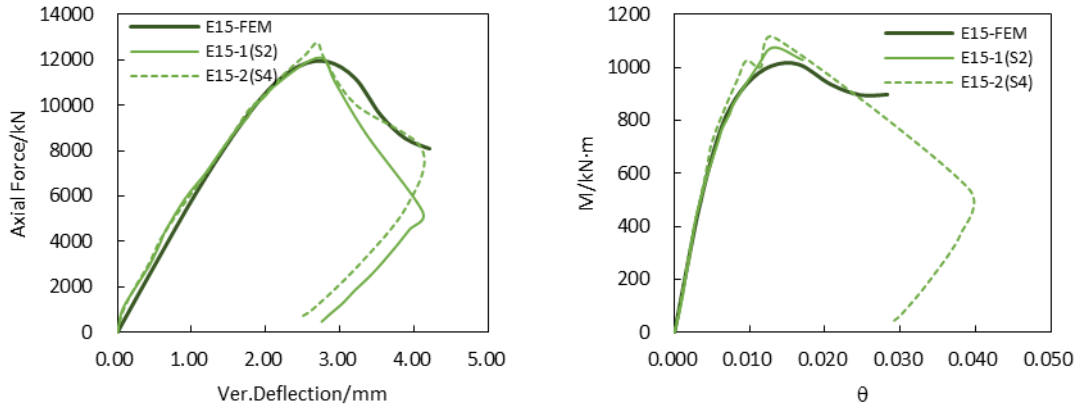

(a) Axial force vs. vertical deflection (b) Bending moment vs. rotation

Figure 5-7 Calculated curve (E15-1 & E15-2)

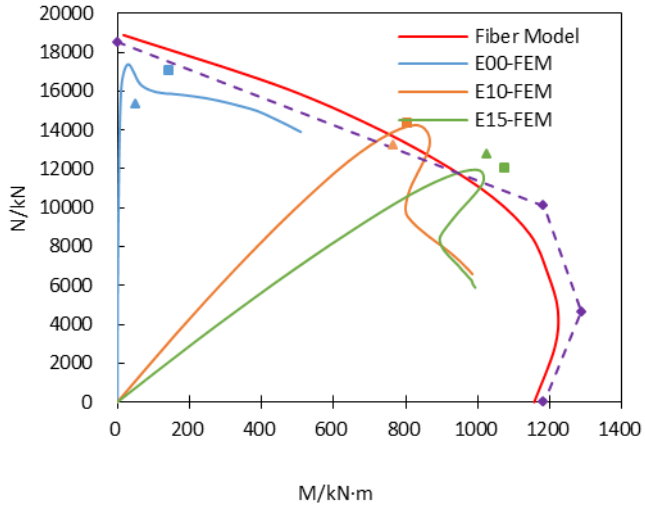

Figure 5-8 Calculated interaction curve – phase 1

5.4 Deformation pattern and stress distribution

5.4.1 Pure axial specimens

Figure 5-9 shows the lateral deformation of a pure axial specimen. The positive direction of lateral deformation is toward right and marked with red color; the negative direction is toward left and marked with blue color. It is clear that the column deflects toward left and the end rotates in clockwise direction.

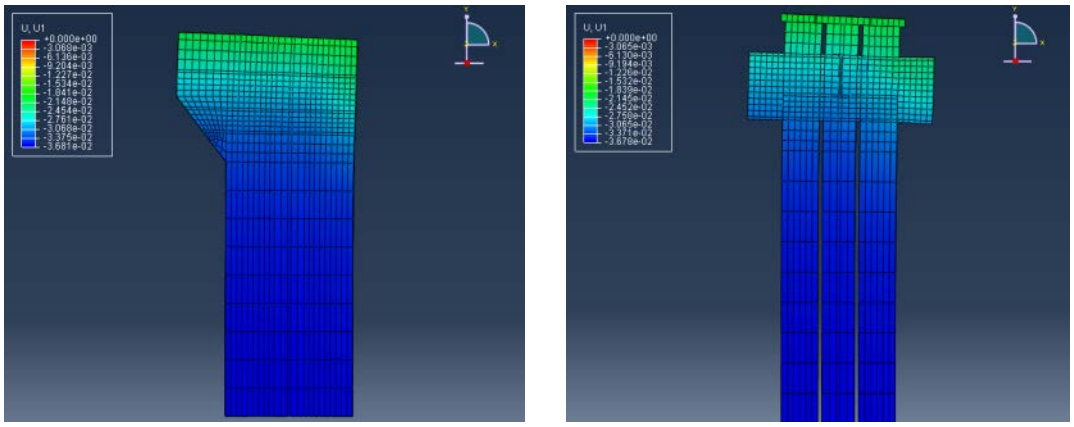

(a) Concrete (b) Steel sections

Figure 5-9 Deformation pattern (e/h=0)

Figure 5-10 shows the distribution of von Mises stress and normal stress of the steel sections. The von Mises stress is almost normally distributed along the steel column.

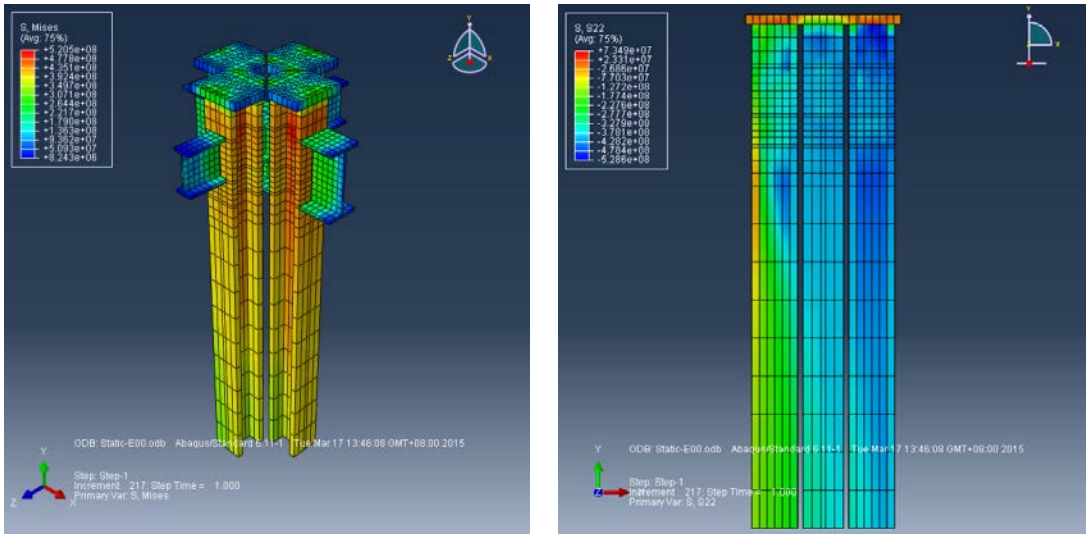

(a) Von Mises stress (b) Normal stress

Figure 5-10 Stress distribution of steel sections (e/h=0)

The shear stress distribution of steel beams is presented in Figure 5-11. As it is shown, the shear stress in the steel beam is very large at the connection between steel beams and steel columns. In fact, the steel beam is like a huge shear stud, providing shear resistance to the steel column to prevent relative slip on concrete-steel interface. Because the shear stiffness of the beams' web is very large, shear stress is more concentrated in the web of the beam.

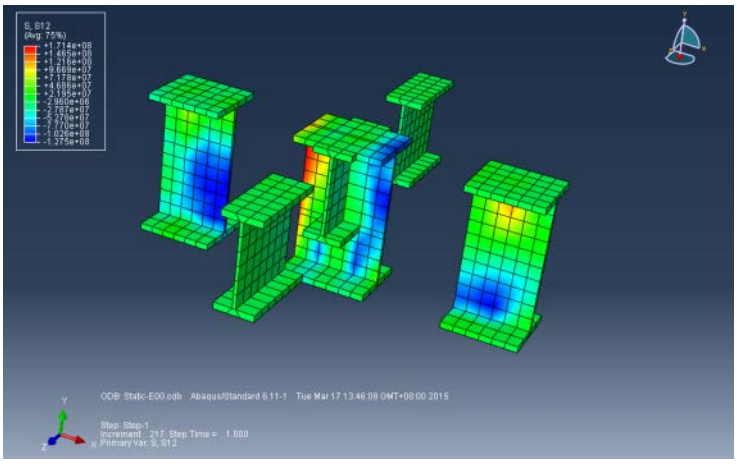

Figure 5-11 Shear stress of steel beams (e/h=0)

5.4.2 Eccentric specimens

The deformation and stress distribution is similar for specimens with e/h=10% and e/h=15%, so specimen e/h=10% serves as an example. The deformation pattern corresponds with the experimental phenomenon – mid-section drifts right.

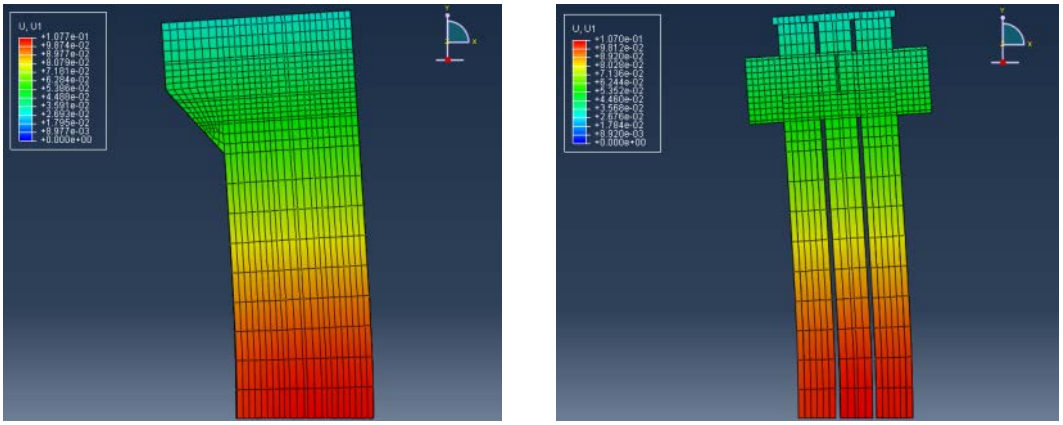

(a) Concrete (b) Steel sections

Figure 5-12 Deformation pattern (e/h=10%)

Stress distribution of the steel column shows that the von Mises stress is significantly greater near the mid-section, which implies that the mid-section is the critical damage section.

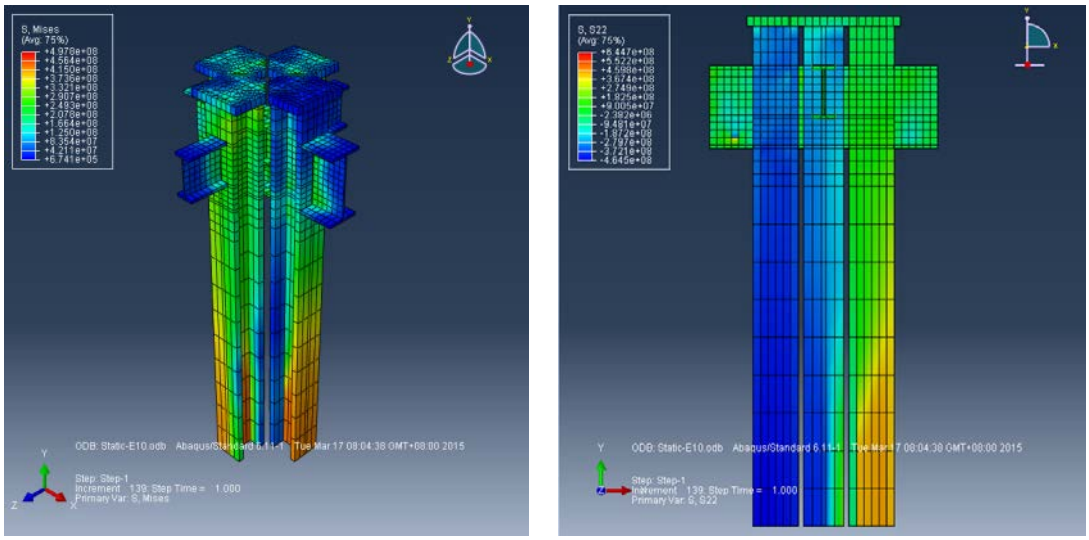

(a) Von Mises stress (b) Normal stress

Figure 5-13 Stress distribution of steel sections (e/h=10%)

The shear stress of the steel beam is also very large. In addition, it is shown that the maximum shear stress on the steel beam, which is between the steel columns (188MPa), is larger than that outside the steel columns (145MPa). Because steel beams within the core are constrained at each end by steel columns, the difference in deformation of steel columns results in a large shear demand in the connection beams. On the outside of the column, however, steel beams are only constrained at one end, so the shear demand is relatively small.

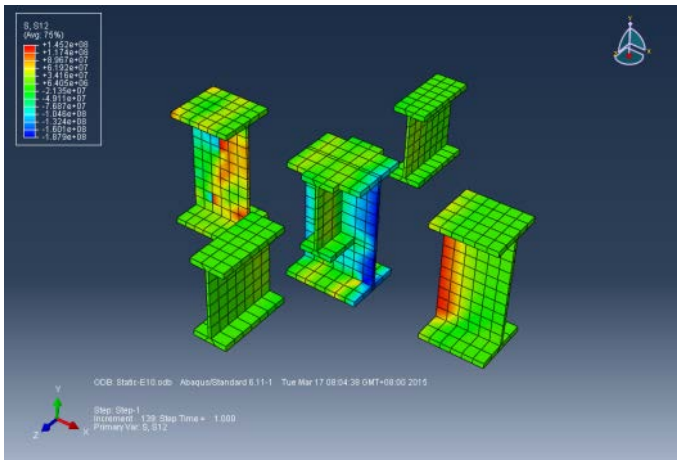

Figure 5-14 Shear stress of steel beams (e/h=10%)

5.5 Analysis of studs

5.5.1 Pure axial specimens

Slip of the concrete-steel interface measures the relative displacement of the interface, as well as load transfer between concrete and steel sections. According to the constitution curve given by Figure 1-3, the direction of restoring force of the spring is always the same as the direction of relative displacement.

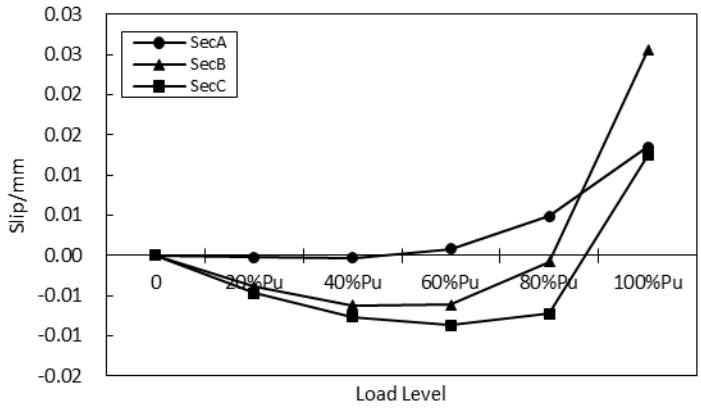

Figure 5-15 Relationship between slip and load level (e/h=0)

Figure 5-15 shows the relationship between the slip of section 'A', 'B' and 'C' (defined in Figure 3-11) and load level for specimens with e/h=0. A positive slip indicates the steel sections are compressed more than the concrete is, thus the force transferred by shear studs exerts compression to the concrete and tension to the steel sections. When the load is small, the magnitudes of slip for all of the three sections are negative, indicating concrete is compressed more, and the axial force is transferred from concrete to steel sections through shear studs. As load increases, the rigidity of concrete reduced due to damage and crack, so steel sections are sustained to a larger load. Therefore, the steel sections are compressed more and the slip goes positive. The maximum slip in FE model is 0.03mm, very similar to experimental result (0.04mm).

The magnitude of slip also varies with elevation (measured from mid-section). Because the mid-section is the symmetry plane of the column, there will be no slip on that section. Meanwhile, the rigidity of the steel beams is very large so that slip is also restricted at the beam-column joint. As shown in Figure 5-16, slip is very small at elevation 50mm and

950mm. In fact, the steel beam is acting as a big shear stud, providing enough shear resistance and rigidity to restrict relative displacement at the joint.

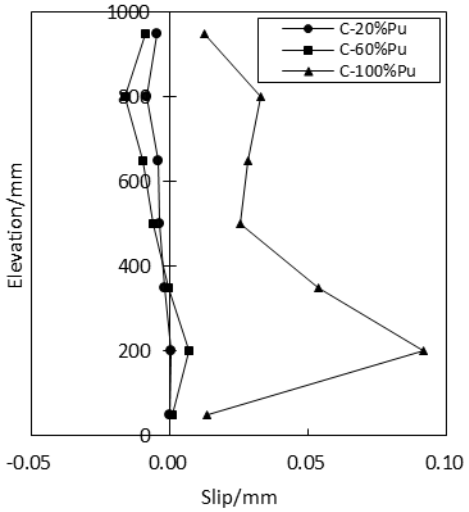

Figure 5-16 Relationship between slip and elevation (e/h=0)

5.5.2 Eccentric specimens

The relationship between slip and load level for specimens with e/h=10% and e/h=15% is presented in Figure 5-17. Two of the four steel sections are presented in the figure: one in the compression zone and the other in the tension zone marked with continuous line and dashed line respectively. When the load is less than 80% of the maximum load, the slip is positive for both the two steel sections, in consistency with pure axial specimens. The deformation of eccentric specimen is contributed by compression effect and flexural effect (Figure 5-18). When the applied load is small, the deformation is dominated by compression effect, so the slip pattern is similar to that of pure axial specimen. The combination of compression and flexural effect causes the slip of compression zone steel section larger than that of tension zone steel section. As load increases, flexural effect dominates the deformation pattern, and the slip changes dramatically when load reaches the capacity.

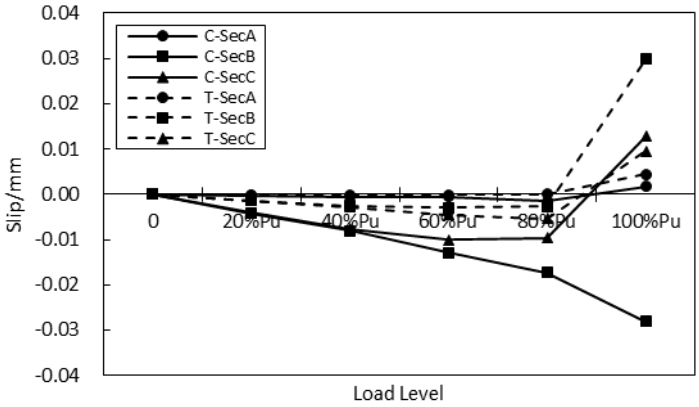

(a) e/h=10%

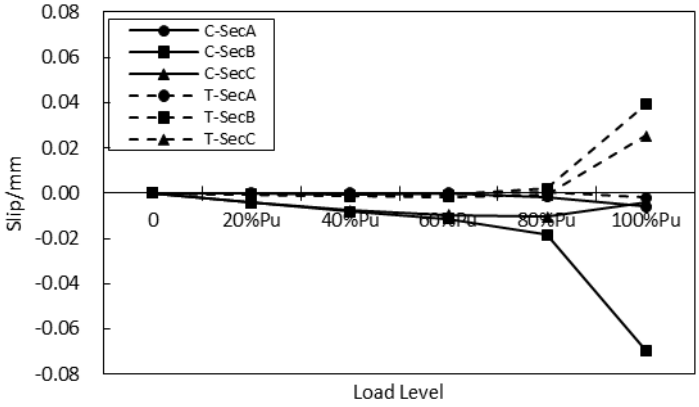

(b) e/h=15%

Figure 5-17 Relationship between slip and load level (e/h=10% and 15%)

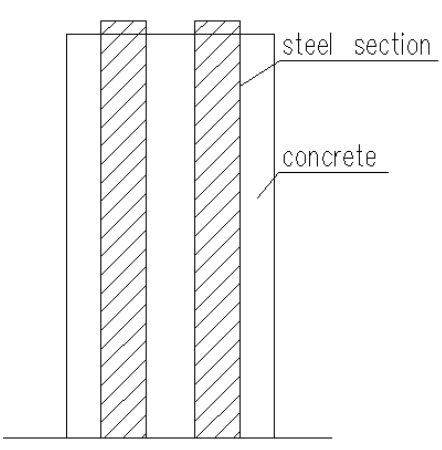

(a) Compression effect

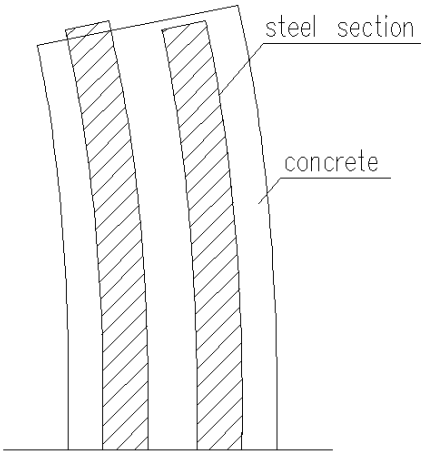

(b) Flexural effect

Figure 5-18 Deformation patterns for eccentric specimens

Figure 5-19 shows the relationship between slip and elevation for specimens with e/h=10% and e/h=15%. It is also evident that slip at the middle and ends of the column is very small, but larger in between.

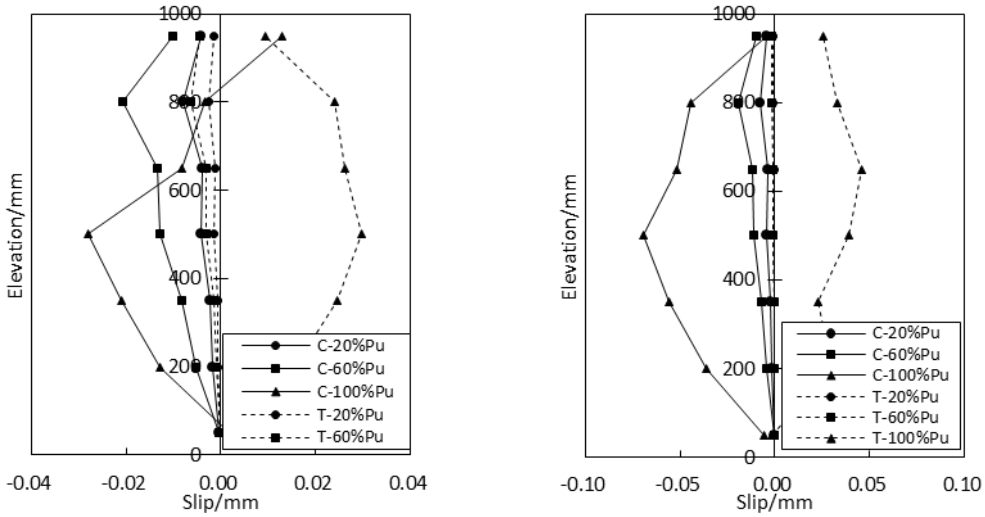

(a) e/h=10% (b) e/h=15%

Figure 5-19 Relationship between slip and elevation (e/h=10% and 15%)

The FEA shows that the steel beams play an important role in providing shear resistance along concrete-steel interface - more than 40% of the shear force along the interface is provided by steel beams. However, the mechanism may change when the boundary condition changes. Phase 2 of the study will illustrate the difference.

5.6 Effect of beam and shear stud

Table 5-2 Actual eccentricities of phase 1specimens

Model name	Beam	Beam connection	Shear stud
BeamStud	Yes	Yes	Yes
BeamNone	Yes	Yes	No
NoneStud	Yes	No	Yes
NoneNone	Yes	No	No

As mentioned above, shear resistance on the concrete-steel interface is contributed by steel beams and shear studs. This section of the report presents the influence of steel beams and shear studs on the capacity of ISRC columns under combined compression and bending. Apart from the FE model mention above, three extra FE models are built. Differences between these models are presented in Table 5-2.

Figure 5-20 and Figure 5-21 shows the capacities of the four different models. It can be concluded that beam connections and shear studs can help increase the capacity of ISRC columns under combined compression and bending, but the effect is very small. For e/h=0, the capacity of ISRC column is about 3% lower if beam connection is removed from the model. For e/h=10% and e/h=15%, the capacity decreases less than 1% if the beam connection is removed. Effect of the shear studs is even smaller. For columns with or without shear studs, the capacity almost remains constant. It should be noticed that this conclusion does not mean shear studs and beam connections are not important in ISRC columns. If the column is subjected to horizontal load, the influence of shear studs will be very strong (Discussed in following chapters).

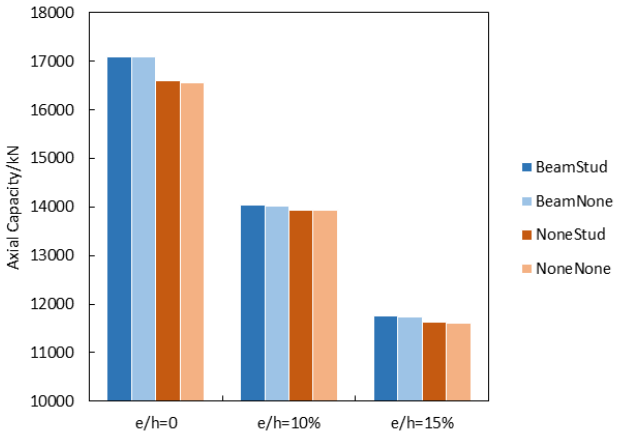

Figure 5-20 Comparison of capacities

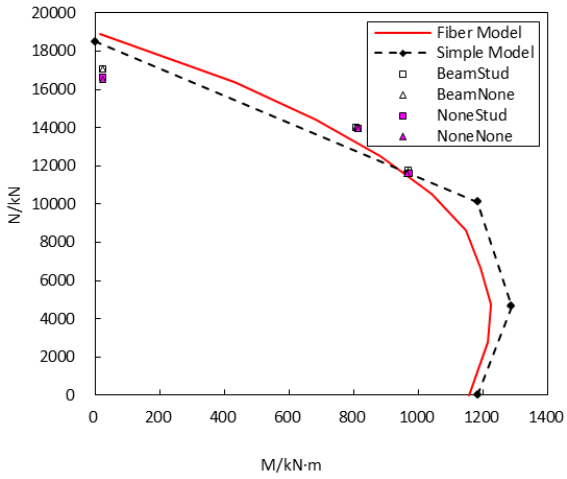

Figure 5-21 Comparison of interaction relationship

The shear stress distribution of steel beams is presented Figure 5-22. The shear stress is very large in the concrete encased steel beam, while there is little shear stress in the other steel beam. By comparing it with Figure 5-14, it is clear that the maximum shear stress is 10% less if the beam connection is removed.

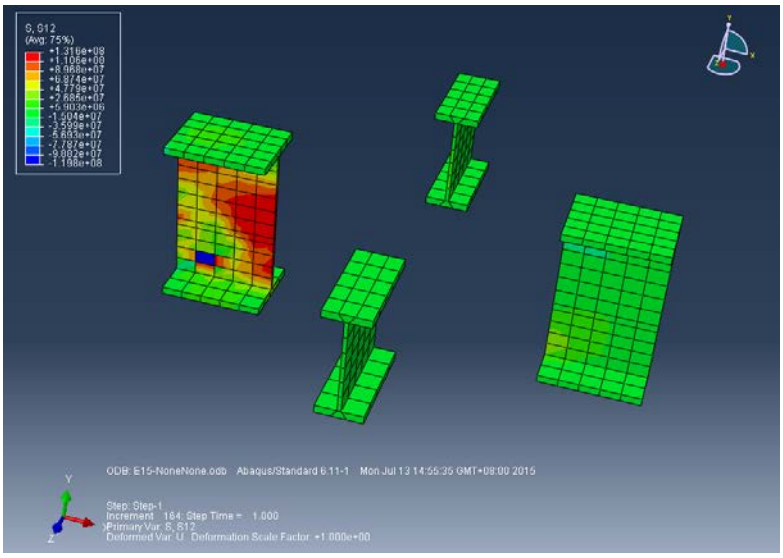

Figure 5-22 Shear stress distribution of steel beams (e/h=10%)

5.7 Summary of phase 1 FEA

1) Nonlinear spring elements are used to simulate the tangential behavior of concrete-steel interface. FEA results and test results agree with each other well.
2) Shear resistance on the concrete-steel interface is contributed by steel beams and shear studs. Because, steel beams behavior as a rigid shear connector, a large portion of the shear resistance is shared by steel beams. Shear stress on the steel beams and beam connections are very large.
3) The capacity of ISRC columns does not drop significantly if the beam connection is removed. Effect of shear studs is also very little. However, this conclusion is only applicable without horizontal load.
4) The maximum shear stress on steel beams is 10% smaller if beam connection is removed.

6 FEA – phase 2

The finite element analysis for quasi-static tests is also conducted in ABAQUS. The material models employed in this chapter are the same as what in chapter 6, so such details are omitted.

6.1 FE model development

To increase the efficiency of numerical analysis, only the upper half of the specimen is built in ABAQUS based on the actual dimensions and configuration of the specimen. The meshing strategy for the concrete and steel profiles is shown in Figure 6-1. C3D8R Solid elements are employed for concrete; T3D2 truss elements are employed for bars; and S4R shell elements are employed for steel profiles.

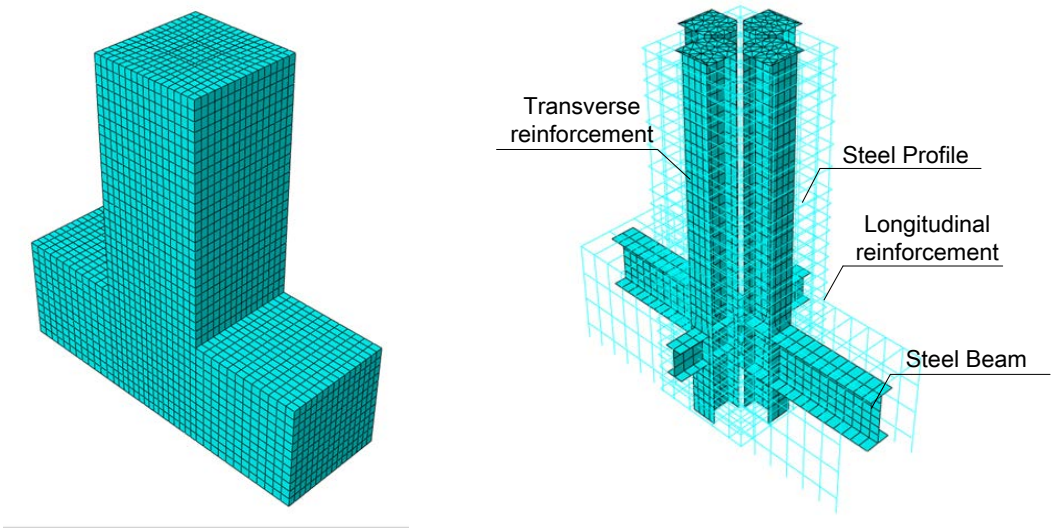

(a) Mesh of concrete (b) Mesh of steel profiles

Figure 6-1 FE model in ABAQUS

The longitudinal bars and transverse bars are embedded in the concrete, namely no relative displacement is allowed between the concrete and the bars. Similarly, tie constraint is employed between the concrete and the steel beams. While the steel profiles are connected with the surrounding concrete with nonlinear spring elements. Details of the spring elements can be referred to section 6.1. The best represent real conditions in the test, the endplates in the FEM model are only connected to the steel profiles, and there is no constraint between the endplates and the concrete.

The material strengths used in the FEM model are listed as follows:

Table 6-1 Material strengths in FEM models

Steel profiles and rebar		
Material	Yield strength f_y/MPa	Ultimate strength f_u/MPa
Steel profile	458	604
Steel beam	235	310
DIA 8	459	689
DIA 6	367	584
DIA3.25	573	638
DIA 2.95	259	371
Concrete		
Specimen	f_{cu}/MPa	
D10-1	70.2	
D10-2	70.1	
D15-1	67.5	
D15-2	76.2	

6.2 Comparison between FEA and test results

6.2.1 Envelop curves

The calculated envelop curves are presented in Figure 6-2. Except for specimen D10-2, the calculated envelop curves of all the other specimens agree with the test results well.

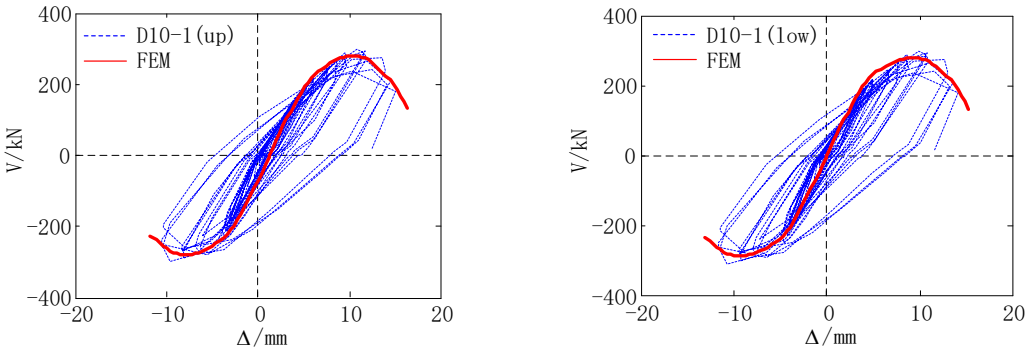

1) Specimen D10-1(up)　　2) Specimen D10-1(low)

Figure 6-2 FEA envelop curves

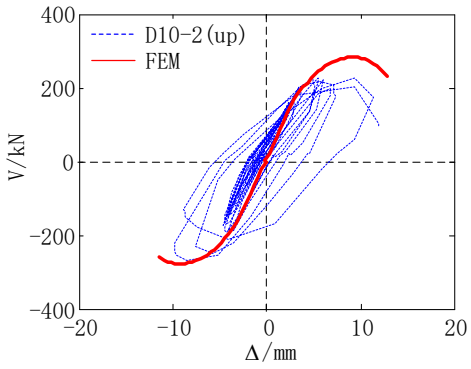

3) Specimen D10-2(up)

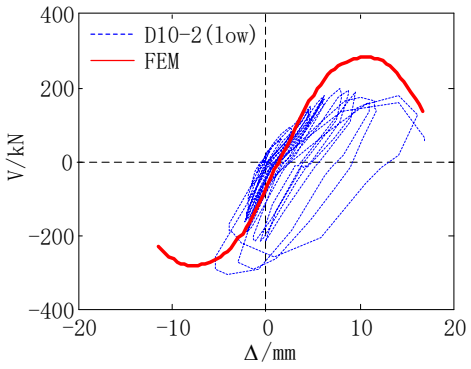

4) Specimen D10-2(low)

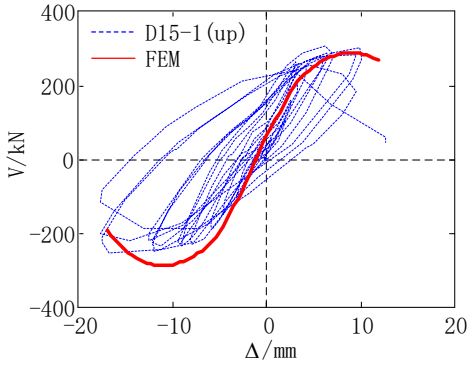

5) Specimen D15-1(up)

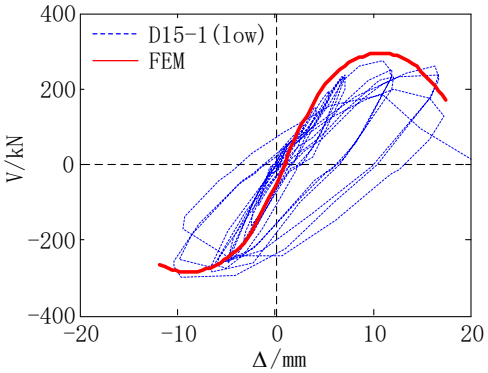

6) Specimen D15-1(low)

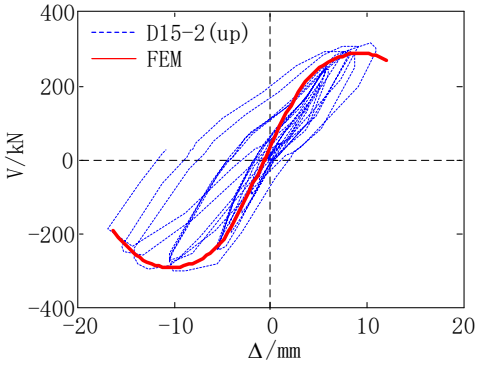

7) Specimen D15-2(up)

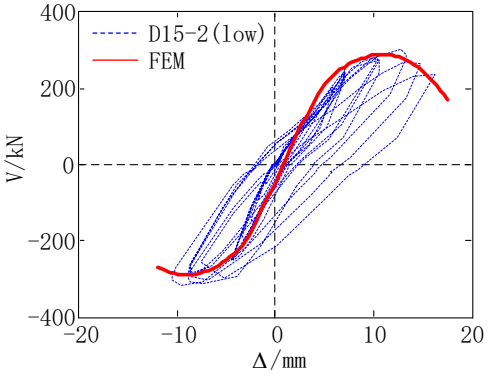

8) Specimen D15-2(low)

Figure 6-2 FEA envelop curves (continued)

6.2.2 Capacities

Figure 6-2 shows the comparison of the test and calculated capacities of the specimens. When defining the capacity a specimen, the listed value is the maximum one among the positive and negative direction. According to this table, the FEA results are close to test results with relative errors ranging from 0.16%~12.26%.

Table 6-2 Comparison of capacities

Specimen	N-tested /kN	M-tested /kN·m	M-calculated /kN·m	Relative errors
D10-1(up)	7426.00	320.40	282.29	-11.89%
D10-1(low)	7427.33	321.58	282.15	-12.26%
D10-2(up)	7190.67	276.20	276.65	0.16%
D10-2(low)	7189.29	272.73	285.10	4.54%
D15-1(up)	6152.00	303.27	292.50	-3.55%
D15-1(low)	6153.91	308.00	292.50	-5.03%
D15-2(up)	6311.63	322.10	289.87	-10.01%
D15-2(low)	6312.36	323.68	292.55	-9.62%

6.3 Stress distributions and deformation patterns

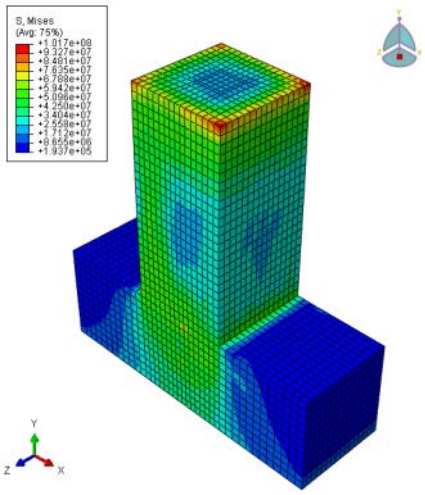

(a) Mises stress for concrete

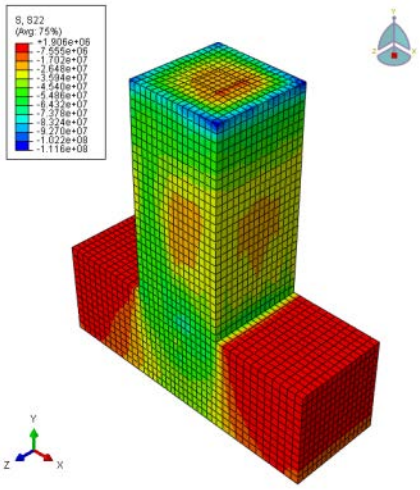

(b) Vertical normal stress for concrete

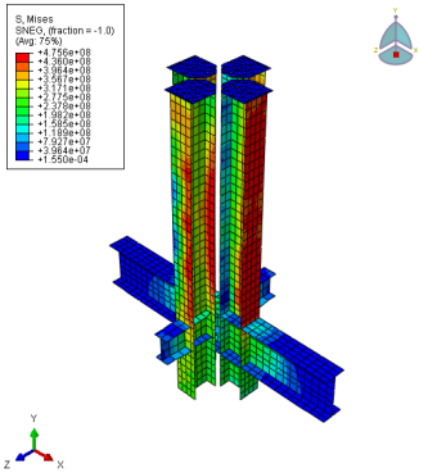

(c) Mises stress for steel profiles

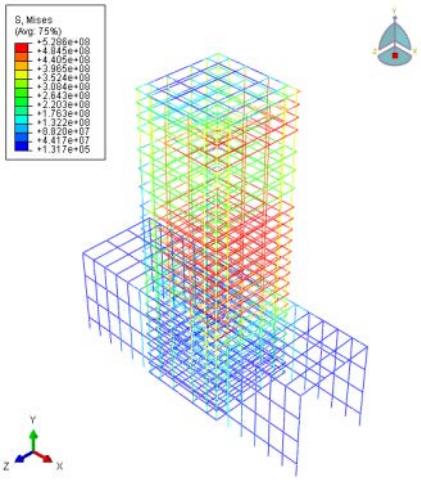

(d) Mises stress for reinforcing bars

Figure 6-3 Stress distribution for specimens with e/h=10%

Abaqus 6.11 can provide clear images of the deformation of the specimens. The FEA shows that even though the deformation patterns of the specimens are similar, the distribution of concrete damage is different for specimens with 10% eccentricity ratio and specimens with 15% eccentricity ratio.

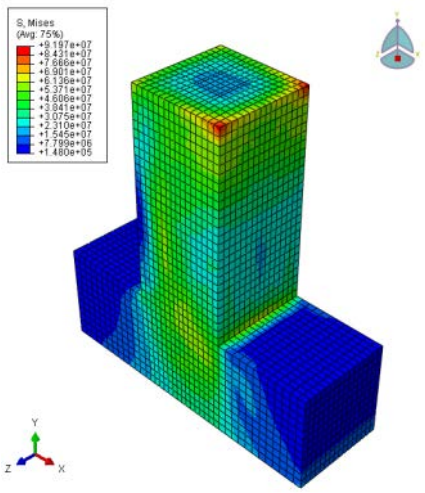

(a) Mises stress for concrete

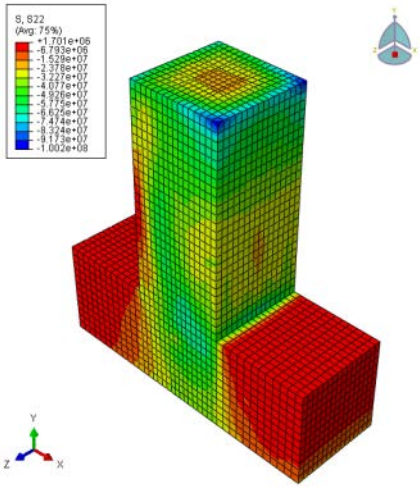

(b) Vertical normal stress for concrete

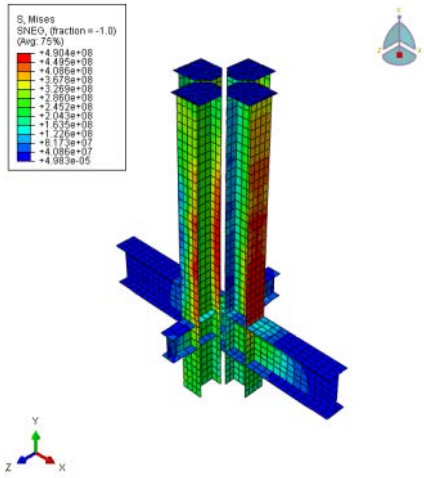

(c) Mises stress for steel profiles

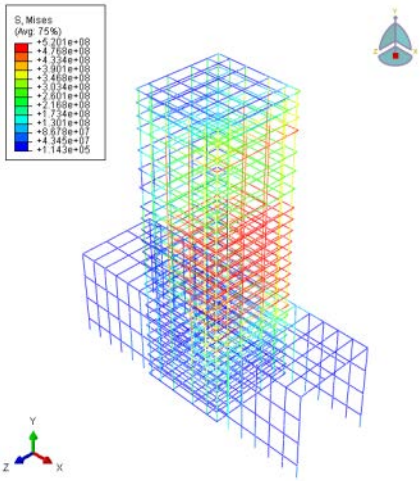

(d) Mises stress for reinforcing bars

Figure 6-4 Stress distribution for specimens with e/h=15%

Figure 6-3 and Figure 6-4 present the stress distributions at failure level of the specimens with 10% and 15% eccentricity ratios respectively. Several discussions are listed as follows:

1) The distribution of Mises stress indicates that the stress at the corners of the column is very large, but this does not necessarily mean that the stress concentration occurs in real structures, since an MPC constraint is employed in the FEA to simulate the boundary conditions of the test. Nevertheless, the stress concentration is limited to the adjacent area of the corners, so the behavior of the whole specimen will not be significantly affected.

2) Figure 6-3 (b) and Figure 6-4 (b) shows the normal stress of the concrete in the longitudinal direction of the specimen. At failure load level, tensile stress occurs in the column of the specimen with 15% eccentricity ratio, but does not occur in that with 10% eccentricity ratio.

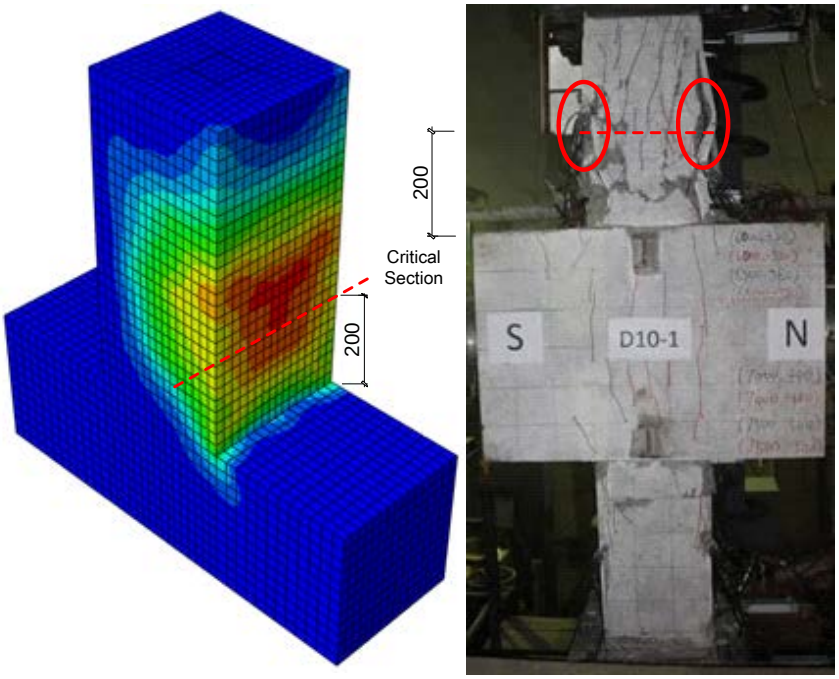

(a) Specimens with e/h=10%

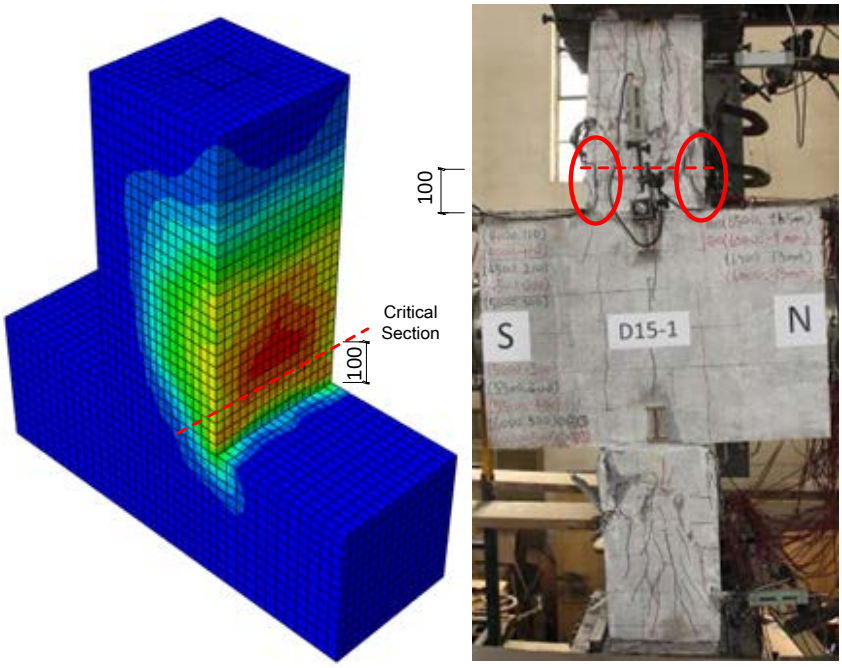

(b) Specimens with e/h=15%

Figure 6-5 Distribution of PEEQ of the concrete

The cumulative damage of the concrete results in a plastic hinge at the bottom of the column, whose length is dependent on the distribution of damage of the concrete. The position of the critical section can be regarded as the center of the plastic hinge. By using plastic damage model of the concrete, the analytical results can sometimes provide a meaningful insight into the damage of the concrete. Shown in Figure 6-5 are the distributions of PEEQ of specimens with 10% and 15% eccentricity ratios respectively. It is obvious that the position of damage is higher for the specimen with 10% eccentricity ratio than that of the specimen with 15% eccentricity ratio. Test results also support this phenomenon. Compared to specimen D15-1, the damage of concrete of specimen D10-1 occurred at a higher place. Based on both the test results and the FEA, the critical section is 200 mm away from the bottom of the column for specimens with 10% eccentricity ratio, and 100 mm away from the bottom of the column for specimens with 15% eccentricity ratio.

6.4 Influence of the shear resistance

Since the number of specimens was limited, a parametric study was conducted to investigate how the shear resistance on the concrete-steel interface would influence the capacity of ISRC columns. According to the superimposition method, the flexural capacity of the composite column is dependent on the axial carried by the concrete and the steel sections, respectively. Since in the longitudinal direction, the axial load between the concrete and the steel sections is transferred by the shear force on the concrete-steel interface. Therefore, the flexural capacity of the composite column is directly related to the shear resistance provided by the combination of bond stress and shear studs.

Shown in Figure 6-6 is a free body diagram of the steel sections. A segment, from the top surface to the critical section of the column, is extracted from one of the steel sections. Based on the equilibrium in vertical forces, one may have the following equation:

$$V = N_2 - N_1 \tag{6.1}$$

where V is the shear force provided by the bond stress and shear studs; N_1 and N_2 are the axial force on the two sides of the segment.

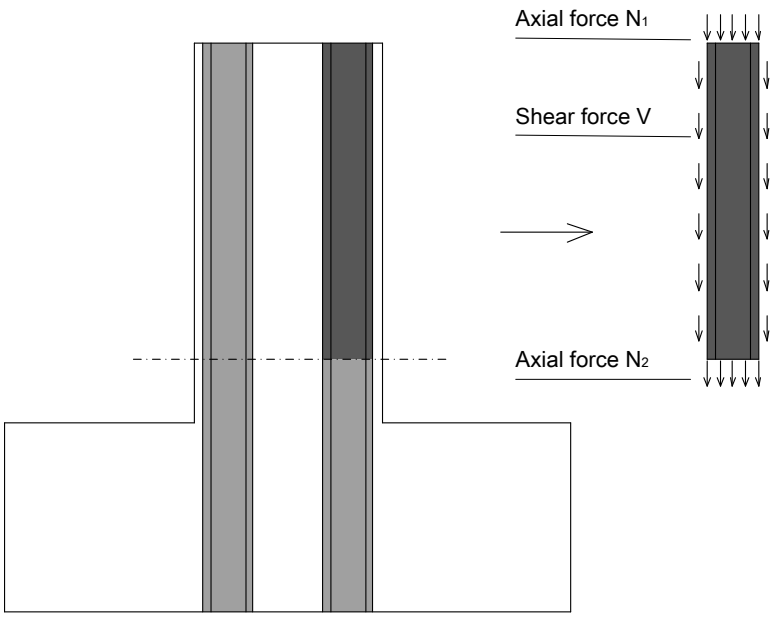

Figure 6-6 Free body diagram of the steel sections

The shear demand along the steel section is determined by N_1 and N_2. N_1 is the axial load carried by the steel section on the top surface of the specimen, which is in proportion to the total axial load. Given a certain axial load, the nominal flexural capacity on the critical cross section can be calculated based on the plastic stress distribution on that cross section. According to the plastic stress distribution, the axial load N_2 carried by the steel section can also be determined. Therefore, the shear demand can be determined. It is obvious that the shear demand varies with the loading conditions of the composite column since it is determined by the difference between N_1 and N_2. To quantify the interface strength provided by the shear connectors, the shear resistance index is defined as follows:

$$\delta = \frac{\sum Q_u}{A_p f_p} \tag{6.2}$$

where Q_u is the shear capacity of one shear stud. According to this definition, the shear resistance index may underestimate the interface strength because the bond stress is not included. However, since the bond stress is relative small, it is reasonable to neglect it when the surfaces of the steel profiles are smooth and enough shear studs are provided.

The finite element analysis indicates that the flexural capacity of the ISRC column grows with the shear resistance index, and that the growth rate gets smaller as the shear resistance index increases (Figure 6-7 (a)). In other words, the marginal effect of the shear studs gets

smaller as the shear resistance index increases. When the shear resistance index is larger than 0.5, providing more shear studs will not significantly improve the capacity of ISRC columns. The flexural capacities of columns with full composite action ($\delta = 1$) are about 20% larger than columns with no composite action ($\delta = 0$).

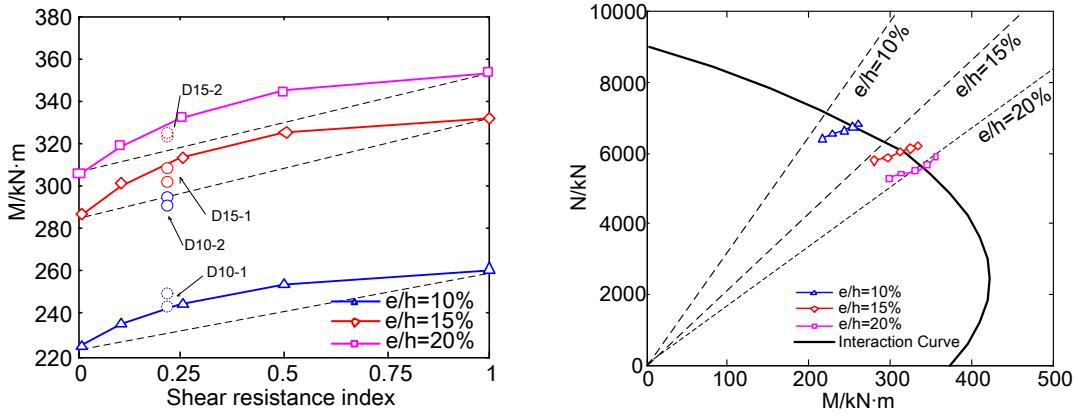

(a) Flexural capacity (b) Interaction relationship

Figure 6-7 Influence of shear resistance index

In practice, accurately predicting the flexural capacity of ISRC columns can be complex, so a more convenient while conservative way to determine the flexural capacity of ISRC columns is to draw a straight line between the starting point and the ending point of the curve, and then determine the flexural capacity according to the actual shear resistance index. For example, the shear resistance index in this test program was:

$$Q_u = \min\{\frac{f_u \pi d^2}{4}, \frac{0.5\pi d^2}{4}\sqrt{f_c E_c}\} = 5.064\,\text{kN} \tag{6.3a}$$

$$\delta = \frac{\sum Q_u}{A_p f_p} = \frac{25 \times 5.064}{2352 \times 460 \times 10^{-3}} \approx 0.12 \tag{6.3b}$$

By conducting linear interpolation, the predicted flexural capacities are $228\text{kN}\cdot\text{m}$ and $288\text{kN}\cdot\text{m}$ for 10% and 15% specimens respectively. Because the actual curves are concave and the contribution of bond stress is not considered, the predictions are conservative.

Note that both the axial capacity and the flexural capacity vary with the shear resistance index because of the special loading protocol employed in this test. In fact, each point on the curves in Figure 6-7 (a) represents a particular axial load. Projecting these points on an M-N coordinate, a more clear relationship between the capacity and the shear resistance index can be obtained (Figure 6-7 (b)). As it is shown in this figure, both the axial capacity and the flexural capacity will be enhanced when the shear resistance index increases.

However, the enhancement of the flexural capacity is not only contributed by the increase in the interface shear strength, but also by the shear stiffness provided by the shear studs. Figure 6-8 illustrates the relationship between the efficiency of the shear resistance and the index δ under the maximum load level, where the vertical axis represents the ratio of the actual shear force to the shear resistance on the steel profiles. Results reveal that the shear force on the concrete-steel interfaces is only 10%~20% of its capacity, which means that the interface strength is by no means fully utilized. Therefore, the enhancement of the flexural capacity of the composite column cannot be entirely explained by the increase of the strength of the shear studs. Previous research (Nie et al, 2003) has shown that the interface stiffness is able to influence the stiffness and capacity of the composite member. Specifically, as the interface stiffness grows, the slip effect will be weakened, thus increasing the composite action between the concrete and the steel profiles.

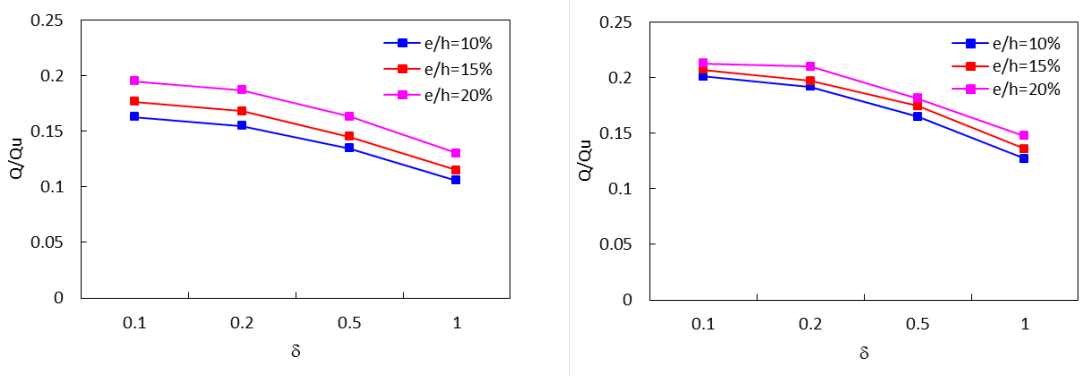

(a) Tensile steel profile (b) Compressive steel profile

Figure 6-8 Efficiency of the shear resistance

What happens in the FEA supports this theory. With the increase of the shear resistance index δ, both the interface strength and interface stiffness increase. Since the interface strength is not fully utilized at all, the interface stiffness explains much of the enhancement of the capacity of the composite column.

Note that the two steel profiles are named after ‘compressive profile’ and ‘tensile profile’ just for distinguishing, and it does not imply the stress distribution of the steel profile. The tensile steel profile, for example, is actually in compression on the bottom of the column due to the limited eccentricity. Since the stress distribution on the composite cross section is a combination of the compression effect and the bending effect, the compressive profile becomes ‘more compressive’ and the tensile profile becomes ‘less compressive’. Several other conclusions can be obtained from the results:

1) The shear force on the compressive steel profile is larger than that on the tensile steel profile with all else equal. This is because the shear demand on the compressive profile is larger than that on the tensile profile, which is a result of the small eccentricity.
2) The shear force on the steel profile increases as the eccentricity increases with all else equal. Similarly, this can also be explained by the shear demand on the interface.
3) The efficiency of the shear resistance drops as the index δ increases. This conclusion, in fact, is a direct inference of the constitutive law of the shear stud. As shown in Figure 5-4, the strength of the shear stud can be reached only when the slip is fully developed. The fact that more shear studs increases the interface stiffness, which leads to smaller slip, which further leads to less effective of utilizing the strength of the shear studs.

In addition, two issues should be noted:

1) This relationship between the capacity and the shear resistance index is only valid when the failure pattern of the composite column is combined compression and bending. The relationship will be violated if other failure patterns occur, such as shear failure or other premature failures.
2) In a real project, the actual shear resistance index can be very small. For example, the shear resistance index in this test program is only 0.12, which means that the composite columns have a large potential to increase the capacities. However, this does not mean that the more shear studs, the better. First, as mentioned above, it is not economical when the shear resistance index is very large. Second, more shear studs will make the construction and fabrication work considerably difficult. Third, more shear studs may further harm the bond conditions between the concrete and the steel sections.

In this phase of the test, since the steel beams are located near the plane of symmetry of the specimens, very little shear demand is created on the interface of the steel beams and the steel sections. As a result, the behavior of the specimens will not be significantly influenced if the steel beams are removed from the model. Similar to the static test, test results and FEA in phase 2 do not mean that the steel beams are not important in real structures. However, this test program cannot reflect the influence of the steel beams.

6.5 Summary of phase 2 FEA

1) The FEA indicates that the position of the critical cross section of the specimen with e/h=10% is higher than that of the specimen with e/h=15%. A similar phenomenon was also observed in the test. In this test program, the distance between the critical section and the bottom of the column is 2/3h and 1/3h for specimens with 10% and 15% eccentricity ratios respectively, where 'h' is the width of the cross section.
2) Shear studs have a strong influence on the flexural capacity of the specimen. The FEA indicates that shear studs are more efficient when the shear resistance index is less than 0.5; otherwise, providing more shear studs will not significantly increase the flexural capacity of the specimen.
3) The enhancement in the capacity of ISRC columns can be explained by both the interface strength and the interface stiffness.
4) In this test program, the existence of steel beams and connections do not have much influence on the capacity of the specimen since the beam-column joint is near the plane of symmetry where the shear demand on the concrete-steel interface is relatively small.

7 Code evaluations

This chapter of the report presents a description of the design philosophies and procedures in current codes from the U.S., Europe, and China. More detailed design procedures in Chinese codes are discussed in the last section of this chapter.

Since the main purpose of the test program is to investigate the performance ISRC columns, this chapter of the report focuses on the code provisions concerning how to determine the resistance of the ISRC columns, and the load factors will not be discussed. Therefore, the safety factors calculated in section 8.1 and 8.2 do not reflect the degree of redundancy of these codes comprehensively. However, the calculated safety factors do provide an insight to evaluate the code provisions to determine the resistance of the composite columns.

7.1 Code predictions on axial resistance

The procedures for determining the pure axial resistance of a composite column include three steps: (1) compute the cross-sectional resistance of the composite column, (2) include the reduction factors to account for the minimum eccentricity ratios, imperfections, and buckling effects to obtain the nominal axial resistance, and (3) include the strength reduction factors to obtain the factored axial resistance of the composite column.

The minimum design eccentricity is included in many codes to serve as a means of reducing the axial design resistance of a section in pure compression to account for accidental eccentricities that may exist in a compression member but not considered in the analysis, and to recognize that concrete strength may be reduced under sustained high loads. In early editions of the codes, the minimum eccentricity requirement was employed to limit the maximum design axial load of a compression member. This is now accomplished directly by limiting the axial resistance of a section in pure compression.

In ACI 318, the nominal axial resistance is limited to 85% and 80% of the cross-sectional axial resistance for spirally reinforced and tied reinforced members, respectively. In Chinese code GB 50010, the nominal axial resistance is limited to 90% of the cross-sectional axial resistance, regardless of the configuration of transverse reinforcement.

In addition to these limitations, the buckling effect should also be included when determining the axial resistance under pure compression.

The AISC-LRFD and Eurocode3 limit the maximum axial resistance load by directly accounting for the buckling effect. Only flexural buckling is discussed in this paper.

For AISC-LRFD, the axial resistance of a composite column is determined as follows:

$$P_n = A_s F_{cr} \tag{7.1}$$

$$\begin{aligned} F_{cr} &= \left(0.658^{\lambda_c^2}\right) F_{my} \quad for\ \lambda_c \le 1.5 \\ F_{cr} &= \frac{0.877}{\lambda_c^2} F_{my} \quad for\ \lambda_c > 1.5 \end{aligned} \tag{7.2}$$

$$\lambda_c = \frac{Kl}{r\pi}\sqrt{\frac{F_{my}}{E_m}} \tag{7.3}$$

Eurocode4 specifies that:

$$\frac{N_{Ed}}{\chi N_{pl,Rd}} \le 1.0 \tag{7.4}$$

where the coefficient χ should be determined in accordance with Eurocode3 (EN 1993-1-1:2004). The design philosophy in Eurocode3 is similar to that in AISC-LRFD.

$$\chi = \frac{1}{\Phi + \sqrt{\Phi^2 - \overline{\lambda}^2}} \le 1.0 \tag{7.5}$$

$$\Phi = 0.5\left[1 + \alpha\left(\overline{\lambda} - 0.2\right) + \overline{\lambda}^2\right] \tag{7.6}$$

where α is an imperfection factor and should be obtained from Table 7-1.

Table 7-1 Imperfection factors for buckling curves

Buckling curve	a0	a	b	c	d
α	0.13	0.21	0.34	0.49	0.76

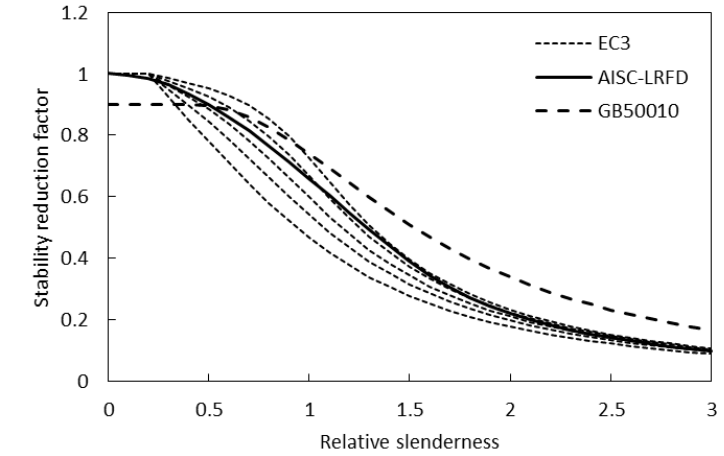

Figure 7-1 Reduction factors

A comparison between the buckling curves from AISC-LRFD, Eurocode3, and GB 50010 is presented in Figure 7-1. Results given by Eurocode3 are plotted in dashed lines, with buckling curves ‘a0’, ‘a’, ‘b’, ‘c’, and ‘d’ ordered from top to bottom. Results suggest that the buckling curve given by AISC-LRFD resembles buckling curves ‘a’ and ‘b’ given by Eurocode3, and that the GB 50010 is less conservative when the relative slenderness is larger than 1.0.

Table 7-2 Redundancy factors of different codes

Specimen	N_{test} /kN	Un-factored				Factored			
		$\frac{N_{test}}{N_{ACI}}$	$\frac{N_{test}}{N_{AISC}}$	$\frac{N_{test}}{N_{EC4}}$	$\frac{N_{test}}{N_{YB}}$	$\frac{N_{test}}{\phi N_{ACI}}$	$\frac{N_{test}}{\phi N_{AISC}}$	$\frac{N_{test}}{\phi N_{EC4}}$	$\frac{N_{test}}{\phi N_{YB}}$
E00-1	17082	1.22	1.25	1.17	1.14	1.87	1.48	1.49	1.46
E00-2	15325	1.13	1.16	1.08	1.07	1.73	1.36	1.37	1.34
	AVE	1.18	1.21	1.13	1.11	1.80	1.42	1.43	1.40

Figure 7-2 shows the ratios of test results to the nominal axial resistance of specimen E00-1 and E00-2. Note that buckling curve ‘b’ is employed in Eurocode4. The AISC-LRFD produces results that are more conservative with the average redundancy of 1.21. However, this does not necessarily mean that the AISC-LRFD provides more conservative results compared with other codes, because the strength reduction factor ϕ has not been included yet.

ACI 318 specifies that the ϕ factor to be taken as 0.65 for compression-controlled sections with tie reinforcement, and the ϕ factor is permitted to be linearly increased from 0.65 to

0.90 as the net tensile strain in the extreme tension steel at nominal strength increases from the compression-controlled strain limit to 0.005. The ϕ factor specified by AISC-LRFD is 0.85 for axial strength. For flexural strength, the ϕ factor is also taken as 0.85 if the nominal flexural strength is determined based on the plastic stress distribution of the composite cross section (If other design philosophies are adopted, the ϕ factor can be different). Chinese codes and Eurocode4 do not apply the strength reduction factors to the calculated strength of the cross section. Rather, the strength reduction factors are applied to the material strength. According to Chinese codes (GB50010 2010; GB50017 2003), the design strength of the material is the characteristic value of the material strength divided by γ_R. The values of γ_R for concrete, reinforcing bars, and steel sections are 1.40, 1.10, and 1.11 respectively. Similarly, the values of γ_R specified by Eurocode2 are 1.50, 1.15, and 1.00 for concrete, reinforcing bars, and steel sections, respectively. In addition, Eurocode4 also employs a ϕ factor to the design flexural resistance. The ϕ factor should be taken as 0.9 for steel grades between S235 to S355, and be taken as 0.8 for steel grades S420 and S460.

With the strength reduction factors being included, the ACI 318 produces the most conservative results with the average redundancy factor of 1.80, while the other three codes produce similar results with redundancy factors around 1.42.

7.2 Code predictions on flexural resistance

Current code provisions provide distinct ways to determine the flexural capacity of concrete-encased composite columns. Most of the design philosophies are based on the following assumptions:

(1) Plane sections remain plane.

(2) Full composite action between the concrete and the steel sections holds effective up to failure of the composite column.

(3) The tensile strength of the concrete is neglected.

According to ACI 318, the flexural capacity of the composite column is determined based on the plastic stress distribution of the cross section. The coefficient of 0.85 is applied to the concrete compressive strength. As mentioned above, the nominal axial resistance of the composite members shall not exceed 85% or 80% of the cross-sectional pure axial resistance, depending on the configurations of the transverse reinforcement.

In AISC-LRFD (1999), the design philosophy for composite columns derives from the design of steel columns. The modified material strength and modulus of elasticity should be calculated based on the configuration of the composite column, and then the nominal axial capacity of the column can be obtained. Similar to ACI 318, the nominal flexural capacity of the composite column is determined based on the plastic stress distribution on the composite cross section. The interaction curve of the column is determined by the following two equations:

$$For \frac{P_u}{\phi P_n} \geq 0.2 \quad \frac{P_u}{\phi P_n} + \frac{8}{9}\frac{M_u}{\phi_b M_n} \leq 1.0 \tag{7.7a}$$

$$For \frac{P_u}{\phi P_n} < 0.2 \quad \frac{P_u}{2\phi P_n} + \frac{M_u}{\phi_b M_n} \leq 1.0 \tag{7.7b}$$

The design philosophy in Chinese code *Technical Specification of Steel-Reinforced Concrete Structures* (YB 9082) derived from the Japan code *AIJ standards for structural calculation of steel reinforced concrete structures* (AIJ-SRC), in which the so called ‘superimposition method’ is used for determining the capacity of concrete-encased composite columns under combined compression and bending. However, YB 9082 employs a more rational strategy to allocate the axial load carried by the concrete and the steel sections respectively, resulting in more accurate predictions on the capacity of the composite columns.

Predictions provided by these codes are presented in Figure 7-2 together with the test results. To evaluate the code provisions, the redundancy factor is defined as follows:
(1) Draw a straight line between the origin and the test result;
(2) The redundancy factor is defined as the ratio of the distance between the origin and the test result to the distance between the origin and the intersection of the straight line and the interactive curve (Figure 7-2).

For un-factored predictions, the ACI 318 and YB 9082 yield similar results, but the YB 9082 has a higher plateau than the ACI 318 since the ACI 318 has a more restrict limitation on the pure axial strength. The key points of Eurocode4 well agreed with ACI 318 and YB 9082, but Eurocode4 is more conservative since a linear relationship between the axial and flexural capacity is employed. Buckling curve ‘b’ is employed in determining the axial strength of the composite columns. As shown in the figure, the buckling curve ‘b’ is close to Chinese codes. The AISC-LRFD provides the most conservative results among these four codes.

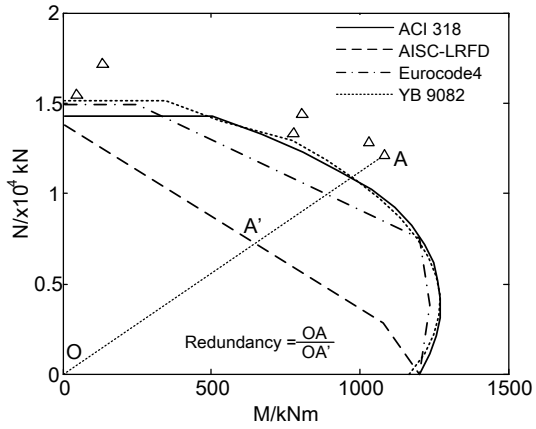

(a) Un-factored
(Material strength using characteristic value)

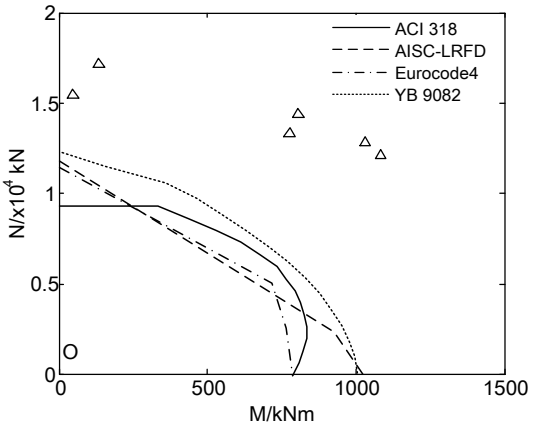

(b) Factored
(Material strength using design value)

Figure 7-2 Code predictions – static tests

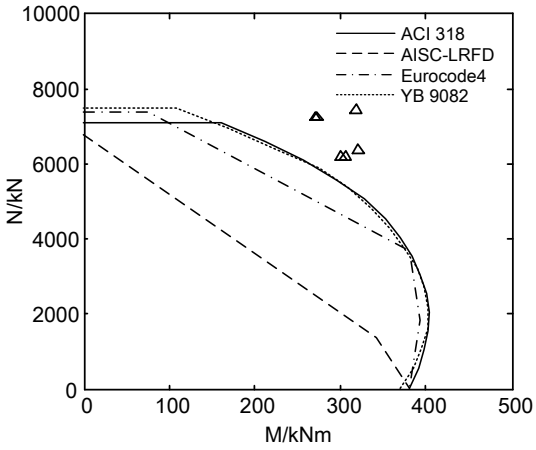

(a) Un-factored
(Material strength using characteristic value)

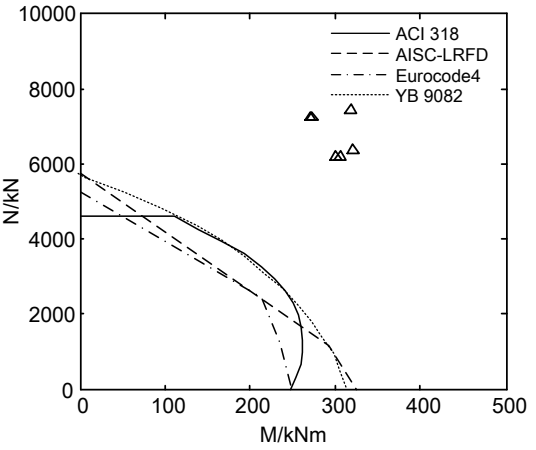

(b) Factored
(Material strength using design value)

Figure 7-3 Code predictions – quasi-static tests

Likewise, the code predictions are somehow meaningless without including the strength reduction factors. Apart from the strength reduction factors, other related specifications should also be included to account for the member imperfections, additional eccentricities, as well as the second order effect. Table 7-3 and Table 7-4 lists the code specifications for these considerations.

Table 7-3 Code provisions for additional eccentricities and imperfections

Code	Specifications
ACI 318	$M_{2,\min} = P_u(15.24 + 0.03h)$
Eurocode4	$e_a = L/200$ or $L/150$
GB 50010	$e_a = \max(20, 30/h)$

Table 7-4 Code provisions for second order effect

Code	Moment amplifier	
ACI 318	$\delta_{ns}=\dfrac{c_m}{1-\dfrac{P_u}{0.75P_c}}\geq 1.0$	$EI=\dfrac{0.2E_cI_c+E_sI_s+E_rI_r}{1+\beta_d}$ $c_m=0.6+0.4\dfrac{M_1}{M_2}\geq 0.4$
Eurocode4	$k=\dfrac{\beta}{1-\dfrac{N_{\mathrm{Ed}}}{N_{\mathrm{cr,eff}}}}\geq 1.0$	$EI_{\mathrm{eff,II}}=0.9\left(0.5E_cI_c+E_sI_s+E_rI_r\right)$ $\beta=0.66+0.44\dfrac{M_1}{M_2}\geq 0.44$
GB 50010	$\delta_{ns}=c_m\eta_{ns}\geq 1.0$	$\eta_{ns}=1+\dfrac{1}{1300\left(M_2/N+e_a\right)/h_0}\left(\dfrac{l_c}{h}\right)^2\dfrac{0.5f_cA}{N}$ $c_m=0.7+0.3\dfrac{M_1}{M_2}\geq 0.7$

When the strength reduction factors are included, the Chinese codes provide the least conservative results with the average redundancy factors of 1.49 and 1.76 for static and quasi-static tests, respectively. The AISC-LRFD and Eurocode4 yield similar results in the flexural part of the curves, while the ACI 318 is more conservative when the eccentricities are very small. Table 7-5 and Table 7-6 present the un-factored and factored code predictions.

Table 7-5 Code predictions on static tests

Specimen	N_{test} /kN	M_{test} /kNm	Un-factored				Factored			
			ACI	AISC	EC4	YB	ACI	AISC	EC4	YB
E00-1	17082	143	1.20	1.33	1.14	1.12	1.84	1.57	1.60	1.45
E00-2	15325	52	1.09	1.15	1.04	1.03	1.64	1.35	1.40	1.26
E10-1	14360	803	1.12	1.67	1.22	1.09	1.74	1.92	1.92	1.55
E10-2	13231	767	1.05	1.53	1.15	1.02	1.60	1.80	1.76	1.44
E15-1	12041	1076	1.12	1.69	1.22	1.14	1.72	1.98	1.91	1.62
E15-2	12759	1026	1.13	1.69	1.23	1.12	1.71	1.98	1.91	1.63
		AVE	1.12	1.51	1.17	1.09	1.71	1.76	1.75	1.49
		COV	0.003	0.050	0.005	0.003	0.007	0.067	0.045	0.020

Table 7-6 Code predictions on quasi-static tests

Specimen	N_{test} /kN	M_{test} /kNm	Un-factored				Factored			
			ACI	AISC	EC4	YB	ACI	AISC	EC4	YB
D10-1(up)	7426	292	1.24	1.84	1.36	1.24	1.74	1.96	2.04	1.74
D10-1(low)	7427	294	1.24	1.84	1.36	1.24	1.76	1.98	2.07	1.76
D10-2(up)	7190	249	1.14	1.71	1.26	1.14	1.89	2.17	2.21	1.89
D10-2(low)	7189	242	1.14	1.71	1.26	1.14	1.89	2.17	2.21	1.89
D15-1(up)	6152	303	1.07	1.60	1.19	1.07	1.66	1.91	1.95	1.66
D15-1(low)	6153	308	1.08	1.65	1.19	1.08	1.67	1.92	1.96	1.67
D15-2(up)	6311	322	1.11	1.69	1.24	1.11	1.73	1.98	1.98	1.73
D15-2(low)	6312	324	1.11	1.69	1.24	1.11	1.73	1.98	1.98	1.73
		AVE	1.14	1.72	1.26	1.14	1.76	2.01	2.05	1.76
		COV	0.004	0.007	0.005	0.004	0.008	0.011	0.012	0.008

7.3 Design approaches for Chinese codes

Based on the previous studies, test results of this program, and the evaluations on the current code provisions, simplified design approaches are proposed for the design of ISRC columns in accordance with Chinese codes. There are two codes in China to guide the design of composite columns, one of them is *Technical Specification of Steel-Reinforced Concrete Structures* (YB 9082 2006), the other one is *Technical Specification for Steel Reinforced Concrete Composite Structures* (JGJ 138 2001).

The simplified design approaches may contain three steps:

1) Determine the design loads;

2) Transfer the cross sections for simplification;

3) Determine the factored resistance of the composite columns.

These three steps are discussed in details in the following:

1. Determine the design loads

The design loads (N,M), including axial loads and bending moments, can be obtained from the first order elastic analysis of the structures in accordance with *Code for Design of*

Concrete Structures (GB 50010 2010), *Code for Design of Steel Structures* (GB 50017 2003), and *Technical Specification for Concrete Structures of Tall Buildings* (JGJ 3 2010). The load factors should be included to amplify the calculated internal forces to obtain sufficient redundancy.

When the factored design loads have been obtained, the bending moment has to be enlarged to account for the member imperfections, additional eccentricities, and the second order effect. The GB 50010, JGJ 138, and YB 9082 provide different ways to include these influences:

Table 7-7 Specifications for member imperfection and second order effect in Chinese codes

Codes	Member imperfections	Moment amplifier in second order effect
GB 50010		$M = C_m \eta_{ns} M_2$ $C_m = 0.7 + 0.3\frac{M_1}{M_2}$ $\eta_{ns} = 1 + \frac{1}{1300(M_2 / N + e_a)/h_0}\left(\frac{l_0}{h_c}\right)^2 \zeta_c$ $\zeta_c = \frac{0.5 f_c A_c}{N}$
JGJ 138	$e_i = e_0 + e_a$ $e_0 = \frac{M}{N}$ $e_a = \max(20, \frac{1}{30}h_c)$	$M = \eta N e_i$ $\eta = 1 + \frac{1}{1400 e_0 / h_0}\left(\frac{l_0}{h}\right)^2 \zeta_1 \zeta_2$ $\zeta_1 = \frac{0.5 f_c A}{N}$ $\zeta_2 = 1.15 - 0.01\frac{l_0}{h}$
YB 9082		$M = \eta N e_i$ $\eta = 1 + 1.25\frac{(7-6\alpha)}{e_i / h_c}\zeta\left(\frac{l_0}{h_c}\right)^2 \times 10^{-4}$ $\alpha = \frac{N - N_b}{N_{u0} - N_b}$ $\zeta = 1.3 - 0.026\frac{l_0}{h_c} \le 1.0,\ \zeta \ge 0.7$

2. Transfer the cross sections

Plumier et al (2013) have proposed a method to transfer the I-shaped steel sections into rectangular sections to simplify the calculation procedures, of which the accuracy has been proved. Figure 7-4 shows the cross sections before and after the transformation.

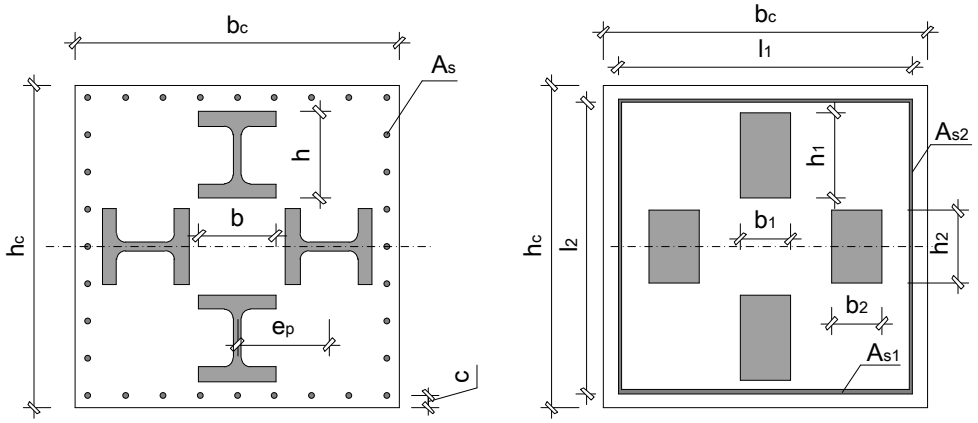

Figure 7-4 Transformation of steel sections and bars

1) The dimensions of the gross cross section remain the same after the transformation, which are b_c and h_c.

2) The longitudinal bars are transferred into continuous steel plates. The number of longitudinal bars on each side of the column is n_1. The area, length, and width of the transferred steel plates can be determined as follows:

$$\begin{aligned} A_{s1} &= n_1 A_b \\ l_1 &= b_c - 2c \\ t_1 &= A_{s1} / l_1 \end{aligned} \tag{7.8a}$$

$$\begin{aligned} A_{s2} &= (n_1 - 2) A_b \\ l_2 &= h_c - 2c \\ t_2 &= A_{s2} / l_2 \end{aligned} \tag{7.8b}$$

3) Assume the bending moment is applied around the horizontal axis. To locate the position of the neutral axis, the dimensions of the steel sections along the vertical direction must not change. For the column presented in Figure 7-4, the transferred dimensions can be obtained as follows:

$$\begin{aligned} A_{p1} &= A_p \\ h_1 &= h \\ b_1 &= A_{p1} / h_1 \end{aligned} \tag{7.9a}$$

$$\begin{aligned} A_{p2} &= A_p \\ h_2 &= b \\ b_2 &= A_{p2} / h_2 \end{aligned} \tag{7.9b}$$

where A_p is the cross area of one steel section. In this way, the plastic moment of inertia will not be changed after the transformation. Since the flexural capacity of the composite column is determined based on the plastic stress distribution of the cross section, this transformation method will have sufficient accuracy when calculating the ultimate strength of the cross section.

3. Determine the factored resistance

To determine the factored resistance of the composite columns, one has to (1) determine the nominal resistance of the column; and (2) include the member imperfections, additional eccentricities, and the second order effect.

The YB 9082 approaches:

According to Chinese code *Technical Specification of Steel-Reinforced Concrete Structures* (YB 9082-2006), the design resistance should satisfy the following requirements:

$$\begin{cases} N \le N_{cy}^{ss} + N_{cu}^{rc} \\ M \le M_{cy}^{ss} + M_{cu}^{rc} \end{cases} \tag{7.10}$$

where N_{cy}^{ss} and N_{cu}^{rc} are the axial load carried by the steel sections and the reinforced concrete, respectively; M_{cy}^{ss} and M_{cu}^{rc} are the flexural resistance of the steel sections and the reinforced concrete, which are related to the axial loads carried by these two parts; *N* and *M* are the design axial load and bending moment of the composite column.

YB 9082 specifies that the axial load be shared by the steel sections and the reinforced concrete by the following principles:

$$N_{cy}^{ss} = \frac{N - N_b}{N_{u0} - N_b} N_{c0}^{ss} \tag{7.11a}$$

$$N_c^{rc} = N - N_{cy}^{ss} \tag{7.11b}$$

where N_{c0}^{ss} is the cross sectional axial resistance of the steel sections, which equals to $f_p A_p$, N_b is the axial load of the composite column corresponding to the balanced strain conditions, which can be taken as $0.4 f_c b_c h_c$, and N_{u0} is the cross sectional axial resistance of the composite column. The bending moment is shared by the following principles:

$$M_{cy}^{ss} = \left(1 - \left|\frac{N_{cy}^{ss}}{N_{c0}^{ss}}\right|^m\right) M_{y0}^{ss} \tag{7.12a}$$

$$M_c^{rc} = M - M_{cy}^{ss} \tag{7.12b}$$

where M_{y0}^{ss} is the pure flexural resistance of the steel sections, and *m* is a coefficient, which can be determined based on the configuration of the cross sections.

For the steel sections part, the axial and flexural resistance of the steel sections automatically exceeds the carried axial load and bending moment according to Eq. 7.11a and Eq. 7.12a. For the reinforced concrete part, the position of the neutral axis can be obtained from the carried axial load N_c^{rc}, and the corresponding axial and flexural resistance can be obtained from the following equations:

$$N \le N_{cu}^{rc} = \alpha_1 f_c bx + f_y^{'} A_s^{'} - \sigma_s A_s - \left(\sigma_{p0}^{'} - f_{p0}^{'}\right) A_p^{'} - \sigma_p A_p \tag{7.13a}$$

$$M \le M_{cu}^{rc} = \alpha_1 f_c bx\left(h_0 - \frac{x}{2}\right) + f_y^{'} A_s^{'}\left(h_0 - a_s^{'}\right) - \left(\sigma_{p0}^{'} - f_{p0}^{'}\right) A_p^{'}\left(h_0 - a_p^{'}\right) \tag{7.13b}$$

In general, the YB 9082 permits to calculate the flexural resistance of the steel sections and the reinforced concrete separately based on the axial loads carried by these two parts, and the flexural resistance of the composite column is the sum of the flexural resistance of these two parts.

JGJ 138 approaches:

The JGJ 138 permits to calculate the nominal resistance of the composite columns based on the plastic stress distribution of the composite cross sections. A simplified method is proposed in JGJ 138 to calculate concrete-encased composite columns with a single I-shaped steel section in the middle of the cross section. This method, however, is not suitable for ISRC columns. Therefore, a more appropriate approach is proposed based on the basic principles of JGJ 138: (1) plane sections remain plane, (2) tensile strength of the concrete is neglected, and (3) the ultimate compressive strain for concrete is 0.0033.

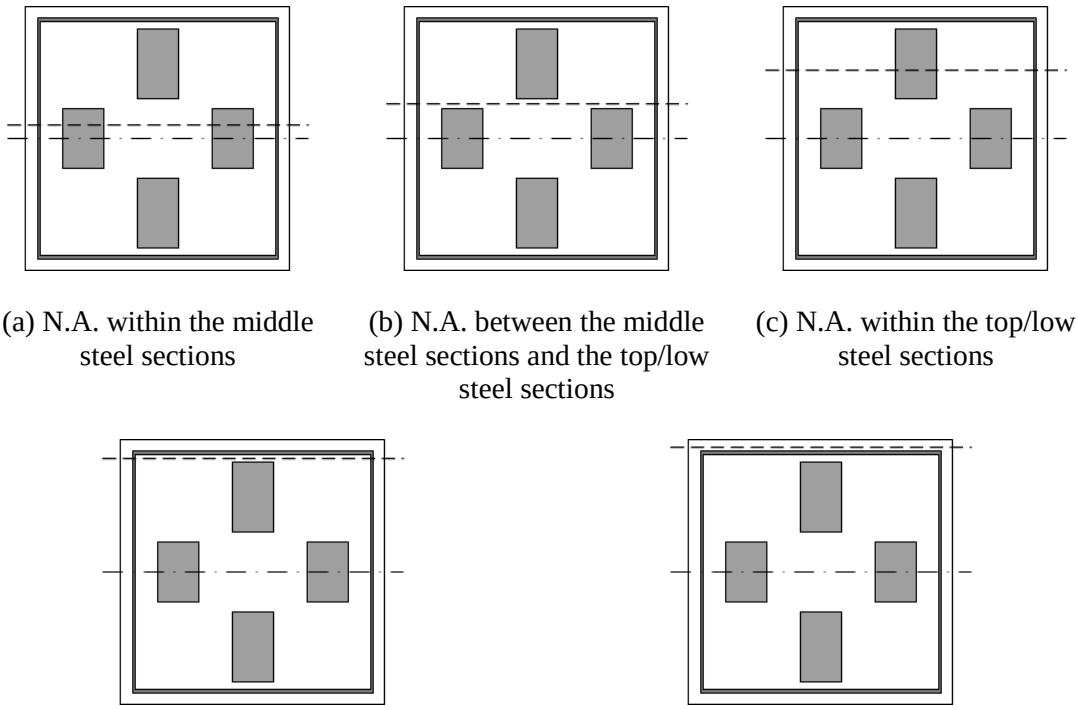

(a) N.A. within the middle steel sections

(b) N.A. between the middle steel sections and the top/low steel sections

(c) N.A. within the top/low steel sections

(d) N.A. between the top/low steel sections and the reinforcing bars

(e) N.A. outside the reinforcing bars

Figure 7-5 Position of the neutral axis

A two-step calculation can be used to determine the flexural resistance of the composite cross section.

Step 1: Determine the position of the neutral axis (N.A.) based on the balance condition of the axial load. There are five distinct situations of the position of the N.A., as shown in Figure 7-5

Step 2: Calculate the flexural resistance of the composite cross section based on the position of the N.A.

8 Conclusions

A series of structural tests were conducted on concrete-encased composite columns with separate steel profiles. The test specimens were designed to achieve high levels of composite action between the concrete and the steel profiles. A two-phase test program was carried out. Phase 1 of the study included six 1/4-scaled static tests, and phase 2 of the study included four 1/6-scaled quasi-static tests. The following sections provide the conclusions found by this research program.

8.1 Comparing results to previous studies

Since very few tests were conducted on ISRC columns, there are limited comparable results. However, comparing the test results to previous SRC tests can still provide some insight.

1. Shear demand for ISRC columns is larger

Previous studies (Ricles and Paboojian, 1994; Mirza et al, 1996) found that the shear connectors had little influence on the ultimate capacity of SRC columns. This is because the shear demand on the concrete-steel interfaces is relatively small for SRC columns. Therefore, installing more shear connectors could not improve the capacity of SRC columns significantly. Test results of this test program revealed that the Plane Section Assumption was generally valid for specimens with e/h=10% and e/h=15%, but the interface slip grew with the eccentricity, which suggested that the shear demand was relatively larger for ISRC columns.

2. Confinement provided by the steel profiles is helpful

The confinement effect may increase the ultimate compressive strain of the concrete, thus improving the ductility of the composite column. For SRC columns, the confinement effect is often provided by transverse reinforcement and the steel flanges. For ISRC columns, however, the concrete core surrounded by the steel profiles was also highly confined, thus increasing the ductility of the ISRC column.

8.2 Comparing results to code provisions

1. Code predictions on ultimate capacity

The current ACI 318, AISC-LRFD, Eurocode4, JGJ 138, and YB 9082 were evaluated in this test program. The first four of these codes are based on the Plane Section Assumption, while the last code is based on the superimposition method. For the test specimens, the current codes were able to provide precise predictions on the axial and flexural capacities with sufficient margins of safety.

2. Requirements for lateral deformation

Both the static and quasi-static specimens showed sufficient deformation capacity. In static tests, the specimens were able to maintain the bending moment as high as the maximum while the curvature was developing up to failure. In quasi-static tests, the ultimate drift ratios of the specimens were 1/54~1/97, which met the minimum requirement - 1/100 - specified by Chinese code *Technical specification for concrete structures of tall building* (JGJ 3 - 2010). Previous studies have revealed that the transverse reinforcement was very helpful in improving the ductility and deformation capacity of SRC columns. The authors believe that the same rule applies to ISRC columns. However, since the test specimens were limited, the influence of transverse reinforcement was not deeply investigated in this test program.

3. Coefficients of stiffness reduction

The code provisions allow the use of the reduced stiffness of a concrete member (or composite member) to calculate the first order elastic reaction of the structure as a simplified way to account for the second order effect and concrete crack under medium or severe earthquakes. Test results of this program support the conclusion that the stiffness reduction factor be taken as 0.7 for ACI 318 method (The factor is applied to the entire composite cross section.) or 0.6 for Eurocode4 method (The factor is applied to the concrete part only.).

4. Simplified design methods

Simplified design approaches were proposed and described in this report in accordance with Chinese codes JGJ 138 and YB 9082. The design approaches are applicable to ISRC columns within 15% eccentricity ratio.

8.3 Insights provided by FEA

The finite element analyses were conducted as a supplementary to the test research. FEA demonstrated that the interface strength and stiffness influenced the capacity of ISRC columns dramatically when subjected lateral loads. This implied that the shear demand on the interfaces became much larger when the steel profiles were separate from one another. Specifically, the flexural capacity of the ISRC column might increase by as much as 20% if enough shear studs were provided.

More thoughtful analyses imply that the enhancement in capacity was contributed by both the interface strength and interface stiffness, and that the efficiency of shear studs got smaller as the number of shear studs grew. In a real structure, however, the shear force between the concrete and the steel profiles is contributed by shear studs, bond stress, and friction, but the FEA results only reflect the influence of shear studs. With the existence of bond stress and friction, the influence of shear studs in a real structure may not be as significant as it is shown in the FEA.

9 Simplified method for the design of composite columns with several embedded steel profiles subjected to axial force and bending moment – according to Eurocode 4

9.1 Introduction. Eurocode 4 Simplified Method.

Eurocode 4 - Clause 6.7 provides two design methods in the design of composite compression members with encased sections, partially encased sections and concrete filled rectangular and circular tubes

The first one is a numerical and general method, while the second one is a simplified analytical method, applied only to doubly symmetrical sections, uniform along the height of the element. By using the simplified method, the interaction curve can be approached by a succession of lines joining 4 points A,B,C,D (stresses are then represented with rectangular stress blocks), as shown in figure below.

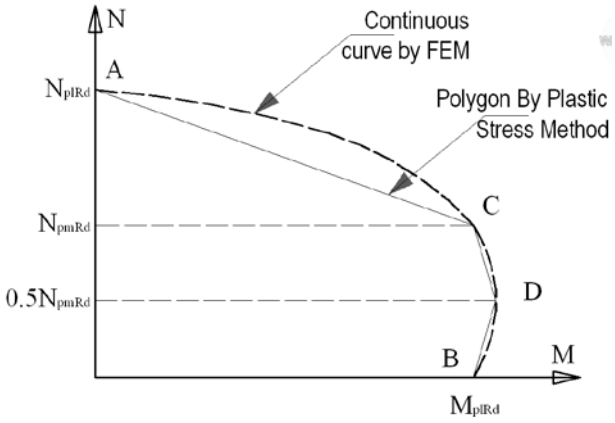

Figure 9-1 Simplified method: point A, B, C, and D

No available design standards are however providing information on how to design properly RC sections with more than one embedded profile. The present document presents therefore the extension of an existing method developed in the first by Roik and Bergman and the adapted in EC4.

EC4 clause 6.7 limits the utilization of the use of simplified method for composite columns:

- The steel grades should be between S235 to S460 and normal weight concrete of strength classes C20/25 to C50/60.
- The steel contribution ratio δ is such as $0.2 \leq \delta \leq 0.9$.
- The considered element must be uniform along its height and its section must be doubly symmetrical
- The relative slenderness $\bar{\lambda}$ should fulfill the following condition : $\bar{\lambda} \leq 2$ [-]
- For fully encased steel profiles, the limits to the maximum thickness of concrete cover that may be used, should fulfill those conditions (with h the profile height and b the profile width) : 40 [mm] $\leq c_y \leq 0.4$ b and 40 [mm] $\leq c_z \leq 0.3$ h (c_y and c_z can have higher values in order to improve the fire resistance, but this supplement is then neglected in the resistance calculation)
- The sum of the rebar sections must represent at least 0,3% of the concrete area and must represent less than 4% of this area (more important sections can be used in order to improve the fire resistance but this supplement is then neglected in the resistance calculation).

The following assumptions should also be considered, because are underlying the prescriptions from EC4:

- There is a complete interaction between steel and concrete.
- The plane sections remain plane after deformation.
- The concrete resistance in traction is neglected.
- The material laws of steel and concrete come from EC2 and EC3.

Point A is characterized by pure compression scenario, as shown in Figure 9-2 :

$N_A = N_{pl,Rd}$

$M_A = 0$

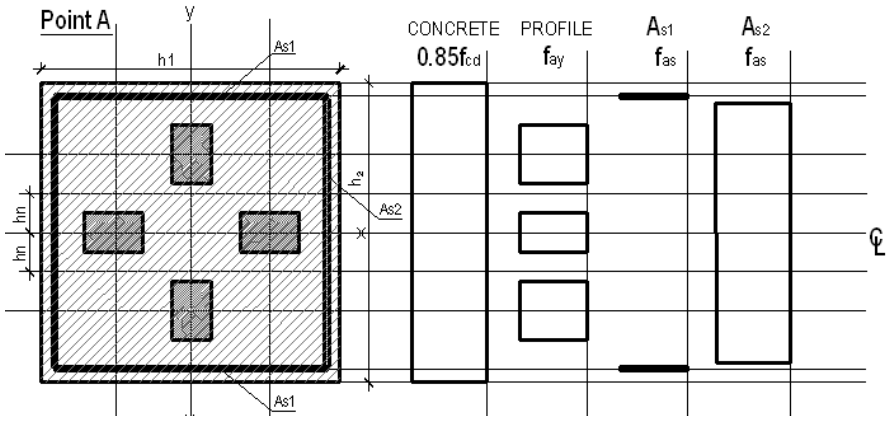

Figure 9-2 Point A – stress distribution

Point B is characterized by pure bending scenario. The plastic neutral is situated at a distance h_n from the axis of symmetry.

$N = 0$

$M = M_{pl,Rd}$

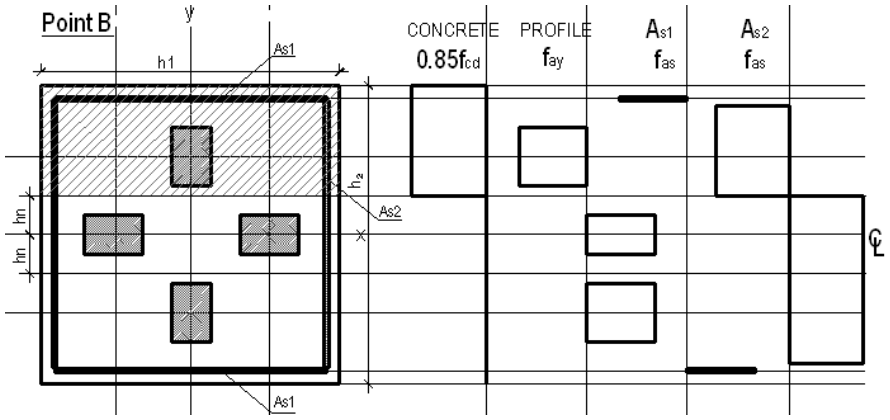

Figure 9-3 Point B – stress distribution

Point C corresponds to pure bending capacity. It is assumed that the concrete part has no tensile strength:

$N_C = N_{pm,Rd}$

$M_C = M_{pl,Rd}$

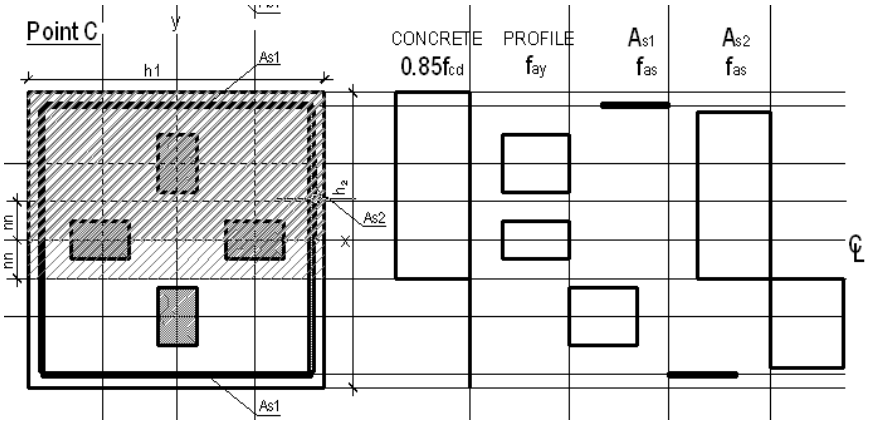

Figure 9-4 Point C – stress distribution

Point D is defined by:

$N_D = 0.5 \cdot N_{pm,Rd}$

$M_D = M_{max,Rd}$

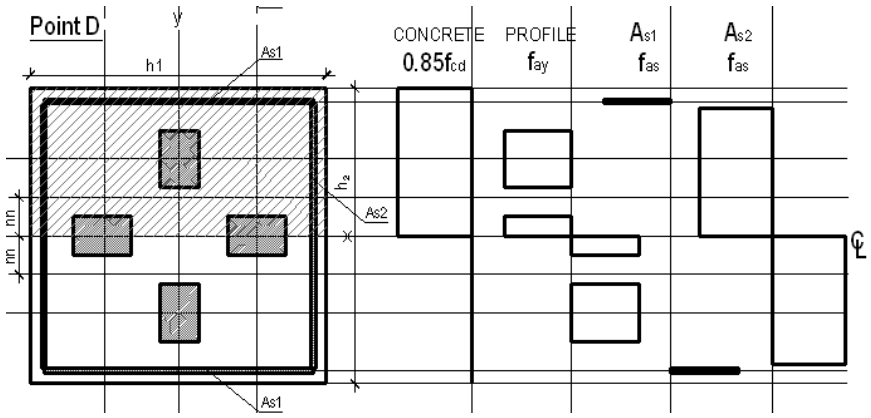

Figure 9-5 Point D – stress distribution

9.2 Equivalent plates for definition of rebar layers and steel profiles.

The development of a method of calculation of concrete sections with several encased steel sections requires the calculation of section characteristics like the moment of inertia, the plastic moment, the elastic neutral axis and the plastic neutral axis. Such calculation can be made numerically or “hand - made”, in which case the calculation becomes tedious. In order to facilitate such calculation two simplifications are proposed, as shown in Figure 9-6. The first one is to replace the amount of longitudinal rebar by equivalent plates.

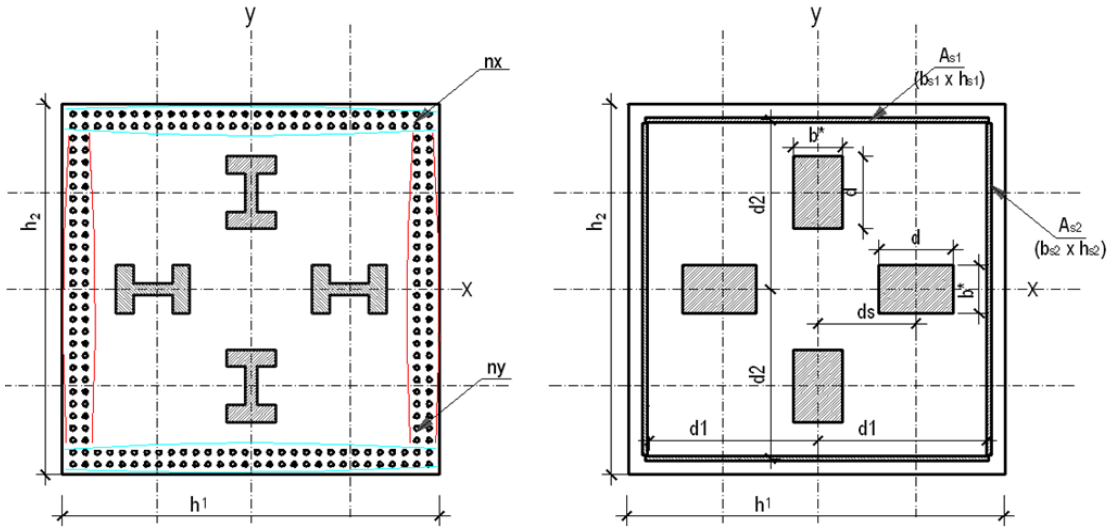

Figure 9-6 Equivalent plates for steel profiles and rebar

9.2.1 Flange layer of rebar.

In order to make calculations easily, the layers of rebar parallel to one considered neutral axis could be substituted by an equivalent plate, see Figure 9-7, with the following properties:

- Plate area: $A_{p:}A_p = 2n\ A_b$, where: A_b is the cross sectional area of one bar and n the number of bars in one layer.
- Distance of plate geometrical center to neutral axis d_p: $d_p = (d_1 + d_2)/2$, where d_1 (respectively d_2) is the distance from the center of rebar of the 1st layer (respectively 2nd layer) to the neutral axis.

It has been shown[1] that the error generated by this simplification. Indeed, if we express $d_1 = d_p + \varepsilon$ and $d_2 = d_p - \varepsilon$, the error is then equal to ε^2/d_p^2 and is acceptable if $(d_1 - d_2) < 0{,}2d_p$. This condition is for an error less than 1% on the moment of inertia of reinforcing bars and checks for a wide range of sections. It should be mentioned that the 1% error on the moment of inertia of reinforcing bars induces a minor error on other parameters like the complete section stiffness. Concerning the plastic moment, the simplification does not imply any change.

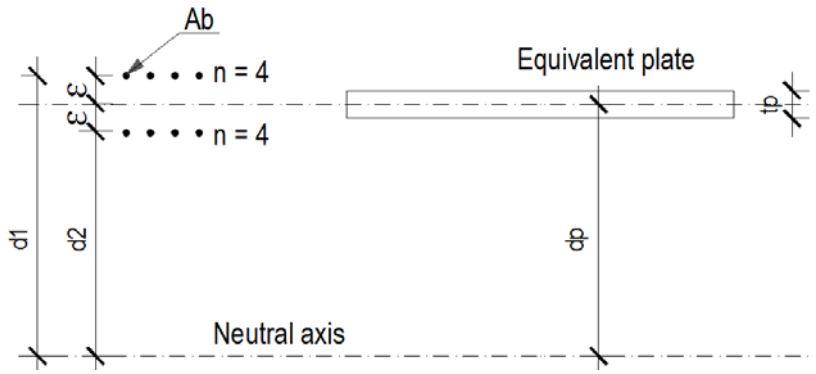

Figure 9-7 Flange layer and the equivalent plate

9.2.2 Web layer of rebar.

Let us consider a layer of (n+1) bars perpendicular to the neutral axis, see Figure 9-8, where s is the step of bars. The total number of bars in one layer is 2n + 1. The total height h of the layer is: $h = 2n\ s$, while A_b is the cross sectional area of one bar. In order to make calculations easier, the layers of rebar perpendicular to one considered neutral axis could be substituted by an equivalent plate, see Figure 9-8, with the properties:

[1] DESIGN OF COLUMN WITH SEVERAL ENCASED STEEL PROFILES FOR COMBINED COMPRESSION AND BENDING, T. Bogdan, A. Plumier, H. Degée (ULg)

$A_p = (2n+1)A_b$ $h_p = (2n+1)s$

$h_p = h + s$ $t_p = (2n+1)\,A_b\,/[(2n+1)s] = A_b\,/s.$

Comparing I_b and I_p it appears that the error is equal to: $(I_b - I_p)/\ I_p = 1/2n$. A simple formulation for the acceptability of the simplification would correspond to a 1% error on EI_{eff}. This condition is fulfilled as long as the number of web rebar in a line are not less than 10 because n is the number of bars for either top or bottom equivalent plate. Concerning the error relative to the plastic moment, The error is: 1/[4(n2 + n)]. With the minimum *s* defined in the previous paragraph (n=10/2=5), the error is equal to:

1/ (4x25 + 4x5) = 1/120 = 0.8%.

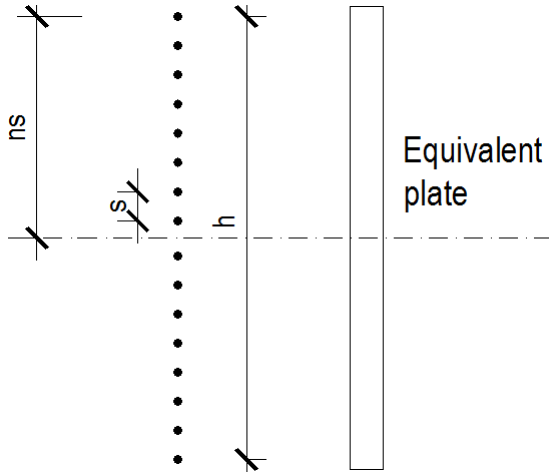

Figure 9-8 Flange layer and the equivalent plate

9.2.3 Equivalent steel profiles.

In order to have an easily calculation of the plastic value of the bending moment of the complete section of the example in which there are 4 encased steel shapes, see Figure 9-6, equivalent rectangular plates are replacing the current steel profiles; the rectangular plates have the following dimensions (d^* x b^*) :

$d^* = d$; $b^* = A_s/d^*$; $I^* = (b^* \text{ x } d^{*3})/12$

where:

d – depth of the steel profile;

A_s – one steel profile area;

*I** – the moment of inertia of equivalent rectangle;

I_{sx} – the moment of inertia of one steel profile

9.3 3 Evaluation of neutral axis position - "hn".

9.3.1 Simplified Method

To determine points A, B, C, D from the interaction curve, as shown in Figure 9-1, the following equations are used:

$$N_{pl,Rd} = A_s \,.\, f_{yd} + A_{sr} \,.\, f_{sd} + A_c \,.\, 0{,}85 \,.\, f_{cd}$$

$$N_{pm,Rd} = A_c \,.\, 0{,}85 \,.\, f_{cd}$$

$$M_{max,Rd} = Z_s \,.\, f_{yd} + Z_{sr} \,.\, f_{sd} + 0{,}5 \,.\, Z_c \,.\, 0{,}85 \,.\, f_{cd}$$

The subscript "d" represents the design value. The overstregth factors are being used for concrete and reinforcement rebars:

$$f_{yd} = f_{yk}/\gamma_a \qquad f_{sd} = f_{sk}/\gamma_s \qquad f_{cd} = f_{ck}/\gamma_c.$$

Where:

$$\gamma_a = 1, \gamma_s = 1.15 \; and \; \gamma_c = 1.5$$

This equation for $M_{max,Rd}$ is due to the fact that for point D, the neutral axis is situated at the axis of symmetry of the cross section (the 0,5 coefficient results from the assumption that concrete tensile strength is neglected).

In order to determine the plastic moment $M_{pl,Rd}$, the position of the neutral axis must be evaluated. Several scenarios needs to be taken into account: they are detailed below while considering different scenarios.

<u>*Scenario 1*</u>

In this scenario, h_n is between the rectangular plates and so $h_n \leq b^*/2$, as shown in Figure 9-9. Let N_B and N_c be the axial effort corresponding to points B and C from the simplified interaction curve, then:

$$N_b - N_c = 0{,}85 \,.\, A_c \,.\, f_{cd}$$

$$N_b - N_c = 2 \,.\, h_n \,.\, h_1 \,.0{,}85 \,.\, f_{cd} + 2 \,.\, h_n \,.\, 2 \,.\, d \,.\, \left(f_{yd} - 0{,}85 \,.\, f_{cd}\right) + 2 \,.\, h_n \,.\, 2 \,.\, b_{s2} \,.\, \left(f_{sd} - 0{,}85 \,.\, f_{cd}\right)$$

This implies that:

$$h_n = \frac{0{,}85 \,.\, A_c \,.\, f_{cd}}{2 \,.\, h_1 \,.0{,}85 \,.\, f_{cd} + 4d \,.\, f_{yd} - 4d \,.0{,}85 \,.\, f_{cd} + 4b_{s2} \,.\, f_{sd} - 4b_{s2} \,.0{,}85 \,.\, f_{cd}}$$

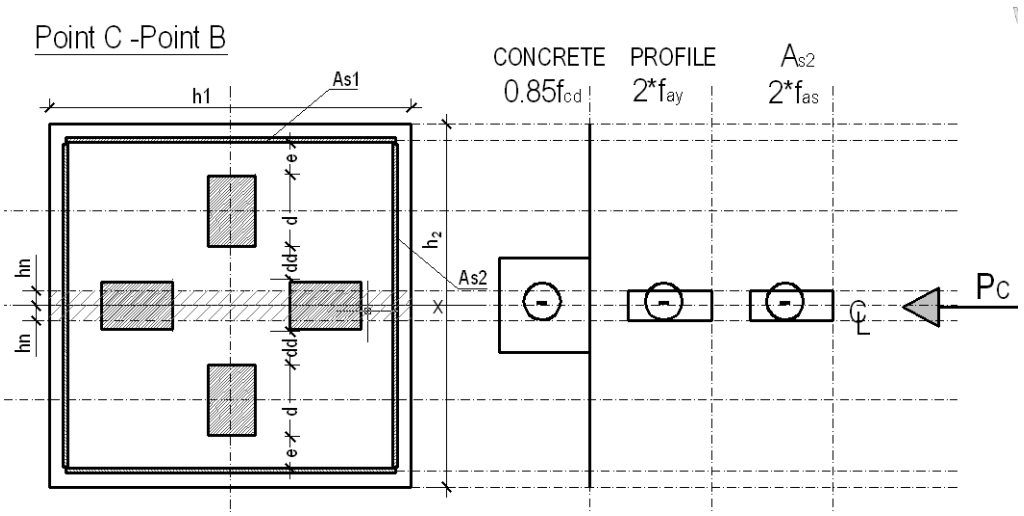

Figure 9-9 Subtracting the components of the stress distribution combination at point B & C – PNA is within the inner profile equivalent rectangular plates

Scenario 2

In this scenario, $\frac{b^*}{2} \leq h_n \leq \frac{d_d}{2}$, see Figure 9-10.

$$N_b - N_c = 0{,}85 \,.\, A_c \,.\, f_{cd}$$

$$N_b - N_c = 2 \,.\, h_n \,.\, h_1 \,.0{,}85 \,.\, f_{cd} + 2 \,.\, A_{prof} \,.\, (f_{yd} - 0{,}85 \,.\, f_{cd}) + 2 \,.\, h_n \,.\, 2 \,.\, b_{s2} \,.\, (f_{sd} - 0{,}85 \,.\, f_{cd})$$

Which implies that:

$$h_n = \frac{0{,}85 \,.\, A_c \,.\, f_{cd} - 2A_{prof} \,.\, (f_{yd} - 0{,}85 \,.\, f_{cd})}{2 \,.\, h_1 \,.0{,}85 \,.\, f_{cd} + 4b_{s2} \,.\, f_{sd} - 4b_{s2} \,.0{,}85 \,.\, f_{cd}}$$

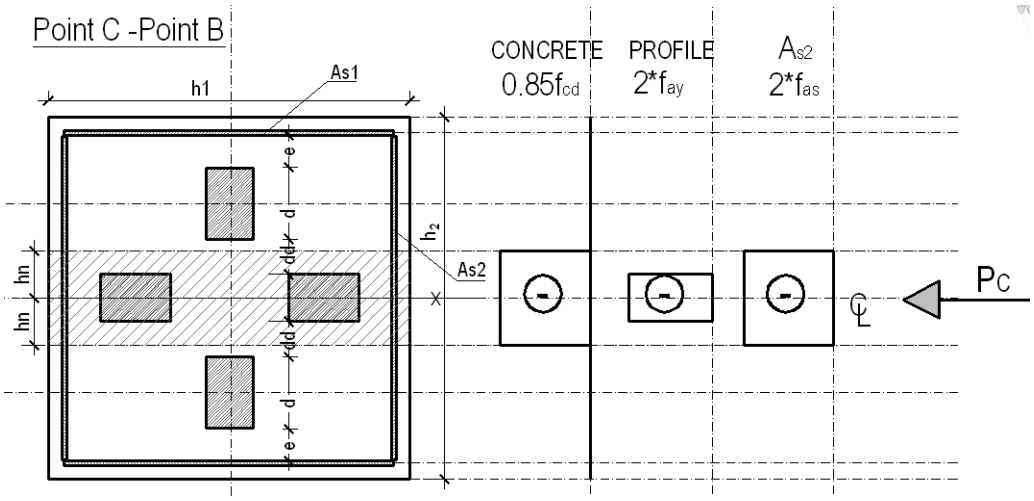

Figure 9-10 Subtracting the components of the stress distribution combination at point B & C – PNA is between the profile equivalent rectangular plates

Scenario 3

In this scenario, $\frac{d_d}{2} \leq h_n \leq \frac{d_d}{2} + d$, see Figure 9-11.

$$N_b - N_c = 0{,}85 \,.\, A_c \,.\, f_{cd}$$

$$N_b - N_c = 2 \,.\, h_n \,.\, h_1 \,.0{,}85 \,.\, f_{cd} + 2 \,.\, A_{prof} \,.\, \left(f_{yd} - 0{,}85 \,.\, f_{cd}\right) + 2 \,.\, \left(h_n - \frac{d_d}{2}\right) \,.\, b^* \,.\, \left(f_{yd} - 0{,}85 \,.\, f_{cd}\right) + 2 \,.\, h_n \,.\, 2 \,.\, b_{s2} \,.\, \left(f_{sd} - 0{,}85 \,.\, f_{cd}\right)$$

This implies that:

$$h_n = \frac{0{,}85 \,.\, A_c \,.\, f_{cd} - 2A_{prof} \,.\, (\, f_{yd} - 0{,}85 \, f_{cd}\,) + \mathrm{d_d} \,.\, \mathrm{b^*} \,.\, \mathrm{f_{yd}} - \mathrm{d_d} \,.\, \mathrm{b^*} \,.0{,}85 \,.\, \mathrm{f_{cd}}}{2.\, h_1 .\, 0{,}85 \, f_{cd} + 2b^* .\, f_{yd} - 2b^* .\, 0{,}85 f_{cd} + 4b_{s2} \,.\, f_{sd} - 4b_{s2} \,.0{,}85 \, f_{cd}}$$

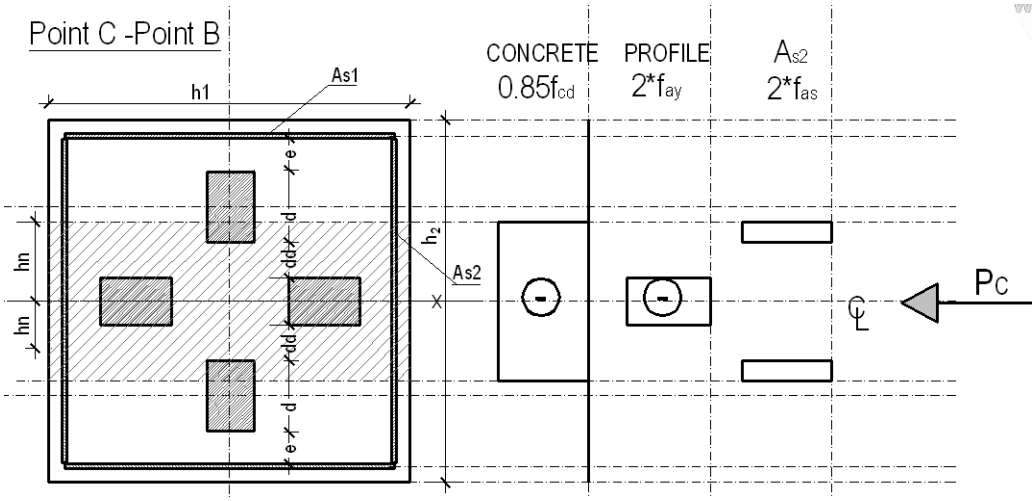

Figure 9-11 Subtracting the components of the stress distribution combination at point B & C – PNA is between the outer profile equivalent rectangular plates

Scenario 4

In this scenario, $\frac{d_d}{2} + d \leq h_n \leq \frac{d_d}{2} + d + e,$, see Figure 9-12.

$$N_b - N_c = 0{,}85 \,.\, A_c \,.\, f_{cd}$$

$$N_b - N_c = 2 \,.\, h_n \,.\, h_1 \,.0{,}85 \,.\, f_{cd} + 4 \,.\, A_{prof} \,.\, \left(f_{yd} - 0{,}85 \,.\, f_{cd}\right) + 2 \,.\, h_n \,.\, 2 \,.\, b_{s2} \,.\, \left(f_{sd} - 0{,}85 \,.\, f_{cd}\right)$$

This implies that:

$$h_n = \frac{0{,}85 \,.\, A_c \,.\, f_{cd} - 4A_{prof} \,.\, (f_{yd} - 0{,}85 \, f_{cd}\,)}{2.\, h_1 .\, 0{,}85 \, f_{cd} + 4b_{s2} \,.\, f_{sd} - 4b_{s2} \,.0{,}85 \,.\, f_{cd}}$$

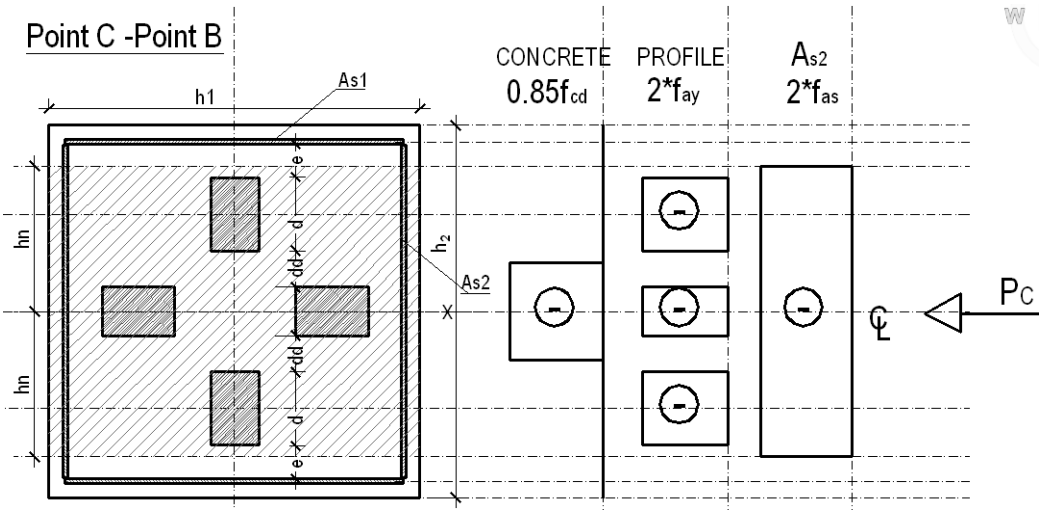

Figure 9-12 Subtracting the components of the stress distribution combination at point B & C – PNA is between the steel profiles and rebar

Scenario 5

In this scenario, $\frac{d_d}{2} + d + e \leq h_n \leq \frac{d_d}{2} + d + e + b_{s1}$, as shown in Figure 9-13.

$$N_b - N_c = 0{,}85 \,.\, A_c \,.\, f_{cd}$$

$$N_b - N_c = 2 \,.\, h_n \,.\, h_1 \,.0{,}85 \,.\, f_{cd} + 4 \,.\, A_{prof} \,.\, \left(f_{yd} - 0{,}85 \,.\, f_{cd}\right) + A_{sr2} \,.\, (f_{sd} -$$

$$0{,}85 \,.\, fcd + \quad 2 \,.\, (hn - hs22) \,.\, hs1 \,.\, (fsd - 0{,}85 \,.\, fcd)$$

This implies that

$$h_n = \frac{0{,}85 \,.\, A_c \,.\, f_{cd} - 4A_{prof} \,.\, \left(f_{yd} - 0{,}85\, f_{cd}\right) + (2h_{s2} \,.\, h_{s1} - A_{sr2}).\, (f_{sd} - 0{,}85\, f_{cd}\,)}{2.\, h_1.\, 0{,}85\, f_{cd} + 2b_{s2} \,.\, h_{s1}.\, (f_{sd} - 0{,}85\, f_{cd}\,)}$$

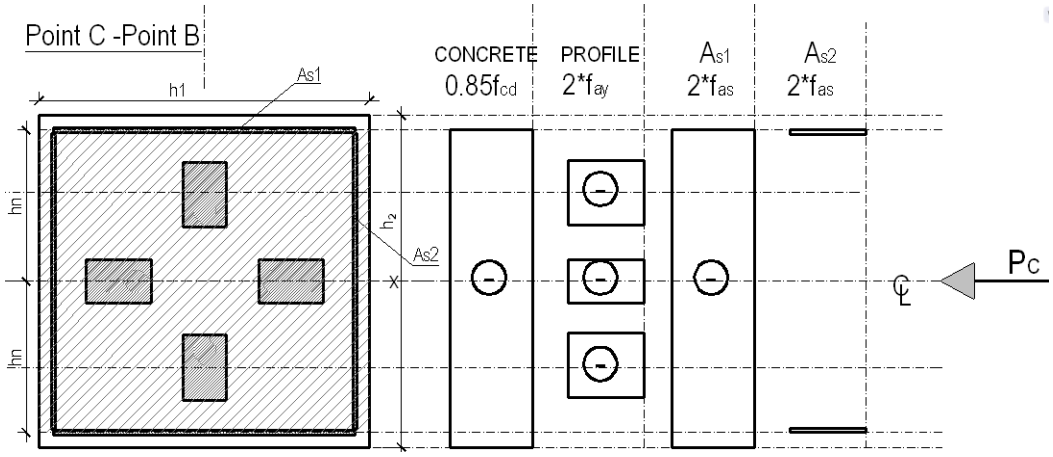

Figure 9-13 Subtracting the components of the stress distribution combination at point B & C – PNA is within the equivalent rebar plates

Scenario 6

In this scenario, $\frac{d_d}{2} + d + e + b_{s1} \leq h_n \leq \frac{h_2}{2}$.

$$N_b - N_c = 0{,}85 \,.\, A_c \,.\, f_{cd}$$

$$N_b - N_c = 2 \,.\, h_n \,.\, h_1 \,.0{,}85 \,.\, f_{cd} + 4 \,.\, A_{prof} \,.\, (f_{yd} - 0{,}85 \,.\, f_{cd}) + A_{sr2} \,.\, (f_{sd} -$$

$$0{,}85 \,.\, fcd + Asr1 \,.\, fs - 0{,}85 \,.\, fc$$

This implies that

$$h_n = \frac{0{,}85 \,.\, A_c \,.\, f_c - 4A_{prof} \,.\, (f_{yd} - 0{,}85\, f_{cd}) - A_{sr2} \,.\, (f_{sd} - 0{,}85\, f_{cd}) - A_{sr1} \,.\, (f_{sd} - 0{,}85 \,.\, f_{cd})}{2.\, h_1 .\, 0{,}85\, f_{cd}}$$

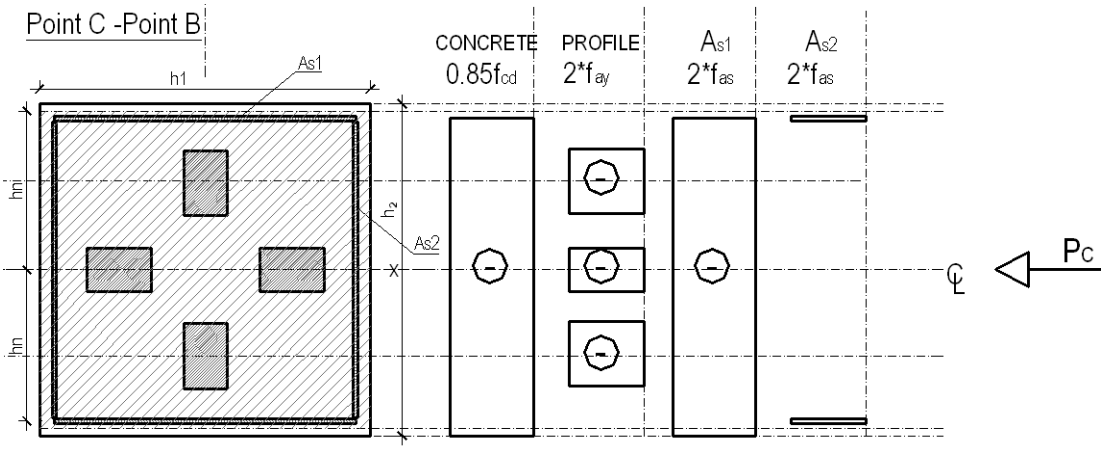

Figure 9-14 Subtracting the components of the stress distribution combination at point B & C – PNA is above the equivalent rebar plates

9.4 Evaluation of M_{plRd}.

The bending moments values corresponding to points A,B,C,D from simplified interaction curve, as shown in Figure 9-1, can be evaluated with the following expressions :

$$M_{max,Rd} = W_y \,.\, f_{yd} + W_s \,.\, f_{sd} + 0{,}5 \,.\, W_c \,.\, 0{,}85 \,.\, f_{cd}$$

$$M_{pl,Rd} = M_{max,Rd} - W_{yn} \,.\, f_{yd} + W_{sn} \,.\, f_{sd} + 0{,}5 \,.\, W_{cn} \,.\, 0{,}85 \,.\, f_{cd}$$

The notations W_y, W_s, W_c represent the plastic bending modulus of the profiles steel, rebar steel, concrete (respectively), according to the neutral axis which is situated at the axis of symmetry of the section because point D is considered. The notations W_{yn}, W_{sn}, W_{cn} represent the plastic bending modulus of the profiles steel, rebar steel, concrete (respectively), within the $2h_n$ zone. Their expressions corresponding to the considered example, examining y-axis, are given, as follows:

$$W_y = 2A_{prof} \,.\, d_{sy} + \left(\frac{d \,.\, b^{*2}}{2}\right)$$

$$W_s = A_{sr1} \,.\, d_{s1} + \left(\frac{b_{s2} \,.\, {h_{s2}}^2}{2}\right)$$

$$W_c = \left(\frac{h_1 \,.\, {h_2}^2}{4}\right) - W_y - W_s$$

If scenario 1 is encountered:

$$W_{yn} = 2d \,.\, {h_n}^2$$

$$W_{sn} = 2b_{s2} \,.\, {h_n}^2$$

$$W_{cn} = h_1 \,.\, {h_n}^2 - W_{yn} - W_{sn}$$

If scenario 2 is encountered:

$$W_{yn} = 0{,}5\, d \,.\, b^{*2}$$

$$W_{sn} = 2b_{s2} \,.\, {h_n}^2$$

$$W_{cn} = h_1 \,.\, {h_n}^2 - W_{yn} - W_{sn}$$

If scenario 3 is encountered:

$$W_{yn} = 0.5\, d \,.\, b^{*2} + 2b^* \left(h_n - \frac{d_{dy}}{2}\right) . \left(\frac{h_n}{2} + \frac{d_{dy}}{4}\right)$$

$$W_{sn} = 2b_{s2} \,.\, {h_n}^2$$

$$W_{cn} = h_1 \,.\, {h_n}^2 - W_{yn} - W_{sn}$$

If scenario 4 is encountered:

$$W_{yn} = 0{,}5\, d \,.\, b^{*2} + 2A_{prof} \,.\, d_{sy}$$

$$W_{sn} = 2b_{s2} \,.\, {h_n}^2$$

$$W_{cn} = h_1 \,.\, {h_n}^2 - W_{yn} - W_{sn}$$

If scenario 5 is encountered:

$$W_{yn} = 0{,}5\, d \,.\, b^{*2} + 2A_{prof} \,.\, d_{sy}$$

$$W_{sn} = 0{,}5\, d \,.\, b^{*2} + 2h_{s1} \left(h_n - \frac{h_{s2}}{2}\right) . \left(\frac{h_n - \frac{h_{s2}}{2}}{2} + \frac{h_{s2}}{2}\right)$$

$$W_{cn} = h_1 \,.\, {h_n}^2 - W_{yn} - W_{sn}$$

If scenario 6 is encountered:

$$W_{yn} = 0{,}5\, d \,.\, b^{*2} + 2A_{prof} \,.\, d_{sy}$$

$$W_{sn} = 0{,}5\, b_{s2} \,.\, {h_{s2}}^2 + 2h_{s1} . b_{s1} . d_{s1}$$

$$W_{cn} = h_1 \,.\, {h_n}^2 - W_{yn} - W_{sn}$$

9.5 Reduction of the N-M interaction curve due to buckling.

In order to have a realistic interaction curve, the buckling effects should be taken into account. This phenomenon of instability lowers the resisting values of bending moment and axial force.

9.5.1 Axial force reduction.

$N_{pl,b,Rd}$ is the plastic resisting axial force, considering buckling. It can be determined by multiplying $N_{pl,Rd}$ by a coefficient χ whose value is between 0 and 1. The evaluation of the coefficient is presented in the following steps.

a) First, the Euler force must be determined: $N_{cr} = \frac{\pi^2 \, EI}{{l_f}^2}$, with l_f the buckling length which depends on the element length but also on the supports. The flexural stiffness is determined with the following formula:

$$EI = E_y \, . \, I_y + E_s \, . \, I_s + K_e . E_{c,eff} . \, I_c$$

Where:

- E_y and E_s the Young modulus of profile steel and rebars steel (respectively),
- I_y, I_s and I_c the inertia of profile steel, rebars steel and concrete (respectively),
- K_e = 0,6
- $E_{c,eff} = E_{cm} \frac{1}{1 + \varphi_t . (\frac{N_{G,Ed}}{N_{Ed}})}$
- E_{cm} the Young modulus of concrete,
- φ_t the creep coefficient of concrete,
- N_{Ed} the total applied axial force,
- $N_{G,Ed}$ the permanent part of this force

b) Next, the relative slenderness can be calculated:

$$\lambda = \sqrt{N_{pl,Rk}/N_{cr}}$$

Where:

$$N_{pl,Rk} = A_s . f_{yk} + A_{sr} . f_{sk} + A_c . 0{,}85 . f_{ck.} \; - \text{ the plastic resisting axial force}$$

c) The coefficient ϕ is equal with $\phi = 0{,}5 \, . \, (1 + \alpha \, . \, (\lambda - 0{,}2) + \lambda^2)$, where α is an imperfection factor whose value depends on the choosed buckling curve. EC4 recommends to use $\alpha = 0.34$ for buckling axis y and $\alpha = 0.49$ for buckling axis z.

d) The coefficient χ is equal to:

$$\frac{1}{\phi + \sqrt{\phi^2 - \lambda^2}} \leq 1$$

9.5.2 Bending moment reduction.

$M_{pl,b,Rd}$ is the plastic resisting bending moment where the buckling effects are taken into account. If we consider a point from interaction curve that corresponds to N=0, then $M_{pl,b,Rd} = M_{pl,Rd}$.

$M_{pl,b,Rd}$ can be determined by dividing $M_{pl,Rd}$ by a coefficient k :

$$k = \frac{\beta}{1 - N_{Ed}/N_{cr,eff}}$$

With β such as defined in Figure 9-15 and with $N_{cr,eff}$ which can be calculated in the same way that N_{cr}, but by taking the length of the element instead of the buckling length.

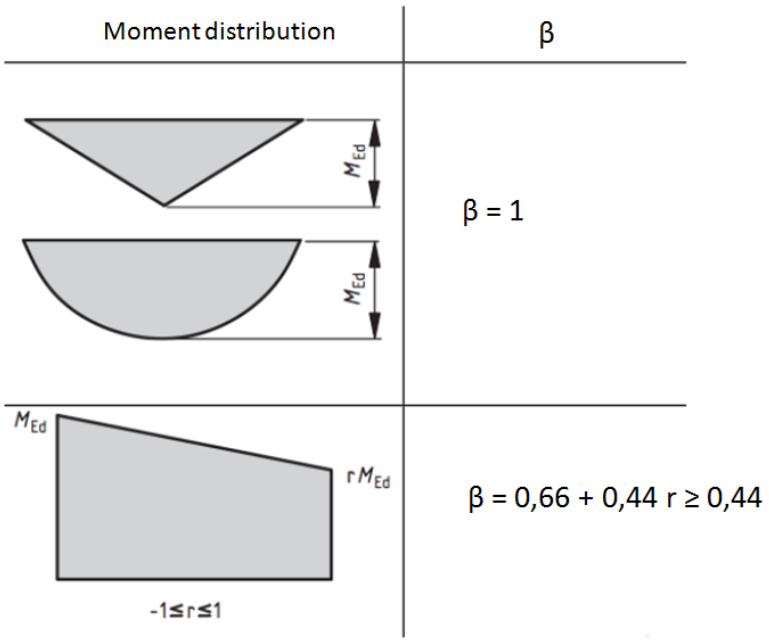

Figure 9-15 Parameter β

Also, $M_{pl,b,Rd} = M_{pl,Rd}$ if $\lambda < 0{,}2\,.\,(2 - r)$ and if $\frac{N_{Ed}}{N_{cr,eff}} < 0{,}1$, with r the ratio between the end moments.

9.6 Validation of the method using FEM numerical models and experimental results

9.6.1 FEM numerical models created in SAFIR.

SAFIR is a computer program that models the behavior of building structures. The structure can be made of a 3D skeleton of linear elements such as beams and columns, in conjunction with planar elements such as slabs and walls. Different materials such as steel, concrete, timber, aluminum, gypsum or thermally insulating products can be used separately or in combination in the model[2].

The numerical model is a 2D Bernouilli fiber element with 3 nodes and 7 degrees of freedom. This number corresponds to one rotational and two translational DOF for each of the two nodes situated at beam element ends and one relative translational DOF for the node situated at the mid-length of the beam element.

The mechanical characteristics of material laws come from EC2 for concrete and from EC3 for steel (the safety coefficients are equal to 1). For the steel elements, a bi-linear law is used while a parabolic law is used for concrete elements.

Model calibration:

First, the considered section has been defined in Safir, with the obtained material characteristics, see Figure 9-16 and Table 3-2. Two different yield strengths are used for the profile flanges and for the profile web, which result from the tests. It is to note that a perfect bond between concrete and steel is assumed in Safir.

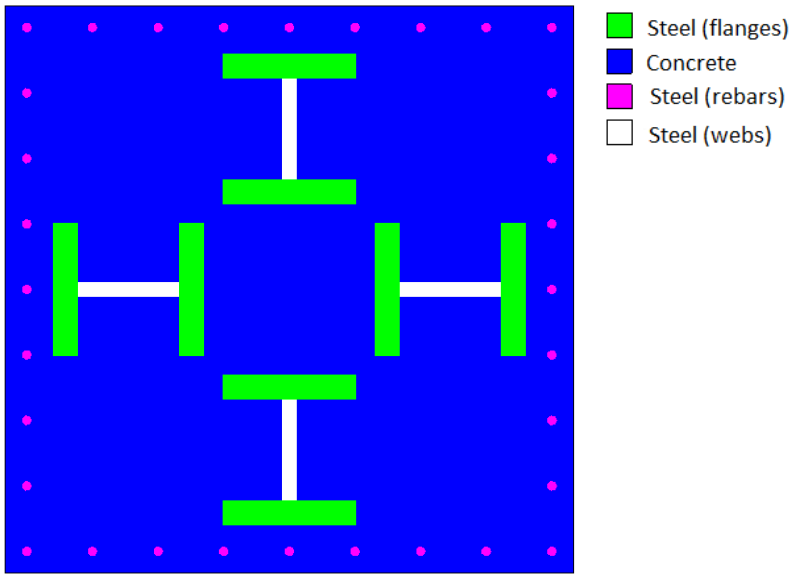

Figure 9-16 Definition of the section in Safir Software (Section 1)

[2] http://www.facsa.ulg.ac.be – ArGenCo - Safir

Definition of the numerical model is presented in Figure 9-17, the length of the specimen is 3.6m and it has an initial eccentricity of L/200 (EC4 – Table 6.5) to be able to take into account the second order effects. The vertical displacement is blocked at the bottom of the column, while the horizontal displacement is blocked at the both the top and bottom (see Figure 18). The column cross section is constant along the length of the element, shown in Figure 9-16.

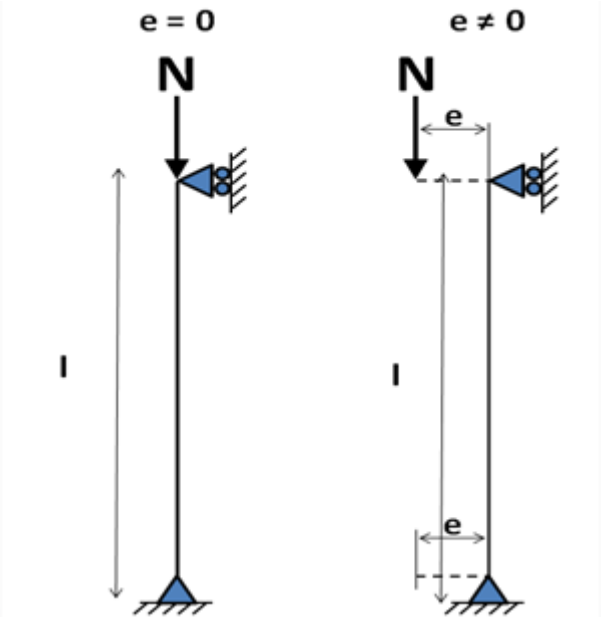

Figure 9-17 Safir – numerical model definition and experimental set-up configuration

The actual length of the tested specimen is 2.7 meters, but the test device has the distance between the two articulations of 3.6 m (Figure 9-19). To be able to take into account the real buckling length, a second cross section is defined at the extremities of the column. The section has the same geometry as the composite one, 450 x 450 mm and contains only one material, steel that has the strength of 450 MPa.

The experimental setup does not contain a constant cross-section along its element (see Figure9-18). To simplify the numerical model, a constant cross section has been defined in Safir. The specimens contains at the both extremities two I shaped steel profiles in order to simulate beam-column joints. Two composite length scenarios have then been considered, as shown in Figure 9-18 – where the Section 1 is composite and section 2 is made of steel:

- Scenario A: for which the section N°2 is assigned on the length where the metallic part is present ($\frac{3,6 - 2,7}{2} = 0,45$ meter at each end)
- Scenario B: for which the section N°2 is assigned on the length where the metallic part and the reinforced part are present (0.9 meter at each end) (see Figure 19).

The obtained results are given in the Table 9-1. The results obtained with scenarios A and B are similar and gives similar results with the experimental part. In order to keep the numerical model simple, the scheme of scenario A is considered thereafter.

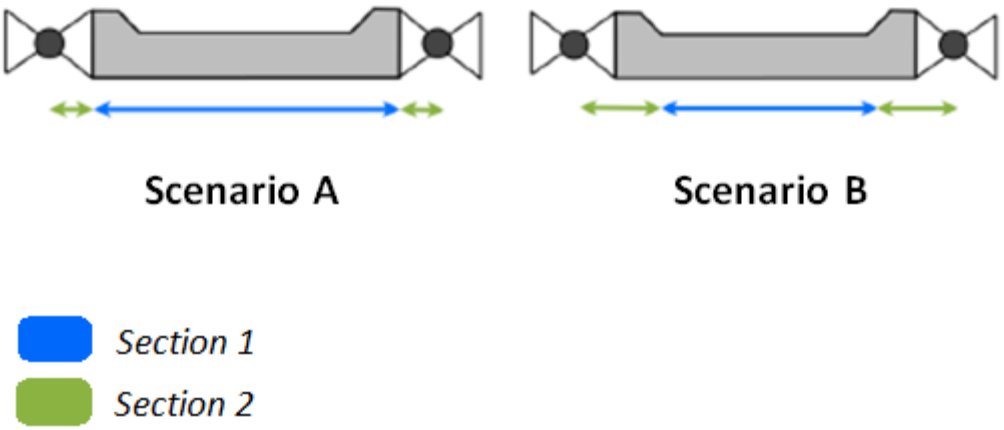

Figure 9-18 Scenario A and B considered in FEM Safir

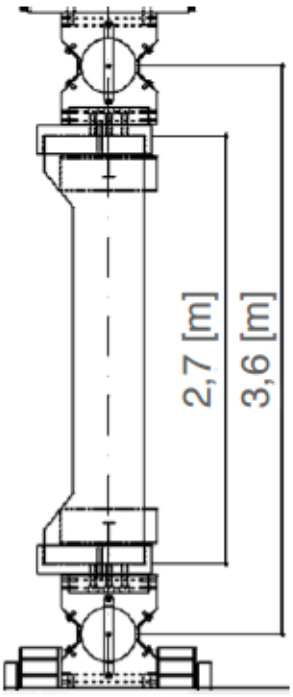

Figure 9-19 Static experimental set-up length

Table 9-1 Comparisons between Scenario A and B

Experimental												
E00-1		**E00-2**		**E10-1**		**E10-2**		**E15-1**		**E15-2**		
f_{ck} [MPa]	61.2	f_{ck} [MPa]	56.6	f_{ck} [MPa]	59.7	f_{ck} [MPa]	68.4	f_{ck} [MPa]	67.5	f_{ck} [MPa]	75.1
$f_{yk(flange)}$ [MPa]	383	$f_{yk(flange)}$ [MPa]	377	$f_{yk(flange)}$ [MPa]	398	$f_{yk(flange)}$ [MPa]	388.5	$f_{yk(flange)}$ [MPa]	408.5	$f_{yk(flange)}$ [MPa]	423
$f_{y(web)}$ [MPa]	415	$f_{y(web)}$ [MPa]	404	$f_{y(web)}$ [MPa]	411	$f_{y(web)}$ [MPa]	405	$f_{y(web)}$ [MPa]	523	$f_{y(web)}$ [MPa]	435
f_{sk} [MPa]	438	f_{sk} [MPa]	438	f_{sk} [MPa]	438	f_{sk} [MPa]	438	f_{sk} [MPa]	438	f_{sk} [MPa]	438
e [%]	0	e [%]	0	e [%]	12.4	e [%]	12.9	e [%]	19.9	e [%]	17.9
M [kNm]	0	M [kNm]	0	M [kNm]	801	M [kNm]	768	M [kNm]	1078	M [kNm]	1028
N[kN]	17082	N[kN]	15325	N[kN]	14360	N[kN]	13231	N[kN]	12041	N[kN]	12759

Safir - scenario A												
E00-1		**E00-2**		**E10-1**		**E10-2**		**E15-1**		**E15-2**		
f_{ck} [MPa]	61.2	f_{ck} [MPa]	56.6	f_{ck} [MPa]	59.7	f_{ck} [MPa]	68.4	f_{ck} [MPa]	67.5	f_{ck} [MPa]	75.1
$f_{yk(flange)}$ [MPa]	383	$f_{yk(flange)}$ [MPa]	377	$f_{yk(flange)}$ [MPa]	398	$f_{yk(flange)}$ [MPa]	388.5	$f_{yk(flange)}$ [MPa]	408.5	$f_{yk(flange)}$ [MPa]	423
$f_{y(web)}$ [MPa]	415	$f_{y(web)}$ [MPa]	404	$f_{y(web)}$ [MPa]	411	$f_{y(web)}$ [MPa]	405	$f_{y(web)}$ [MPa]	523	$f_{y(web)}$ [MPa]	435
f_{sk} [MPa]	438	f_{sk} [MPa]	438	f_{sk} [MPa]	438	f_{sk} [MPa]	438	f_{sk} [MPa]	438	f_{sk} [MPa]	438
e [%]	0	e [%]	0	e [%]	12.4	e [%]	12.9	e [%]	19.9	e [%]	17.9
M [kNm]	0	M [kNm]	0	M [kNm]	0	M [kNm]	0	M [kNm]	0	M [kNm]	0
N[kN]	19240	N[kN]	18020	N[kN]	12280	N[kN]	12800	N[kN]	10160	N[kN]	11600
ratio exp./safir	0.89	ratio exp./safir	0.85	ratio exp./safir	1.17	ratio exp./safir	1.03	ratio exp./safir	1.19	ratio exp./safir	1.10

Safir - scenario B												
E00-1		**E00-2**		**E10-1**		**E10-2**		**E15-1**		**E15-2**		
f_{ck} [MPa]	61.2	f_{ck} [MPa]	56.6	f_{ck} [MPa]	59.7	f_{ck} [MPa]	68.4	f_{ck} [MPa]	67.5	f_{ck} [MPa]	75.1
$f_{yk(flange)}$ [MPa]	383	$f_{yk(flange)}$ [MPa]	377	$f_{yk(flange)}$ [MPa]	398	$f_{yk(flange)}$ [MPa]	388.5	$f_{yk(flange)}$ [MPa]	408.5	$f_{yk(flange)}$ [MPa]	423
$f_{y(web)}$ [MPa]	415	$f_{y(web)}$ [MPa]	404	$f_{y(web)}$ [MPa]	411	$f_{y(web)}$ [MPa]	405	$f_{y(web)}$ [MPa]	523	$f_{y(web)}$ [MPa]	435
f_{sk} [MPa]	438	f_{sk} [MPa]	438	f_{sk} [MPa]	438	f_{sk} [MPa]	438	f_{sk} [MPa]	438	f_{sk} [MPa]	438
e [%]	0	e [%]	0	e [%]	12.4	e [%]	12.9	e [%]	19.9	e [%]	17.9
M [kNm]	0	M [kNm]	0	M [kNm]	0	M [kNm]	0	M [kNm]	0	M [kNm]	0
N[kN]	19300	N[kN]	18060	N[kN]	12480	N[kN]	12980	N[kN]	10320	N[kN]	11780
ratio exp./safir	0.89	ratio exp./safir	0.85	ratio exp./safir	1.15	ratio exp./safir	1.02	ratio exp./safir	1.17	ratio exp./safir	1.08

9.6.2 Validation of neutral axis position.

With Safir software, is possible to get the stress distribution in a certain section. The (N, M) values corresponding to point D of the simplified interaction curve (i.e. $N_{pm,Rd}$ and $M_{max,Rd}$) obtained with the EC4 method, using mechanical characteristics of E00-1 and E00-2 specimens, are applied to the column in Safir.

In the first case (using E00-1 data), the stress distribution in the mid-height section that is obtained is represented on Figure 9-20. It can be seen that the neutral axis (i.e. the axis where the stress have zero value) is placed at the middle of the section. This position corresponds to the position given by EC4. In the second case (using E00-2 data), the stress distribution in the mid-height section that is obtained is represented on Figure 9-21. The same conclusion can be drawn concerning the neutral axis.

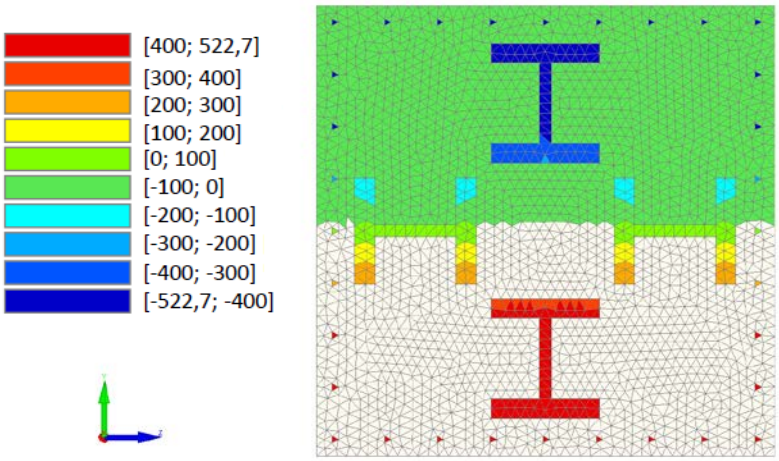

Figure 9-20 Stress distribution in the mid-height section (E00-1) subject to $N_{pm,Rd}$

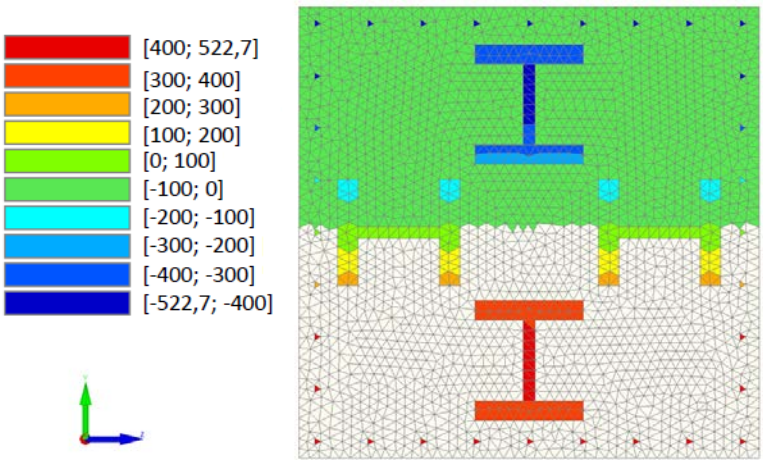

Figure 9-21 Stress distribution in the mid-height section (E00-2) subject to $N_{pm,Rd}$

9.6.3 FEM numerical models created in Abaqus.

The numerical model created in Abaqus, is presented in Figure 9-22 and contains a simplification of the experimental part. The column is considered with a constant cross section of 450 x 450 mm. The concrete and the steel sections are simulated by three dimensional eight-mode solid elements and the rebar are simulated by two dimensional three-node truss elements. The interface between concrete and steel profiles is TIE connected, while the rebar are perfectly embedded in the concrete part.

To keep the buckling length chosen by the experimental part, 5.9 m, two steel cubes are defined in the top and bottom of the composite model. The boundary conditions are defined in the reference points RP-1 and RP-2, while the force is applied in RP-2, for the models that have the axial load applied with eccentricity (E 10-1).

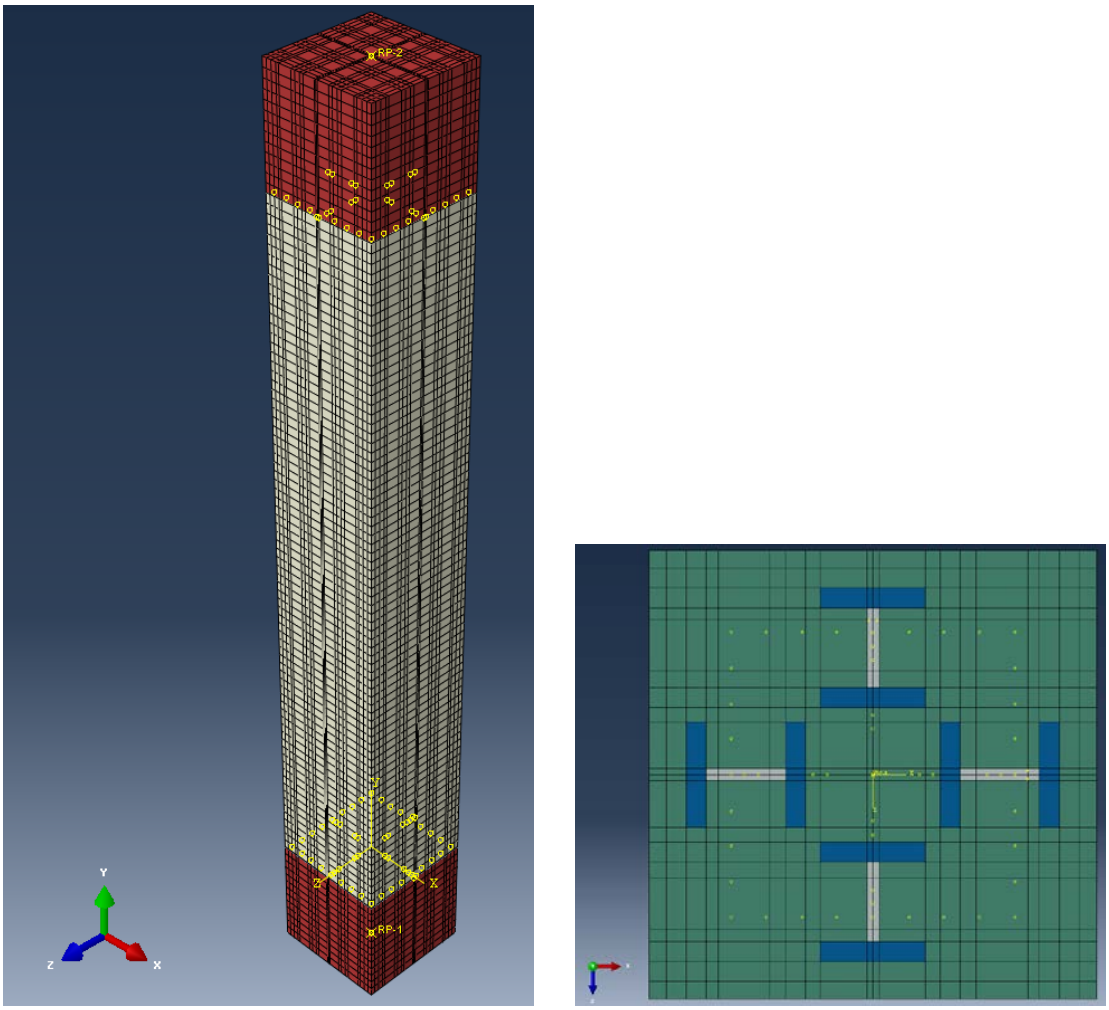

Figure 9-22 Abaqus FE Model – static specimen

The definition of the concrete behavior has been made by using a concrete damage plasticity model. The uni-axial constitutive law for concrete material has been obtained using the Eurocode 2 material law as show in Figure 9-23:

$$\frac{\sigma_c}{f_{cm}} = \frac{k\eta - \eta^2}{1 + (k-2)\eta}$$

Where:

$$\eta = {\varepsilon_c}/{\varepsilon_{c1}}$$

$$k = {1.05E_{cm} \times |\varepsilon_{c1}|}/{f_{cm}}$$

$$E_{cm} = 22[{f_{cm}}/{10}]^{0.3}$$

$$\varepsilon_{c1}(‰) = 0.7{f_{cm}}^{0.31} < 2.8$$

$$\varepsilon_{cu1}(‰) = 2.8 + 27[(98 - f_{cm})/100]^4$$

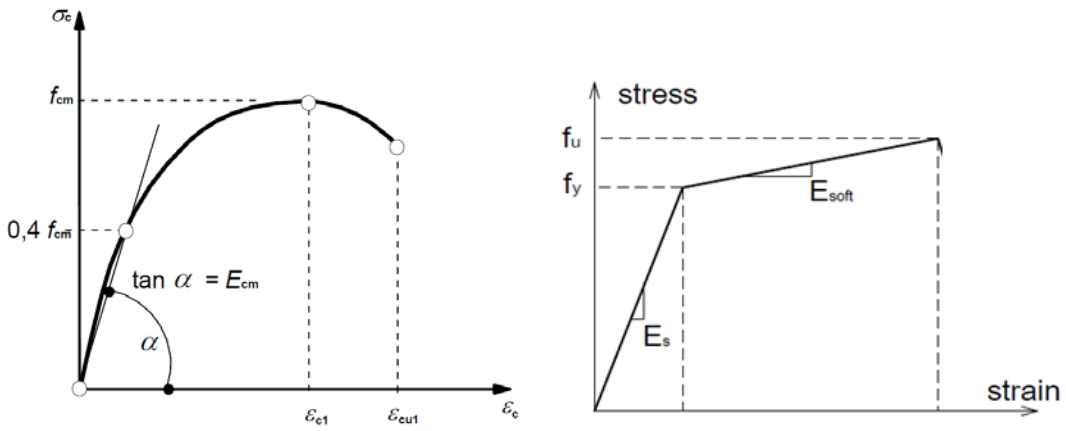

Figure 9-23 Static experimental set-up length

A bilinear constitutive model is adopted for longitudinal bar and for the steel profiles, where fu and f_y are obtained from the experimental tests, as shown in Table 9-2.

Table 9-2 Steel profile material strength – static tests

Specimen ID	Location	Yield Strength/Mpa	Ultimate Strength/Mpa	Elongation %
E00 – 1	Flange	410 407	539	33.9
	Web	523	546	27.1
E00 – 2	Flange	404 392	528	33.8
	Web	411	535	27.3
E10 – 1	Flange	433 413	554	32.4
	Web	435	568	26.0
E10 – 2	Flange	420 346	534	33.80
	Web	415	530	28.9
E15 – 1	Flange	378 376	500	32.8
	Web	404	529	29.9
E15– 2	Flange	393 384	516	34.6
	Web	405	520	30.2

Table 9-3 contains a comparison between the experimental results and the numerical models. The peak values and the corresponding displacement are compared. It can be observed that the numerical results are similar with the experimental part.

Table 9-3 Comparisons between peak load vs. corresponding deflection

Specimen ID	Experimental values		Numerical values	
	Capacity P_u /kN	Vertical deflection P_u / mm	Capacity P_u /kN	Vertical deflection P_u / mm
E00 – 1	17082	4.17	17006.8	3.98
E00 - 2	15325	3.43	15879	4.25
E10 – 1	14360	3.55	14500	3.60
E10 - 2	13231	3.46	14031	3.34
E15 – 1	12041	2.79	12521	3.35
E15 - 2	12759	2.70	13012	3.43

Figures 9-24 - 9-26 presents a comparison between the load – top displacement curves. It can be observed that for the specimens that have no eccentricity in the load application (E00-1 and E00 -2) the rigidity of the numerical model is similar with the experimental tests.

The concrete law influences the behavior of the numerical model and a slight change in the elastic modulus of the concrete material can change completely the numerical model behavior. In E10 and E15 models, there is a difference in the rigidity, but the peak values of the axial force are obtained at a similar top displacement, as shown in Table 9-3.

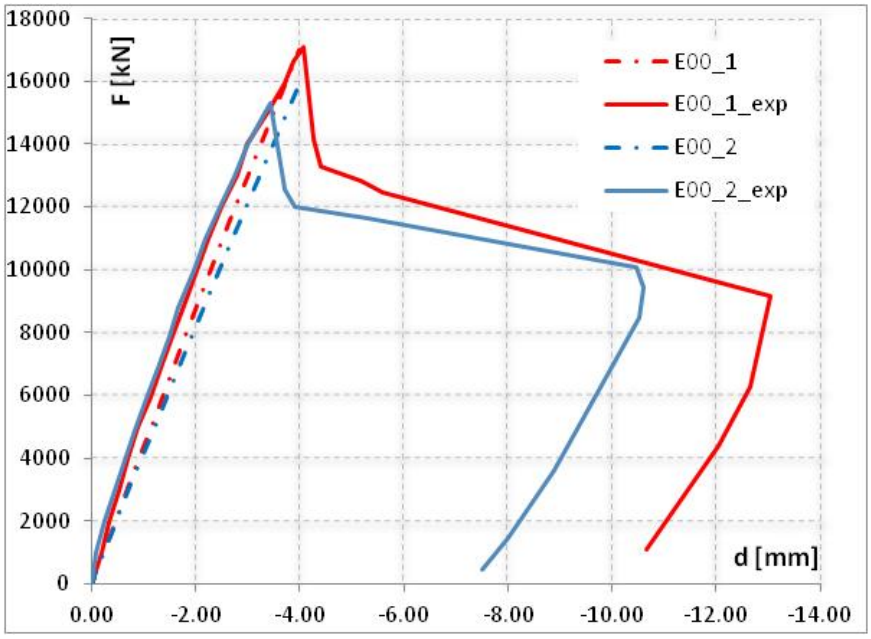

Figure 9-24 Deformed shape for E00-1 and E00-2 specimens

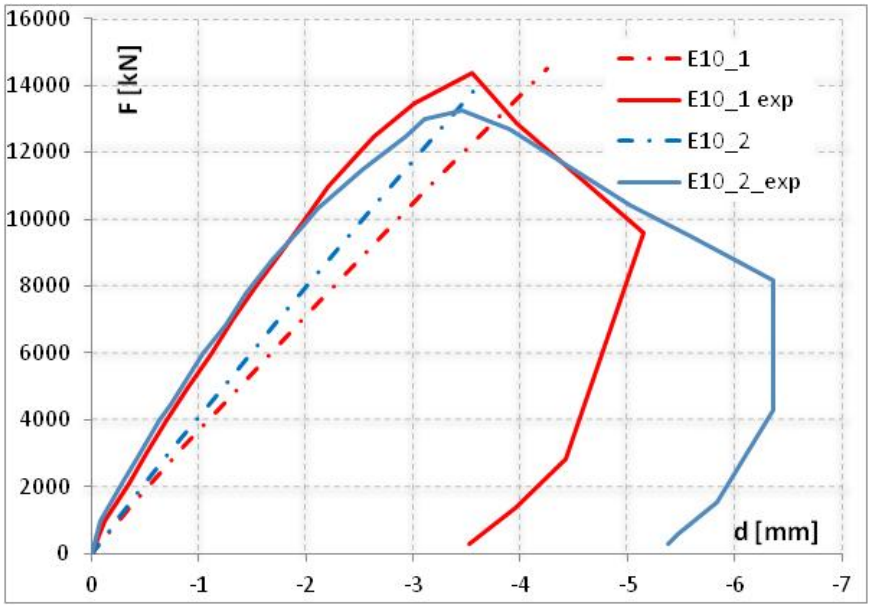

Figure 9-25 Deformed shape for E10-1 and E10-2 specimens

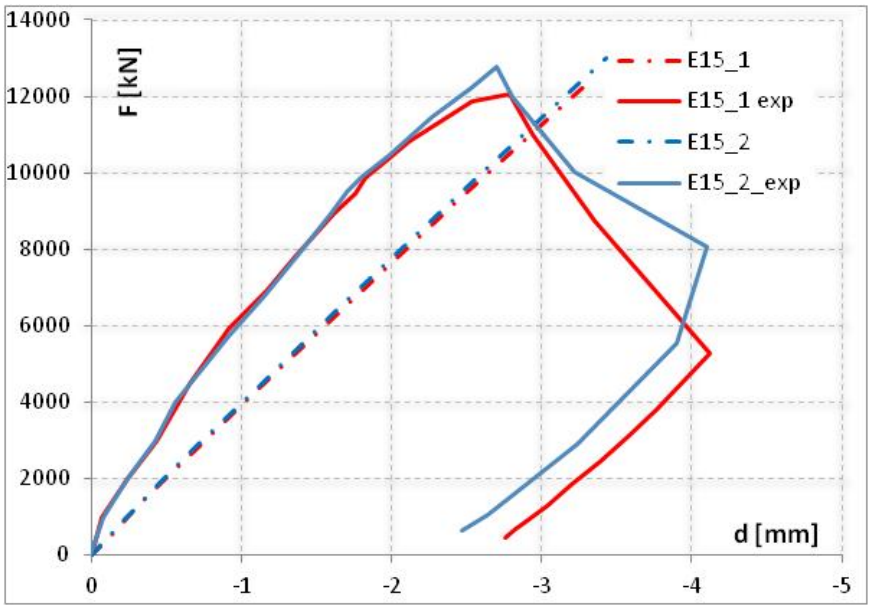

Figure 9-26 Deformed shape for E15-1 and E15-2 specimens

A new extended method based on Eurocode 4 design has been developed in order to design the composite columns with several steel profiles embedded. The method is an extension of the Plastic Distribution Method and takes into account all the assumptions that are defined in EC 4 - Clause 6.7.

Two numerical models have been created in order to simulate the behavior experimental tests. Simplified model have been chosen to facilitate furthermore a parametric study of the steel-concrete composite columns.

Figures 9-27- 9-29 presents a comparison between the adapted simplified method, the experimental results and the two simplified numerical model created in Abaqus and Safir. It can be observed that similar result to the experimental part is obtained by using the Simplified Method.

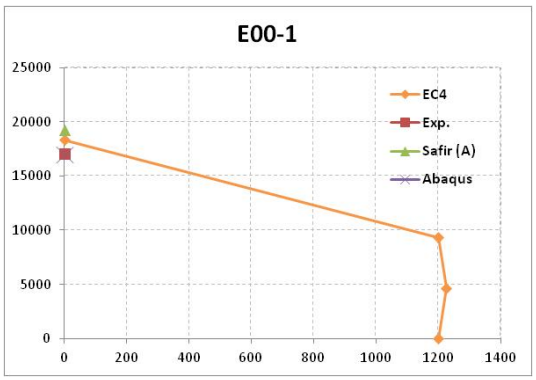

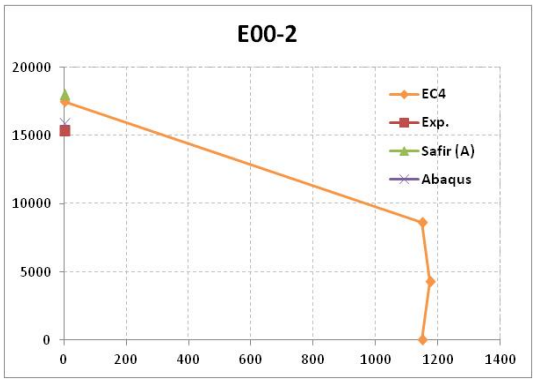

Figure 9-27 N – M Interaction curves for specimens E00-1 and E00-2

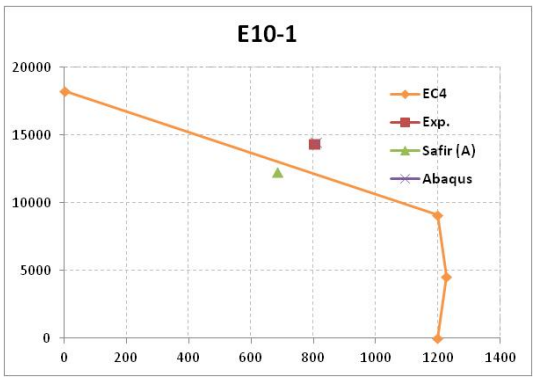

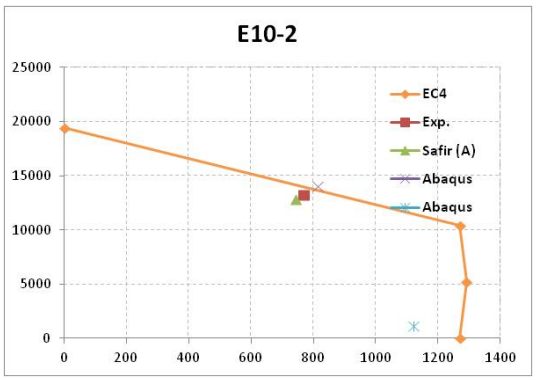

Figure 9-28 N – M Interaction curves for specimens E10-1 and E10-2

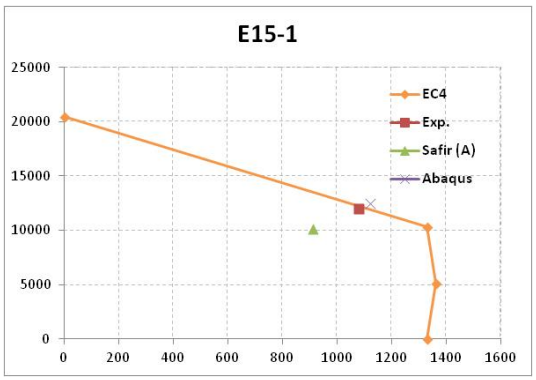

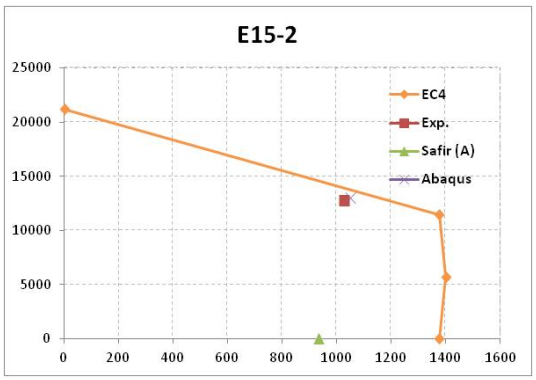

Figure 9-29 N – M Interaction curves for specimens E15-1 and E15-2

10 Simplified Design method and examples of codes application

10.1 Case 1: Eurocode 4

10.1.1 Example 1

Example 1: Composite column with four encased profiles in combined axial compression and flexure about the (x-x) axis, and the steel profiles are in the same orientation.

Given: The encased composite member, illustrated in Figure 10-1, is subject to axial force, bending moment, and shear force. The composite member consists of 4 HD 400x1299 ASTM A913- 11 grade steel profiles, encased in concrete with a specified compressive strength of 50 MPa, and 224 rebar with 40 mm diameter, S500 grade distributed in 2 layers at the perimeter. The buckling length (L_o) of the column is 18 m.

Check that the capacity of the composite column it is subject to the following demands:

N_{Ed} = 300000 kN;

M_{Ed} = 250000 kN;

V_{Ed} = 20000 kN;

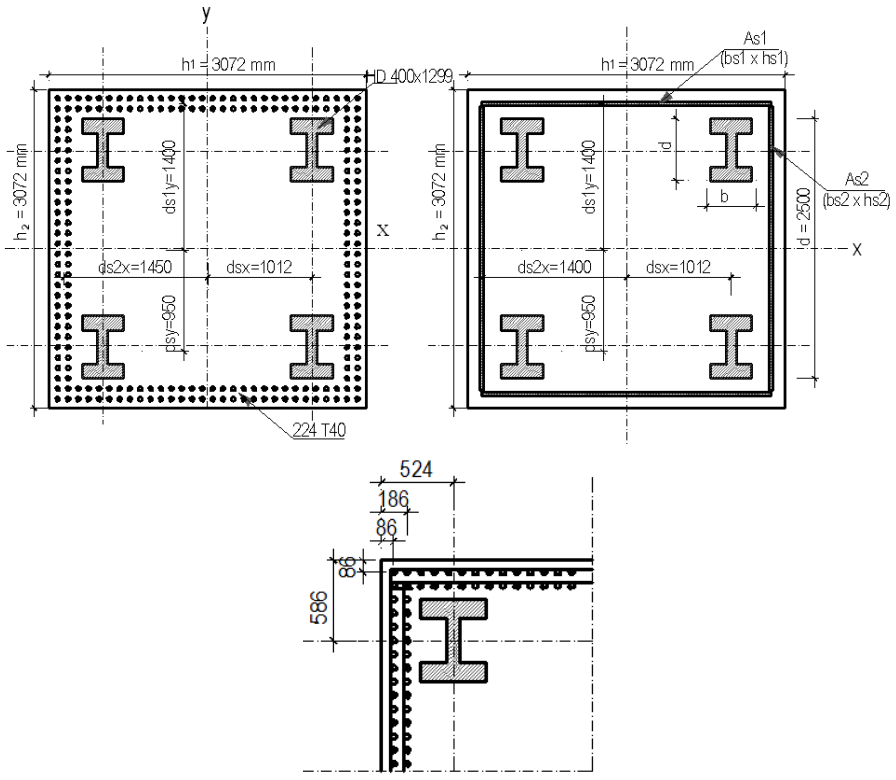

Figure 10-1 Encased composite member section (EC4 Design) – Example 1

Steel profile HD 400x1299 (W14x16x873) properties are:

ASTM A913- 11 Grade 65 - f_y = 450MPa;

E_s = 210000 MPa;

b = 476 mm;

d = 600 mm;

t_w = 100 mm;

t_f = 140 mm;

Z_{sx} = 33250 cm^3;

Z_{sy} = 16670 cm^3;

$I_{HDx} = 754600 \cdot 10^4 \text{mm}^4$;

$I_{HDy} = 254400 \cdot 10^4 \text{mm}^4$;

A_a = 165000 mm^2;

$A_s = \sum_{i=1}^{4} A_a = 4 \cdot 165000\text{mm}^2 = 660000\text{mm}^2$;

d_{sx} = 1012 mm;

d_{sy} = 950mm;

d_x = 2500 mm;

d_y = 2500mm;

Reinforcement properties are:

224 = total amount of vertical rebar;

d_b = 40mm for a T40 diameter bar;

f_s = 500MPa;

E_{sr} = 200000 MPa;

$A_{sri} = 1256.63\text{mm}^2$;

$A_{sr} = \sum_{i=1}^{n} A_{sri} = 281486.7\text{mm}^2$;

Concrete section's properties are:

h_1 = 3072mm;

h_2 = 3072mm;

c_x = 86mm;

c_y = 86mm;

Concrete class C50: f_{ck} = 50MPa;

$f_{cm} = f_{ck} + 8$ MPa=58 MPa;

$E_{cm} = 22 \cdot \left(\frac{f_{cm}}{10} \right)^{0.3} = 22 \cdot \left(\frac{58}{10} \right)^{0.3} = 37278\text{MPa}$;

$A_g = h_1 \cdot h_2 = (3072\text{mm}) \times (3072\text{mm}) = 9437184\text{mm}^2$;

Solution:

- **The partial safety factors for materials:**

To determine resistance, the following partial safety factors should be applied to the following materials:

γ_a the partial factor for structural steel

γ_s the partial factor for the reinforcement

γ_c the partial factor for reinforced concrete

Thus:

$f_{yd} = f_y / \gamma_a = 450\text{MPa} / 1 = 450\text{MPa}$

the design value of yield strength of the structural steel

$f_{sd} = f_s / \gamma_a = 500\text{MPa} / 1.15 = 434.78\text{MPa}$

the design value of yield strength of the reinforcement

$f_{cd} = f_c / \gamma_c = 50\text{MPa} / 1.5 = 33.33\text{MPa}$

the design value of yield strength of the concrete

- **Definition of plates equivalent to rebar:**

The definition of the equivalent horizontal plates (A_{s1} and A_{s2}) is based off the following:

1) A_{s1} plate:

i = 2 = the amount of rebar layers in one equivalent plate

n_x = 30 = the amount of rebar in one layer

s_x = 100 mm = the spacing between 2 vertical rebar

$$A_{s1} = i \cdot n_x \cdot A_{sri} = 2 \cdot 30 \cdot 1256.64\text{mm}^2 = 75398.2\text{mm}^2$$

$$b_{s1} = \frac{A_{s1}}{h_{s1}} = \frac{75398.2\text{mm}^2}{2900\text{mm}} = 26\text{mm}$$

$$d_{1y} = \frac{3072\text{mm}}{2} - 86\text{mm} = 1450\text{mm}$$

$$d_{2y} = \frac{3072\text{mm}}{2} - 186\text{mm} = 1350\text{mm}$$

$$d_{s1y} = \sum d_{iy} / i = (1450\text{mm} + 1350\text{mm}) / 2 = 1400\text{mm}$$

$$Z_{sr1x} = 2 \cdot A_{s1} \cdot d_{s1y} = 2 \cdot 75398.2\text{mm}^2 \cdot 1400\text{mm} = 2.1112 \cdot 10^8\,\text{mm}^3$$

$$I_{sr1x} = 2 \cdot \text{i} \cdot n_x \cdot A_{sri} \cdot d_{s1y}{}^2 = 2 \cdot 2 \cdot 30 \cdot 1256.64\text{mm}^2 \cdot (1400\text{mm})^2 = 2.9556 \cdot 10^{11}\,\text{mm}^4$$

2) A_{s2} plate:

$A_{s2} = n_y \cdot A_{sri} = b_{s2} \cdot h_{s2}$

j = 2 = the number of rebar layers in one equivalent plate

n_y = 26 = the number of rebar in one layer

$A_{s2} = j \cdot n_y \cdot A_{sri} = 2 \cdot 26 \cdot 1256.64\text{mm}^2 = 65345.1\text{mm}^2$

$h_{s2} = (n_y - 1) \cdot s_y = 25 \cdot 100\text{mm} = 2500\text{mm}$

$b_{s2} = \frac{A_{s2}}{h_{s2}} = \frac{65345\text{mm}^2}{2500\text{mm}} = 26.1\text{mm}$

$d_{1x} = \frac{3072\text{mm}}{2} - 86\text{mm} = 1450\text{mm}$

$d_{2x} = \frac{3072\text{mm}}{2} - 186\text{mm} = 1350\text{mm}$

$d_{s2x} = \sum d_{jx} / j = 1450\text{mm} + 1350\text{mm} / 2 = 1400\text{mm}$

$Z_{sr2x} = 2 \cdot \frac{b_{s2} \cdot h_{s2}^2}{4} = \frac{26.1\text{mm} \cdot (2500\text{mm})^2}{2} = 8.168 \cdot 10^7\,\text{mm}^3$

$I_{sr2x} = 2 \cdot \frac{b_{s2} \cdot h_{s2}^3}{12} = \frac{26.1\text{mm} \cdot (2500\text{mm})^3}{6} = 6.807 \cdot 10^{10}\,\text{mm}^4$

- **Definition of plates equivalent to steel profiles:**

The definition of the equivalent horizontal plates is made according to the following:

$d^* = d = 600\text{mm}$

$b^* = \frac{A_s}{d^*} = \frac{6.6 \cdot 10^5\,\text{mm}^2}{600\text{mm}} = 275\text{mm}$

$Z_{sx} = n \cdot A_a \cdot d_{sy} = 4 \cdot 1.65 \cdot 10^5\,\text{mm}^2 \cdot 950\text{mm} = 6.27 \cdot 10^8\,\text{mm}^3$

$I_{sx} = n \cdot A_a \cdot d_{sy}^2 + n \cdot I_x = 4 \cdot 1.65 \cdot 10^5\,\text{mm}^2 \cdot (950\text{mm})^2 + 4 \cdot 7.564 \cdot 10^9\,\text{mm}^4 = 6.258 \cdot 10^{11}\,\text{mm}^4$

- **Stiffness evaluation:**

$$(EI)_{eff} = E_s \cdot I_s + E_{sr} \cdot I_{sr} + K_e \cdot E_{c,eff} \cdot I_c$$
$$= 2.1 \cdot 10^5 \text{MPa} \cdot 6.258 \cdot 10^{11} \text{mm}^4 + 2.0 \cdot 10^5 \text{MPa} \cdot (2.955 \cdot 10^{11} \text{mm}^4 + 6.81 \cdot 10^{10} \text{mm}^4) +$$
$$+0.6 \cdot 1.75 \cdot 10^4 \text{MPa} \cdot 6.43 \cdot 10^{12} \text{mm}^4$$
$$= 2.719 \cdot 10^{17} \text{N} \cdot \text{mm}^2$$

$$N_{cr} = \frac{\pi^2 \cdot (EI)_{eff}}{L_o^2} = \frac{\pi^2 \cdot 2.719 \cdot 10^{17} \text{N} \cdot \text{mm}^2}{(18\text{m})^2} = 8.281 \cdot 10^9 \text{N}$$

$$E_{c,eff} = E_{cm} \frac{1}{1 + \left(N_{G,Ed} / N_{Ed} \right) \cdot \varphi_t} = E_{cm} \frac{1}{1 + 0.75 \cdot 1.5} = 0.47 \cdot 37278 \text{ MPa} = 17543 \text{ MPa}$$

where:

- $K_e = 0.6$ the correction factor
- φ_t is the creep coefficient according to EN 1992-1-1, 3.1.4 or 11.3.3, depending on the age (t) of the concrete at the moment considered at the age (t_o) at loading. In this example, we consider the creep coefficient equal to 1.5.
- N_{Ed} is the total design force
- $N_{G,Ed}$ is the part of the normal force that is permanent

In high-rise buildings, there is a significant amount of long-term loads, approximately 75% of total loads. Therefore, the ratio of the normal forces in this example is considered equal to:

$$N_{G,Ed} / N_{Ed} = 0.75$$

- **Limitation when using the extended simplified method:**

1) The steel contribution ratio δ should fulfill the following condition $0.2 < \delta < 0.9$

$$\delta = \frac{A_s \cdot f_{yd}}{N_{pl.Rd}} = \frac{6.6 \cdot 10^5 \text{mm}^2 \cdot 450\text{MPa}}{660096.9\text{kN}} = 0.45 \qquad \text{EN 1994-1-1:2004 – Eq (6.27)}$$

where:

$$N_{pl.Rd} = A_s \cdot f_{yd} + A_{sr} \cdot f_{sd} + 0.85 \cdot A_c \cdot f_{cd}$$
$$= 6.6 \cdot 10^5 \text{mm}^2 \cdot 450\text{MPa} + 3.81 \cdot 10^5 \text{mm}^2 \cdot 434.78\text{MPa} + 8.455 \cdot 10^6 \text{mm}^2 \cdot (0.85 \cdot 33.3\text{MPa})$$
$$= 660096.9\text{kN}$$

2) The relative slenderness $\bar{\lambda} \le 2$

$$\bar{\lambda} = \sqrt{\frac{N_{pl.Rk}}{N_{cr}}} = \sqrt{\frac{797810\text{kN}}{5.476 \cdot 10^{10}\text{kN}}} = 0.121 < 2 \qquad \text{EN 1994-1-1:2004 – Eq (6.28)}$$

where

$$\begin{aligned} N_{pl.Rk} &= A_s \cdot f_y + A_{sr} \cdot f_{sy} + 0.85 \cdot A_c \cdot f_{ck} \\ &= 6.6 \cdot 10^5\,\text{mm}^2 \cdot 450\text{MPa} + 3.81 \cdot 10^5\,\text{mm}^2 \cdot 500\text{MPa} + 8.455 \cdot 10^6\,\text{mm}^2 \cdot (0.85 \cdot 50\text{MPa}) \\ &= 798810\text{kN} \end{aligned}$$

$$N_{cr} = \frac{\pi^2 \cdot (EI)_{eff}}{L_o^2} = \frac{\pi^2 \cdot 2.719 \cdot 10^{17}\,\text{N} \cdot \text{mm}^2}{(18\text{m})^2} = 8.281 \cdot 10^9\,\text{N}$$

3) Other limitations

- Longitudinal reinforcement area:

$$0.3\% \le \frac{A_{sr}}{A_c} = \frac{2.814 \cdot 10^5\,\text{mm}^2}{8.50 \cdot 10^6\,\text{mm}^2} = 3.31\% \le 6\%$$

For a fully encased section, limits to minimum and maximum thickness to concrete cover are based off of EN 1994-1-1:2004 – Eq (6.29):

$40\text{mm} \le c_y = 286\text{ mm} \le 0.3h_2 = 921\text{ mm}$

$40\text{mm} \le c_x = 286\text{ mm} \le 0.3h_1 = 921\text{ mm}$

- The ratio of the cross-section depth h_2 to width h_1, should be within the limits:

$0.2 \le h_1 / h_2 = 1 \le 5.0$ EN 1994-1-1:2004 –Clause 6.7.3.1(4)

- **Interaction of axial force and flexure:**

In order to determine the axial force N – bending moment M interaction curve, critical points are determined. The detailed definition of such points is as follows:

- A – pure axial capacity point

$N_A = N_{pl.Rd}$

$M_A = 0$ MPa

- B - pure flexural bending point

$N_B = 0$

$M_B = M_{pl,Rd}$

- C – point with bending moment equal to the pure bending capacity and axial compressive load greater than 0

$N_C = N_{pm,Rd}$

$M_C = M_{pl,Rd}$

- D – the maximum bending moment point

$N_D = 0{,}5 \; . \; N_{pm,Rd}$

$M_D = M_{max,Rd}$

Rigid – plastic material behavior is assumed in order to evaluate these key points. Steel is assumed to have reached yield stress in either tension or compression. Concrete is assumed to have reached its peak stress in compression and have the tensile strength equal to zero. For one equivalent rectangular stress block, the peak stress in compression in this example is:

$$0.85 \cdot f_{cd} = 0.85 \cdot 33.3\text{MPa} = 28.3\text{MPa}$$

- **Evaluation of the plastic resistance to axial force $N_{pl,Rd}$ and $N_{pm,Rd}$:**

The plastic resistance to axial force combines the individual resistances of the steel profile, the concrete and reinforcement. For fully or partially concrete – encased steel sections:

$$\begin{aligned} N_{pl.Rd} &= A_s \cdot f_{yd} + (A_{s1} + A_{s2}) \cdot f_{sd} + A_c \cdot 0.85 \cdot f_{cd} \\ &= 6.6 \cdot 10^5 \cdot \text{mm}^2 \cdot 450\text{MPa} + (7.54 \cdot 10^4 \cdot \text{mm}^2 + 6.53 \cdot 10^4 \cdot \text{mm}^2) \cdot 434.7\text{MPa} + \\ &\quad + 8.5 \cdot 10^6 \cdot \text{mm}^2 \cdot 0.85 \cdot 33.3\text{MPa} \\ &= 660097\text{kN} \end{aligned}$$

$$\begin{aligned} N_{pm.Rd} &= A_c \cdot 0.85 \cdot f_{cd} \\ &= 8.5 \cdot 10^6 \text{mm}^2 \cdot 0.85 \cdot 33.3\text{MPa} \\ &= 240711\text{kN} \end{aligned}$$

$$\begin{aligned} 0.5 \cdot N_{pm.Rd} &= 0.5 \cdot A_c \cdot 0.85 \cdot f_{cd} \\ &= 0.5 \cdot 8.5 \cdot 10^6 \text{mm}^2 \cdot 0.85 \cdot 33.3\text{MPa} \\ &= 120356\text{kN} \end{aligned}$$

- **Evaluation of the reduced axial force parameter χ:**

The reduction factor χ for relevant buckling mode in terms of relative slenderness is determined with the following formulae:

$$\chi = \frac{1}{\phi + \sqrt{\phi^2 - \lambda^2}} \leq 1$$

$$\chi = \frac{1}{0.567 + \sqrt{0.567^2 - 0.311^2}} = 0.960$$

Where:

$$\phi = 0.5 \cdot \left(1 + \alpha \cdot (\lambda - 0.2) + \lambda^2\right) = 0.5 \cdot \left(1 + 0.34 \cdot (0.311 - 0.2) + 0.311^2\right) = 0.567$$

$\alpha = 0.34$ - parameter that depends on the chosen buckling curve defined in EN 1994-1-1 Table 6.5. EC4 recommends using $\alpha = 0.34$ for buckling axis y and $\alpha = 0.49$ for buckling axis z.

In conclusion, the amplification factor of the axial force will be considered as equal with:

$$\chi = 0.96$$

$$N_{pl.b.Rd} = \chi \cdot N_{pl.Rd} = 0.96 \cdot 660097 \text{ kN} = 633833 \text{ kN}$$

$$N_{pm.b.Rd} = \chi \cdot N_{pm.Rd} = 0.96 \cdot 240071 \text{ kN} = 231134 \text{ kN}$$

where:

$N_{pl,b,Rd}$ is the plastic resisting axial force, considering the buckling effects

- **Evaluation of the maximum moment resistance $M_{max.Rd}$:**

$$\begin{aligned} M_{max.Rd} &= Z_{sx} \cdot f_{yd} + \left(Z_{r1x} + Z_{r2x}\right) \cdot f_{sd} + 0.5 \cdot Z_{cx} \cdot \left(0.85 \cdot f_{cd}\right) \\ &= 6.27 \cdot 10^8 \text{mm}^3 \cdot 450\text{MPa} + \left(2.111 \cdot 10^8 \text{mm}^3 + 8.168 \cdot 10^8 \text{mm}^3\right) \cdot 434.7\text{MPa} + \\ &\quad + 0.5 \cdot 6.33 \cdot 10^9 \text{mm}^3 \cdot \left(0.85 \cdot 33.3\text{MPa}\right) \\ &= 499099\text{kNm} \end{aligned}$$

$$\begin{aligned} Z_{cx} &= \frac{h_1 \cdot h_2^2}{4} - Z_{r1x} - Z_{r2x} - Z_{sx} \\ &= \frac{3072\text{mm} \cdot (3072\text{mm})^2}{4} - 2.111 \cdot 10^8 \text{mm}^3 - 8.168 \cdot 10^8 \text{mm}^3 - 6.27 \cdot 10^8 \text{mm}^3 \\ &= 6.33 \cdot 10^9 \text{mm}^3 \end{aligned}$$

- **Evaluation of the plastic bending moment resistance $M_{pl.Rd}$:**

In order to evaluate the plastic bending moment value, first we need to determine the position of the neutral axis. Different assumptions of the neutral axis position have been taken into consideration. The position of the neutral axis is determined by subtracting the stress distribution combination at point B and C, considering normal forces only.

Assumption 1: h_{nx} between the two profiles $\left(h_{nx} \le d_{sy} - \frac{d}{2}\right)$:

$$\begin{aligned} h_{nx} &= \frac{N_C}{(2 \cdot h_1 - 4 \cdot b_{s2}) \cdot \left(0.85 \cdot f_{cd}\right) + 4 \cdot b_{s2} \cdot f_{sd}} \\ &= \frac{240711\text{kN}}{(2 \cdot 3072\text{mm} - 4 \cdot 26.1\text{mm})\left(0.85 \cdot 33.3\text{MPa}\right) + 4 \cdot 26.1\text{mm} \cdot 434.7\text{MPa}} \\ &= 975.4\text{mm} \end{aligned}$$

Check assumption $\left(h_{nx} \le d_{sy} - \frac{d}{2}\right)$: assumption **not ok**

$$h_{nx} = 975.4\text{mm} \le d_{sy} - \frac{d}{2} = 950\text{mm} - \frac{600\text{mm}}{2} = 650\text{mm}$$

Assumption 2: h_{nx} is placed within the steel profiles $\left(d_{sy} - \frac{d}{2} < h_{nx} \le d_{sy} + \frac{d}{2} \right)$:

$$h_{nx} = \frac{N_C + 4 \cdot (d_{sy} - d/2) \cdot b^* \cdot (f_{yd} - 0.85 \cdot f_{cd})}{(2 \cdot h_1 - 4 \cdot b^* - 4 \cdot b_{s2}) \cdot (0.85 \cdot f_{cd}) + 4 \cdot b^* \cdot f_{yd} + 4 \cdot b_{s2} \cdot f_{sd}}$$

$$= \frac{240711\text{kN} + 4 \cdot (950\text{mm} - 600\text{mm}/2) \cdot 275\text{mm} \cdot (434.7\text{MPa} - 0.85 \cdot 33.3\text{MPa})}{(2 \cdot 3072\text{mm} - 4 \cdot 275\text{mm} - 4 \cdot 26.1\text{mm})(0.85 \cdot 33.3\text{MPa}) + 4 \cdot 26.1\text{mm} \cdot 434.7\text{MPa} + 4 \cdot 275\text{mm} \cdot 450\text{MPa}}$$

$$= 1032\text{mm}$$

Check assumption $\left(d_{sy} - \frac{d}{2} < h_{nx} \le d_{sy} + \frac{d}{2} \right)$: assumption **ok**

$$d_{sy} - \frac{d}{2} = 950\text{mm} - \frac{600\text{mm}}{2} = 650\text{mm} < h_{nx} = 1032\text{mm} \le d_{sy} + \frac{d}{2} = 950\text{mm} + \frac{600\text{mm}}{2} = 1250\text{mm}$$

$$M_{pl.Rd} = M_{max.Rd} - Z_{r2xn} \cdot f_{sd} - Z_{sxn} \cdot f_{yd} - 1/2 \cdot Z_{cxn} \cdot (0.85 \cdot f_{cd})$$

$$= 499099\text{kNm} - 5.57 \cdot 10^7\,\text{mm}^3 \cdot 434.7\text{MPa} - 3.938 \cdot 10^8\,\text{mm}^3 \cdot 450\text{MPa} -$$

$$- 1/2 \cdot 2.824 \cdot 10^9\,\text{mm}^3 \cdot (0.85 \cdot 33.3\text{MPa})$$

$$= 427820\text{kNm}$$

where:

$$Z_{sxn} = b^* \cdot \left[h_{nx} - \left(d_{sy} - d/2 \right) \right] \cdot \left[3 \cdot h_{nx} + \left(d_{sy} - d/2 \right) \right]$$

$$= 275\text{mm} \cdot \left[1032\text{mm} - \left(950\text{mm} - 600\text{mm}/2 \right) \right] \cdot \left[3 \cdot 1032\text{mm} + \left(950\text{mm} - 600\text{mm}/2 \right) \right]$$

$$= 3.938 \cdot 10^8\,\text{mm}^3$$

$$Z_{r2xn} = 2 \cdot b_{s2} \cdot h_{nx}^2$$

$$= 2 \cdot 26.1\text{mm} \cdot (1032\text{mm})^2$$

$$= 5.570 \cdot 10^7\,\text{mm}^3$$

$$Z_{cxn} = h_1 \cdot h_{nx}^2 - Z_{r2xn} - Z_{sxn}$$

$$= 3072\text{mm} \cdot (1032\text{mm})^2 - 5.570 \cdot 10^7\,\text{mm}^3 - 3.938 \cdot 10^8\,\text{mm}^3$$

$$= 2.824 \cdot 10^9\,\text{mm}^3$$

- **Evaluation of the reduced interaction curve axial force bending moment:**

$$M_{pl.b.Rd} = {M_{pl.Rd}}/{k}$$

where:

$M_{pl,b,Rd}$ is the plastic resisting bending moment where the buckling effects are taken into account.

$$k = \frac{\beta}{1 - {N_{Ed}}/{N_{cr,eff}}} = \frac{1}{1 - {180000\text{kN}}/{8.09 \cdot 10^6\,\text{kN}}} = 1.04$$

β coefficient is defined in EN 1994-1-1 Table 6.4 – depends on the distribution of the bending moment along the element. In this example, the coefficient is considered equal with $\beta = 1$

$$N_{cr,eff} = N_{cr}$$

$M_{pl,b,Rd} = M_{pl,Rd}$ if $\lambda < 0{,}2\,.\,(2 - r)$ and if $\frac{N_{Ed}}{N_{cr,eff}} < 0{,}1$, with r the ratio between the end moments.

- **Interaction curve bending moment axial force:**

The plastic distribution method gives the following values:

Point A : $N_A = N_{pl.Rd} = 660096\text{kN}$ $M_A = 0$ kNm

Point B : $N_B = 0$ $M_B = M_{pl,Rd} = 427820$ kNm

Point C : $N_C = N_{pm,Rd} = 240711.4$ kN $M_C = M_{pl,Rd} = 427820$ kNm

Point D: $N_D = 0{,}5\,.\,N_{pm,Rd} = 120355.7$ kN $M_D = M_{max,Rd} = 499099$ kNm

Considering the buckling effects:

Point A': $N_A = N_{pl.Rd} = 633833\text{kN}$ $M_A = 0$ kNm

Point B': $N_B = 0$ $M_B = M_{pl,Rd} = 427819$ kNm

Point C': $N_C = N_{pm,Rd} = 231134$ kN $M_C = M_{pl,Rd} = 427819$ kNm

Point D': $N_D = 0{,}5\,.\,N_{pm,Rd} = 115567$ kN $M_D = M_{max,Rd} = 499098$ kNm

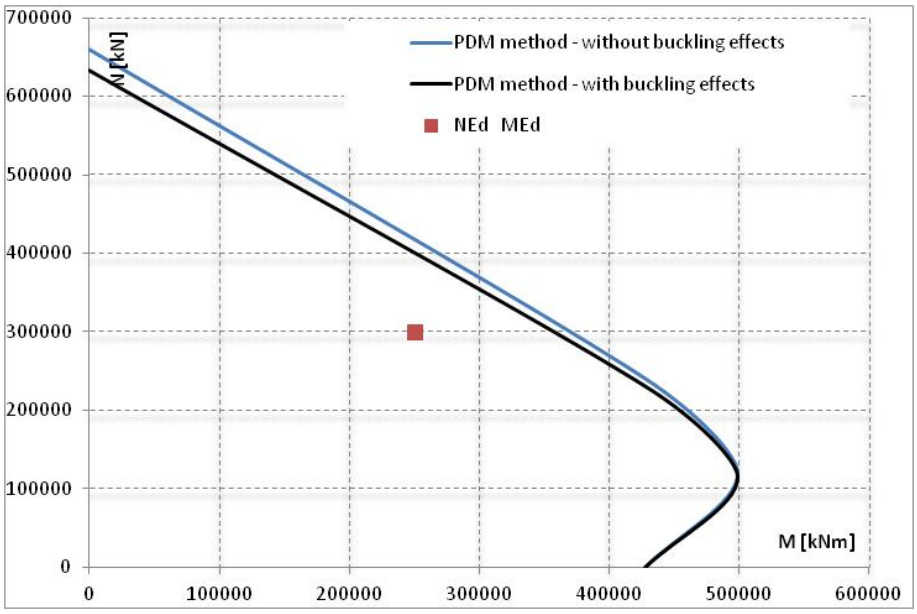

Figure 10-2 Axial force - bending moment interaction curve (EC4 Design) – Example 1

- **Shear force evaluation:**

The evaluation of the shear force is made according to the report "Design Example of a column with 4 encased steel profiles" prepared by ArcelorMittal in collaboration with University of Liege. This procedure is to evaluate the composite behavior as a whole and additional considerations should be taken into account in order to ensure adequate load paths from the concrete to steel or vice versa at the load application points.

The definition of the used symbols is defined in Figure 10-3:

$b_{c3} = 286\text{mm}$

$b_s = 476\text{mm}$

$b_{c4} = 3072\text{mm} - 2 \cdot (286\text{mm} + 476\text{mm}) = 1548\text{mm}$

The applied shear force is V_{Ed} is distributed between sections b_{c3}, b_{c4} and b_s proportionally to their stiffness:

$$V_{Ed,bc3} = V_{Ed} \cdot EI_{eff,bc3} / EI_{eff}$$

$$V_{Ed,bc4} = V_{Ed} \cdot EI_{eff,bc4} / EI_{eff}$$

$$V_{Ed,bs} = V_{Ed} \cdot EI_{eff,bs} / EI_{eff}$$

The effective bending stiffness of the column is: $EI_{eff} = 2.719 \cdot 10^{17}\ \text{Nmm}$

The total effective bending stiffness is the sum of individual EI_{eff} established for sections b_{c3}, b_{c4} and b_s respectively.

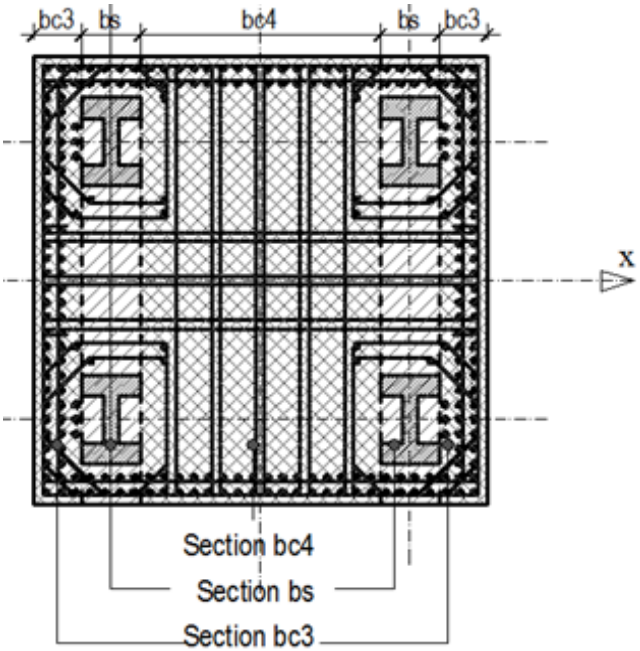

Figure 10-3 Definition of sections bc3, bc4, and bs (EC4 Design) – Example 1

1) Section b_{c3}: $EI_{eff,bc3} = E_{sr} \cdot I_{sr,bc3} + K_e \cdot E_{c,eff} \cdot I_{c,bc3}$

To calculate $I_{sr,bc3}$ of the reinforcing bars, it is considered one equivalent plate A_{s2} and 2x2 bars on the top and bottom.

For each face:

- The number of bars is: 30+30+4+4 = 68 bars
- The area of those bars is: $A_{sr,bc3} = 68 \cdot A_{sri} = 85451\text{mm}^2$
- The thickness of the equivalent plate is:

$$t_p = {A_{sr,side}}/{h_{s1}} = 85451\text{mm}^2 / 2900\text{mm} = 29.5\text{mm}$$

$$I_{cg,bc3} = \frac{b_{c3} \cdot h_1^3}{12} = \frac{286\text{mm} \cdot (3072\text{mm})^3}{12} = 6.91 \cdot 10^{11}\,\text{mm}^4$$

$$I_{sr,bc3} = \frac{t_p \cdot h_{s1}^3}{12} = \frac{29.4\text{mm} \cdot 2900\text{mm}^3}{12} = 5.99 \cdot 10^{10}\,\text{mm}^4$$

$$I_{c,bc3} = I_{cg,bc3} - I_{sr,bc3} = 6.91 \cdot 10^{11}\,\text{mm}^4 - 6.91 \cdot 10^{10}\,\text{mm}^4 = 6.31 \cdot 10^{11}\,\text{mm}^4$$

$$\begin{aligned} EI_{eff,bc3} &= E_{sr} \cdot I_{sr,bc3} + K_e \cdot E_{c,eff} \cdot I_{c,bc3} \\ &= 200000\text{MPa} \cdot 3.40 \cdot 10^{10}\,\text{mm}^4 + 0.6 \cdot 17543\text{MPa} \cdot 6.3110^{11}\,\text{mm}^4 \\ &= 1.86 \cdot 10^{16}\,\text{Nmm}^2 \end{aligned}$$

2) Section b_{c4}: $EI_{eff,bc4} = E_{sr} \cdot I_{sr,bc4} + K_e \cdot E_{c,eff} \cdot I_{c,bc4}$

To calculate $I_{sr,bc4}$, two equivalent (one top and one bottom) steel plates replace the reinforcing bars. Each plate has the same total area, and contains 36 rebar:

$$A_{sr,bc4} = 36 \cdot A_{sri} = 45238\text{mm}^2$$

$$I_{sr,bc4} = 2 \cdot A_{sr,bc4} \cdot d_{s1y}{}^2 = 2 \cdot 45238\text{mm}^2 \cdot \left(1400\text{mm}\right)^2 = 1.77 \cdot 10^{11}\,\text{mm}^4$$

$$I_{cg,bc4} = \frac{b_{c4} \cdot h_1{}^3}{12} = \frac{1548\text{mm} \cdot \left(3072\text{mm}\right)^3}{12} = 3.74 \cdot 10^{12}\,\text{mm}^4$$

$$I_{c,bc4} = I_{cg,bc4} - I_{sr,bc4} = 3.74 \cdot 10^{12}\,\text{mm}^4 - 1.77 \cdot 10^{11}\,\text{mm}^4 = 3.563 \cdot 10^{12}\,\text{mm}^4$$

$$\begin{aligned} EI_{eff,bc4} &= E_{sr} \cdot I_{sr,bc4} + K_e \cdot E_{c,eff} \cdot I_{c,bc4} \\ &= 200000\text{MPa} \cdot 1.77 \cdot 10^{11}\,\text{mm}^4 + 0.6 \cdot 17543\text{MPa} \cdot 3.563 \cdot 10^{12}\,\text{mm}^4 \\ &= 7.30 \cdot 10^{16}\,\text{Nmm}^2 \end{aligned}$$

3) Section b_s: $EI_{eff,bs} = E_s \cdot I_{s,bs} + E_{sr} \cdot I_{sr,bs} + K_e \cdot E_{c,eff} \cdot I_{c,bs}$

To calculate $I_{sr,bs}$, two equivalent (one top and one bottom) steel plates replace the reinforcing bars. Each plate has the same total area, and contains 8 rebar:

$$A_{sr,bs} = 8 \cdot A_{sri} = 10053\text{mm}^2$$

$$I_{sr,bs} = 2 \cdot A_{sr,bs} \cdot d_{s1y}{}^2 = 2 \cdot 10053\text{mm}^2 \cdot \left(1400\text{mm}\right)^2 = 3.94 \cdot 10^{10}\,\text{mm}^4$$

$$I_{s,bs} = 2 \cdot A_a \cdot d_{sy}{}^2 + 2 \cdot I_x = 2 \cdot 165000\text{mm}^2 \cdot \left(950\text{mm}\right)^2 + 2 \cdot 7.546 \cdot 10^9\,\text{mm}^4 = 3.129 \cdot 10^{11}\,\text{mm}^4$$

$$I_{cg,bs} = \frac{b_s \cdot h_1{}^3}{12} = \frac{476\text{mm} \cdot \left(3072\text{mm}\right)^3}{12} = 1.15 \cdot 10^{12}\,\text{mm}^4$$

$$I_{c,bs} = I_{cg,bs} - I_{sr,bs} - I_{s,bs} = 1.15 \cdot 10^{12}\,\text{mm}^4 - 3.94 \cdot 10^{10}\,\text{mm}^4 - 3.129 \cdot 10^{11}\,\text{mm}^4 = 8.199 \cdot 10^{11}\,\text{mm}^4$$

$$\begin{aligned} EI_{eff,bs} &= E_s \cdot I_{s,bs} + E_{sr} \cdot I_{sr,bs} + K_e \cdot E_{c,eff} \cdot I_{c,bs} \\ &= 210000\text{MPa} \cdot 8.199 \cdot 10^{11}\,\text{mm}^4 + 200000\text{MPa} \cdot 2.955 \cdot 10^{10}\,\text{mm}^4 + 0.6 \cdot 17543\text{MPa} \cdot 8.13 \cdot 10^{11}\,\text{mm}^4 \\ &= 8.199 \cdot 10^{16}\,\text{Nmm}^2 \end{aligned}$$

$$\begin{aligned} EI_{eff} &= 2 \cdot (EI_{eff,bc3}) + EI_{eff,bc4} + 2 \cdot (EI_{eff,bs}) \\ &= 2 \cdot (1.86 \cdot 10^{16}\,\text{Nmm}^2) + 7.30 \cdot 10^{16}\,\text{Nmm}^2 + 2 \cdot (8.199 \cdot 10^{16}\,\text{Nmm}^2) \\ &= 2.472 \cdot 10^{17}\,\text{Nmm}^2 \end{aligned}$$

The factored shear force V_{Ed} = 20000 kN for the complete section is distributed in the 5 sections (2 b_{c3}, 2 b_s and 1 b_{c4}) :

$$V_{Ed,bc3} = V_{Ed} \cdot \frac{EI_{eff,bc3}}{EI_{eff}} = 20000\text{kN} \cdot \frac{1.86 \cdot 10^{16}\,\text{Nmm}^2}{2.742 \cdot 10^{17}\,\text{Nmm}^2} = 1358\text{kN}$$

$$V_{Ed,bc4} = V_{Ed} \cdot \frac{EI_{eff,bc4}}{EI_{eff}} = 20000\text{kN} \cdot \frac{7.30 \cdot 10^{16}\,\text{Nmm}^2}{2.742 \cdot 10^{17}\,\text{Nmm}^2} = 5322\text{kN}$$

$$V_{Ed,bs} = V_{Ed} \cdot \frac{EI_{eff,bs}}{EI_{eff}} = 20000\text{kN} \cdot \frac{8.199 \cdot 10^{16}\,\text{Nmm}^2}{2.742 \cdot 10^{17}\,\text{Nmm}^2} = 5981\text{kN}$$

- **Calculation of shear in section b_s:**

Section b_s is a composite steel-concrete section having 2 reinforced concrete flanges, 2 steel "flanges" (the HD sections) and 1 reinforced concrete web. To establish longitudinal shear in section b_s, it is convenient to transform the composite section into a single material section or "homogenized" section. The single material can be either steel or concrete.

Choosing concrete, the moment of inertia of the homogenized concrete section I_c* is such that the stiffness $E_c\, I_c$* of the homogenized section is equal to the stiffness $EI_{eff,bs}$:

$$I_c^* = EI_{eff,bs} \Big/ E_{cm} = 8.199 \cdot 10^{16}\,\text{Nmm}^2 \Big/ 37278\text{MPa} = 2.119 \cdot 10^{12}\,\text{mm}^4$$

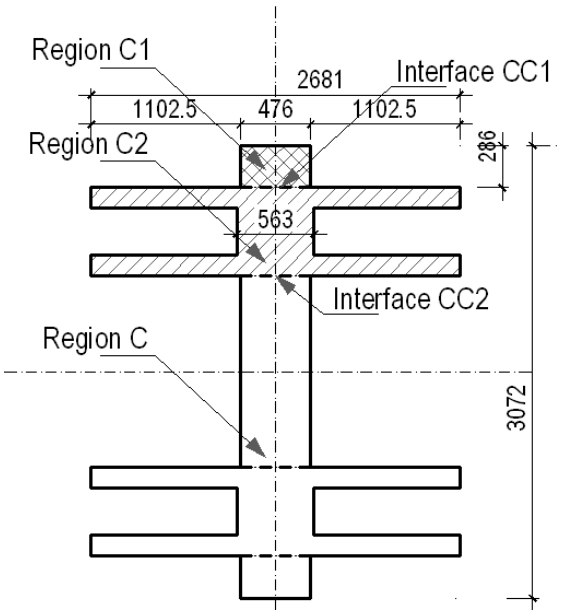

Figure 10-4 Homogenized equivalent concrete section bs – Example 1

In a homogenized concrete section (Figure 10-4), the width of the concrete equivalent to the width of the steel flanges is:

$$b_s^* = b_s \cdot E_s \Big/ E_{cm} = 476\text{mm} \cdot 210000\text{MPa} \Big/ 37278\text{MPa} = 2681\text{mm}$$

The width of the concrete equivalent to the width of the steel web is:

$$t_w^* = t_w \cdot E_s \Big/ E_{cm} = 100\text{mm} \cdot 210000\text{MPa} \Big/ 37278\text{MPa} = 563\text{mm}$$

The resultant longitudinal shear force on interfaces like CC1 and CC2 in Figure 10-4 is:

$$V_{Ed,l} = \frac{V_{Ed,bs} \cdot \mathrm{S}}{I_\mathrm{c}^*}$$

where:

S is the first moment of areas of regions C1 and C2 taken about the neutral axis of the section as illustrated as illustrated in Figure 10-4.

Using S, the longitudinal shear is calculated at the steel-concrete interfaces CC1 and CC2 in order to size the force transfer mechanisms required for the member to act as a fully composite section.

- **Calculation of longitudinal shear force applied at interface CC1:**

S_{CC1} is the section modulus for the region C1 as defined in Figure 10-4:

The height of the C1 region is:

$$h_1' = \frac{h_1}{2} - \left(d_{sy} + \frac{d}{2} \right) = \frac{3072\text{mm}}{2} - \left(950\text{mm} + \frac{600\text{mm}}{2} \right) = 286\text{mm}$$

The area is:

$$A_1 = b \cdot h_1' = 476\text{mm} \cdot 286\text{mm} = 136136\text{mm}^2$$

$$S_{CC1} = A_1 \cdot \left(\frac{h_1}{2} - \frac{h_1'}{2} \right) = 136136\text{mm}^2 \cdot \left(\frac{3072\text{mm}}{2} - \frac{286\text{mm}}{2} \right) = 1.896 \cdot 10^8\,\text{mm}^3$$

The resultant longitudinal shear force at interface CC1 is:

$$V_{Ed,CC1} = \frac{V_{Ed,bs} \cdot S_{CC1}}{I_\mathrm{c}^*} = \frac{5981\text{kN} \cdot 1.896 \cdot 10^8\,\text{mm}^3}{2.199 \cdot 10^{16}\,\text{mm}^4} = 515.6 \frac{\mathrm{N}}{\mathrm{mm}}$$

On 1-meter length of column:

$$V_{Ed,CC1} = 515.6 \frac{\mathrm{kN}}{\mathrm{m}}$$

- **Calculation of longitudinal shear force applied at interface CC2:**

S_{CC2} is the section modulus for the combined regions C1 and C2 (the HD profile):

The equivalent area in concrete for the HD profile is:

$A_a = 165000\text{mm}^2$

The equivalent are in concrete for the HD profile is:

$$A_a^* = A_a \cdot E_s / E_{cm} = 165000\text{mm}^2 \cdot 210000\text{MPa} / 37278\text{MPa} = 929506\text{mm}^2$$

The distance of HD center to the neutral axis is:

$d_{sy} = 950$ mm

The moment of area of the equivalent steel profile is:

$$S_{HD} = A_a^* \cdot d_{sy} = 929506\text{mm}^2 \cdot 950\text{mm} = 8.83 \cdot 10^8\,\text{mm}^3$$

Area of concrete between the flanges:

$$A_{c\_CC2}^* = b \cdot d\text{-}A_a = 476\text{mm} \cdot 600\text{mm} - 165000\text{mm}^2 = 120600\text{mm}^2$$

Moment of area of concrete between the flanges:

$$S_{c\_CC2}^* = A_{c\_CC2}^* \cdot d_{sy} = 120600\text{mm}^2 \cdot 950\text{mm} = 1.146 \cdot 10^8\,\text{mm}^3$$

The section modulus corresponding to the combined regions C1 and C2 is equal to:

$$S_{CC2} = S_{c\_CC2}^* + S_{HD} + S_{CC1} = 1.146 \cdot 10^8\,\text{mm}^3 + 8.83 \cdot 10^8\,\text{mm}^3 + 1.896 \cdot 10^8\,\text{mm}^3 = 1.19 \cdot 10^9\,\text{mm}^3$$

The resultant longitudinal shear force at interface CC2 is:

$$V_{Ed,CC2} = \frac{V_{Ed,bs} \cdot S_{CC2}}{I_c^*} = \frac{5981\text{kN} \cdot 1.19 \cdot 10^9\,\text{mm}^3}{2.199 \cdot 10^{12}\,\text{mm}^4} = 3229.3\frac{\text{N}}{\text{mm}}$$

On 1-meter length of column:

$$V_{Ed,CC2} = 3229.3\frac{\text{kN}}{\text{m}}$$

- **Evaluation of necessary amount of shear studs:**

Geometrical characteristic of the shear studs correspond to State of Art – Table 3.2.2 where:

d = 25 mm – diameter of the shear stud;

h_{sc} = 100 mm – stud height; $3d$ = 75 mm ≤ h_{sc} ;

s_c – longitudinal spacing; $5d$ = 150 mm ≤ sc ≤ min(6 h_{sc}; 800mm)=600mm;

s_x –transversal spacing; $2.5d$ = 62.5 mm ≤ sx ;

f_u = 450 MPa – maximum stud tensile strength;

For a shear stud with a diameter d = 25 mm, the design shear strength is equal to:

$$P_{Rk} = \min\left(\frac{0.8\cdot f_u\cdot\pi\cdot d^2/4}{\gamma_V}, \frac{0.29\cdot\alpha\cdot d^2\cdot\sqrt{f_{ck}\cdot E_{cm}}}{\gamma_V}\right) = \min\left(176.71\text{kN}, 247.45\text{kN}\right) = 176.71\text{kN}$$

where:

$$\alpha = \begin{cases} 0.2\left(\frac{h_{sc}}{d}+1\right) \text{ for } 3\le\frac{h_{sc}}{d}\le 4 \\ 1 \text{ for } \frac{h_{sc}}{d} > 4 \end{cases} = 1$$

$$\gamma_V = 1$$

$$\frac{0.8\cdot f_u\cdot\pi\cdot d^2/4}{\gamma_V} = \frac{0.8\cdot 450\text{MPa}\cdot\pi\cdot\left(25\text{mm}\right)^2/4}{1} = 176.71\text{kN}$$

$$\frac{0.29\cdot\alpha\cdot d^2\cdot\sqrt{f_{ck}\cdot E_{cm}}}{\gamma_V} = \frac{0.29\cdot 1\cdot\left(25\text{mm}\right)^2\cdot\sqrt{50\text{MPa}\cdot 37278\text{MPa}}}{1} = 247.45\text{kN}$$

For 1 m column length, the necessary amount of shear studs at each flange interface is:

$$n_{studs\_CC1} = \frac{V_{Ed1\_CC1}\cdot 1\text{m}}{P_{Rk}} = \frac{515.6\frac{\text{kN}}{\text{m}}\cdot 1\text{m}}{176.71\text{kN}} = 2.91 \Rightarrow 3 \text{ studs} / 1\text{m}$$

$$n_{studs\_CC2} = \frac{V_{Ed1\_CC2}\cdot 1\text{m}}{P_{Rk}} = \frac{3228.3\frac{\text{kN}}{\text{m}}\cdot 1\text{m}}{176.71\text{kN}} = 18.3 \Rightarrow 19 \text{ studs} / 1\text{m}$$

10.1.1 Example 2

Example 2: Composite column with four encased profiles in combined axial compression and flexure about the (x-x) axis, and the steel profiles have a different orientation

Given:

The encased composite member, illustrated in Figure 10-5, is subject to axial force, bending moment, and shear force. The composite member consist of 4 HD 400x634 S460 grade steel profiles, encased in concrete with a specified compressive strength of 60 MPa, and 32 pieces of rebar with 32 mm diameter, grade HRB 400 (f_{sy} = 400MPa, distributed in 1 layer at the perimeter. The buckling length (L_o) of the column is 18 m.

Check the capacity of the composite column subjected to the following demands:

N_{Ed} = 150000 kN;

M_{Ed} = 40000 kN;

V_{Ed} = 8000 kN;

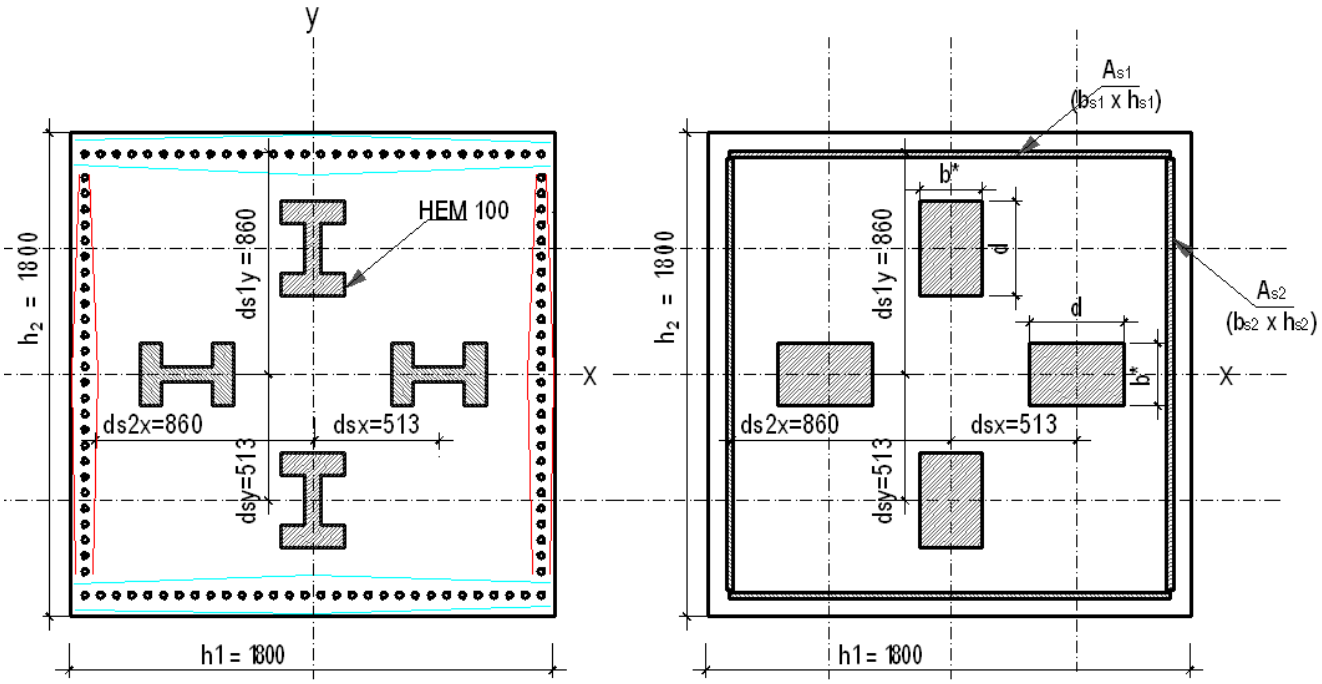

Figure 10-5 Encased composite member section (EC4 Design) – Example 2

Steel profile HD 400x634 properties are:

HISTAR 460 - f_y = 460MPa;

E_s = 210000 MPa;

b = 424 mm;

d = 474 mm;

t_w = 51.2 mm;

t_f = 81.5 mm;

$Z_{sx} = 14220 \cdot 10^3$ mm^3;

$Z_{sy} = 4978 \cdot 10^3$ mm^3; $I_{HDx} = 180200 \cdot 10^4$ mm^4;

$I_{HDy} = 98250 \cdot 10^4$ mm^4;

$A_a = 808 \cdot 10^2$ mm^2;

$A_s = \sum_{i=1}^{4} A_a = 4 \cdot 808 \cdot 10^2$ mm^2 $= 323200$mm^2;

$d_{sx} = 513$mm;

$d_{sy} = 513$mm;

d_x = 375 mm;

d_y = 375mm;

Reinforcement properties are:

32 = the total number of vertical rebar;

d_b = 32mm for a T32 diameter rebar;

f_s = 400MPa;

E_{sr} = 200000 MPa;

$A_{sri} = 804.24$mm^2;

$A_{sr} = \sum_{i=1}^{n} A_{sri} = 25735.93$mm^2;

Concrete section's properties are:

f_{ck} = 60MPa;

E_{cm} = 39100 MPa

h_1 = 1800 mm;

h_2 = 1800 mm;

c_x = 40 mm;

c_y = 40 mm;

$A_g = h_1 \cdot h_2 = (1800\text{mm}) \times (1800\text{mm}) = 3.24 \cdot 10^6$ mm^2;

$A_c = A_g - A_{sr} - A_s = 3.24 \cdot 10^6$ mm^2 $- 25735.93$mm^2 $- 323200$mm^2 $= 2.89 \cdot 10^6$ mm^2

Solution:

- **The partial safety factors for materials:**

For the determination of resistance, the following partial safety factors should be applied for different materials:

γ_a is the partial factor for structural steel

γ_s is the partial factor for the reinforcement

γ_c is the partial factor for reinforced concrete

Thus:

$$f_{yd} = f_y / \gamma_a = 460\text{MPa} / 1 = 460\text{MPa}$$

is the design value of yield strength of the structural steel

$$f_{sd} = f_s / \gamma_a = 400\text{MPa} / 1.15 = 347.8\text{MPa}$$

is the design value of yield strength of the reinforcement

$$f_{cd} = f_c / \gamma_c = 60\text{MPa} / 1.5 = 40\text{MPa}$$

is the design value of yield strength of the concrete

- **Definition of plates equivalent to rebar:**

The definition of the equivalent horizontal plates (A_{s1} and A_{s2}) is as follows:

1) A_{s1} plate:

i = 1 = the number of rebar layers in one equivalent plate

n_x = 9 = the amount of rebar in one layer

$$A_{s1} = i \cdot n_x \cdot A_{sri} = 1 \cdot 9 \cdot 804.24\text{mm}^2 = 7.24 \cdot 10^3\text{mm}^2$$

$$h_{s1} = (n_x - 1) \cdot s_x = (9-1) \cdot 215\text{mm} = 1720\text{mm}$$

$$b_{s1} = \frac{A_{s1}}{h_{s1}} = 4.2\text{mm}$$

$$d_{1y} = \frac{1800\text{mm}}{2} - 40\text{mm} = 760\text{mm}$$

$$d_{s1y} = \sum d_{iy} / i = 760\text{mm}$$

$$Z_{sr1x} = 2 \cdot A_{s1} \cdot d_{s1y} = 2 \cdot 7.24 \cdot 10^3\text{mm}^2 \cdot 760\text{mm} = 1.1 \cdot 10^7\text{mm}^3$$

$$I_{sr1x} = 2 \cdot i \cdot n_x \cdot A_{sri} \cdot d_{s1y}^2 = 2 \cdot 1 \cdot 9 \cdot 804.24\text{mm}^2 \cdot (760\text{mm})^2 = 2.837 \cdot 10^{10}\text{mm}^4$$

2) A_{s2} plate:

$$A_{s2} = n_y \cdot A_{sri} = b_{s2} \cdot h_{s2}$$

j = 1 = the number of rebar layers in one equivalent plate

n_y = 7 = the amount of rebar in one layer

$$A_{s2} = j \cdot n_y \cdot A_{sri} = 1 \cdot 7 \cdot 804.24\text{mm}^2 = 5.63 \cdot 10^3\,\text{mm}^2$$

$$h_{s2} = (n_y - 1) \cdot s_y = 6 \cdot 215\text{mm} = 1290\text{mm}$$

$$b_{s2} = \frac{A_{s2}}{h_{s2}} = 4.4\text{mm}$$

$$d_{1x} = \frac{1800\text{mm}}{2} - 40\text{mm} = 760\text{mm}$$

$$d_{s2x} = \sum d_{jx} \Big/ j = 760\text{mm}$$

$$Z_{sr2x} = 2 \cdot \frac{b_{s2} \cdot h_{s2}^2}{4} = \frac{4.4\text{mm} \cdot (1290\text{mm})^2}{2} = 3.631 \cdot 10^6\,\text{mm}^3$$

$$I_{sr2x} = 2 \cdot \frac{b_{s2} \cdot h_{s2}^3}{12} = \frac{4.4\text{mm} \cdot (1290\text{mm})^3}{6} = 1.561 \cdot 10^9\,\text{mm}^4$$

- **Definition of plates equivalent to steel profiles:**

The definition of the equivalent horizontal plates is made according the following:

$$d^* = d = 474\text{mm}$$

$$b^* = \frac{A_a}{d^*} = \frac{80800\text{mm}^2}{474\text{mm}} = 170.5\text{mm}$$

$$Z_{sx} = 2 \cdot A_a \cdot d_{sy} + 2 \cdot Z_y = 2 \cdot 80800\text{mm}^2 \cdot 760\text{mm} + 2 \cdot 7117 \cdot 10^3\,\text{mm}^2 = 9.713 \cdot 10^7\,\text{mm}^3$$

$$I_{sx} = 2 \cdot A_a \cdot d_{sy}^2 + 2 \cdot I_x = 2 \cdot 80800\text{mm}^2 \cdot (760\text{mm})^2 + 2 \cdot 250200 \cdot 10^4\,\text{mm}^4 = 4.449 \cdot 10^{10}\,\text{mm}^4$$

- **Stiffness evaluation:**

$$(EI)_{eff} = E_s \cdot I_{sx} + E_{sr} \cdot I_{srx} + K_e \cdot E_{c,eff} \cdot I_{cx}$$

$$= 2.1 \cdot 10^5\,\text{MPa} \cdot 4.45 \cdot 10^{10}\,\text{mm}^4 + 2.0 \cdot 10^5\,\text{MPa} \cdot (2.837 \cdot 10^{10}\,\text{mm}^4 + 1.561 \cdot 10^{10}\,\text{mm}^4) +$$

$$+0.6 \cdot 18400\text{MPa} \cdot 8.004 \cdot 10^{11}\,\text{mm}^4$$

$$= 2.417 \cdot 10^{16}\,\text{N} \cdot \text{mm}^2$$

$$N_{cr} = \frac{\pi^2 \cdot (EI)_{eff}}{L_o^2} = \frac{\pi^2 \cdot 2.417 \cdot 10^{16}\,\text{N} \cdot \text{mm}^2}{(18\text{m})^2} = 7.362 \cdot 10^8\,\text{N}$$

$$E_{c,eff} = E_{cm}\frac{1}{1+\left(N_{G,Ed}/N_{Ed}\right)\cdot\varphi_t} = E_{cm}\frac{1}{1+0.75\cdot1.5} = 0.47\cdot39100\ \text{MPa}=18400\ \text{MPa}$$

Where:

$K_e = 0.6$ the correction factor

φ_t is the creep coefficient according to EN 1992-1-1, 3.1.4 or 11.3.3, depending on the age (t) of the concrete at the moment considered at the age (t_o) at loading. In this example, we consider the creep coefficient equal to 1.5.

N_{Ed} is the total design force

$N_{G,Ed}$ is the part f the normal force that is permanent

In high-rise buildings, there is a significant amount of long-term loads, approximately 75% of total loads. Therefore, the ratio of the normal forces in this example is considered equal to:

$$N_{G,Ed}/N_{Ed} = 0.75$$

- **Limitation when using the extended simplified method:**

1) The steel contribution ratio δ should fulfill the following condition $0.2 < \delta < 0.9$

$$\delta = \frac{A_s\cdot f_{yd}}{N_{pl.Rd}} = \frac{6.6\cdot10^5\,\text{mm}^2\cdot460\text{MPa}}{255920\text{kN}} = 0.58 \qquad \text{EN 1994-1-1:2004 – Eq (6.27)}$$

where:

$$\begin{aligned} N_{pl.Rd} &= A_s\cdot f_{yd} + A_{sr}\cdot f_{sd} + 0.85\cdot A_c\cdot f_{cd} \\ &= 323200\text{mm}^2\cdot460\text{MPa} + 25375.92\text{mm}^2\cdot347.82\text{MPa} + 2.89\cdot10^6\,\text{mm}^2\cdot\left(0.85\cdot40\text{MPa}\right) \\ &= 255920\text{kN} \end{aligned}$$

2) The relative slenderness $\bar{\lambda} \le 2$

$$\bar{\lambda} = \sqrt{\frac{N_{pl.Rk}}{N_{cr}}} = \sqrt{\frac{306410\text{kN}}{7.362\cdot10^8\,\text{N}}} = 0.589 < 2 \qquad \text{EN 1994-1-1:2004 – Eq (6.28)}$$

Where:

$$\begin{aligned} N_{pl.Rk} &= A_s\cdot f_y + A_{sr}\cdot f_{sy} + 0.85\cdot A_c\cdot f_{ck} \\ &= 323200\text{mm}^2\cdot460\text{MPa} + 25375.92\text{mm}^2\cdot400\text{MPa} + 2.89\cdot10^6\,\text{mm}^2\cdot\left(0.85\cdot60\text{MPa}\right) \\ &= 306410\text{kN} \end{aligned}$$

$$N_{cr} = \frac{\pi^2\cdot\left(EI\right)_{eff}}{L_o^2} = \frac{\pi^2\cdot2.417\cdot10^{16}\,\text{N}\cdot\text{mm}^2}{(18\text{m})^2} = 7.362\cdot10^8\,\text{N}$$

3) Other limitations

- Longitudinal reinforcement area:

$$0.3\% \le \frac{A_{sr}}{A_c} = \frac{25735.93\text{mm}^2}{2.89 \cdot 10^6 \text{mm}^2} = 0.89\% \le 6\%$$

For a fully encased section, limits to minimum and maximum thickness to concrete cover are shown in EN 1994-1-1:2004 – Eq (6.29):

$$40\text{mm} \le c_y = 40 \text{ mm} \le 0.3h_2 = 540 \text{ mm}$$
$$40\text{mm} \le c_x = 40 \text{ mm} \le 0.3h_1 = 540 \text{ mm}$$

- The ratio of the cross-section depth h2 to width h1, should be within the limits:

$0.2 \le h1/h2 = 1 \le 5.0$ EN 1994-1-1:2004 – Clause 6.7.3 (4)

- **Interaction of axial force and flexure:**

In order to determine the axial force N – bending moment M interaction curve, a few points are determined. The detailed definition of the points are as follows:

- A – pure axial capacity point

$$N_A = N_{pl.Rd}$$

$$M_A = 0 \text{ MPa}$$

- B - pure flexural bending point

$$N_B = 0$$
$$M_B = M_{pl,Rd}$$

- C – point with bending moment equal to the pure bending capacity and axial compressive load greater than 0

$$N_C = N_{pm,Rd}$$
$$M_C = M_{pl,Rd}$$

- D – the maximum bending moment point

$$N_D = 0{,}5 \, . \, N_{pm,Rd}$$
$$M_D = M_{max,Rd}$$

Rigid – plastic material behavior is assumed in order to evaluate these key points. Steel is assumed to have reached yield stress in either tension or compression. Concrete is assumed to have reached its peak stress in compression and have the tensile strength equal to zero. For one equivalent rectangular stress block, the peak stress in compression in this example is:

$$0.85 \cdot f_{\text{cd}} = 0.85 \cdot 40\text{MPa} = 34\text{MPa}$$

- **Evaluation of the plastic resistance to axial force $N_{pl.Rd}$ and $N_{pm.Rd}$:**

The plastic resistance to axial force combines the individual resistances of the steel profile, the concrete and reinforcement. For fully or partially concrete – encased steel sections:

$$N_{pl.Rd} = A_s \cdot f_{yd} + A_{sr} \cdot f_{sd} + 0.85 \cdot A_c \cdot f_{cd}$$
$$= 323200\text{mm}^2 \cdot 460\text{MPa} + 25375.92\text{mm}^2 \cdot 347.82\text{MPa} + 2.89 \cdot 10^6\,\text{mm}^2 \cdot (0.85 \cdot 40\text{MPa})$$
$$= 255920\text{kN}$$

$$N_{pm.Rd} = A_c \cdot 0.85 \cdot f_{cd}$$
$$= 2.89 \cdot 10^6\,\text{mm}^2 \cdot 0.85 \cdot 40\text{MPa}$$
$$= 98296\text{kN}$$

$$0.5 \cdot N_{pm.Rd} = 0.5 \cdot A_c \cdot 0.85 \cdot f_{cd}$$
$$= 0.5 \cdot 2.89 \cdot 10^6\,\text{mm}^2 \cdot 0.85 \cdot 40\text{MPa}$$
$$= 49148\text{kN}$$

- **Evaluation of the reduced axial force parameter χ :**

The reduction factor χ for the relevant buckling mode in terms of the relevant relative slenderness is determined with the following formulae:

$$\chi = \frac{1}{\phi + \sqrt{\phi^2 - \lambda^2}} \le 1$$

$$\chi = \frac{1}{0.74 + \sqrt{0.74^2 - 0.589^2}} = 0.84$$

where:

$$\phi = 0.5 \cdot \left(1 + \alpha \cdot (\lambda - 0.2) + \lambda^2\right) = 0.5 \cdot \left(1 + 0.34 \cdot (0.58 - 0.2) + 0.58^2\right) = 0.74$$

$\alpha = 0.34$ - parameter that depends on the chosen buckling curve defined in EN 1994-1-1 Table 6.5. EC4 recommends using $\alpha = 0.34$ for buckling axis y and $\alpha = 0.49$ for buckling axis z.

In conclusion, the amplification factor of the axial force will be considered as equal with:

$$\chi = 0.84$$

$$N_{pl.b.Rd} = \chi \cdot N_{pl.Rd} = 0.84 \cdot 255920\text{kN} = 215545\text{kN}$$

$$N_{pm.b.Rd} = \chi \cdot N_{pm.Rd} = 0.84 \cdot 98296\text{kN} = 82788\text{kN}$$

Where:

$N_{pl,b,Rd}$ is the plastic resisting axial force, considering the buckling effects

- **Evaluation of the maximum moment resistance $M_{max.Rd}$.:**

$$M_{max.Rd} = Z_{sx} \cdot f_{yd} + \left(Z_{r1x} + Z_{r2x}\right) \cdot f_{sd} + 0.5 \cdot Z_{cx} \cdot \left(0.85 \cdot f_{cd}\right)$$
$$= 9.71 \cdot 10^7\,\text{mm}^3 \cdot 460\text{MPa} + \left(1 \cdot 10^7\,\text{mm}^3 + 3.63 \cdot 10^6\,\text{mm}^3\right) \cdot 347.8\text{MPa} +$$
$$+ 0.5 \cdot 1.35 \cdot 10^9\,\text{mm}^3 \cdot \left(0.85 \cdot 40\text{MPa}\right)$$
$$= 76696\text{kNm}$$

$$Z_{cx} = \frac{h_1 \cdot h_2^2}{4} - Z_{r1x} - Z_{r2x} - Z_{sx}$$
$$= \frac{1800\text{mm} \cdot (1800\text{mm})^2}{4} - 1.1 \cdot 10^7\,\text{mm}^3 - 3.63 \cdot 10^6\,\text{mm}^3 - 9.71 \cdot 10^7\,\text{mm}^3$$
$$= 1.35 \cdot 10^9\,\text{mm}^3$$

- **Evaluation of the plastic bending moment resistance $M_{pl.Rd.}$:**

In order to evaluate the plastic bending moment value, first we need to determine the position of the neutral axis. Different assumptions of the neutral axis position have been taken into consideration. The position of the neutral axis is determined by subtracting the stress distribution combination at point B and C, considering normal forces only.

Assumption 1: h_{nx} between the two profiles $\left(h_{nx} \le \frac{b^*}{2}\right)$:

$$h_{nx} = \frac{N_C}{(2 \cdot h_1 - 2 \cdot d - 4 \cdot b_{s2}) \cdot \left(0.85 \cdot f_{cd}\right) + 2 \cdot d \cdot f_{yd} + 4 \cdot b_{s2} \cdot f_{sd}}$$
$$= \frac{98296\text{kN}}{(2 \cdot 1800\text{mm} - 2 \cdot 474\text{mm} - 4 \cdot 4.4\text{mm})\left(0.85 \cdot 40\text{MPa}\right) + 2 \cdot 474\text{mm} \cdot 460\text{MPa} + 4 \cdot 4.4\text{mm} \cdot 347.8\text{MPa}}$$
$$= 179.5\text{mm}$$

Check assumption $\left(h_{nx} \le \frac{b^*}{2}\right)$: assumption **not ok**

$$h_{nx} = 179.5\text{mm} \le \frac{b^*}{2} = \frac{170.5\text{mm}}{2} = 85.25\text{mm}$$

Assumption 2: h_{nx} is placed within the steel profiles $\left(b^*/2 < h_{nx} \le d_{sy} - d/2\right)$:

$$h_{nx} = \frac{N_C + 2 \cdot A_a \cdot 0.85 \cdot f_{cd} - 2 \cdot A_a \cdot f_{yd}}{(2 \cdot h_1 - 4 \cdot b_{s2}) \cdot \left(0.85 \cdot f_{cd}\right) + 4 \cdot b_{s2} \cdot f_{sd}}$$
$$= \frac{98296\text{kN} + 2 \cdot 80800\text{mm}^2 \cdot 0.85 \cdot 40\text{MPa} - 2 \cdot 80800\text{mm}^2 \cdot 460\text{MPa}}{(2 \cdot 1800\text{mm} - 2 \cdot 4.4\text{mm})\left(0.85 \cdot 40\text{MPa}\right) + 4 \cdot 4.4\text{mm} \cdot 347.8\text{MPa}}$$
$$= 230\text{mm}$$

Check assumption $\left(b^*/2 < h_{nx} \le d_{sy} - d/2\right)$: assumption **ok**

$$b^*/2 = 170.5\text{mm}/2 = 85.25\text{mm} < h_{nx} = 230\text{mm} \le d_{sy} - d/2 = 513\text{mm} - 474\text{mm}/2 = 276\text{mm}$$

$$\begin{aligned} Z_{r2xn} &= 2 \cdot b_{s2} \cdot h_{nx}^2 \\ &= 2 \cdot 4.4\text{mm} \cdot (230\text{mm})^2 \\ &= 4.631 \cdot 10^5\,\text{mm}^3 \end{aligned}$$

$$Z_{sxn} = 2 \cdot Z_y = 2 \cdot 7.12 \cdot 10^6\,\text{mm}^3 = 1.423 \cdot 10^6\,\text{mm}^3$$

$$\begin{aligned} Z_{cxn} &= h_1 \cdot h_{nx}^2 - Z_{r2xn} - Z_{sxn} \\ &= 450\text{mm} \cdot (157\text{mm})^2 - 4.631 \cdot 10^5\,\text{mm}^3 - 1.423 \cdot 10^6\,\text{mm}^3 \\ &= 8.08 \cdot 10^6\,\text{mm}^3 \end{aligned}$$

$$\begin{aligned} M_{pl.Rd} &= M_{max.Rd} - Z_{r2xn} \cdot f_{sd} - Z_{sxn} \cdot f_{yd} - 1/2 \cdot Z_{cxn} \cdot (0.85 \cdot f_{cd}) \\ &= 76696\text{kNm} - 4.631 \cdot 10^5\,\text{mm}^3 \cdot 347.8\text{MPa} - 1.423 \cdot 10^6\,\text{mm}^3 \cdot 460\text{MPa} - 1/2 \cdot 8.08 \cdot 10^6\,\text{mm}^3 \cdot (0.85 \cdot 40\text{MPa}) \\ &= 75162\text{kNm} \end{aligned}$$

- **Evaluation of the reduced interaction curve axial force bending moment:**

$$M_{pl.b.Rd} = M_{pl.Rd}/k$$

where:

$M_{pl,b,Rd}$ is the plastic resisting bending moment where the buckling effects are taken into account.

$$k = \frac{\beta}{1 - N_{Ed}/N_{cr,eff}} = \frac{1}{1 - 150000\text{kN}/7.362 \cdot 10^8\,\text{N}} = 1.26$$

$\beta = 1$ coefficient is defined in EN 1994-1-1 Table 6.4 – depends on the distribution of the bending moment along the element.

$$N_{cr,eff} = N_{cr} = 7.362 \cdot 10^8\,\text{N}$$

$M_{pl,b,Rd} = M_{pl,Rd}$ if $\lambda < 0{,}2\,.\,(2 - r)$ and if $\frac{N_{Ed}}{N_{cr,eff}} < 0{,}1$, with r the ratio between the end moments.

- **Interaction curve bending moment axial force:**

The plastic distribution method gives the following values:

Point A : $N_A = N_{pl.Rd} = 255919\text{kN}$ $M_A = 0$ kNm

Point B : $N_B = 0$ $M_B = M_{pl,Rd} = 75162$ kNm

Point C : $N_C = N_{pm,Rd} = 98296$ kN $M_C = M_{pl,Rd} = 75162$ kNm

Point D: $N_D = 0{,}5 \cdot N_{pm,Rd} = 49148$ kN $M_D = M_{max,Rd} = 76696$ kNm

Taking the buckling effects into account:

Point A' : $N_A = N_{pl.Rd} = 215545.4\text{kN}$ $M_A = 0$ kNm

Point B' : $N_B = 0$ $M_B = M_{pl,Rd} = 59847$ kNm

Point C' : $N_C = N_{pm,Rd} = 82788$ kN $M_C = M_{pl,Rd} = 59847$ kNm

Point D': $N_D = 0{,}5 \cdot N_{pm,Rd} = 41394$ kN $M_D = M_{max,Rd} = 61069$ kNm

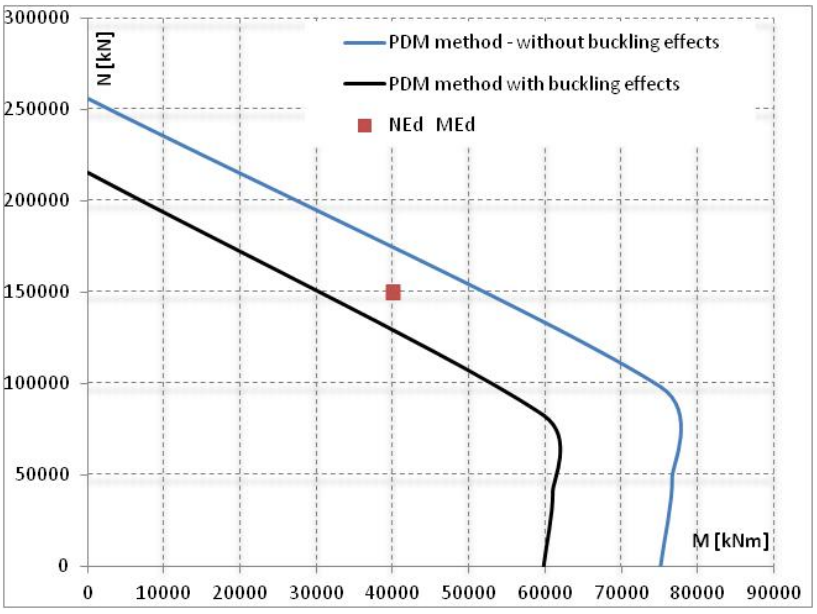

Figure 10-6 Axial force - bending moment interaction curve (EC4 Design) – Example 2

- **Shear force evaluation:**

The evaluation of the shear force is made according to the report "Design Example of a column with 4 encased steel profiles" prepared by ArcelorMittal in collaboration with University of Liege. This procedure is to evaluate the composite behavior as a whole and additional considerations should be taken into account in order to ensure adequate load paths from the concrete to steel or vice versa at the load application points.

The definition of the used symbols is defined in Figure 10-7:

$b_{c1} = 150\text{mm}$

$b_{s2} = 474\text{mm}$

$b_{c3} = 64\text{mm}$

$b_{s4} = 424\text{mm}$

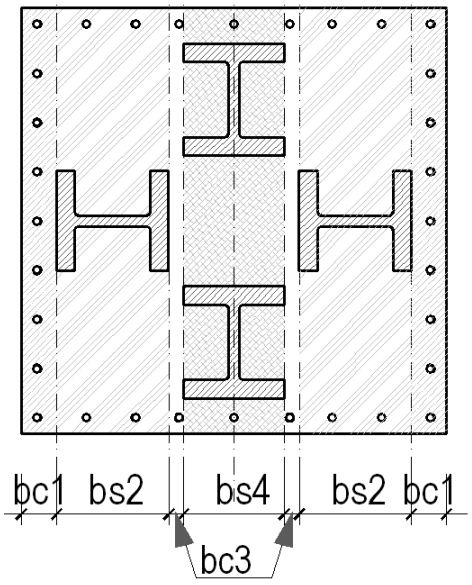

Figure 10-7 Definition of sections bc1, bc3, bs2, and bs4 (EC4 Design) – Example 2

The applied shear force is V_{Ed} is distributed between sections b_{c3}, b_{c4} and b_s proportionally to their stiffness:

$$V_{Ed,bc1} = V_{Ed} \cdot EI_{eff,bc1} / EI_{eff}$$

$$V_{Ed,bc3} = V_{Ed} \cdot EI_{eff,bc3} / EI_{eff}$$

$$V_{Ed,bs1} = V_{Ed} \cdot EI_{eff,bs1} / EI_{eff}$$

$$V_{Ed,bs2} = V_{Ed} \cdot EI_{eff,bs2} / EI_{eff}$$

The effective bending stiffness of the column is:

$$EI_{eff} = 2.417 \cdot 10^{16}\ \text{Nmm}$$

The total effective bending stiffness is the sum of individual EI_{eff} established for sections b_{c1}, b_{c3}, b_{s2} and b_{s4} respectively.

1) Section b_{c1}: $EI_{eff,bc3}1 = E_{sr} \cdot I_{sr,bc1} + K_e \cdot E_{c,eff} \cdot I_{c,bc1}$

To calculate $I_{sr,bc3}$ of the reinforcing bars, it is considered one equivalent plate A_{s2}.
For each face:

- The number of bars is: 9 bars
- The area of those bars is: $A_{sr,bc3} = 9 \cdot A_{sri} = 85451\text{mm}^2$
- The thickness of the equivalent plate is:

$$t_p = {A_{sr,bc1}}/{h_{s1}} = 7238\text{mm}^2/1720\text{mm} = 4.2\text{mm}$$

$$I_{cg,bc1} = \frac{b_{c1} \cdot h_1^{\,3}}{12} = \frac{150\text{mm} \cdot (1800\text{mm})^3}{12} = 7.29 \cdot 10^{10}\,\text{mm}^4$$

$$I_{sr,bc1} = \frac{t_p \cdot h_{s1}^{\,3}}{12} = \frac{4.4\text{mm} \cdot 1720\text{mm}^3}{12} = 1.784 \cdot 10^{9}\,\text{mm}^4$$

$$I_{c,bc1} = I_{cg,bc1} - I_{sr,bc1} = 6.91 \cdot 10^{11}\,\text{mm}^4 - 1.784 \cdot 10^{9}\,\text{mm}^4 = 7.112 \cdot 10^{10}\,\text{mm}^4$$

$$\begin{aligned} EI_{eff,bc1} &= E_{sr} \cdot I_{sr,bc1} + K_e \cdot E_{c,eff} \cdot I_{c,bc1} \\ &= 200000\text{MPa} \cdot 1.784 \cdot 10^{9}\,\text{mm}^4 + 0.6 \cdot 18400\text{MPa} \cdot 7.112 \cdot 10^{10}\,\text{mm}^4 \\ &= 1.142 \cdot 10^{15}\,\text{Nmm}^2 \end{aligned}$$

2) Section b_{c3}: $EI_{eff,bc3} = E_{sr} \cdot I_{sr,bc3} + K_e \cdot E_{c,eff} \cdot I_{c,bc3}$

To calculate $I_{sr,bc3}$, two equivalent (one top and one bottom) steel plates replace the reinforcing bars. Each plate has the same total area, and contains 1 rebar:

$$A_{sr,bc3} = 1 \cdot A_{sri} = 804.2\text{mm}^2$$

$$I_{sr,bc3} = 2 \cdot A_{sr,bc3} \cdot d_{s1y}^{\,2} = 2 \cdot 804.2\text{mm}^2 \cdot (860\text{mm})^2 = 1.222 \cdot 10^{6}\,\text{mm}^4$$

$$I_{cg,bc3} = \frac{b_{c3} \cdot h_1^{\,3}}{12} = \frac{64\text{mm} \cdot (1800\text{mm})^3}{12} = 3.110 \cdot 10^{10}\,\text{mm}^4$$

$$I_{c,bc3} = I_{cg,bc3} - I_{sr,bc3} = 1.222 \cdot 10^{6}\,\text{mm}^4 - 3.110 \cdot 10^{10}\,\text{mm}^4 = 3.110 \cdot 10^{10}\,\text{mm}^4$$

$$\begin{aligned} EI_{eff,bc3} &= E_{sr} \cdot I_{sr,bc3} + K_e \cdot E_{c,eff} \cdot I_{c,bc3} \\ &= 200000\text{MPa} \cdot 1.222 \cdot 10^{6}\,\text{mm}^4 + 0.6 \cdot 18400\text{MPa} \cdot 3.110 \cdot 10^{10}\,\text{mm}^4 \\ &= 3.436 \cdot 10^{14}\,\text{Nmm}^2 \end{aligned}$$

3) Section b_{s2}: $EI_{eff,bs2} = E_s \cdot I_{s,bs2} + E_{sr} \cdot I_{sr,bs2} + K_e \cdot E_{c,eff} \cdot I_{c,bs2}$

To calculate $I_{sr,bs2}$, two equivalent (one top and one bottom) steel plates replace the reinforcing bars. Each plate has the same total area, and contains 2 rebar:

$$A_{sr,bs2} = 2 \cdot A_{sri} = 1608.5\text{mm}^2$$

$$I_{sr,bs2} = 2 \cdot A_{sr,bs2} \cdot {d_{s1y}}^2 = 2 \cdot 1608.5\text{mm}^2 \cdot \left(860\text{mm}\right)^2 = 1.858 \cdot 10^9\,\text{mm}^4$$

$$I_{s,bs2} = I_y = 9.825 \cdot 10^8\,\text{mm}^4$$

$$I_{cg,bs2} = \frac{b_{s2} \cdot {h_1}^3}{12} = \frac{476\text{mm} \cdot \left(1800\text{mm}\right)^3}{12} = 2.304 \cdot 10^{11}\,\text{mm}^4$$

$$I_{c,bs2} = I_{cg,bs4} - I_{sr,bs2} - I_{s,bs2} = 2.304 \cdot 10^{11}\,\text{mm}^4 - 1.858 \cdot 10^9\,\text{mm}^4 - 9.825 \cdot 10^8\,\text{mm}^4 = 3.090 \cdot 10^{15}\,\text{mm}^4$$

$$\begin{aligned} EI_{eff,bs2} &= E_s \cdot I_{s,bs2} + E_{sr} \cdot I_{sr,bs2} + K_e \cdot E_{c,eff} \cdot I_{c,bs2} \\ &= 210000\text{MPa} \cdot 9.825 \cdot 10^8\,\text{mm}^4 + 200000\text{MPa} \cdot 1.858 \cdot 10^9\,\text{mm}^4 + 0.6 \cdot 18400\text{MPa} \cdot 2.304 \cdot 10^{11}\,\text{mm}^4 \\ &= 3.090 \cdot 10^{15}\,\text{Nmm}^2 \end{aligned}$$

4) Section b_{s4}: $EI_{eff,bs4} = E_s \cdot I_{s,bs4} + E_{sr} \cdot I_{sr,bs4} + K_e \cdot E_{c,eff} \cdot I_{c,bs4}$

To calculate $I_{sr,bs4}$, two equivalent (one top and one bottom) steel plates replace the reinforcing bars. Each plate has the same total area, and contains 1 rebar:

$$A_{sr,bs4} = 1 \cdot A_{sri} = 804.2\text{mm}^2$$

$$I_{sr,bs4} = 2 \cdot A_{sr,bs4} \cdot {d_{s1y}}^2 = 2 \cdot 804.2\text{mm}^2 \cdot \left(860\text{mm}\right)^2 = 9.291 \cdot 10^8\,\text{mm}^4$$

$$I_{s,bs4} = 2 \cdot A_{\text{a}} \cdot {d_{sy}}^2 = 2 \cdot 80800\text{mm}^2 \cdot \left(513\text{mm}\right)^2 = 4.801 \cdot 10^{10}\,\text{mm}^4$$

$$I_{cg,bs4} = \frac{b_{s4} \cdot {h_1}^3}{12} = \frac{424\text{mm} \cdot \left(1800\text{mm}\right)^3}{12} = 2.061 \cdot 10^{11}\,\text{mm}^4$$

$$I_{c,bs4} = I_{cg,bs4} - I_{sr,bs4} - I_{s,bs4} = 2.061 \cdot 10^{11}\,\text{mm}^4 - 9.291 \cdot 10^8\,\text{mm}^4 - 4.801 \cdot 10^{10}\,\text{mm}^4 = 2.061 \cdot 10^{11}\,\text{mm}^4$$

$$\begin{aligned} EI_{eff,bs4} &= E_s \cdot I_{s,bs4} + E_{sr} \cdot I_{sr,bs4} + K_e \cdot E_{c,eff} \cdot I_{c,bs4} \\ &= 210000\text{MPa} \cdot 4.253 \cdot 10^{10}\,\text{mm}^4 + 200000\text{MPa} \cdot 9.291 \cdot 10^8\,\text{mm}^4 + 0.6 \cdot 18400\text{MPa} \cdot 2.061 \cdot 10^{11}\,\text{mm}^4 \\ &= 1.254 \cdot 10^{16}\,\text{Nmm}^2 \end{aligned}$$

$$EI_{eff} = 2\cdot(EI_{eff,bc1}) + 2\cdot(EI_{eff,bs2}) + 2\cdot(EI_{eff,bc3}) + EI_{eff,bs4}$$
$$= 2\cdot(1.142\cdot10^{15}\,\text{Nmm}^2) + 2\cdot(3.090\cdot10^{15}\,\text{Nmm}^2) + 2\cdot(3.436\cdot10^{14}\,\text{Nmm}^2) + 1.254\cdot10^{16}\,\text{Nmm}^2$$
$$= 2.169\cdot10^{16}\,\text{Nmm}^2$$

The factored shear force V_{Ed} = 20000 kN for the complete section is distributed in the 5 sections (2 b_{c3}, 2 b_s and 1 b_{c4}):

$$V_{Ed,bc1} = V_{Ed}\cdot\frac{EI_{eff,bc1}}{EI_{eff}} = 20000\text{kN}\cdot\frac{1.142\cdot10^{16}\,\text{Nmm}^2}{2.169\cdot10^{16}\,\text{Nmm}^2} = 421\text{kN}$$

$$V_{Ed,bc3} = V_{Ed}\cdot\frac{EI_{eff,bc1}}{EI_{eff}} = 20000\text{kN}\cdot\frac{3.436\cdot10^{14}\,\text{Nmm}^2}{2.169\cdot10^{16}\,\text{Nmm}^2} = 127\text{kN}$$

$$V_{Ed,bs2} = V_{Ed}\cdot\frac{EI_{eff,bs2}}{EI_{eff}} = 20000\text{kN}\cdot\frac{3.090\cdot10^{15}\,\text{Nmm}^2}{2.169\cdot10^{16}\,\text{Nmm}^2} = 1139\text{kN}$$

$$V_{Ed,bs4} = V_{Ed}\cdot\frac{EI_{eff,bs4}}{EI_{eff}} = 20000\text{kN}\cdot\frac{1.254\cdot10^{16}\,\text{Nmm}^2}{2.169\cdot10^{16}\,\text{Nmm}^2} = 4626\text{kN}$$

- **Calculation of shear in section b_{s4}:**

Section b_{s2} is a composite steel-concrete section having 2 reinforced concrete flanges, 2 steel "flanges" (the HD sections) and 1 reinforced concrete web. To establish longitudinal shear in section b_s, it is convenient to transform the composite section into a single material section or "homogenized" section. The single material can be either steel or concrete.

Choosing concrete, the moment of inertia of the homogenized concrete section I_c* is such that the stiffness $E_c\,I_c$* of the homogenized section is equal to the stiffness $EI_{eff,bs2}$:

$$I_c^* = EI_{eff,bs4} \Big/ E_{cm} = 1.254\cdot10^{16}\,\text{Nmm}^2 \Big/ 39100\text{MPa} = 3.208\cdot10^{11}\,\text{mm}^4$$

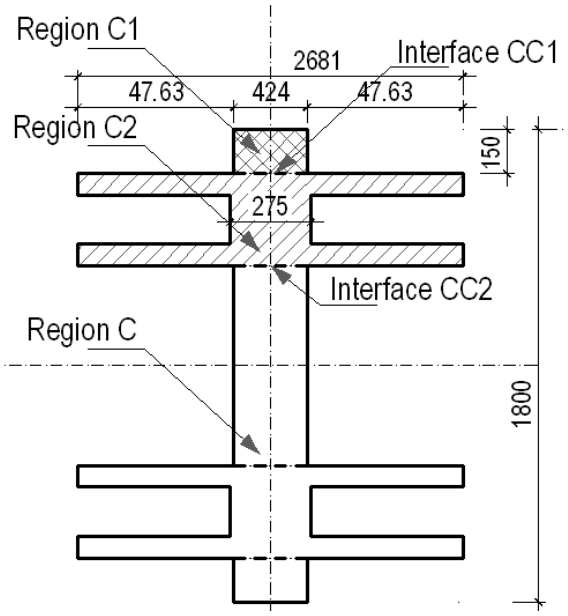

Figure 10-8 Homogenized equivalent concrete section bs – Example 2

In a homogenized concrete section (Figure 10-8), the width of the concrete equivalent to the width of the steel flanges is:

$$b_s^* = b_{s4} \cdot {E_s}/{E_{cm}} = 424\text{mm} \cdot {210000\text{MPa}}/{39100\text{MPa}} = 2277\text{mm}$$

The width of the concrete equivalent to the width of the steel web is:

$$t_w^* = t_w \cdot {E_s}/{E_{cm}} = 51.2\text{mm} \cdot {210000\text{MPa}}/{39100\text{MPa}} = 275\text{mm}$$

The resultant longitudinal shear force on interfaces like CC1 and CC2 in Figure 10-8 is:

$$V_{Ed,l} = \frac{V_{Ed,bs2} \cdot \mathrm{S}}{I_c^*}$$

where:

S is the first moment of areas of regions C1 or C2 taken about the neutral axis of the section as illustrated in Figure 10-8.

Using S, the longitudinal shear is calculated at the steel-concrete interfaces CC1 and CC2 in order to size the force transfer mechanisms required for the member to act as a fully composite section.

- **Calculation of longitudinal shear force applied at interface CC1:**

S_{CC1} is the section modulus for the region C1 as defined in Figure 10-8:

The height of the C1 region is:

$$h_1' = \frac{h_1}{2} - \left(d_{sy} + \frac{d}{2} \right) = \frac{1800\text{mm}}{2} - \left(513\text{mm} + \frac{474\text{mm}}{2} \right) = 150\text{mm}$$

The area is:

$$A_1 = b \cdot h_1' = 424\text{mm} \cdot 150\text{mm} = 63600\text{mm}^2$$

$$S_{CC1} = A_1 \cdot \left(\frac{h_1}{2} - \frac{h_1'}{2} \right) = 63600\text{mm}^2 \cdot \left(\frac{1800\text{mm}}{2} - \frac{150\text{mm}}{2} \right) = 5.247 \cdot 10^7\,\text{mm}^3$$

The resultant longitudinal shear force on interface CC1 is:

$$V_{Ed,CC1} = \frac{V_{Ed,bs} \cdot S_{CC1}}{I_c^*} = \frac{4045\text{kN} \cdot 5.247 \cdot 10^7\,\text{mm}^3}{3.208 \cdot 10^{11}\,\text{mm}^4} = 757\frac{\text{N}}{\text{mm}}$$

On 1-meter length of column:

$$V_{Ed,CC1} = 757\frac{\text{kN}}{\text{m}}$$

- **Calculation of longitudinal shear force applied at interface CC2:**

S_{CC2} is the section modulus for the combined regions C1 and C2 (the HD profile):
The equivalent area in concrete for the HD profile is:

A_a =80800 mm^2

The equivalent are in concrete for the HD profile is:

$$A_a^* = A_a \cdot E_s / E_{cm} = 80800\text{mm}^2 \cdot 210000\text{MPa} / 39100\text{MPa} = 433966\text{mm}^2$$

The distance of HD center to the neutral axis is:

d_{sy} = 513 mm

The moment of area of the equivalent steel profile is:

$$S_{HD} = A_a^* \cdot d_{sy} = 433966\text{mm}^2 \cdot 513\text{mm} = 2.226 \cdot 10^8\,\text{mm}^3$$

Area of concrete between the flanges:

$$A_{c\_CC2}^* = b \cdot d - A_a = 424\text{mm} \cdot 474\text{mm} - 80800\text{mm}^2 = 120176\text{mm}^2$$

Moment of area of concrete between the flanges:

$$S^{*}_{c\_CC2} = A^{*}_{c\_CC2} \cdot d_{sy} = 120176\text{mm}^2 \cdot 513\text{mm} = 6.165 \cdot 10^7\,\text{mm}^3$$

The section modulus of combined regions C1 and C2, is equal to:

$$S_{CC2} = S^{*}_{c\_CC2} + S_{HD} + S_{CC1} = 6.165 \cdot 10^7\,\text{mm}^3 + 2.226 \cdot 10^8\,\text{mm}^3 + 5.247 \cdot 10^7\,\text{mm}^3 = 3.367 \cdot 10^8\,\text{mm}^3$$

The resultant longitudinal shear force at interface CC2 is:

$$V_{Ed,CC2} = \frac{V_{Ed,bs} \cdot S_{CC2}}{I^{*}_{c}} = \frac{4045\text{kN} \cdot 3.367 \cdot 10^8\,\text{mm}^3}{3.208 \cdot 10^{11}\,\text{mm}^4} = 4855\frac{\text{N}}{\text{mm}}$$

On 1-meter length of column:

$$V_{Ed,CC2} = 4855\frac{\text{kN}}{\text{m}}$$

- **Evaluation of necessary amount of shear studs:**

Geometrical characteristic of the shear studs correspond to State of Art – Table 3.2.2 where:

d = 25 mm – diameter of the shear stud;

h_{sc} = 100 mm – stud height; $3d = 75\text{ mm} \le h_{sc}$;

s_c – longitudinal spacing; $5d = 150\text{ mm} \le sc \le \min(6\,h_{sc};\ 800\text{mm}) = 600\text{mm}$;

s_x –transversal spacing; $2.5d = 62.5\text{ mm} \le s_x$;

f_u = 450 MPa – maximum stud tensile strength;

For a shear stud with a diameter d = 25 mm, the design shear strength is equal to:

$$P_{Rk} = \min\left(\frac{0.8 \cdot f_u \cdot \pi \cdot d^2/4}{\gamma_V}, \frac{0.29 \cdot \alpha \cdot d^2 \cdot \sqrt{f_{ck} \cdot E_{cm}}}{\gamma_V}\right) = \min\left(176.71\text{kN}, 247.45\text{kN}\right) = 176.71\text{kN}$$

Where:

$$\alpha = \begin{cases} 0.2\left(\frac{h_{sc}}{d}+1\right) \text{ for } 3 \le \frac{h_{sc}}{d} \le 4 \\ 1 \text{ for } \frac{h_{sc}}{d} > 4 \end{cases} = 1$$

$$\gamma_V = 1$$

$$\frac{0.8 \cdot f_u \cdot \pi \cdot d^2/4}{\gamma_V} = \frac{0.8 \cdot 450\text{MPa} \cdot \pi \cdot (25\text{mm})^2/4}{1} = 176.71\text{kN}$$

$$\frac{0.29 \cdot \alpha \cdot d^2 \cdot \sqrt{f_{ck} \cdot E_{cm}}}{\gamma_V} = \frac{0.29 \cdot 1 \cdot (25\text{mm})^2 \cdot \sqrt{50\text{MPa} \cdot 37278\text{MPa}}}{1} = 247.45\text{kN}$$

For a length of a column of 1 m, the necessary amount of shear studs at the steel profile interfaces is:

$$n_{studs\_CC1} = \frac{V_{Ed1\_CC1} \cdot 1\text{m}}{P_{Rk}} = \frac{757\frac{\text{kN}}{\text{m}} \cdot 1\text{m}}{176.71\text{kN}} = 4.28 \Rightarrow 5 \text{ studs} / 1\text{m}$$

$$n_{studs\_CC2} = \frac{V_{Ed1\_CC2} \cdot 1\text{m}}{P_{Rk}} = \frac{4855\frac{\text{kN}}{\text{m}} \cdot 1\text{m}}{176.71\text{kN}} = 27.47 \Rightarrow 28 \text{ studs} / 1\text{m}$$

10.2 Case 2: AISC 2016 draft version / ACI 318-14

10.2.1 Example 1

Example 1: Composite column with four encased profiles in combined axial compression and flexure about the (x-x) axis, and the steel profiles have the same orientation

Given:

The encased composite member, illustrated in Figure 10-9, is subject to axial force, bending moment, and shear force. The composite member consist of 4 W 14x16x873 (HD 400x1299) ASTM A913 - 11 grade steel profiles, encased in concrete with a specified compressive strength of 7.25 ksi (50 MPa), and 224 pieces of rebar with 1.57 in (40 mm) diameter, S500 grade distributed in 2 layers at the perimeter. The buckling length (L_o) of the column is 708.7 in (18 m).

Check the capacity of the composite column subjected to the following demands:

N_{Ed} = 67443 kip (300000 kN);

M_{Ed} = 221269kip in (250000 kN);

V_{Ed} = 4496 kip (20000 kN);

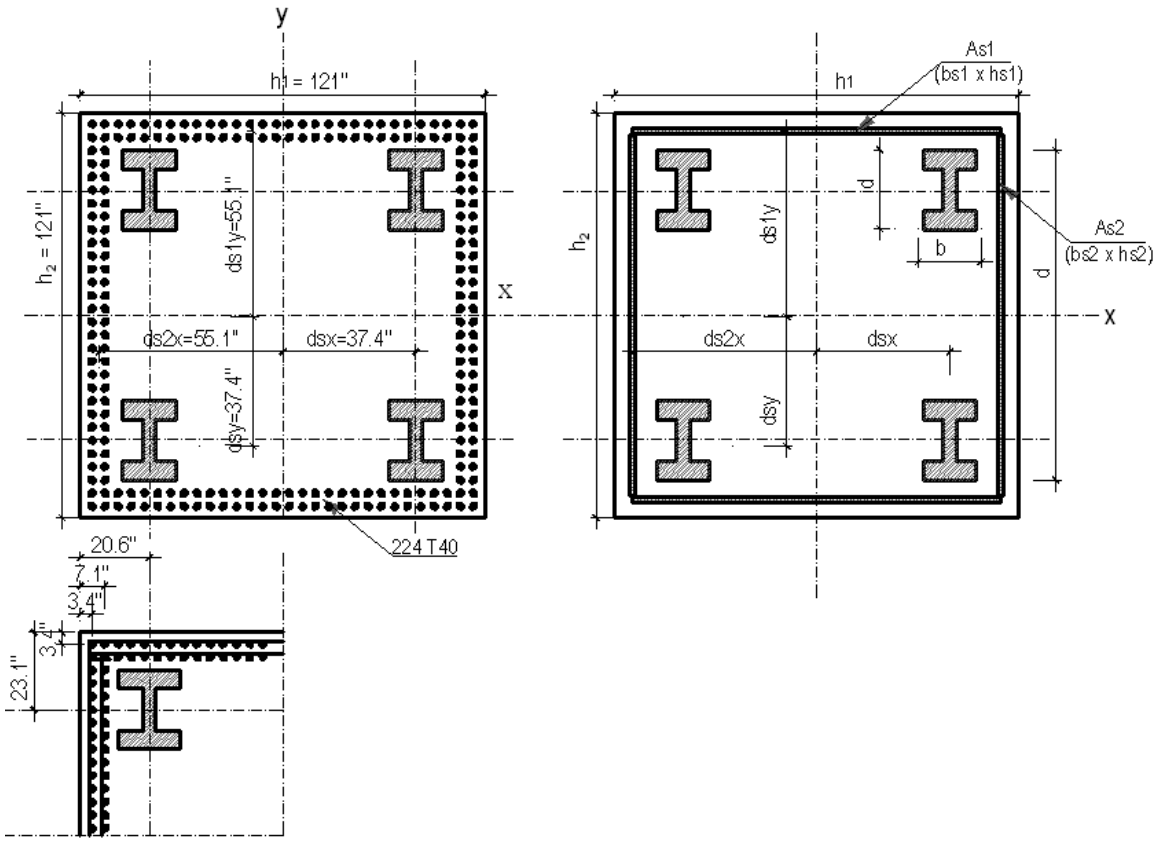

Figure 10-9 Encased composite member section (AISC Design) – Example 1

Steel profile W14x16x873 (HD 400x1299) properties are:

ASTM A913- 11 Grade 65 - f_y = 65 ksi;

E_s = 29000 ksi;

b = 18.7 in;

d = 23.62 in;

t_w = 3.9 in;

t_f = 5.5 in;

Z_{sx} = 2029 in^3;

Z_{sy} = 1017.3 in^3;

$I_{HDx} = 18129.4\text{in.}^4$;

$I_{HDy} = 6112\text{in.}^4$;

A_a = 255.8 in^2;

$A_s = \sum_{i=1}^{4} A_a = 4 \cdot 255.8\text{in}^2 = 1023\text{in}^2$;

d_{sx} = 37.4in.;

d_{sy} = 37.4in.;

d_x = 98.4in.;

d_y = 98.4in.;

Reinforcement properties are:

224 = the total number of vertical rebar;

d_b = 1.57in (equivalent of T40 – with diameter of 40 mm);

f_s = 72.5 ksi.;

E_{sr} = 29000 ksi;

$A_{sri} = 1.95\text{in}^2$;

$A_{sr} = \sum_{i=1}^{n} A_{sri} = 436.3\text{in.}^2$;

Concrete's section properties are:

h_1 = 121 in.;

h_2 = 121 in.;

c_x = 3.4 in.;

c_y = 3.4 in.;

Concrete:

f_c=7251.9 psi;

$E_c = \text{w}_c^{1.5} \cdot \sqrt{f_c} = \left(155 \text{lb}/\text{ft}^3\right)^{1.5} \cdot \sqrt{7.3\text{ksi}} = 5196.6\text{ksi}$;

$A_g = h_1 \cdot h_2 == 14627.7\text{in.}^2$;

$A_c = A_g - A_{sr} - A_s = 13168.4\text{in.}^2$

Solution:

- **Definition of plates equivalent to rebar:**

The definition of the equivalent horizontal plates (A_{s1} and A_{s2}) is made according to the following:

1) A_{s1} plate:

i = 2 = the number of rebar layers in one equivalent plate

n_x = 30 = the amount of rebar in one layer

s_x = 3.9in = the spacing between 2 vertical rebar

$$A_{s1} = i \cdot n_x \cdot A_{sri} = 116.9\text{in.}^2$$

$$h_{s1} = (n_x - 1) \cdot s_x = 114.2\text{in.}$$

$$b_{s1} = \frac{A_{s1}}{h_{s1}} = 1.0\text{in.}$$

$$d_{s1y} = \sum d_{iy} \Big/ i = 55.1\text{in.}$$

$$Z_{sr1x} = 2 \cdot A_{s1} \cdot d_{s1y} = 12883.1\text{in.}^3$$

$$I_{sr1x} = 2 \cdot \mathrm{i} \cdot n_{\mathrm{x}} \cdot A_{sri} \cdot d_{s1y}{}^2 = 710089.8\text{in.}^4$$

2) A_{s2} plate:

$$A_{s2} = n_y \cdot A_{sri} = b_{s2} \cdot h_{s2}$$

j = 2 = the number of rebar layers on one equivalent plate

n_y = 26 = the amount of rebar on one layer

$$A_{s2} = j \cdot n_{\mathrm{y}} \cdot A_{sri} = 101.3\text{in.}^2$$

$$h_{s2} = (n_y - 1) \cdot s_y = 98.4\text{in.}$$

$$b_{s2} = \frac{A_{s2}}{h_{s2}} = 1.0\text{in.}$$

$$d_{s2x} = \sum d_{jx} \Big/ j = 55.1\text{in.}$$

$$Z_{sr2x} = 2 \cdot \frac{b_{s2} \cdot h_{s2}{}^2}{4} = 4984.5\text{in.}^3$$

$$I_{sr2x} = 2 \cdot \frac{b_{s2} \cdot h_{s2}{}^3}{12} = 163534\text{in.}^4$$

- **Definition of plates equivalent to steel profiles:**

The definition of the equivalent horizontal plates is made according to the following:

$$d^* = d = 23.6\text{in.}$$

$$b^* = \frac{A_s}{d^*} = 10.8\text{in.}$$

$$Z_{sx} = n \cdot A_a \cdot d_{sy} = 38261.9\text{in}^3$$

$$I_{sx} = n \cdot A_a \cdot d_{sy}^{\,2} + n \cdot I_x = 1503575.4\text{in.}^4$$

- **Stiffness evaluation:**

$$(EI)_{eff} = E_s \cdot I_s + E_{sr} \cdot I_{sr} + C_1 \cdot E_c \cdot I_c = 1.131 \cdot 10^{11}\,\text{kip} \cdot \text{in}^2$$

$$C_1 = 0.25 + 3 \cdot \frac{A_s + A_{sr}}{A_g} = 0.55 \le 0.7$$

where:

C_1 coefficient for calculation of effective rigidity of an encased composite compression member

- **Limitation when using the extended simplified method:**

1) Concrete cover

ACI 318-14 Table 20.6.1.3.1 contains the requirements for concrete cover. For cast-in-place non-presstresed concrete not exposed to weather or in contact with ground, the required cover for column ties is 1.5 in (38 mm).

$cover = 3.4\text{in} > 1.5\text{in}$ **o. k.**

2) Structural steel minimum reinforcement ratio: AISC 360-11 Section I2.1a.1

$A_s / A_g = 0.07 \ge 0.01$ **o. k.**

3) Minimum longitudinal reinforcement ratio: AISC 360-11 Section I2.1a.1

$A_{sr} / A_g = 0.03 \ge 0.004$ **o. k.**

4) Maximum longitudinal reinforcement ratio: ACI 318-14 Section 10.6.1

$$\rho_{sr} = \frac{A_{sr}}{A_g} = 0.03 \le 0.08$$ **o. k.**

5) Minimum number of longitudinal bars:

ACI 318-14 Section 10.6.1 requires a minimum of four longitudinal bars within rectangular or circular members with ties and six bars for columns utilizing spiral ties. The intent for rectangular sections is to provide a minimum of one bar in each corner, so irregular geometries with multiple corners require additional longitudinal bars.

224 bars provided **o. k.**

6) Clear spacing between longitudinal bars:

ACI 318-14 Section 25.2.3 requires a clear distance between bars of 1.5db or 1.5 in (38 mm).

$$s_{min} = \max\begin{Bmatrix} 1.5 \cdot d_b = 2.4\text{in} \\ 1.5\text{in} \end{Bmatrix} = 2.4\text{in} \geq s_{min}$$ **o. k.**

7) Clear spacing between longitudinal bars and the steel core:

AISC Specification Section I2.1e requires a minimum clear spacing between the steel core and longitudinal reinforcement of 1.5 reinforcing bar diameters, but not less than 1.5 in (38 mm).

$$s_{min} = \max\begin{Bmatrix} 1.5 \cdot d_b = 2.4\text{in} \\ 1.5\text{in} \end{Bmatrix} = 2.4\text{in}$$

The distance from the steel core and the longitudinal bars is determined from Figure 10-9, on x direction: $s = 26\text{in} \geq s_{min}$ **o. k.**

The distance from the steel core and the longitudinal bars is determined from Figure 10-9, on y direction as follows: $s = 3.9\text{in} \geq s_{min}$ **o. k.**

8) Concrete cover for longitudinal reinforcement:

ACI 318-14 Section 10.7 provides concrete cover requirements for reinforcement. The cover requirements for column ties and primary reinforcement are the same, and the tie cover was previously determined to be acceptable, thus the longitudinal reinforcement cover is acceptable by inspection.

- **Interaction of axial force and flexure:**

In order to determine the axial force N – bending moment M interaction curve, critical points are determined. The detailed definition of such points is as follows:

- A – pure axial capacity point

  $N_A = P_n$

  $M_A = 0$ MPa

- B - pure flexural bending point

  $N_B = 0$

  $M_B = M_{pl,Rd}$

- C – point where bending moment = pure bending capacity and axial compressive load > 0

  $N_C = P_{pm,Rd}$

  $M_C = M_{pl,Rd}$

- D – the maximum bending moment point

  $N_D = 0{,}5 \; . \; P_{pm,Rd}$

  $M_D = M_{max,Rd}$

Rigid – plastic material behavior is assumed in order to evaluate these key points. Steel is assumed to have reached yield stress in either tension or compression. Concrete is assumed to have reached its peak stress in compression and have the tensile strength equal to zero. For one equivalent rectangular stress block, the peak stress in compression in this example is:

$$0.85 \cdot f_c = 0.85 \cdot 7.3\text{ksi} = 6.21\text{ksi}$$

- **Evaluation of the plastic resistance to axial force:**

The plastic resistance to axial force combines the individual resistances of the steel profile, the concrete and reinforcement. For concrete – encased steel sections:

$$P_e = \frac{\pi^2 \cdot (EI)_{eff}}{L_o^2} = 2.222 \cdot 10^9 \text{ kip.}$$

$$P_n = \begin{cases} 0.877 P_{no} \cdot 0.658^{P_{no}/P_e} & \text{if } P_{no}/P_e \le 2.25 \\ 0.877 \cdot P_e & \text{if } P_{no}/P_e > 2.25 \end{cases} = 1.736 \cdot 10^8 \text{ kip}$$

Where:

$$P_{no} = A_s \cdot f_{yd} + (A_{s1} + A_{s2}) \cdot f_{sd} + A_c \cdot 0.85 \cdot f_c = 1.796 \cdot 10^8 \text{ kip}$$

$$P_{pm.Rd} = 0.85 \cdot A_c \cdot f_c = 81171.1 \text{kip}$$

$$0.5 \cdot P_{pm.Rd} = 0.5 \cdot A_c \cdot 0.85 \cdot f_c = 40585.6 \text{kip}$$

- **Evaluation of the reduced axial force parameter λ:**

In accordance with AISC Specifications, commentary I5, the same slenderness reduction is applied to each of the remaining points on the interaction surface, using the coefficient λ, which reduce only the axial force values.

$$\lambda = \frac{P_n}{P_{no}} = 0.967$$

- **Evaluation of the maximum moment resistance $M_{max.Rd}$.:**

$$Z_{cx} = \frac{h_1 \cdot h_2^2}{4} - Z_{r1x} - Z_{r2x} - Z_{sx} = 3.862 \cdot 10^5 \text{ in}^3$$

$$M_{max.Rd} = Z_{sx} \cdot f_{yd} + (Z_{r1x} + Z_{r2x}) \cdot f_{sd} + 0.5 \cdot Z_{cx} \cdot (0.85 \cdot f_c) = 4.983 \cdot 10^6 \text{ kip} \cdot \text{in}$$

- **Evaluation of the plastic bending moment resistance $M_{pl.Rd.}$:**

In order to evaluate the plastic bending moment value, first we need to determine the position of the neutral axis. Different assumptions of the neutral axis position have been taken into consideration. The position of the neutral axis is determined by subtracting the stress distribution combination at point B and C, considering normal forces only.

Assumption 1: h_{nx} between the two profiles $\left(h_{nx} \le d_{sy} - \frac{d}{2} \right)$:

$$h_{nx} = \frac{N_C}{(2 \cdot h_1 - 4 \cdot b_{s2}) \cdot (0.85 \cdot f_{cd}) + 4 \cdot b_{s2} \cdot f_{sd}} = 40.1\text{in}$$

Check assumption $\left(h_{nx} \le d_{sy} - \frac{d}{2} \right)$: assumption **not ok**

$$h_{nx} = 40.\text{in} \le d_{sy} - \frac{d}{2} = 25.6\text{in}$$

Assumption 2: h_{nx} is placed within the steel profiles $\left(d_{sy} - \frac{d}{2} < h_{nx} \le d_{sy} + \frac{d}{2} \right)$:

$$h_{nx} = \frac{N_C + 4 \cdot (d_{sy} - d/2) \cdot b^* \cdot (f_{yd} - 0.85 \cdot f_c)}{(2 \cdot h_1 - 4 \cdot b^* - 4 \cdot b_{s2}) \cdot (0.85 \cdot f_c) + 4 \cdot b^* \cdot f_{yd} + 4 \cdot b_{s2} \cdot f_{sd}} = 42.8\text{in}$$

Check assumption $\left(d_{sy} - \frac{d}{2} < h_{nx} \le d_{sy} + \frac{d}{2} \right)$: assumption **ok**

$$d_{sy} - \frac{d}{2} = 25.6\text{in} < h_{nx} = 42.8\text{in} \le d_{sy} + \frac{d}{2} = 49.2\text{in}$$

$$M_{pl.Rd} = M_{max.Rd} - Z_{r2xn} \cdot f_{sd} - Z_{sxn} \cdot f_{yd} - \frac{1}{2} \cdot Z_{cxn} \cdot (0.85 \cdot f_c) = 4.024 \cdot 10^6 \,\text{kip} \cdot \text{in}$$

where:

$$Z_{sxn} = b^* \cdot \left[h_{nx} - \left(d_{sy} - d/2 \right) \right] \cdot \left[3 \cdot h_{nx} + \left(d_{sy} - d/2 \right) \right] = 2.869 \cdot 10^4 \,\text{mm}^3$$

$$Z_{r2xn} = 2 \cdot b_{s2} \cdot h_{nx}^2 = 3.770 \cdot 10^3 \,\text{mm}^3$$

$$Z_{cxn} = h_1 \cdot h_{nx}^2 - Z_{r2xn} - Z_{sxn} = 1.891 \cdot 10^5 \,\text{mm}^3$$

- **Interaction curve bending moment axial force:**

LFRD	ASD
Design compressive strength: $\phi_C = 0.75$ $P_{X''} = \phi_C \cdot P_X \cdot \lambda$ where *X = A,B,C or D*	Allowable compressive strength: $\Omega_C = 2.00$ $P_{X''} = \frac{P_X \cdot \lambda}{\Omega_C}$ where *X = A,B,C or D*
$P_{A''} = \phi_C \cdot P_A \cdot \lambda = 130205\text{kip}$ $P_{B''} = \phi_C \cdot P_B \cdot \lambda = 0\text{kip}$	$P_{A''} = \frac{P_A \cdot \lambda}{\Omega_C} = 86803\text{kip}$
$P_{C''} = \phi_C \cdot P_C \cdot \lambda = 60878\text{kip}$	$P_{B''} = \frac{P_B \cdot \lambda}{\Omega_C} = 0\text{kip}$
$P_{D''} = \phi_c \cdot P_D \cdot \lambda = 30439\text{kip}$	$P_{C''} = \frac{P_C \cdot \lambda}{\Omega_C} = 40586\text{kip}$
Design flexural strength: $\phi_B = 0.90$	$P_{D''} = \frac{P_D \cdot \lambda}{\Omega_C} = 20293\text{kip}$
$M_{X''} = \phi_B \cdot M_X$ where *X = A,B,C or D*	Allowable flexural strength: $\Omega_b = 1.67$
$M_{Ax''} = \phi_B \cdot M_{Ax} = 0\text{kip} \cdot \text{in}$	$M_{X''} = \frac{M_X}{\Omega_b}$ where *X = A,B,C or D*
$M_{Bx''} = \phi_B \cdot M_{Bx} = 3621692\text{kip} \cdot \text{in}$	$M_{Ax''} = \frac{M_{Ax}}{\Omega_b} = 0\text{kip} \cdot \text{in}$
$M_{Cx''} = \phi_B \cdot M_{Cx} = 3621692\text{kip} \cdot \text{in}$	$M_{Bx''} = \frac{M_{Bx}}{\Omega_b} = 2409642\text{kip} \cdot \text{in}$
$M_{Dx''} = \phi_B \cdot M_{Dx} = 4484814\text{kip} \cdot \text{in}$	$M_{Cx''} = \frac{M_{Cx}}{\Omega_b} = 2409642\text{kip} \cdot \text{in}$
	$M_{Dx''} = \frac{M_{Dx}}{\Omega_b} = 2983908\text{kip}$

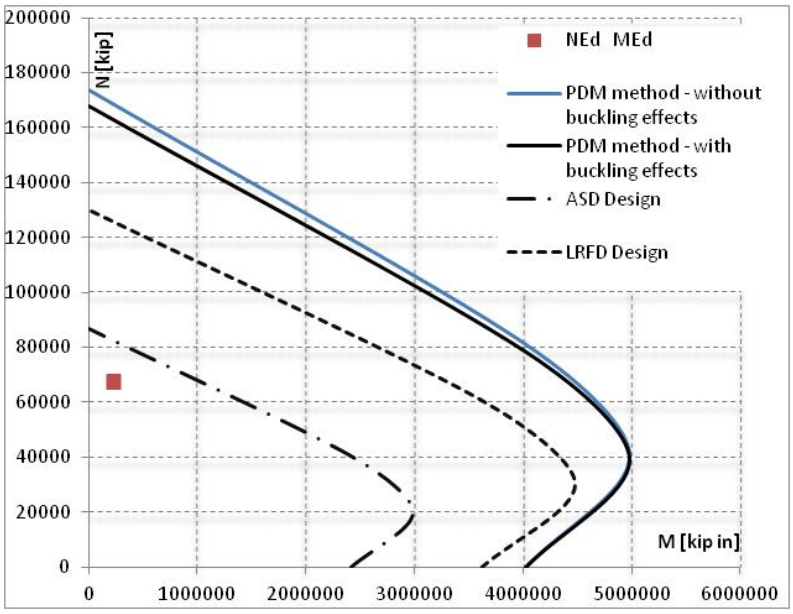

Figure 10-10 Axial force - bending moment interaction curve (AISC Design) – Example 1

- **Shear force evaluation:**

The evaluation of the shear force is made according to the report "Design Example of a column with 4 encased steel profiles" prepared by ArcelorMittal in collaboration with University of Liege. This procedure is to evaluate the composite behavior as a whole and additional considerations should be taken into account in order to ensure adequate load paths from the concrete to steel or vice versa at the load application points. The definition of the used symbols is defined in Figure 10-11:

$b_{c3} = 11.26\text{in}$

$b_s = 18.74\text{in}$

$b_{c4} = 60.94\text{in}$

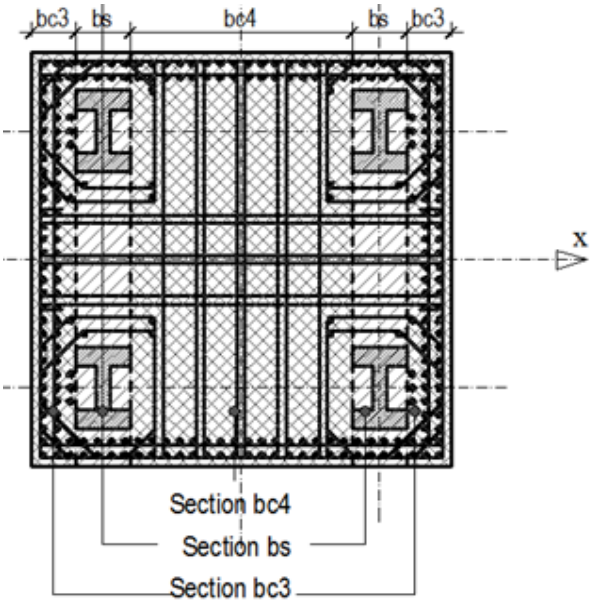

Figure 10-11 Definition of sections bc3, bc4, and bs (AISC Design) – Example 1

The applied shear force is V_{Ed} is distributed between sections b_{c3}, b_{c4} and b_s proportionally to their stiffness:

$$V_{Ed,bc3} = V_{Ed} \cdot {EI_{eff,bc3}}/{EI_{eff}}$$

$$V_{Ed,bc4} = V_{Ed} \cdot {EI_{eff,bc4}}/{EI_{eff}}$$

$$V_{Ed,bs} = V_{Ed} \cdot {EI_{eff,bs}}/{EI_{eff}}$$

The effective bending stiffness of the column is:

$$EI_{eff} = 3.244 \cdot 10^{17}\,\text{kip} \cdot \text{in}^2$$

The total effective bending stiffness is the sum of individual EI_{eff} established for sections b_{c3}, b_{c4} and b_s respectively.

1) Section b_{c3}: $EI_{eff,bc3} = E_{sr} \cdot I_{sr,bc3} + C_1 \cdot E_c \cdot I_{c,bc3}$

To calculate $I_{sr,bc3}$ of the reinforcing bars, it is considered one equivalent plate A_{s2} and 2x2 bars on the top and bottom.

For each face:

- The number of bars is: 30+30+4+4 = 68 bars
- The area of those bars is: $A_{sr,bc3} = 68 \cdot A_{sri} = 132.45\text{in}^2$
- The thickness of the equivalent plate is:

$$t_p = {A_{sr,side}}/{h_{s1}} = 1.16\text{in}$$

$$I_{cg,bc3} = \frac{b_{c3} \cdot h_1^3}{12} = 1.660 \cdot 10^6\,\text{in}^4;$$

$$I_{sr,bc3} = \frac{t_p \cdot h_{s1}^3}{12} = 1.439 \cdot 10^5\,\text{in}^4;$$

$$I_{c,bc3} = I_{cg,bc3} - I_{sr,bc3} = 1.516 \cdot 10^6\,\text{in}^4;$$

$$EI_{eff,bc3} = E_{sr} \cdot I_{sr,bc3} + C_1 \cdot E_c \cdot I_{c,bc3} = 8.501 \cdot 10^9\,\text{kip} \cdot \text{in}^2;$$

2) Section b_{c4}: $EI_{eff,bc4} = E_{sr} \cdot I_{sr,bc4} + C_1 \cdot E_c \cdot I_{c,bc4}$

To calculate $I_{sr,bc4}$, two equivalent (one top and one bottom) steel plates replace the reinforcing bars. Each plate has the same total area, and contains 36 pieces of rebar:

$$A_{sr,bc4} = 36 \cdot A_{sri} = 70.12\text{in}^2$$

$$I_{sr,bc4} = 2 \cdot A_{sr,bc4} \cdot d_{s1y}{}^2 = 4.261 \cdot 10^5 \text{in}^4$$

$$I_{cg,bc4} = \frac{b_{c4} \cdot h_1^3}{12} = 8.985 \cdot 10^6 \text{in}^4$$

$$I_{c,bc4} = I_{cg,bc4} - I_{sr,bc4} = 8.559 \cdot 10^6 \text{mm}^4$$

$$EI_{eff,bc4} = E_{sr} \cdot I_{sr,bc4} + C_1 \cdot E_c \cdot I_{c,bc4} = 3.679 \cdot 10^{10} \text{kip} \cdot \text{in}^2$$

3) Section b_s: $EI_{eff,bs} = E_s \cdot I_{s,bs} + E_{sr} \cdot I_{sr,bs} + C_1 \cdot E_c \cdot I_{c,bs}$

To calculate $I_{sr,bs}$, two equivalent (one top and one bottom) steel plates replace the reinforcing bars. Each plate has the same total area, and contains 8 pieces of rebar:

$$A_{sr,bs} = 8 \cdot A_{sri} = 15.58\text{in}^2$$

$$I_{sr,bs} = 2 \cdot A_{sr,bs} \cdot d_{s1y}{}^2 = 9.468 \cdot 10^4 \text{in}^4$$

$$I_{s,bs} = 2 \cdot A_a \cdot d_{sy}{}^2 + 2 \cdot I_{sx} = 2.151 \cdot 10^{10} \text{in}^4$$

$$I_{cg,bs} = \frac{b_s \cdot h_1^3}{12} = 1.15 \cdot 10^{12} \text{in}^4$$

$$I_{c,bs} = I_{cg,bc4} - I_{sr,bc4} - I_{s,bs} = 2.453 \cdot 10^6 \text{in}^4$$

$$EI_{eff,bs} = E_s \cdot I_{s,bs} + E_{sr} \cdot I_{sr,bs} + C_1 \cdot E_c \cdot I_{c,bc4} = 1.599 \cdot 10^{10} \text{kip} \cdot \text{in}^2$$

$$EI_{eff} = 2 \cdot (EI_{eff,bc3}) + EI_{eff,bc4} + 2 \cdot (EI_{eff,bc4}) = 8.577 \cdot 10^{17} \text{kip} \cdot \text{in}^2$$

The factored shear force V_{Ed} = 4496 kip (20000 kN) for the complete section is distributed in the 5 sections (2 b_{c3}, 2 b_s and 1 b_{c4}) :

$$V_{Ed,bc3} = V_{Ed} \cdot \frac{EI_{eff,bc3}}{EI_{eff}} = 446\text{kip}$$

$$V_{Ed,bc4} = V_{Ed} \cdot \frac{EI_{eff,bc4}}{EI_{eff}} = 1929\text{kip}$$

$$V_{Ed,bs} = V_{Ed} \cdot \frac{EI_{eff,bs}}{EI_{eff}} = 838\text{kip}$$

- **Calculation of shear in section b_s:**

Section b_s is a composite steel-concrete section having 2 reinforced concrete flanges, 2 steel "flanges" (the HD sections) and 1 reinforced concrete web. To establish longitudinal shear in section b_s, it is convenient to transform the composite section into a single material section or "homogenized" section. The single material can be either steel or concrete.

Choosing concrete, the moment of inertia of the homogenized concrete section I_c* is such that the stiffness $E_c\ I_c$* of the homogenized section is equal to the stiffness $EI_{eff,bs}$:

$$I_c^* = EI_{eff,bs} \Big/ E_c = 3.077 \cdot 10^6 \text{in}^4$$

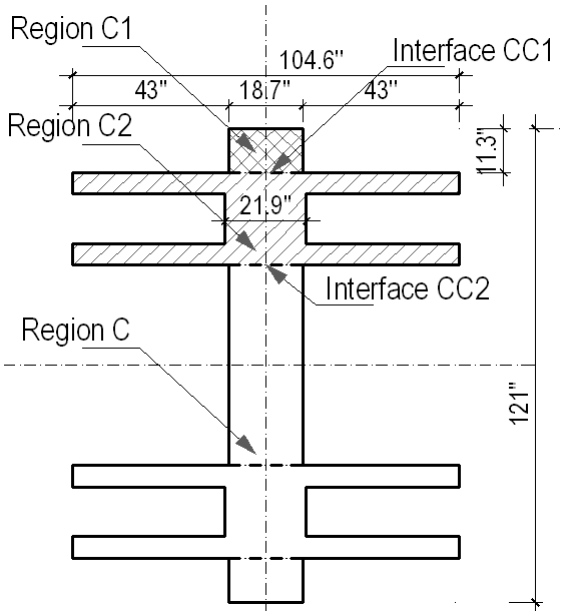

Figure 10-12 Homogenized equivalent concrete section bs – Example 1

In a homogenized concrete section (Figure 10-12), the width of the concrete equivalent to the width of the steel flanges is:

$$b_s^* = b_s \cdot E_s \Big/ E_{cm} = 104.6\text{in}$$

The width of the concrete equivalent to the width of the steel web is:

$$t_w^* = t_w \cdot E_s \Big/ E_{cm} = 21.9\text{in}$$

The resultant longitudinal shear force on regions like CC1 and CC2 in Figure 10-12 is:

$$V_{Ed,l} = \frac{V_{Ed,bs} \cdot \text{S}}{I_c^*}$$

where:

S is the first moment of areas of regions C1 or C2 taken about the natural axis of the section as illustrated in Figure 10-12.

Using S, the longitudinal shear is calculated at the steel-concrete interfaces between CC1 and CC2 in order to size the force transfer mechanisms required for the member to act as a fully composite section.

- **Calculation of longitudinal shear force applied at interface CC1:**

S_{CC1} is the section modulus for the region C1 ranging from the edge to outer HD flange:
The height of the C1 region is:

$$h_1' = \frac{h_1}{2} - \left(d_{sy} + \frac{d}{2} \right) = 11.26\text{in}$$

The area is:

$$A_1 = b \cdot h_1' = 211.01\text{in}^2$$

$$S_{CC1} = A_1 \cdot \left(\frac{h_1}{2} - \frac{h_1'}{2} \right) = 1.157 \cdot 10^4 \text{in}^3$$

The resultant longitudinal shear force at interface CC1 is:

$$V_{Ed,CC1} = \frac{V_{Ed,bs} \cdot S_{CC1}}{I_c^*} = 3.15 \frac{\text{kip}}{\text{in}}$$

- **Calculation of longitudinal shear force applied at interface CC2:**

S_{CC2} is the section modulus for the region C1 plus C2 (the HD profile):
The equivalent area in concrete for the HD profile is:

$$A_a = 255.8\text{in}^2$$

The equivalent are in concrete for the HD profile is:

$$A_a^* = A_a \cdot E_s / E_{cm} = 1427.6\text{in}^2$$

The distance of HD center to the neutral axis is:

$$d_{sy} = 37.4 \text{ in}$$

The moment of area of the equivalent steel profile is:

$$S_{HD} = A_a^* \cdot d_{sy} = 5.339 \cdot 10^4 \text{in}^3$$

Area of concrete between the flanges:

$$A_{c\_CC2}^* = b \cdot d - A_a = 186.93\text{in}^2$$

Moment of area of concrete between the flanges:

$$S^{*}_{c\_CC2} = A^{*}_{c\_CC2} \cdot d_{sy} = 6.992 \cdot 10^{3}\,\text{in}^{3}$$

The section modulus corresponding to the area C1 and C2 limited by sections CC2 is equal to:

$$S_{CC2} = S^{*}_{c\_CC2} + S_{HD} + S_{CC1} = 7.196 \cdot 10^{4}\,\text{in}^{3}$$

The resultant longitudinal shear force on section CC2 is:

$$V_{Ed,CC2} = \frac{V_{Ed,bs} \cdot S_{CC2}}{I^{*}_{c}} = 19.60\,\frac{\text{kip}}{\text{in}}$$

- **Evaluation of necessary amount of shear studs:**

Where concrete breakout strength in shear is not an applicable limit state, the design shear strength $\phi_v Q_{nv}$ and allowable shear strength Q_{nv}/Ω_v shall be determined according to AISC 2015 Specifications Eq. I8-3:

$$Q_{nv} = F_u \cdot A_{sa}$$

where:

$\phi_v = 0.65$ (LRFD)

$\Omega_v = 2.31$ (ASD)

Q_{nv} nominal shear strength of steel headed stud anchor, kips

F_u specified minimum tensile strength of a steel headed stud anchor, ksi

A_{sa} cross-sectional area of steel-headed stud anchor, in^2

$A_{sa} = \pi \cdot (0.75)^2/4 = 0.44\,\text{in}^2$ per steel headed stud anchor diameter 0.75in

$F_u = 63.3\,\text{ksi}$

$\phi_v Q_{nv} = 0.65 \cdot 63.3\,\text{ksi} \cdot 0.44\,\text{in}^2 = 18\,\text{kip}$

The necessary amount of shear studs to different interfaces is:

$$n_{studs\_CC1} = \frac{V_{Ed1\_CC1}}{\phi_v Q_{nv}} = \frac{3.15\,\frac{\text{kip}}{\text{in}}}{18\,\text{kip}} = \frac{37.82\,\frac{\text{kip}}{\text{ft}}}{18\,\text{kip}} \Rightarrow 3\ \text{studs / 1ft}$$

$$n_{studs\_CC2} = \frac{V_{Ed1\_CC2}}{\phi_v Q_{nv}} = \frac{19.60\,\frac{\text{kip}}{\text{in}}}{18\,\text{kip}} = \frac{235.22\,\frac{\text{kip}}{\text{ft}}}{18\,\text{kip}} \Rightarrow 13\ \text{studs / 1ft}$$

10.2.2 Example 2

Example 2: Composite column with four encased profiles in combined axial compression and flexure about the (x-x) axis, and the steel profiles have different orientations

Given:

The encased composite member, illustrated in Figure 10-13, is subject to axial force, bending moment, and shear force. The composite member consist of 4 W 14x16x426 (HD 400x634) HISTAR 460 grade steel profiles, encased in concrete with a specified compressive strength of 8.7 ksi (60 MPa), and 32 pieces of rebar with 1.3 in (32 mm) diameter, HRB 400 grade distributed in 1 layer at the perimeter. The buckling length (L_o) of the column is 708.7 in (18m).

Check the capacity of the composite column subjected to the following demands:

N_{Ed} = 33721 kip (150000 kN);

M_{Ed} = 35403 kip in (40000 kN);

V_{Ed} = 1798 kip (8000 kN);

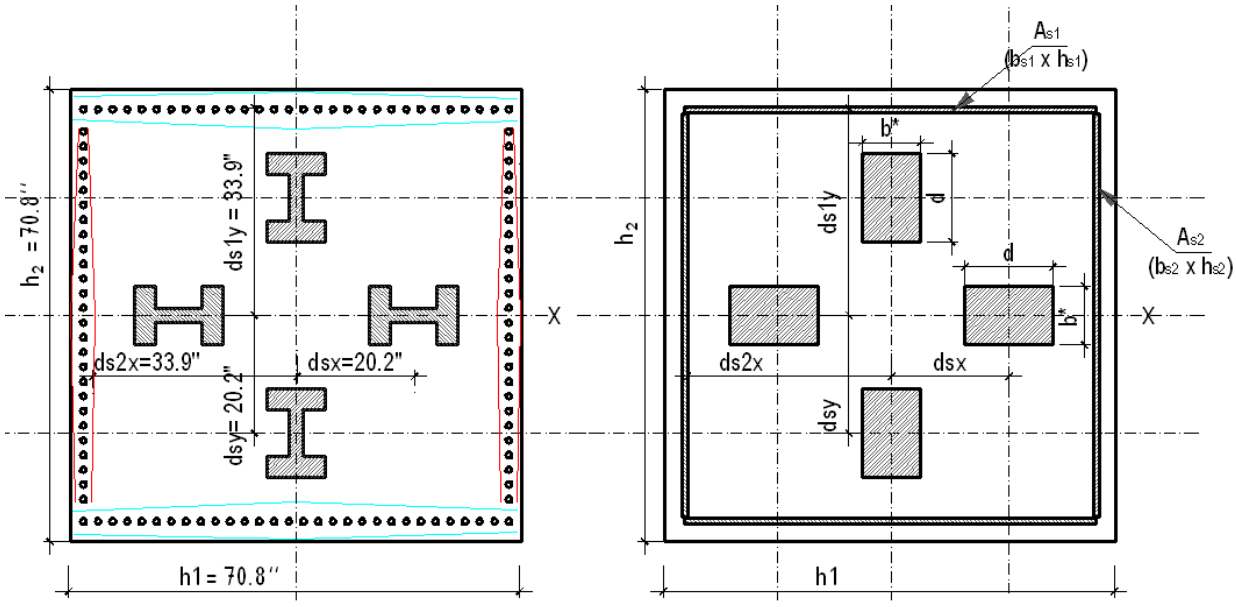

Figure 10-13 Encased composite member section (AISC Design) – Example 2

Steel profile W 14x16 x426 (HD 400x634) properties are:

HISTAR 460 - f_y = 66.7 ksi;

E_s = 29000 ksi;

b = 16.7 in;

d = 18.7 in;

t_w = 2.0 in;

t_f = 3.2 in;

Z_{sx} = 867.8 in^3;

Z_{sy} = 434.3 in^3;

$I_{HDx} = 6578.7 in^4$;

$I_{HDy} = 2360.5 in^4$

$A_a = 125.2 in^2$;

$A_s = \sum_{i=1}^{4} A_a = 4 \cdot 125.2\ in^2 = 501\ in^2$;

$d_{sx} = d_{sy} = 20.2 in$

$d_x = d_y$ = 14.8 in;

Reinforcement properties are:

32 = the total number of vertical rebar;

d_b = 1.3 in equivalent T32 diameter rebar;

f_s = 58.ksi;

E_{sr} = 29000 ksi;

$A_{sri} = 1.25 in^2$;

$A_{sr} = \sum_{i=1}^{n} A_{sri} = 39.9 in^2$;

Concrete section's properties are:

f_c = 8.7 ksi;

E_c = 5692.6 ksi

h_1 = 70.9 in;

h_2 = 70.9 in;

c_x = 1.6 in;

c_y = 1.6 in;

$A_g = h_1 \cdot h_2 = 5022 in^2$;

$A_c = A_g - A_{sr} - A_s = 4481.2 in^2$

Solution:

- **Definition of plates equivalent to rebar:**

The definition of the equivalent horizontal plates (A_{s1} and A_{s2}) is made according to the following:

1) A_{s1} plate:

i = 1= the number of rebar layers in one equivalent plate

n_x = 9 = the amount of rebar in one layer

$A_{s1}=i \cdot n_x \cdot A_{sri}=11.2\text{in}^2$;

$h_{s1} = 67.7\text{in} \qquad b_{s1} = \frac{A_{s1}}{h_{s1}} = 0.2\text{in}$

$d_{s1y} = \sum d_{iy} / i = 29.9\text{in}$

$Z_{sr1x} = 2 \cdot A_{s1} \cdot d_{s1y} = 1236.8\text{in}^3$

$I_{sr1x} = 2 \cdot i \cdot n_x \cdot A_{sri} \cdot d_{s1y}{}^2 = 2.009 \cdot 10^4 \text{in}^4$

2) A_{s2} plate:

$A_{s2} = n_y \cdot A_{sri} = b_{s2} \cdot h_{s2}$

j = 1= the number of rebar layers in one equivalent plate

n_y = 7 = the amount of rebar in one layer

$A_{s2}=j \cdot n_y \cdot A_{sri}=8.7\text{in}^2$; $\quad h_{s2} = (n_y - 1) \cdot s_y = 50.8\text{in};$

$b_{s2} = \frac{A_{s2}}{h_{s2}} = 0.2\text{in}$;

$d_{s2x} = \sum d_{jx} / j = 29.9\text{in}$;

$Z_{sr2x} = 2 \cdot \frac{b_{s2} \cdot h_{s2}{}^2}{4} = 221.6\text{in}^3$;

$I_{sr2x} = 2 \cdot \frac{b_{s2} \cdot h_{s2}{}^3}{12} = 3.751 \cdot 10^3 \text{in}^4$

- **Definition of plates equivalent to steel profiles:**

The definition of the equivalent horizontal plates is made according to the following:

$d^* = d = 23.6\text{in};$

$b^* = \frac{A_a}{d^*} = 5.3\text{in};$

$Z_{sx} = 2 \cdot A_a \cdot d_{sy} + 2 \cdot Z_y = 1.012 \cdot 10^4 \text{in}^3;$

$I_{sx} = 2 \cdot A_a \cdot d_{sy}{}^2 + 2 \cdot I_x = 2.307 \cdot 10^5 \text{in}^4;$

- **Stiffness evaluation**

$(EI)_{eff} = E_s \cdot I_s + E_{sr} \cdot I_{sr} + C_1 \cdot E_c \cdot I_c = 1.341 \cdot 10^{10} \text{kip} \cdot \text{in}^2$

$C_1 = 0.25 + 3 \cdot \frac{A_s + A_{sr}}{A_g} = 0.57 \leq 0.7$

where:

C_1 coefficient for calculation of effective rigidity of an encased composite compression member

- **Limitation when using the extended simplified method:**

1) Concrete cover

ACI 318-14 Table 20.6.1.3.1 contains the requirements for concrete cover. For cast-in-place non-presstresed concrete not exposed to weather or in contact with ground, the required cover for column ties is 1.5 in (38 mm).

$cover = 1.6\text{in} > 1.5\text{in}$ **o. k.**

2) Structural steel minimum reinforcement ratio: AISC 360-11 Section I2.1a.1

$A_s / A_g = 0.1 \geq 0.01$ **o. k.**

3) Minimum longitudinal reinforcement ratio: AISC 360-11 Section I2.1a.1

$A_{sr} / A_g = 0.01 \geq 0.004$ **o. k.**

4) Maximum longitudinal reinforcement ratio: ACI 318-14 Section 10.6.1

$\rho_{sr} = \frac{A_{sr}}{A_g} = 0.01 \leq 0.08$ **o. k.**

5) Minimum number of longitudinal bars:

ACI 318-14 Section 10.6.1 requires a minimum of four longitudinal bars within rectangular or circular members with ties and six bars for columns utilizing spiral ties. The intent for rectangular sections is to provide a minimum of one bar in each corner, so irregular geometries with multiple corners require additional longitudinal bars.

224 bars provided **o. k.**

6) Clear spacing between longitudinal bars:

ACI 318-14 Section 25.2.3 requires a 1.5db or 1.5in (38mm) distance between bars.

$$s_{min} = \max\begin{Bmatrix} 1.5 \cdot d_b = 1.9\text{in} \\ 1.5\text{in} \end{Bmatrix} = 1.9\text{in} \geq s_{min}$$ **o. k.**

7) Clear spacing between longitudinal bars and the steel core:

AISC Specification Section I2.1e requires a minimum clear spacing between the steel core and longitudinal reinforcement of 1.5 reinforcing bar diameters, but not less than 1.5 in (38 mm).

$$s_{min} = \max\begin{Bmatrix} 1.5 \cdot d_b = 1.9\text{in} \\ 1.5\text{in} \end{Bmatrix} = 1.5\text{in}$$

The distance from the steel core and the longitudinal bars is determined from Figure 10-13, on x direction: $s = 8.5\text{in} \geq s_{min}$ **o. k.**

The distance from the steel core and the longitudinal bars is determined from Figure 10-13, on y direction as follows: $s = 8.5\text{in} \geq s_{min}$ **o. k.**

8) Concrete cover for longitudinal reinforcement:

ACI 318-14 Section 10.7 provides concrete cover requirements for reinforcement. The cover requirements for column ties and primary reinforcement are the same, and the tie cover was previously determined to be acceptable, thus the longitudinal reinforcement cover is acceptable by inspection.

- **Interaction of axial force and flexure:**

In order to determine the axial force N – bending moment M interaction curve, critical points are determined. The detailed definition of such points is as follows:

- A – pure axial capacity point

$N_A = P_n$

$M_A = 0$ MPa

- B - pure flexural bending point

$N_B = 0$

$M_B = M_{pl,Rd}$

- C – point with bending moment equal to the pure bending capacity and axial compressive load greater than 0.

$N_C = P_{pm,Rd}$

$M_C = M_{pl,Rd}$

- D – the maximum bending moment point

$N_D = 0{,}5 \; . \; P_{pm,Rd}$

$M_D = M_{max,Rd}$

Rigid – plastic material behavior is assumed in order to evaluate these key points. Steel is assumed to have reached yield stress in either tension or compression. Concrete is assumed to have reached its peak stress in compression and have the tensile strength equal to zero. For one equivalent rectangular stress block, the peak stress in compression in this example is:

$$0.85 \cdot f_{cd} = 0.85 \cdot 8.7\text{ksi} = 7.4\text{ksi}$$

- **Evaluation of the plastic resistance to axial force:**

The plastic resistance to axial force combines the individual resistances of the steel profile, the concrete and reinforcement. For concrete – encased steel sections:

$$P_e = \frac{\pi^2 \cdot (EI)_{eff}}{L_o^2} = 2.635 \cdot 10^8 \text{ kip.}$$

$$P_n = \begin{cases} 0.877 P_{no} \cdot 0.658^{P_{no}/P_e} & \text{if } P_{no}/P_e \le 2.25 \\ 0.877 \cdot P_e & \text{if } P_{no}/P_e > 2.25 \end{cases} = 6.175 \cdot 10^7 \text{ kip}$$

where:

$$P_{no} = A_s \cdot f_{yd} + (A_{s1} + A_{s2}) \cdot f_{sd} + A_c \cdot 0.85 \cdot f_c = 6.888 \cdot 10^7 \text{ kip}$$

$$P_{pm.Rd} = 0.85 \cdot A_c \cdot f_c = 33146.8 \text{kip}$$

$$0.5 \cdot P_{pm.Rd} = 0.5 \cdot A_c \cdot 0.85 \cdot f_c = 16573.4 \text{kip}$$

- **Evaluation of the reduced axial force parameter λ:**

In accordance with AISC Specifications, commentary I5, the same slenderness reduction is applied to each of the remaining points on the interaction surface, using the coefficient λ, which reduce the axial forces value.

$$\lambda = \frac{P_n}{P_{no}} = 0.896$$

- **Evaluation of the maximum moment resistance $M_{max.Rd.}$:**

$$Z_{cx} = \frac{h_1 \cdot h_2^2}{4} - Z_{r1x} - Z_{r2x} - Z_{sx} = 7.740 \cdot 10^4 \text{ in}^3$$

$$M_{max.Rd} = Z_{sx} \cdot f_{yd} + (Z_{r1x} + Z_{r2x}) \cdot f_{sd} + 0.5 \cdot Z_{cx} \cdot (0.85 \cdot f_c) = 1.046 \cdot 10^6 \text{ kip} \cdot \text{in}$$

- **Evaluation of the plastic bending moment resistance $M_{pl.Rd.}$:**

In order to evaluate the plastic bending moment value, first we need to determine the position of the neutral axis. Different assumptions of the neutral axis position have been taken into consideration. The position of the neutral axis is determined by subtracting the stress distribution combination at point B and C, considering normal forces only.

Assumption 1: h_{nx} between the two profiles $\left(h_{nx} \le \frac{b^*}{2}\right)$:

$$h_{nx} = \frac{N_C}{(2 \cdot h_1 - 2 \cdot d - 4 \cdot b_{s2}) \cdot (0.85 \cdot f_c) + 2 \cdot d \cdot f_{yd} + 4 \cdot b_{s2} \cdot f_{sd}} = 8.5\text{in}$$

Check assumption $\left(h_{nx} \le \frac{b^*}{2}\right)$: assumption **not ok**

$$h_{nx} = 8.5 \le \frac{b^*}{2} = 2.7\text{in}$$

Assumption 2: h_{nx} is placed within the steel profiles $\left(b^*/2 < h_{nx} \le d_{sy} - d/2\right)$:

$$h_{nx} = \frac{N_C + 2 \cdot A_a \cdot 0.85 \cdot f_c - 2 \cdot A_a \cdot f_{yd}}{(2 \cdot h_1 - 4 \cdot b_{s2}) \cdot (0.85 \cdot f_c) + 4 \cdot b_{s2} \cdot f_{sd}} = 16.9\text{in}$$

Check assumption $\left(b^*/2 < h_{nx} \le d_{sy} - d/2\right)$: assumption **ok**

$$b^*/2 = 2.7\text{in} < h_{nx} = 16.9\text{in} \le d_{sy} - d/2 = 32\text{in}$$

$$Z_{r2xn} = 2 \cdot b_{s2} \cdot h_{nx}^2 = 9.796 \cdot 10^1 \text{in}^3$$

$$Z_{sxn} = 2 \cdot Z_y = 8.686 \cdot 10^2 \text{in}^3$$

$$Z_{cxn} = h_1 \cdot h_{nx}^2 - Z_{r2xn} - Z_{sxn} = 1.924 \cdot 10^4 \text{in}^3$$

$$M_{pl.Rd} = M_{max.Rd} - Z_{r2xn} \cdot f_{sd} - Z_{sxn} \cdot f_{yd} - 1/2 \cdot Z_{cxn} \cdot (0.85 \cdot f_c) = 9.565 \cdot 10^5 \text{kip} \cdot \text{in}$$

- **Interaction curve bending moment axial force:**

LFRD	ASD
Design compressive strength: $\phi_C = 0.75$ $P_{X''} = \phi_C \cdot P_X \cdot \lambda$ where *X = A,B,C or D* $P_{A''} = \phi_C \cdot P_A \cdot \lambda = 46309\text{kip}$ $P_{B''} = \phi_C \cdot P_B \cdot \lambda = 0\text{kip}$ $P_{C''} = \phi_C \cdot P_C \cdot \lambda = 24860\text{kip}$ $P_{D''} = \phi_c \cdot P_D \cdot \lambda = 12430\text{kip}$ Design flexural strength: $\phi_B = 0.90$ $M_{X''} = \phi_B \cdot M_X$ where *X = A,B,C or D* $M_{Ax''} = \phi_B \cdot M_{Ax} = 0\text{kip} \cdot \text{in}$ $M_{Bx''} = \phi_B \cdot M_{Bx} = 860862\text{kip} \cdot \text{in}$ $M_{Cx''} = \phi_B \cdot M_{Cx} = 860862\text{kip} \cdot \text{in}$ $M_{Dx''} = \phi_B \cdot M_{Dx} = 941301\text{kip} \cdot \text{in}$	Allowable compressive strength: $\Omega_C = 2.00$ $P_{X''} = \frac{P_X \cdot \lambda}{\Omega_C}$ where *X = A,B,C or D* $P_{A''} = \frac{P_A \cdot \lambda}{\Omega_C} = 30873\text{kip}$ $P_{B''} = \frac{P_B \cdot \lambda}{\Omega_C} = 0\text{kip}$ $P_{C''} = \frac{P_C \cdot \lambda}{\Omega_C} = 16573\text{kip}$ $P_{D''} = \frac{P_D \cdot \lambda}{\Omega_C} = 8287\text{kip}$ Allowable flexural strength: $\Omega_b = 1.67$ $M_{X''} = \frac{M_X}{\Omega_b}$ where *X = A,B,C or D* $M_{Ax''} = \frac{M_{Ax}}{\Omega_b} = 0\text{kip} \cdot \text{in}$ $M_{Bx''} = \frac{M_{Bx}}{\Omega_b} = 572762\text{kip} \cdot \text{in}$ $M_{Cx''} = \frac{M_{Cx}}{\Omega_b} = 572762\text{kip} \cdot \text{in}$ $M_{Dx''} = \frac{M_{Dx}}{\Omega_b} = 626282\text{kip} \cdot \text{in}$

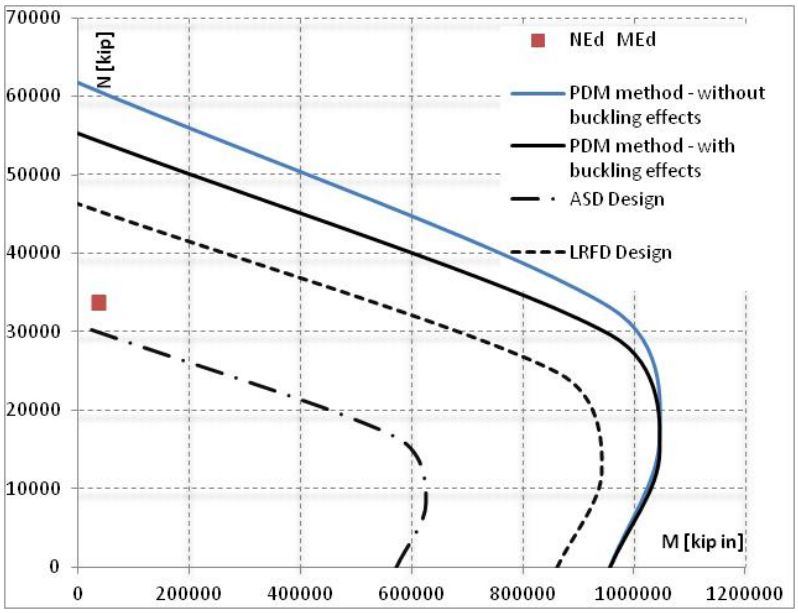

Figure 10-14 Axial force - bending moment interaction curve (AISC Design) – Example 2

- **Shear force evaluation:**

The evaluation of the shear force is made according to the report "Design Example of a column with 4 encased steel profiles" prepared by ArcelorMittal in collaboration with University of Liege. This procedure is to evaluate the composite behavior as a whole and additional considerations should be taken into account in order to ensure adequate load paths from the concrete to steel or vice versa at the load application points. The definition of the used symbols is defined in Figure 10-15:

$b_{c1} = 5.91\text{in}$;

$b_{s2} = 16.69\text{in}$;

$b_{c3} = 2.52\text{in}$;

$b_{s4} = 16.7\text{in}$;

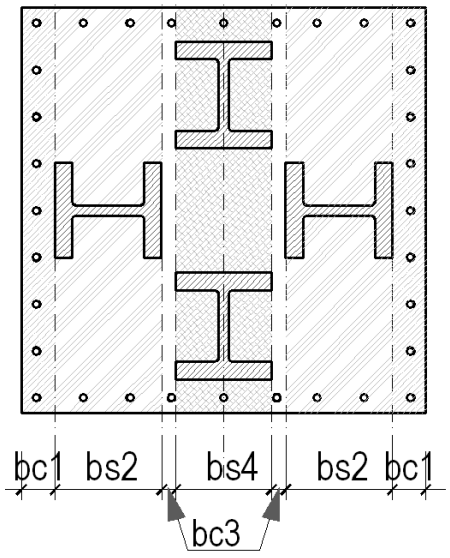

Figure 10-15 Definition of sections bc1, bc3, bs2, and bs4 (AISC Design) – Example 2

The applied shear force is V_{Ed} is distributed between sections b_{c3}, b_{c4} and b_s proportionally to their stiffness:

$$V_{Ed,bc1} = V_{Ed} \cdot {EI_{eff,bc1}}/{EI_{eff}}$$

$$V_{Ed,bc3} = V_{Ed} \cdot {EI_{eff,bc3}}/{EI_{eff}}$$

$$V_{Ed,bs1} = V_{Ed} \cdot {EI_{eff,bs1}}/{EI_{eff}}$$

$$V_{Ed,bs2} = V_{Ed} \cdot {EI_{eff,bs2}}/{EI_{eff}}$$

The effective bending stiffness of the column is:

$$EI_{eff} = 3.848 \cdot 10^{16}\,\text{kip} \cdot \text{in}^2$$

The total effective bending stiffness is the sum of individual EI_{eff} established for sections b_{c1}, b_{c3}, b_{s2} and b_{s4} respectively.

1) Section b_{c1}: $EI_{eff,bc1} = E_{sr} \cdot I_{sr,bc1} + C_1 \cdot E_c \cdot I_{c,bc1}$

To calculate $I_{sr,bc3}$ of the reinforcing bars, it is considered one equivalent plate A_{s2}.
For each face:

- The number of bars is: 9 bars
- The area of those bars is: $A_{sr,bc1} = 9 \cdot A_{sri} = 11.22\text{in}^2$
- The thickness of the equivalent plate is: $t_p = {A_{sr,bc1}}/{h_{s1}} = 0.17\text{in}$

$$I_{cg,bc1} = \frac{b_{c1} \cdot h_1^{\,3}}{12} = 1.751 \cdot 10^5\,\text{in}^4;$$

$$I_{sr,bc1} = \frac{t_p \cdot h_{s1}^{\,3}}{12} = 4.287 \cdot 10^3\,\text{in}^4;$$

$$I_{c,bc1} = I_{cg,bc1} - I_{sr,bc1} = 1.709 \cdot 10^5\,\text{in}^4;$$

$$EI_{eff,bc1} = E_{sr} \cdot I_{sr,bc1} + C_1 \cdot E_c \cdot I_{c,bc1} = 6.818 \cdot 10^8\,\text{kip} \cdot \text{in}^2$$

2) Section b_{c3}: $EI_{eff,bc3} = E_{sr} \cdot I_{sr,bc3} + C_1 \cdot E_c \cdot I_{c,bc3}$

To calculate $I_{sr,bc3}$, two equivalent (one top and one bottom) steel plates replace the reinforcing bars. Each plate has the same total area, and contains 1 rebar:

$$A_{sr,bc3} = 1 \cdot A_{sri} = 1.25\text{in}^2;$$

$$I_{sr,bc3} = 2 \cdot A_{sr,bc3} \cdot d_{s1y}^{\,2} = 2.232 \cdot 10^3\,\text{in}^4$$

$$I_{cg,bc3} = \frac{b_{c3} \cdot h_1^{\,3}}{12} = 7.437 \cdot 10^4 \text{in}^4 \quad ;$$

$$I_{c,bc3} = I_{cg,bc3} - I_{sr,bc3} = 7.250 \cdot 10^4 \text{in}^4$$

$$EI_{eff,bc3} = E_{sr} \cdot I_{sr,bc3} + C_1 \cdot E_c \cdot I_{c,bc3} = 3.013 \cdot 10^8 \text{kip} \cdot \text{in}^2$$

3) Section b_{s2}: $EI_{eff,bs2} = E_s \cdot I_{s,bs2} + E_{sr} \cdot I_{sr,bs2} + C_1 \cdot E_{c,eff} \cdot I_{c,bs2}$

To calculate $I_{sr,bs2}$, two equivalent (one top and one bottom) steel plates replace the reinforcing bars. Each plate has the same total area, and contains 2 rebar:

$$A_{sr,bs2} = 2 \cdot A_{sri} = 2.49 \text{in}^2 ;$$

$$I_{sr,bs2} = 2 \cdot A_{sr,bs2} \cdot d_{s1y}{}^2 = 4.464 \cdot 10^3 \text{in}^4 ;$$

$$I_{s,bs2} = I_y = 2.360 \cdot 10^3 \text{in}^4$$

$$I_{cg,bs2} = \frac{b_{s2} \cdot h_1^{\,3}}{12} = 4.951 \cdot 10^5 \text{in}^4$$

$$I_{c,bs2} = I_{cg,bs4} - I_{sr,bs2} - I_{s,bs2} = 4.882 \cdot 10^5 \text{in}^4$$

$$EI_{eff,bs2} = E_s \cdot I_{s,bs2} + E_{sr} \cdot I_{sr,bs2} + K_e \cdot E_{c,eff} \cdot I_{c,bs2} = 1.791 \cdot 10^9 \text{kip} \cdot \text{in}^2$$

4) Section b_{s4}: $EI_{eff,bs4} = E_s \cdot I_{s,bs4} + E_{sr} \cdot I_{sr,bs4} + C_1 \cdot E_c \cdot I_{c,bs4}$

To calculate $I_{sr,bs4}$, two equivalent (one top and one bottom) steel plates replace the reinforcing bars. Each plate has the same total area, and contains 1 rebar:

$$A_{sr,bs4} = 1 \cdot A_{sri} = 16.7 \text{in}^2$$

$$I_{sr,bs4} = 2 \cdot A_{sr,bs4} \cdot d_{s1y}{}^2 = 3.907 \cdot 10^5 \text{in}^4$$

$$I_{s,bs4} = 2 \cdot A_a \cdot d_{sy}{}^2 + 2 \cdot I_{sx} = 1.153 \cdot 10^5 \text{in}^4$$

$$I_{cg,bs4} = \frac{b_{s4} \cdot h_1^{\,3}}{12} = 4.951 \cdot 10^5 \text{in}^4$$

$$I_{c,bs4} = I_{cg,bs4} - I_{sr,bs4} - I_{s,bs4} = 3.775 \cdot 10^5 \text{in}^4$$

$$EI_{eff,bs4} = E_s \cdot I_{s,bs4} + E_{sr} \cdot I_{sr,bs4} + C_1 \cdot E_{c,eff} \cdot I_{c,bs4} = 3.411 \cdot 10^9 \text{kip} \cdot \text{in}^2$$

$$EI_{eff} = 2 \cdot (EI_{eff,bc1}) + 2 \cdot (EI_{eff,bs2}) + 2 \cdot (EI_{eff,bc3}) + EI_{eff,bs4} = 8.275 \cdot 10^9 \text{kip} \cdot \text{in}^2$$

The factored shear force V_{Ed} = 1798 kip (8000 kN) for the complete section is distributed in the 5 sections (2 b_{c3}, 2 b_s and 1 b_{c4}) :

$$V_{Ed,bc1} = V_{Ed} \cdot \frac{EI_{eff,bc1}}{EI_{eff}} = 142\text{kip}$$

$$V_{Ed,bc3} = V_{Ed} \cdot \frac{EI_{eff,bc1}}{EI_{eff}} = 63\text{kip}$$

$$V_{Ed,bs2} = V_{Ed} \cdot \frac{EI_{eff,bs2}}{EI_{eff}} = 372\text{kip}$$

$$V_{Ed,bs4} = V_{Ed} \cdot \frac{EI_{eff,bs4}}{EI_{eff}} = 709\text{kip}$$

- **Calculation of shear in section b_{s4}:**

Section b_{s2} is a composite steel-concrete section having 2 reinforced concrete flanges, 2 steel "flanges" (the HD sections) and 1 reinforced concrete web. To establish longitudinal shear in section b_s, it is convenient to transform the composite section into a single material section or "homogenized" section. The single material can be either steel or concrete.

Choosing concrete, the moment of inertia of the homogenized concrete section I_c* is such that the stiffness $E_c\, I_c$* of the homogenized section is equal to the stiffness $EI_{eff,bs2}$:

$$I_c^* = {EI_{eff,bs4}}\Big/{E_{cm}} = 3.146 \cdot 10^5\,\text{in}^4$$

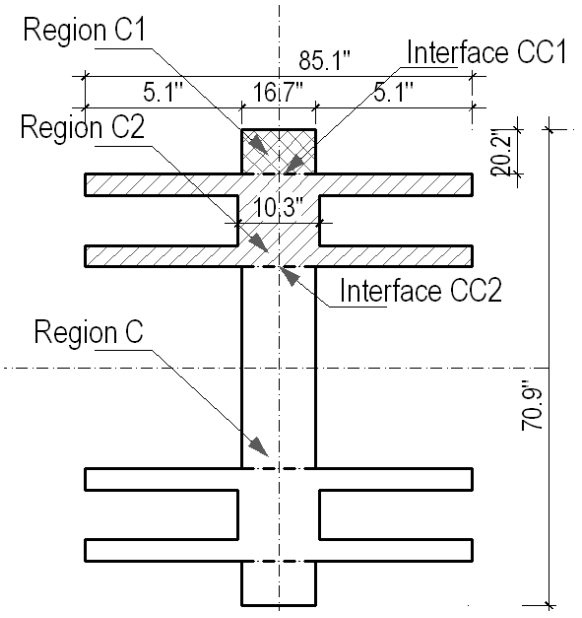

Figure 10-16 Homogenized equivalent concrete section bs – Example 2

In a homogenized concrete section (Figure 10-16), the width of the concrete equivalent to the width of the steel flanges is:

$$b_s^* = b_{s4} \cdot E_s / E_{cm} = 85.06\text{in}$$

The width of the concrete equivalent to the width of the steel web is:

$$t_w^* = t_w \cdot E_s / E_{cm} = 10.27\text{in}$$

The resultant longitudinal shear force on interfaces like CC1 and CC2 in Figure 10-16 is:

$$V_{Ed,l} = \frac{V_{Ed,bs2} \cdot \mathrm{S}}{I_c^*}$$

where:

S is the first moment of areas of regions C1 or C2 taken about the neutral axis of the section as illustrated in Figure 10-16.

Using S, the longitudinal shear is calculated at the steel-concrete interfaces CC1 and CC2 in order to size the force transfer mechanisms required for the member to act as a fully composite section.

- **Calculation of longitudinal shear force applied at interface CC1:**

S_{CC1} is the section modulus for the section C1, as defined in Figure 10-16.

The height of the C1 region is:

$$h_1' = 5.91\text{in}$$

The area is:

$$A_1 = b \cdot h_1' = 98.58\text{in}^2$$

$$S_{CC1} = A_1 \cdot \left(\frac{h_1}{2} - \frac{h_1'}{2} \right) = 3.202 \cdot 10^3 \text{in}^3$$

The resultant longitudinal shear force on interface CC1 is:

$$V_{Ed,CC1} = \frac{V_{Ed,bs} \cdot S_{CC1}}{I_c^*} = 3.79 \frac{\text{kip}}{\text{in}}$$

- **Calculation of longitudinal shear force applied at interface CC2:**

S_{CC2} is the section modulus for the combined regions C1 and C2.

The equivalent area in concrete for the HD profile is:

$A_a = 125.24\ \text{in}^2$

The equivalent are in concrete for the HD profile is:

$$A_a^* = A_a \cdot E_s / E_{cm} = 638.18\text{in}^2$$

The distance of HD center to the neutral axis is:

$d_{sy} = 20.2\ \text{in}$

The moment of area of the equivalent steel profile is:

$$S_{HD} = A_a^* \cdot d_{sy} = 1.289 \cdot 10^4\ \text{in}^3$$

Area of concrete between the flanges:

$$A_{c\_CC2}^* = b \cdot d\text{-}A_a = 186.27\text{in}^2$$

Moment of area of concrete between the flanges:

$$S_{c\_CC2}^* = A_{c\_CC2}^* \cdot d_{sy} = 3.762 \cdot 10^3\ \text{in}^3$$

The section modulus of the combined regions C1 and C2:

$$S_{CC2} = S_{c\_CC2}^* + S_{HD} + S_{CC1} = 1.985 \cdot 10^4\ \text{mm}^3$$

The resultant longitudinal shear force at interface CC2 is:

$$V_{Ed,CC2} = \frac{V_{Ed,bs} \cdot S_{CC2}}{I_c^*} = 23.48 \frac{\text{kip}}{\text{in}}$$

- **Evaluation of necessary amount of shear studs:**

Where concrete breakout strength in shear is not an applicable limit state, the design shear strength $\phi_v Q_{nv}$ and allowable shear strength Q_{nv} / Ω_v shall be determined according to AISC 2015 Specifications Eq. I8-3:

$$Q_{nv} = F_u \cdot A_{sa}$$

where:

$\phi_v = 0.65$ (LRFD)

$\Omega_v = 2.31$ (ASD)

Q_{nv} nominal shear strength of steel headed stud anchor, kips

F_u specified minimum tensile strength of a steel headed stud anchor, ksi

A_{sa} cross-sectional area of steel-headed stud anchor, in^2

$A_{sa} = \pi \cdot (0.75)^2 / 4 = 0.44 in^2$ per steel headed stud anchor diameter 0.75in

$F_u = 63.3 ksi$

$\phi_v Q_{nv} = 0.65 \cdot 63.3 ksi \cdot 0.44 in^2 = 18 kip$

The necessary amount of shear studs to different interfaces is:

$$n_{studs\_CC1} = \frac{V_{Ed1\_CC1}}{\phi_v Q_{nv}} = \frac{3.79 \frac{kip}{in}}{18 kip} = \frac{45.43 \frac{kip}{ft}}{18 kip} \Rightarrow 3 \text{ studs} / 1 ft$$

$$n_{studs\_CC2} = \frac{V_{Ed1\_CC2}}{\phi_v Q_{nv}} = \frac{23.48 \frac{kip}{in}}{18 kip} = \frac{281.74 \frac{kip}{ft}}{18 kip} \Rightarrow 16 \text{ studs} / 1 ft$$

10.3 Case 3: Chinese code JGJ 138-2016: Code for Design of Composite Structures

Chinese codes use the 'Plane section assumptions' (PSA) to calculate the flexural capacity of composite columns if full composite actions can be realized. Material properties and the equivalent stress distribution are defined in different ways compared to American and European codes.

10.3.1 Design approaches.

The framework of the design approaches in Chinese codes can be presented by the procedures shown below. There are three steps in designing a composite member. These design examples mainly focus on the third step, and detailed procedures will be discussed in each part.

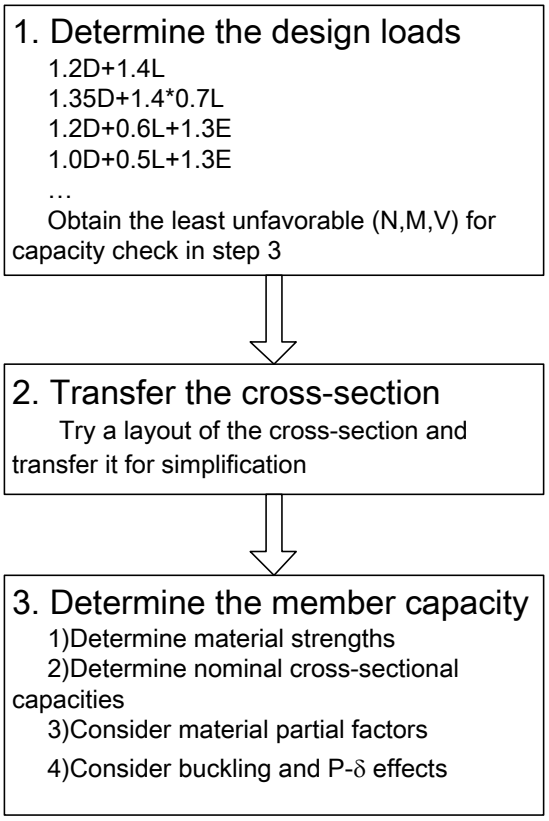

10.3.2 Material properties.

- **Concrete:**

According to GB 50010-2010, the concrete properties are listed in Table 10-1, where f_{ck} is the characteristic (5%) strength in compression and f_{cd} is the design concrete strength in compression. Tensile strengths are not included in this Table since tensile strengths are often neglected when calculating the flexural capacity. The characteristic strength is usually used for checking the serviceability limit states (SLS), while the design strength is usually for ultimate limit states (ULS). The α and β are two factors used for defining the effective rectangular stress distribution of the concrete.

Table 10-1 Material properties of concrete

Grade	f_{ck}/MPa	f_{cd}/MPa	$\alpha-$factor	$\beta-$factor
C15	10.0	7.2	1.0	0.8
C20	13.4	9.6	1.0	0.8
C25	16.7	11.9	1.0	0.8
C30	20.1	14.3	1.0	0.8
C35	23.4	16.7	1.0	0.8
C40	26.8	19.1	1.0	0.8
C45	29.6	21.2	1.0	0.8
C50	32.4	23.1	1.0	0.8
C55	35.5	25.3	0.99	0.79
C60	38.5	27.5	0.98	0.78
C65	41.5	29.7	0.97	0.77
C70	44.5	31.8	0.96	0.76
C75	47.4	33.8	0.95	0.75
C80	50.2	35.9	0.94	0.74

However, the f_{ck} in EC 2 and GB 50010 have different meanings because these two codes use different ways to classify the concrete strength. In Chinese codes, the concrete is classified by 150 x 150 x 150 mm cube strengths, that is $f_{cu,k}$. For example, if the cube strength of concrete is 60 MPa, namely $f_{cu,k} = 60$ MPa, then the concrete class is C60, but the f_{ck} is actually 26.8 MPa. In EC 2, however, the concrete is classified by its cylinder strength. For example, if the cylinder strength of concrete is 60 MPa, namely $f_{ck} = 60$ MPa, then the concrete class is C60. In this report, concrete strengths and partial factors are listed in Table 10-2.

Table 10-2 strengths and partial factors of concrete

Concrete class	f_{ck}/MPa		γ_C	
	EC	GB	EC	GB
C40	40	19.1	1.5	1.4
C50	50	23.1		
C60	60	27.5		

To make the calculation results comparable, the concrete compressive strength f_{ck} used in this report are determined based on EC2. For example, if the concrete class is C60, we take f_{ck} = 60 MPa during calculations.

- **Reinforcing bars:**

Shown in Table 10-3 are the material properties of reinforcing bars according to GB 50010-2010, where f_{yk} is the characteristic yield strength and f_{yd} is the design yield strength. Note that for HRB500 and HRBF500 bars, the design yield strength in compression is smaller than that in tension. If very high strength reinforcing bars are used, it is very likely that concrete crush occurs before the compressive yield strength is reached, thus reducing the actual capacity of the reinforcing bars. Therefore, a smaller value is used for compressive yield strength for HRB500 and HRBF500 to account for this effect. The nominal strengths and partial factors for HRB400 and HRB500 are presented in Table 10-4.

Table 10-3 Material properties of reinforcing bars

Grade	f_{yk}/MPa	f_{yd}/MPa (in compression)	f_{yd}/MPa (in tension)
HPB300	300	270	270
HRB335,HRBF335	335	300	300
HRB400,HRBF400,RRB400	400	360	360
HRB500,HRBF500	500	410	435

Table 10-4 Strengths and partial factors of reinforcing bars

Grade	f_{yk}/MPa		γ_S	
	EC	GB	EC	GB
HRB400	400	400	1.15	1.11
HRB500	500	500		1.15

- **Structural steel:**

GB 50017-2003 specifies four grades for structural steels, ranging from Q235 to Q420, but only Q235 and Q345 are recommended in JGJ 138. However, steels with higher strengths may still be used if the material properties can be effectively confirmed. For strengths higher than Q420, there is no data available in Chinese codes, so the nominal strengths are determined based on European code EC 3.

Table 10-5 Material properties of steel profiles

Grade	Thickness/mm	f_{yk}/MPa	f_{yd}/MPa	
			compression tension flexure	shear
Q235	≤16	235	215	125
	16~40	225	205	120
	40~60	215	200	115
	60~100	205	200	115
Q345	≤16	345	310	180
	16~35	325	295	170
	35~50	295	265	155
	50~100	275	250	145
Q390	≤16	390	350	205
	16~35	370	335	190
	35~50	350	315	180
	50~100	330	295	170
Q420	≤16	420	380	220
	16~35	400	360	210
	35~50	380	340	195
	50~100	360	325	185

Table 10-6 Strengths and partial factors of steel profiles

Grade	f_{yk}/MPa		γ_S	
	Thickness	EC&GB	EC	GB
S355	t ≤ 40 mm	355	1.0	1.1
	40 mm < t ≤ 80 mm	355		
S450	t ≤ 40 mm	440		
	40 mm < t ≤ 80 mm	410		
S460	t ≤ 40 mm	460		
	40 mm < t ≤ 80 mm	430		

- **Equivalent steel distribution:**

PSA in Chinese codes slightly differs from PDM in American and European codes in the following two aspects:

1. In American and European codes, a 0.85 factor is used to discount the compressive strength of the concrete. This 0.85 factor is not included in Chinese codes. Only the $\alpha -$ factor is used to discount the effective strength of the concrete (see Table 10-1).
2. The actual concrete compressive stress distribution is represented by an equivalent rectangular diagram, where concrete strength is assumed to be αf_c and height of the equivalent rectangular diagram is β times the actual height of the compressive stress distribution (see Figure 10-17).

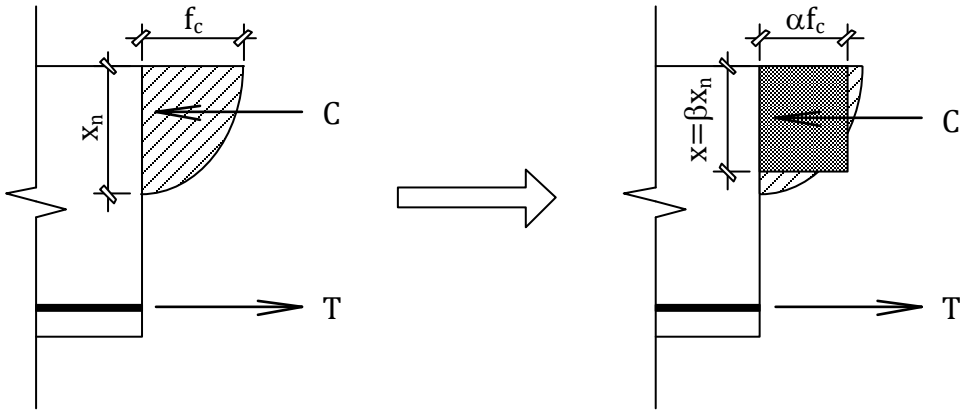

Figure 10-17 Equivalent stress distribution

Although similar specifications are included in EC2 and ACI 318, EC4 also allows using another method to construct the plastic stress distribution of the concrete such that 'the effective area of concrete in compression resists a stress of $0.85f_{cd}$, constant over the whole depth between the plastic neutral axis and the most compressed fiber of the concrete', which is the so called 'plastic stress distribution method' (PDM). However, Chinese standard only provides the PSA method but not the PDM method. Consequently, results obtained from these codes may be different.

10.3.3 Example 1.

Given:

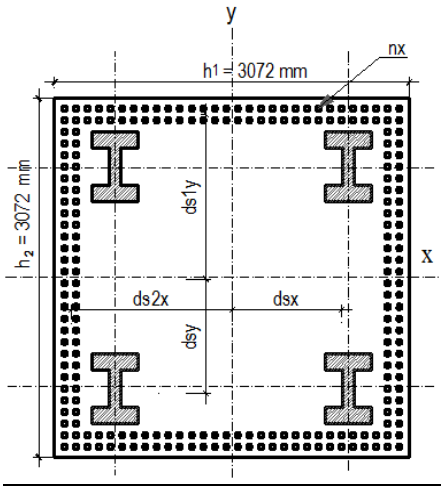

Figure 10-18 Section 1 dimensions

Steel profiles: 4 HD 400 x 1299 ASTM A913-11
Grade 65 – fy = 450 MPa
d_{sx} = 1012mm; d_{sy} = 950 mm ;
Reinforcement rebar: 224 φ 40mm –S500
ds2x = ds1y = 1400 mm ;
Concrete: h_1 =h_2= 3072 mm
concrete class : C60: fck = 60 MPa
Buckling length : L= 18000 mm

Solution:

- **Design equations:**

A two-step procedure can be developed to determine the flexural resistance of the composite section under compression and uni-axial bending. First, locate the neutral axis (NA) based on the balance of axial forces. Second, calculate the flexural resistance based on the position of the NA.

After the section transformation, reinforcing bars are replaced by four equivalent steel plates. To simplify the design procedures, thickness of the steel plates is neglected when locating the NA. Namely, there are no such cases that the NA is located within the steel plates. Therefore, four cases can be derived for this cross-section.

Procedures of transforming the real cross-section to the simplified one can be found. Three more variables are defined as follows:

$$y_1 = d_{sx} - d/2$$
$$y_2 = d_{sx} + d/2$$
$$y_3 = h_1/2 - c_y - s_y(i-1)/2$$

Table 10-7 Determining the moment capacity at a given axial load – example 1

Case 1. $|y| \le y_1$

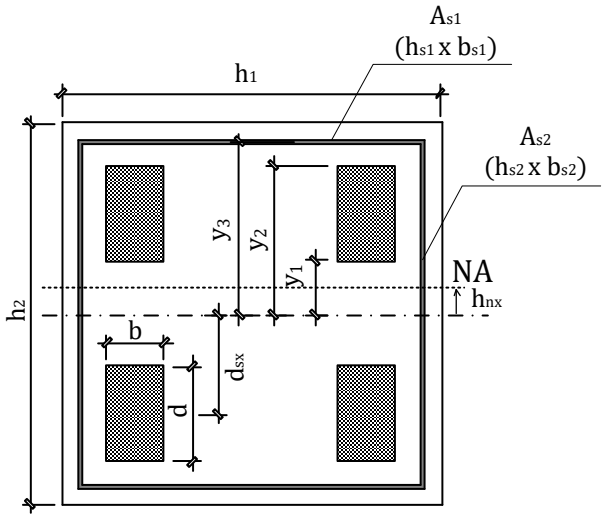

$$h_{nx} = \frac{N - f_c\left(\beta h_2 h_1 / 2 - 2A_a - A_{s1} - h_{s2} b_{s2}\right)}{-4 b_{s2} f_{sy} - \beta h_1 f_c + 2 b_{s2} f_c}$$

$$Z_{sr} = Z_{srx} - 2 b_{s2} h_{nx}^2$$

$$M_{sr} = Z_{sr} f_{sy}$$

$$Z_s = Z_{sx}$$

$$M_s = Z_s f_y$$

$$x = \beta\left(\frac{h_2}{2} - h_{nx}\right)$$

$$M_c = f_c\left[x h_1\left(\frac{h_2}{2} - \frac{x}{2}\right) - \frac{Z_s}{2} - \frac{Z_{sr}}{2}\right]$$

$$M = M_c + M_{sr} + M_s$$

Case 2. $y_1 < |y| \le y_2$

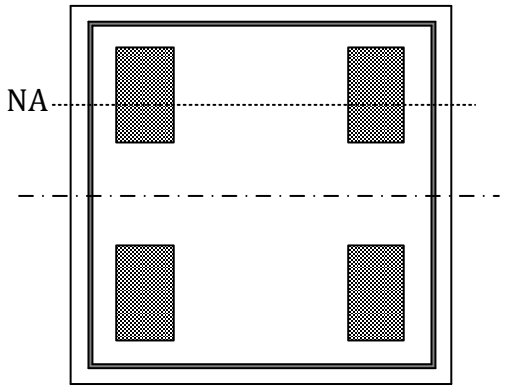

Define $S = sign\left(A_c f_c / 2 - N\right)$. If S=1, the NA is on the upper half. If S=-1, the NA is on the lower half.

$$h_{nx} = \frac{N - 4y_1 b f_y S - f_c\left(\beta h_1 h_2 / 2 - 2A_a - 2y_1 bS - A_{s1} - h_{s2} b_{s2}\right)}{-4bf_y - 4b_{s2} f_{sy} - \beta h_1 f_c + 2bf_c + 2b_{s2} f_c}$$

$$Z_{sr} = Z_{srx} - 2b_{s2} h_{nx}^2$$

$$M_{sr} = Z_{sr} f_{sy}$$

$$d_n = \left|h_{nx}\right| - y_1$$

$$Z_s = Z_{sx} - 4\left[d_n b\left(y_1 + \frac{d_n}{2}\right)\right]$$

$$M_s = Z_s f_y$$

$$x = \beta\left(\frac{h_2}{2} - h_{nx}\right)$$

$$M_c = f_c\left[x h_1\left(\frac{h_2}{2} - \frac{x}{2}\right) - \frac{Z_s}{2} - \frac{Z_{sr}}{2}\right]$$

$$M = M_c + M_{sr} + M_s$$

Case 3. $y_2 < |y| \leq y_3$

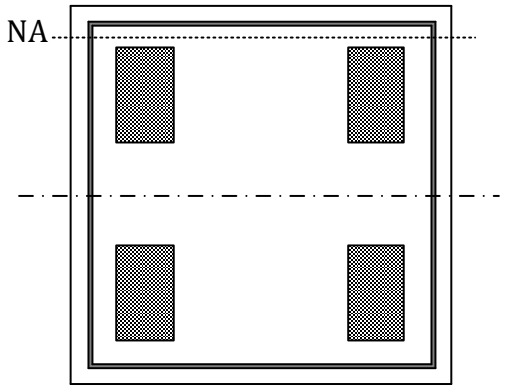

$$h_{nx} = \frac{N + A_s f_y S - f_c \left(\beta h_1 h_2 / 2 - 2A_a + 2A_a S - A_{s1} - h_{s2} b_{s2} \right)}{-4 b_{s2} f_{sy} - \beta h_1 f_c + 2 b_{s2} f_c}$$

$$Z_{sr} = Z_{srx} - 2 b_{s2} h_{nx}^2$$

$$M_{sr} = Z_{sr} f_{sy}$$

$$Z_s = 0$$

$$M_s = Z_s f_y$$

$$x = \beta \left(\frac{h_2}{2} - h_{nx} \right)$$

$$M_c = f_c \left[x h_1 \left(\frac{h_2}{2} - \frac{x}{2} \right) - \frac{Z_s}{2} - \frac{Z_{sr}}{2} \right]$$

$$M = M_c + M_{sr} + M_s$$

Case 4. $|y| \geq y_3$

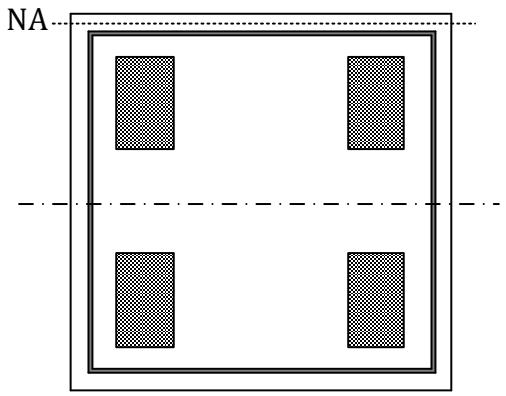

$$h_{nx} = \frac{N + A_s f_y S + A_{sr} f_{sy} S - f_c \left(\beta h_1 h_2 / 2 - A_s / 2 + S A_s / 2 - A_{sr} / 2 + S A_{sr} / 2 \right)}{-\beta h_1 f_c}$$

$$Z_{sr} = Z_{srx} - 2 b_{s2} h_{nx}^2$$

$$M_{sr} = Z_{sr} f_{sy}$$

$$Z_s = 0$$

$$M_s = Z_s f_y$$

$$x = \beta \left(\frac{h_2}{2} - h_{nx} \right)$$

$$M_c = f_c \left[x h_1 \left(\frac{h_2}{2} - \frac{x}{2} \right) - \frac{Z_s}{2} - \frac{Z_{sr}}{2} \right]$$

$$M = M_c + M_{sr} + M_s$$

- **Interaction curves – nominal strengths:**

The N-M interaction curves are calculated based on the nominal material strengths, and no reduction factors are considered. Besides, the buckling effects and $P-\delta$ effects are not considered either. Therefore, the N-M curves reflect the pure cross-sectional capacity of the composite members. The fiber results are obtained based on the FEM numerical calculations.

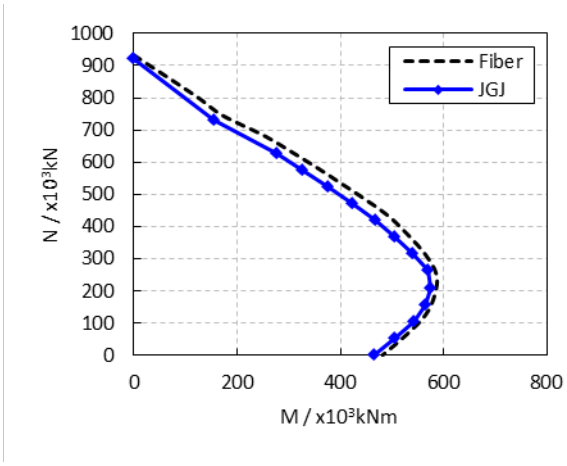

Figure 10-19 Interaction curves with nominal strengths - Section 1

- **Interaction curve – partial factors:**

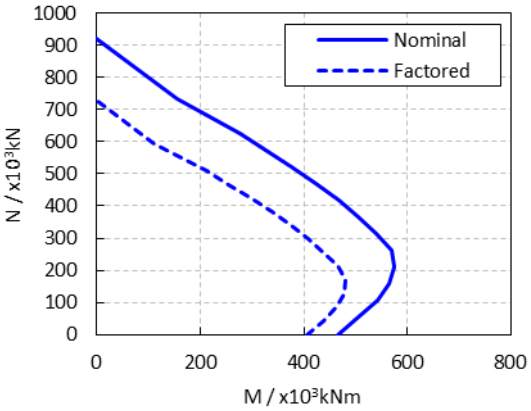

Figure 10-20 Interaction curves with and without material partial factors - Section 1

- **Buckling and second order effects:**

1) Axial capacity

In Chinese codes, the axial capacity of a composite column should be determined based on the following equation:

$$N \le 0.9\varphi(f_c A_c + f_{ys} A_s + f_{ya} A_a)$$

The buckling curve for composite columns can be determined based on 'Code for design of composite structures' (JGJ 138), using the following Table:

Table 10-8 Reduction factor for buckling

l_0 / i	≤ 28	35	42	48	55	62	69	76	83	90	97	104
φ	1.00	0.98	0.95	0.92	0.87	0.81	0.75	0.70	0.65	0.60	0.56	0.52

where:

l_0 = buckling length of the column

i = radius of gyration of the composition cross-section, which can be calculated as:

$$i = \sqrt{\frac{E_c I_c + E_a I_a}{E_c A_c + E_a A_a}}$$

The buckling length for section 1and section 3 is 18m. This value is calculated considering a four-story high lobby with the story height of 4.5m. The buckling length for section 2 is still 3.6m to comply with the test.

Table 10-9 Axial capacity

	Section 1	Section 2	Section 3
Buckling reduction factor	1.000	0.994	0.970
Nominal axial capacity	921085	20988	322734
Axial capacity considering buckling effects only	921085	20873	313044
Axial capacity considering buckling effects & material partial factors	657046	14954	225536

2) Moment capacity:

Chinese standard specifies that the second order $P-\delta$ effect can be ignored if the following three criteria are satisfied:

(1) $M_1 / M_2 \le 0.9$
(2) $N / N_u \le 0.9$
(3) $l_c / i \le 32 - 12(M_1 / M_2)$

where:

M_1 = smallest design bending moment within the composite member
M_2 = largest design bending moment within the composite member
N = design axial force
N_u = short-column axial capacity of the composite member
l_c = buckling capacity
i = radius of gyration of the composite cross-section

If the criteria are not satisfied, the $P-\delta$ effect needs to be considered by multiplying the design bending moment with a coefficient that is greater than 1.0.

$$M = C_m \eta_{ns} M_2$$

$$C_m = 0.7 + 0.3\frac{M_1}{M_2}$$

$$\eta_{ns} = 1 + \frac{1}{1300(M_2 N + e_a)/h_0}\left(\frac{l_c}{h_c}\right)^2 \zeta_c$$

$$\zeta_c = \frac{0.5 f_c A_g}{N}$$

where:

e_a = max{20mm,1/30h_c}
h_0 = effective height of the composite cross-section
h_c = cross-section dimension along the direction that the bending moment is considered
f_c = concrete compressive strength
A_g = gross area of the cross-section

Shown in Figure 10-21 are the interaction curves given by Chinese with and without buckling and second order effects. The interaction curves have considered the material partial factors.

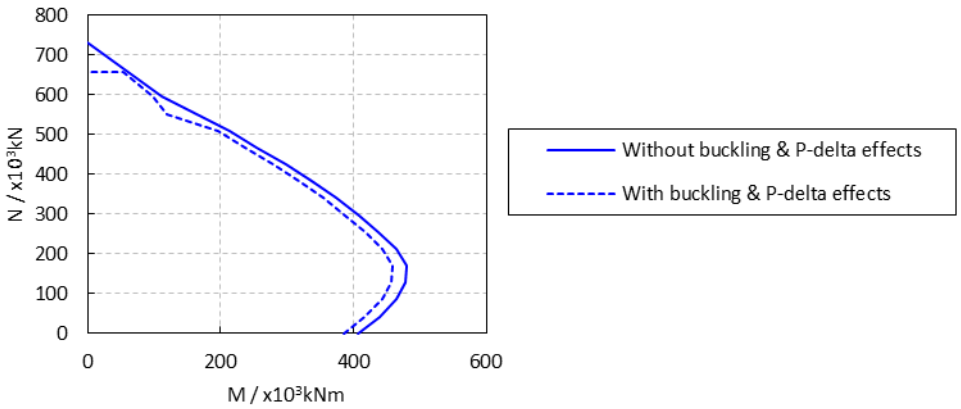

Figure 10-21 Interaction curves with and without considering buckling and second order effects (Material partial factors have already been considered) - Section 1

- **Shear force evaluation:**

The longitudinal shear force of the steel sections should be checked to avoid large slip and to ensure enough composite action. However, a unified method is still lacked in Chinese code to provide general design guidance. As a comparison between Chinese codes, European codes, and American codes, this part of the report checks the longitudinal shear force based on Chinese codes by using the same method proposed by ArcelorMittal and the University of Liege.

Check the shear capacity of the composite column subjected to the following demands: (the same with the design capacities in Section 4.2.7)

N_{Ed} = 300000 kN;

M_{Ed} = 250000 kN;

V_{Ed} = 20000 kN;

The definition of the used symbols is defined in Figure 10-22:

$b_{c3} = 286\text{mm}$

$b_s = 476\text{mm}$

$b_{c4} = 3072\text{mm} - 2\cdot(286\text{mm} + 476\text{mm}) = 1548\text{mm}$

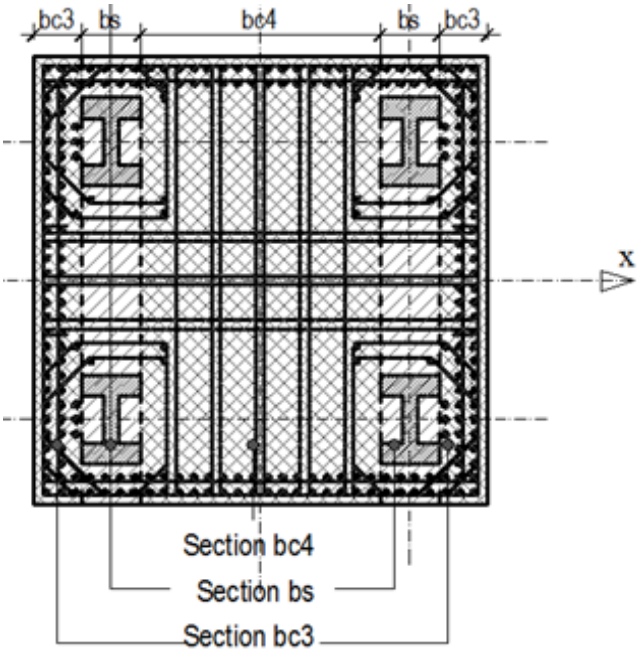

Figure 10-22 Definition of sections bc3, bc4, and bs (EC4 Design) – Example 1

The applied shear force is V_{Ed} is distributed between sections b_{c3}, b_{c4} and b_s proportionally to their stiffness:

$$V_{Ed,bc3} = V_{Ed} \cdot EI_{eff,bc3} \Big/ EI_{eff}$$

$$V_{Ed,bc4} = V_{Ed} \cdot EI_{eff,bc4} \Big/ EI_{eff}$$

$$V_{Ed,bs} = V_{Ed} \cdot EI_{eff,bs} \Big/ EI_{eff}$$

Chinese standards do not use any reduction factors to discount the flexural stiffness of the composite column. Namely: $EI_{eff} = E_s \cdot I_s + E_{sr} \cdot I_{sr} + E_c \cdot I_c$, where the concrete Young's Modulus is calculated by using the following equation:

$$E_c = \frac{10^5}{2.2 + \frac{34.7}{f_{cu,k}}} (MPa)$$

The effective bending stiffness of the column is:

$$EI_{eff} = 4.461 \cdot 10^{17} \text{ Nmm}$$

The total effective bending stiffness is the sum of individual EI_{eff} established for sections b_{c3}, b_{c4} and b_s respectively.

1) Section b_{c3}: $EI_{eff,bc3} = E_{sr} \cdot I_{sr,bc3} + E_c \cdot I_{c,bc3}$

To calculate $I_{sr,bc3}$ of the reinforcing bars, it is considered one equivalent plate A_{s2} , and 2x2 bars on the top and bottom.

For each face:

- The number of bars is: 30+30+4+4 = 68 bars
- The area of those bars is: $A_{sr,bc3} = 68 \cdot A_{sri} = 85451\text{mm}^2$
- The thickness of the equivalent plate is:

$$t_p = {A_{sr,side}}\Big/{h_{s1}} = 85451\text{mm}^2 \Big/ 2900\text{mm} = 29.5\text{mm}$$

$$I_{cg,bc3} = \frac{b_{c3} \cdot h_1^{\,3}}{12} = \frac{286\text{mm} \cdot (3072\text{mm})^3}{12} = 6.91 \cdot 10^{11}\,\text{mm}^4$$

$$I_{sr,bc3} = \frac{t_p \cdot h_{s1}^{\,3}}{12} = \frac{29.4\text{mm} \cdot 2900\text{mm}^3}{12} = 5.99 \cdot 10^{10}\,\text{mm}^4$$

$$I_{c,bc3} = I_{cg,bc3} - I_{sr,bc3} = 6.91 \cdot 10^{11}\,\text{mm}^4 - 5.99 \cdot 10^{10}\,\text{mm}^4 = 6.31 \cdot 10^{11}\,\text{mm}^4$$

$$\begin{aligned} EI_{eff,bc3} &= E_{sr} \cdot I_{sr,bc3} + E_c \cdot I_{c,bc3} \\ &= 200000\text{MPa} \cdot 5.99 \cdot 10^{10}\,\text{mm}^4 + 38000\text{MPa} \cdot 6.31 \cdot 10^{11}\,\text{mm}^4 \\ &= 3.596 \cdot 10^{16}\,\text{Nmm}^2 \end{aligned}$$

2) Section b_{c4}: $EI_{eff,bc4} = E_{sr} \cdot I_{sr,bc4} + E_c \cdot I_{c,bc4}$

To calculate $I_{sr,bc4}$, two equivalent (one top and one bottom) steel plates replace the reinforcing bars. Each plate has the same total area, and contains 36 rebar:

$$A_{sr,bc4} = 36 \cdot A_{sri} = 45238\text{mm}^2$$

$$I_{sr,bc4} = 2 \cdot A_{sr,bc4} \cdot d_{s1y}^{\,2} = 2 \cdot 45238\text{mm}^2 \cdot (1400\text{mm})^2 = 1.77 \cdot 10^{11}\,\text{mm}^4$$

$$I_{cg,bc4} = \frac{b_{c4} \cdot h_1^{\,3}}{12} = \frac{1548\text{mm} \cdot (3072\text{mm})^3}{12} = 3.74 \cdot 10^{12}\,\text{mm}^4$$

$$I_{c,bc4} = I_{cg,bc4} - I_{sr,bc4} = 3.74 \cdot 10^{12}\,\text{mm}^4 - 1.77 \cdot 10^{11}\,\text{mm}^4 = 3.563 \cdot 10^{12}\,\text{mm}^4$$

$$\begin{aligned} EI_{eff,bc4} &= E_{sr} \cdot I_{sr,bc4} + E_c \cdot I_{c,bc4} \\ &= 200000\text{MPa} \cdot 1.77 \cdot 10^{11}\,\text{mm}^4 + 38000\text{MPa} \cdot 3.563 \cdot 10^{12}\,\text{mm}^4 \\ &= 1.390 \cdot 10^{17}\,\text{Nmm}^2 \end{aligned}$$

3) Section b_s: $EI_{eff,bs} = E_s \cdot I_{s,bs} + E_{sr} \cdot I_{sr,bs} + E_c \cdot I_{c,bs}$

To calculate $I_{sr,bs}$, two equivalent (one top and one bottom) steel plates replace the reinforcing bars. Each plate has the same total area, and contains 8 rebar:

$$A_{sr,bs} = 8 \cdot A_{sri} = 10053\text{mm}^2$$

$$I_{sr,bs} = 2 \cdot A_{sr,bs} \cdot {d_{s1y}}^2 = 2 \cdot 10053\text{mm}^2 \cdot \left(1400\text{mm}\right)^2 = 3.94 \cdot 10^{10}\,\text{mm}^4$$

$$I_{s,bs} = 2 \cdot A_a \cdot {d_{sy}}^2 + 2 \cdot I_x = 2 \cdot 165000\text{mm}^2 \cdot \left(950\text{mm}\right)^2 + 2 \cdot 7.546 \cdot 10^9\,\text{mm}^4 = 3.129 \cdot 10^{11}\,\text{mm}^4$$

$$I_{cg,bs} = \frac{b_s \cdot {h_1}^3}{12} = \frac{476\text{mm} \cdot \left(3072\text{mm}\right)^3}{12} = 1.15 \cdot 10^{12}\,\text{mm}^4$$

$$I_{c,bs} = I_{cg,bs} - I_{sr,bs} - I_{s,bs} = 1.15 \cdot 10^{12}\,\text{mm}^4 - 3.94 \cdot 10^{10}\,\text{mm}^4 - 3.129 \cdot 10^{11}\,\text{mm}^4 = 8.199 \cdot 10^{11}\,\text{mm}^4$$

$$\begin{aligned} EI_{eff,bs} &= E_s \cdot I_{s,bs} + E_{sr} \cdot I_{sr,bs} + E_c \cdot I_{c,bs} \\ &= 206000\text{MPa} \cdot 3.129 \cdot 10^{11}\,\text{mm}^4 + 200000\text{MPa} \cdot 3.94 \cdot 10^{10}\,\text{mm}^4 + 38000\text{MPa} \cdot 8.199 \cdot 10^{11}\,\text{mm}^4 \\ &= 1.035 \cdot 10^{17}\,\text{Nmm}^2 \end{aligned}$$

$$EI_{eff} = 2 \cdot (EI_{eff,bc3}) + EI_{eff,bc4} + 2 \cdot (EI_{eff,bs}) = 4.179 \cdot 10^{17}\,\text{Nmm}^2$$

The factored shear force V_{Ed} = 20000 kN for the complete section is distributed in the 5 sections (2 b_{c3}, 2 b_s and 1 b_{c4}) :

$$V_{Ed,bc3} = V_{Ed} \cdot \frac{EI_{eff,bc3}}{EI_{eff}} = 20000\text{kN} \cdot \frac{3.596 \cdot 10^{16}\,\text{Nmm}^2}{4.179 \cdot 10^{17}\,\text{Nmm}^2} = 1720\text{kN}$$

$$V_{Ed,bc4} = V_{Ed} \cdot \frac{EI_{eff,bc4}}{EI_{eff}} = 20000\text{kN} \cdot \frac{1.390 \cdot 10^{17}\,\text{Nmm}^2}{4.179 \cdot 10^{17}\,\text{Nmm}^2} = 6652\text{kN}$$

$$V_{Ed,bs} = V_{Ed} \cdot \frac{EI_{eff,bs}}{EI_{eff}} = 20000\text{kN} \cdot \frac{1.035 \cdot 10^{17}\,\text{Nmm}^2}{4.179 \cdot 10^{17}\,\text{Nmm}^2} = 4953\text{kN}$$

- **Calculation of shear in section b_s:**

Section b_s is a composite steel-concrete section having 2 reinforced concrete flanges, 2 steel "flanges" (the HD sections) and 1 reinforced concrete web. To establish longitudinal shear in section b_s, it is convenient to transform the composite section into a single material section or "homogenized" section. The single material can be either steel or concrete.

Choosing concrete, the moment of inertia of the homogenized concrete section I_c* is such that the stiffness $E_c\ I_c$* of the homogenized section is equal to the stiffness $EI_{eff,bs}$:

$$I_c^* = {EI_{eff,bs}}\Big/{E_{cm}} = 1.035 \cdot 10^{17}\,\text{Nmm}^2 \Big/ 38000\text{MPa} = 2.724 \cdot 10^{12}\,\text{mm}^4$$

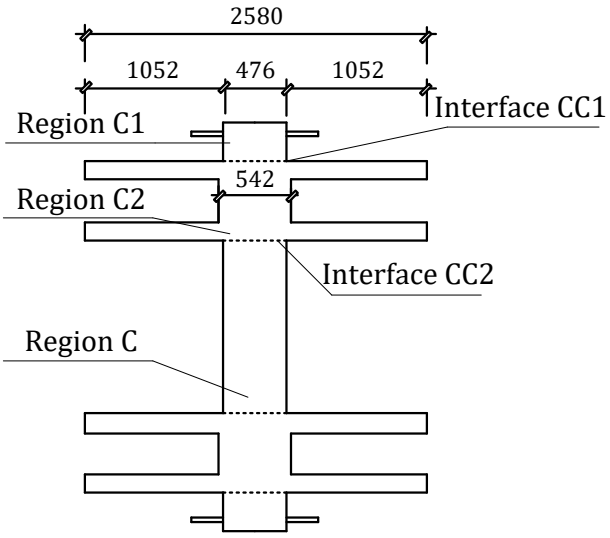

Figure 10-23 Homogenized equivalent concrete section bs – Example 1

In a homogenized section in concrete (Figure 10-23), the width of the concrete equivalent to the width of the steel flanges is:

$$b_s^* = b_s \cdot E_s / E_{cm} = 476\text{mm} \cdot 206000\text{MPa} / 38000\text{MPa} = 2580\text{mm}$$

The width of the concrete equivalent to the width of the steel web is:

$$t_w^* = t_w \cdot E_s / E_{cm} = 100\text{mm} \cdot 206000\text{MPa} / 38000\text{MPa} = 542\text{mm}$$

The resultant longitudinal shear force on sections like CC and CC2in Figure 10-23 is:

$$V_{Ed,l} = \frac{V_{Ed,bs} \cdot \mathrm{S}}{I_c^*}$$

where:

S is the first moment of areas of regions C1 and C2 taken about the neutral axis of the section as illustrated as illustrated in Figure 10-23.

Using S, the longitudinal shear is calculated at the steel-concrete interfaces CC1 and CC2 in order to size the force transfer mechanisms required for the member to act as a fully composite section.

- **Calculation of longitudinal shear force applied at interface CC1:**

S_{CC1} is the section modulus for the region C1 as defined in Figure 10-23:

The height of the C1 section is:

$$h_1' = \frac{h_1}{2} - \left(d_{sy} + \frac{d}{2} \right) = \frac{3072\text{mm}}{2} - \left(950\text{mm} + \frac{600\text{mm}}{2} \right) = 286\text{mm}$$

The area is:

$$A_1 = b \cdot h_1' = 476\text{mm} \cdot 286\text{mm} = 136136\text{mm}^2$$

$$S_{CC1} = A_1 \cdot \left(\frac{h_1}{2} - \frac{h_1'}{2} \right) = 136136\text{mm}^2 \cdot \left(\frac{3072\text{mm}}{2} - \frac{286\text{mm}}{2} \right) = 1.896 \cdot 10^8\,\text{mm}^3$$

The resultant longitudinal shear force at interface CC1 is:

$$V_{Ed,CC1} = \frac{V_{Ed,bs} \cdot S_{CC1}}{I_c^*} = \frac{4953\text{kN} \cdot 1.896 \cdot 10^8\,\text{mm}^3}{2.72 \cdot 10^{12}\,\text{mm}^4} = 345.3\frac{\text{N}}{\text{mm}}$$

On 1-meter length of column:

$$V_{Ed,CC1} = 345.3\frac{\text{kN}}{\text{m}}$$

- **Calculation of longitudinal shear force applied at interface CC2:**

S_{CC2} is the section modulus for the combined regions C1 and C2 (the HD profile):

The equivalent area in concrete for the HD profile is:

$A_a = 165000\text{mm}^2$

The equivalent are in concrete for the HD profile is:

$$A_a^* = A_a \cdot E_s / E_{cm} = 165000\text{mm}^2 \cdot 206000\text{MPa} / 38000\text{MPa} = 894474\text{mm}^2$$

The distance of HD center to the neutral axis is:

$d_{sy} = 950$ mm

The moment of area of the equivalent steel profile is:

$$S_{HD} = A_a^* \cdot d_{sy} = 894474\text{mm}^2 \cdot 950\text{mm} = 8.50 \cdot 10^8\,\text{mm}^3$$

Area of concrete between the flanges:

$$A^*_{c\_CC2} = b \cdot d\text{-}A_a = 476\text{mm} \cdot 600\text{mm} - 165000\text{mm}^2 = 120600\text{mm}^2$$

Moment of area of concrete between the flanges:

$$S^*_{c\_CC2} = A^*_{c\_CC2} \cdot d_{sy} = 120600\text{mm}^2 \cdot 950\text{mm} = 1.146 \cdot 10^8\,\text{mm}^3$$

The section modulus corresponding to the combined regions C1 and C2 is equal to:

$$S_{CC2} = S^*_{c\_CC2} + S_{HD} + S_{CC1} = 1.146 \cdot 10^8\,\text{mm}^3 + 8.83 \cdot 10^8\,\text{mm}^3 + 1.896 \cdot 10^8\,\text{mm}^3 = 1.19 \cdot 10^9\,\text{mm}^3$$

The resultant longitudinal shear force at interface CC2 is:

$$V_{Ed,CC2} = \frac{V_{Ed,bs} \cdot S_{CC2}}{I^*_c} = \frac{4953\text{kN} \cdot 1.19 \cdot 10^9\,\text{mm}^3}{2.72 \cdot 10^{12}\,\text{mm}^4} = 2167\frac{\text{N}}{\text{mm}}$$

On 1-meter length of column:

$$V_{Ed,CC2} = 2167\frac{\text{kN}}{\text{m}}$$

- **Evaluation of necessary amount of shear studs:**

Geometrical characteristic of the shear studs correspond to State of Art – Table 3.2.2 where:

d = 25 mm – diameter of the shear stud;

h_{sc} = 100 mm – stud height; Stud length is **OK**.

f_u = 450 MPa – maximum stud tensile strength;

For a shear stud with a diameter d = 25 mm, the design shear strength is equal to:

$$P_{Rk} = \min\left(0.43 A_s \sqrt{E_c f_c}, 0.7 f_u A_s\right) = \min\left(246.1\text{kN}, 154.4\text{kN}\right) = 154.4\text{kN}$$

For a length of a column of 1 m, the necessary amount of shear studs to different interfaces is:

$$n_{studs\_CC1} = \frac{V_{Ed1\_CC1} \cdot 1\text{m}}{P_{Rk}} = \frac{345.3\frac{\text{kN}}{\text{m}} \cdot 1\text{m}}{154.4\text{kN}} = 2.24 \Rightarrow 3\text{ studs} / 1\text{m}$$

$$n_{studs\_CC2} = \frac{V_{Ed1\_CC2} \cdot 1\text{m}}{P_{Rk}} = \frac{2176\frac{\text{kN}}{\text{m}} \cdot 1\text{m}}{154.4\text{kN}} = 14.1 \Rightarrow 15\text{ studs} / 1\text{m}$$

Suppose the studs are installed in three rows, then the space of the studs is 200mm. The JGJ code specifies that the space should not be less than 6 times the diameter of the stud, which is 150mm in this example. The space is **OK**.

10.3.4 Example 2 and 3

Given:

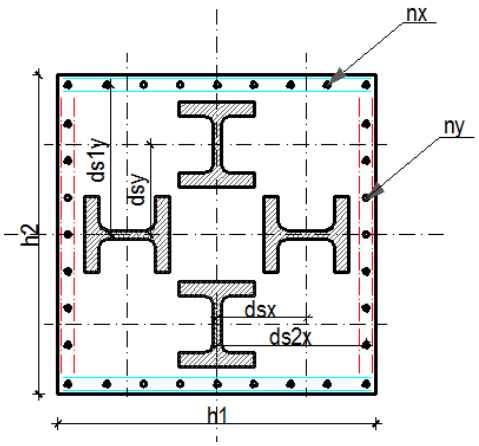

Figure 10-24 Section 2 dimensions

Steel profiles: 4 HEM 100 – fy = 406 MPa - average values from material tests (Table 10-12)
$d_{sx} = d_{sy} = 127.5$ mm ;
Reinforcement rebar: 32φ8mm – fys = 438 Mpa
ds1x = ds1y = 208 mm ;
Concrete: $h_1 = h_2 = 450$mm - fck = 64.8 MPa - average values from material tests
Buckling length : L= 3600 mm

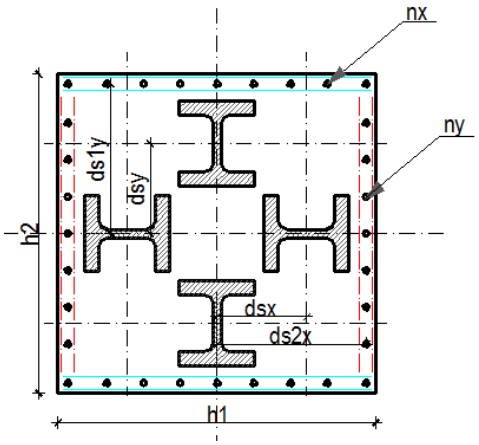

Figure 10-25 Section 3 dimensions

Steel profiles : 4 HD 400 x 634 HISTAR 460
$d_{sx} = d_{sy} = 513$ mm ;
Reinforcement rebar: 32 φ 32mm –HRB 400
$d_{s2x} = d_{s1y} = 550$ mm ;
Concrete: $h_1 = h_2 = 1800$mm - C60: fck = 60 MPa
Buckling length : L= 18000 mm

Solution:

- **Design equations:**

Likewise, the transformation of the real cross-section to the simplified one can found. Several other variables are defined as follows:

$$y_1 = d_2 / 2$$
$$y_2 = d_{sx} - d_1 / 2$$
$$y_3 = d_{sx} + d_1 / 2$$
$$y_4 = d_{s2x}$$

Table 10-10 Determining the moment capacity at a given axial load – example 2

Case 1. $|y| \le y_1$

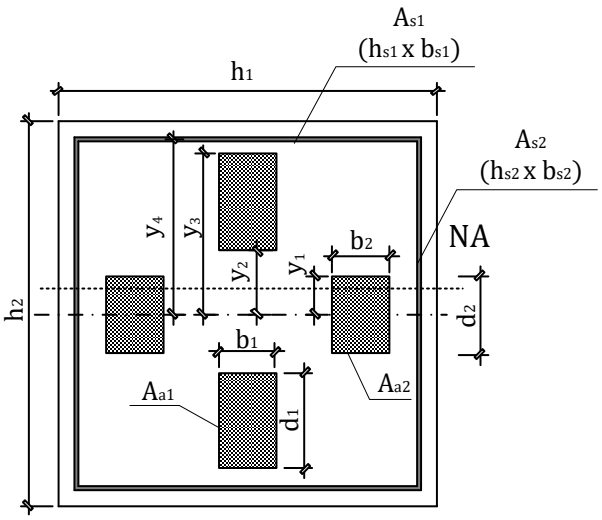

$$h_{nx} = \frac{N - f_c\left(\beta h_1 h_2 / 2 - A_{a1} - A_{a2} - A_{s1} - b_{s2} h_{s2}\right)}{\left(-\beta h_1 + 2b_2 + 2b_{s2}\right) f_c - 4b_2 f_y - 4b_{s2} f_{sy}}$$

$$Z_{sr} = Z_{srx} - 2b_{s2} h_{nx}^2$$

$$M_{sr} = Z_{sr} f_{sy}$$

$$Z_s = Z_{sx} - 2b_2 h_{nx}^2$$

$$M_s = Z_s f_y$$

$$x = \beta\left(\frac{h_2}{2} - h_{nx}\right)$$

$$M_c = f_c\left[x h_1\left(\frac{h_2}{2} - \frac{x}{2}\right) - \frac{Z_s}{2} - \frac{Z_{sr}}{2}\right]$$

$$M = M_c + M_{sr} + M_s$$

Case 2. $\mathbf{y_1 < |y| \leq y_2}$

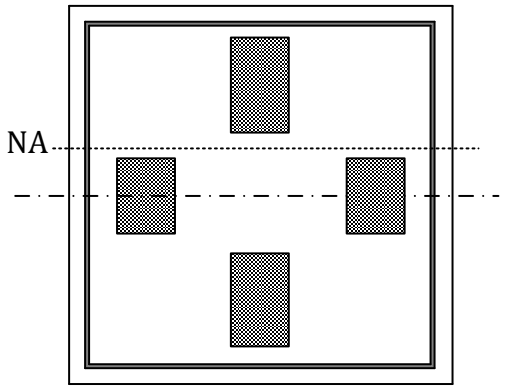

$$h_{nx} = \frac{N + 2A_{a2} f_y S - f_c \left(\beta h_1 h_2 / 2 - A_{a1} - A_{a2} + A_{a2} S - A_{s1} - b_{s2} h_{s2} \right)}{\left(-\beta h_1 + 2b_{s2} \right) f_c - 4 b_{s2} f_{sy}}$$

$$Z_{sr} = Z_{srx} - 2 b_{s2} h_{nx}^2$$

$$M_{sr} = Z_{sr} f_{sy}$$

$$Z_s = 2 A_{a1} d_{sx}$$

$$M_s = Z_s f_y$$

$$x = \beta \left(\frac{h_2}{2} - h_{nx} \right)$$

$$M_c = f_c \left[x h_1 \left(\frac{h_2}{2} - \frac{x}{2} \right) - \frac{Z_s}{2} - \frac{Z_{sr}}{2} \right]$$

$$M = M_c + M_{sr} + M_s$$

Case 3. $\mathbf{y_2 < |y| \leq y_3}$

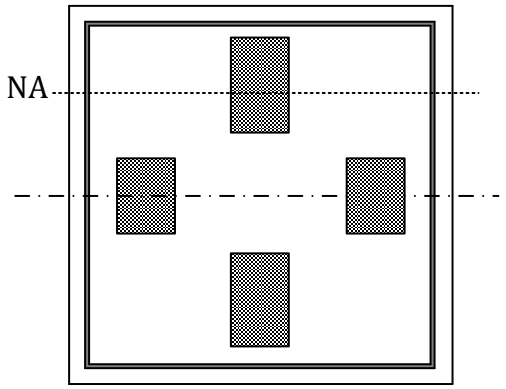

$$h_{nx} = \frac{N + 2\left(A_{a2} - b_1 y_2\right) f_y S - f_c\left[\beta h_1 h_2 / 2 - A_{a1} - A_{a2} + \left(A_{a2} - b_1 y_2\right) S - A_{s1} - b_{s2} h_{s2}\right]}{\left(-\beta h_1 + b_1 + 2b_{s2}\right) f_c - 4 b_{s2} f_{sy} - 2 b_1 f_y}$$

$$Z_{sr} = Z_{srx} - 2 b_{s2} h_{nx}^2$$

$$M_{sr} = Z_{sr} f_{sy}$$

$$d_n = \left|h_{nx}\right| - y_2$$

$$Z_s = 2 A_{a1} d_{sx} - 2 d_n b_1 \left(y_2 + \frac{d_n}{2}\right)$$

$$M_s = Z_s f_y$$

$$x = \beta\left(\frac{h_2}{2} - h_{nx}\right)$$

$$M_c = f_c\left[x h_1\left(\frac{h_2}{2} - \frac{x}{2}\right) - \frac{Z_s}{2} - \frac{Z_{sr}}{2}\right]$$

$$M = M_c + M_{sr} + M_s$$

Case 4. $\mathbf{y_3 < |y| \leq y_4}$

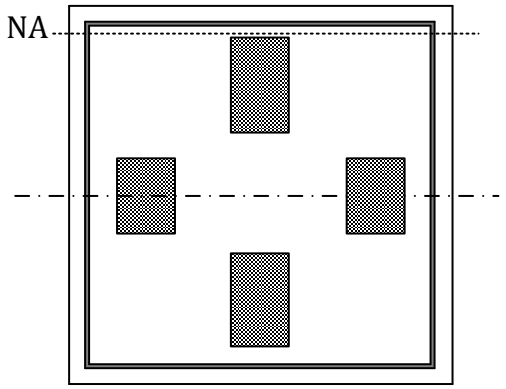

$$h_{nx} = \frac{N + A_s f_y S - f_c\left(\beta h_1 h_2 / 2 - A_s / 2 + S A_s / 2 - A_{s1} - b_{s2} h_{s2}\right)}{\left(-\beta h_1 + 2 b_{s2}\right) f_c - 4 b_{s2} f_{sy}}$$

$$Z_{sr} = Z_{srx} - 2 b_{s2} h_{nx}^2$$

$$M_{sr} = Z_{sr} f_{sy}$$

$$Z_s = 0$$

$$M_s = Z_s f_y$$

$$x = \beta\left(\frac{h_2}{2} - h_{nx}\right)$$

$$M_c = f_c\left[x h_1\left(\frac{h_2}{2} - \frac{x}{2}\right) - \frac{Z_s}{2} - \frac{Z_{sr}}{2}\right]$$

$$M = M_c + M_{sr} + M_s$$

Case 5. $|y| \geq y_4$

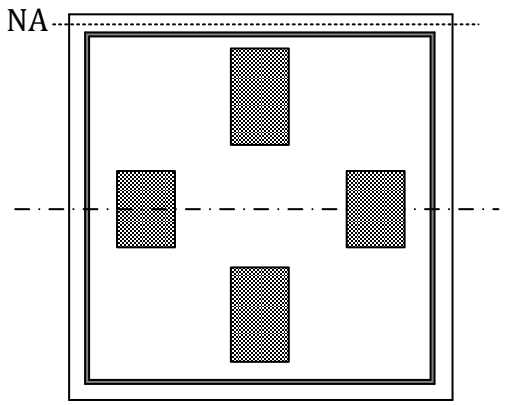

$$h_{nx} = \frac{N + A_s f_y S + A_{sr} f_{sy} S - f_c \left(\beta h_1 h_2 / 2 - A_s / 2 + S A_s / 2 - A_{sr} / 2 + S A_{sr} / 2 \right)}{-\beta h_1 f_c}$$

$$Z_{sr} = 0$$

$$M_{sr} = Z_{sr} f_{sy}$$

$$Z_s = 0$$

$$M_s = Z_s f_y$$

$$x = \beta \left(\frac{h_2}{2} - h_{nx} \right)$$

$$M_c = f_c \left[x h_1 \left(\frac{h_2}{2} - \frac{x}{2} \right) - \frac{Z_s}{2} - \frac{Z_{sr}}{2} \right]$$

$$M = M_c + M_{sr} + M_s$$

- **Interaction curve – nominal strength:**

The N-M interaction curves are calculated based on the nominal material strengths, and no reduction factors are considered. Besides, the buckling effects and $P-\delta$ effects are not considered either. Therefore, the N-M curves reflect the pure cross-sectional capacity of the composite members. The fiber results are obtained based on the FEM numerical calculations.

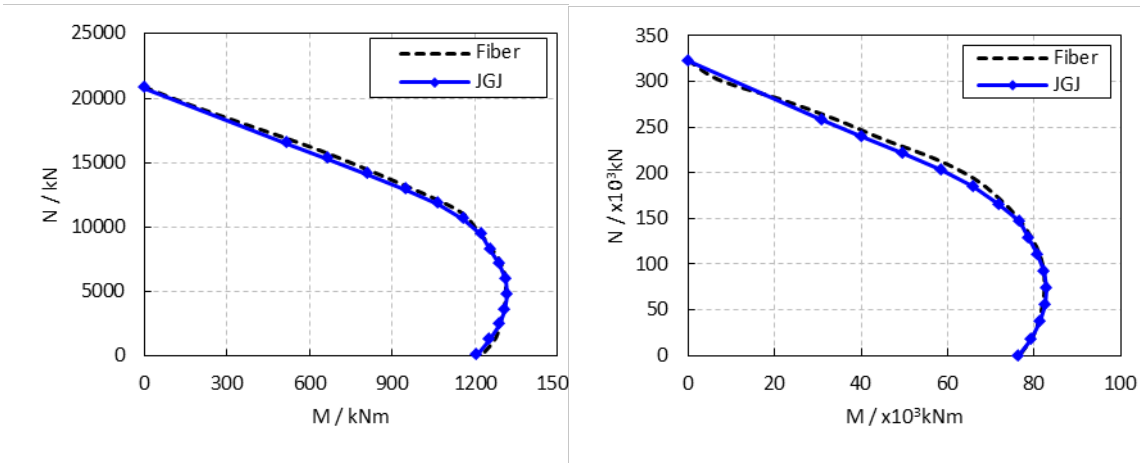

(a) Section 2 (b) Section 3

Figure 10-26 Interaction curves with nominal strengths

- **Interaction curve – partial factors:**

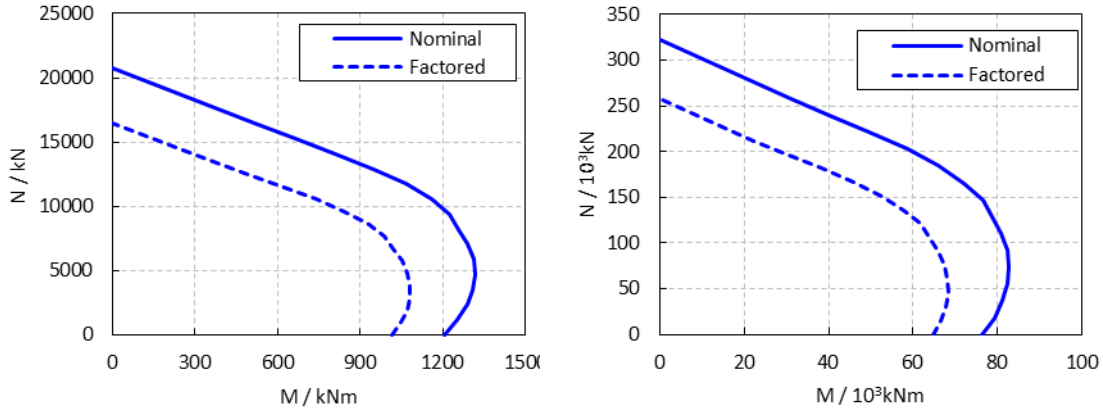

(a) Section 2 (b) Section 3

Figure 10-27 Interaction curves with and without material partial factors

- **Interaction curve - Buckling and second order effects:**

1) Axial capacity

In Chinese codes, the axial capacity of a composite column should be determined based on the following equation:

$$N \le 0.9\varphi(f_c A_c + f_{ys} A_s + f_{ya} A_a)$$

The buckling curve for composite columns can be determined based on 'Code for design of composite structures' (JGJ 138), using the following Table:

Table 10-11 Reduction factor for buckling

l_0 / i	≤ 28	35	42	48	55	62	69	76	83	90	97	104
φ	1.00	0.98	0.95	0.92	0.87	0.81	0.75	0.70	0.65	0.60	0.56	0.52

where:

l_0 = buckling length of the column

i = radius of gyration of the composition cross-section, which can be calculated as:

$$i = \sqrt{\frac{E_c I_c + E_a I_a}{E_c A_c + E_a A_a}}$$

The buckling length for section 1and section 3 is 18m. This value is calculated considering a four-story high lobby with the story height of 4.5m. The buckling length for section 2 is still 3.6m to comply with the test.

Table 10-12 Axial capacity

	Section 1	Section 2	Section 3
Buckling reduction factor	1.000	0.994	0.970
Nominal axial capacity	921085	20988	322734
Axial capacity considering buckling effects only	921085	20873	313044
Axial capacity considering buckling effects & material partial factors	657046	14954	225536

2) Moment capacity

Chinese standard specifies that the second order $P-\delta$ effect can be ignored if the following three criteria are satisfied:

(1) $M_1 / M_2 \le 0.9$
(2) $N / N_u \le 0.9$
(3) $l_c / i \le 32 - 12(M_1 / M_2)$

where:

M_1 = smallest design bending moment within the composite member
M_2 = largest design bending moment within the composite member
N = design axial force
N_u = short-column axial capacity of the composite member
l_c = buckling capacity
i = radius of gyration of the composite cross-section

If the criteria are not satisfied, the $P-\delta$ effect needs to be considered by multiplying the design bending moment with a coefficient that is greater than 1.0.

$$M = C_m \eta_{ns} M_2$$

$$C_m = 0.7 + 0.3\frac{M_1}{M_2}$$

$$\eta_{ns} = 1 + \frac{1}{1300(M_2 N + e_a)/h_0}\left(\frac{l_c}{h_c}\right)^2 \zeta_c$$

$$\zeta_c = \frac{0.5 f_c A_g}{N}$$

where:

e_a = max{20mm,1/30h_c}
h_0 = effective height of the composite cross-section
h_c = cross-section dimension along the direction that the bending moment is considered
f_c = concrete compressive strength
A_g = gross area of the cross-section

Shown in Figure 10-28 are the interaction curves given by Chinese with and without buckling and second order effects. The interaction curves have considered the material partial factors.

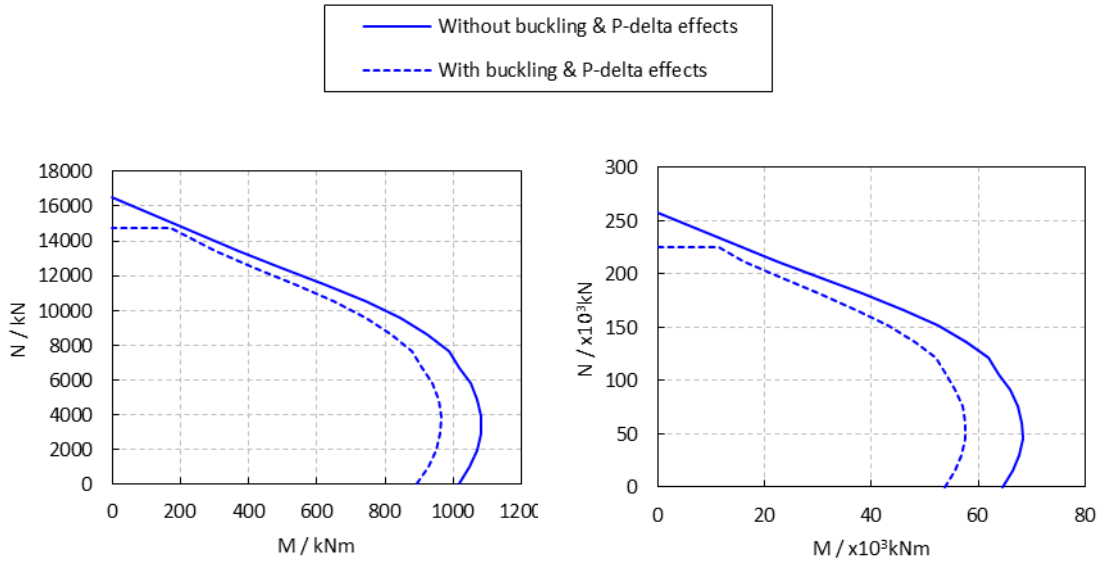

(a) Section 2 (b) Section 3

Figure 10-28 Interaction curves with and without considering buckling and second order effects (Material partial factors have already been considered)

- **Shear force evaluation:**

Check the capacity of the composite column subjected to the following demands:

N_{Ed} = 150000 kN;

M_{Ed} = 40000 kN;

V_{Ed} = 8000 kN;

The definition of the used symbols is defined in Figure 10-29:

$b_{c1} = 150\text{mm}$

$b_{s2} = 474\text{mm}$

$b_{c3} = 64\text{mm}$

$b_{s4} = 424\text{mm}$

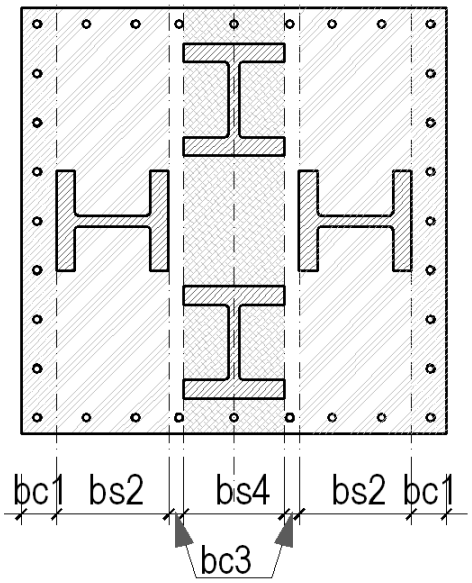

Figure 10-29 Definition of sections bc1, bc3, bs2, and bs4 (EC4 Design) – Example 2

The applied shear force is V_{Ed} is distributed between sections b_{c3}, b_{c4} and b_s proportionally to their stiffness:

$$V_{Ed,bc1} = V_{Ed} \cdot EI_{eff,bc1} / EI_{eff}$$

$$V_{Ed,bc3} = V_{Ed} \cdot EI_{eff,bc3} / EI_{eff}$$

$$V_{Ed,bs1} = V_{Ed} \cdot EI_{eff,bs1} / EI_{eff}$$

$$V_{Ed,bs2} = V_{Ed} \cdot EI_{eff,bs2} / EI_{eff}$$

The effective bending stiffness of the column is:

$EI_{eff} = 4.43 \cdot 10^{16}$ Nmm

The total effective bending stiffness is the sum of individual EI_{eff} established for sections b_{c1}, b_{c3}, b_{s2} and b_{s4} respectively.

1) Section b_{c1}: $EI_{eff,bc3}1 = E_{sr} \cdot I_{sr,bc1} + E_c \cdot I_{c,bc1}$

To calculate $I_{sr,bc1}$ of the reinforcing bars, it is considered one equivalent plate A_{s2}.
For each face:

- The number of bars is: 9 bars
- The area of those bars is: $A_{sr,bc3} = 9 \cdot A_{sri} = 7238\text{mm}^2$
- The thickness of the equivalent plate is:

$$t_p = A_{sr,bc1} \Big/ h_{s1} = 7238\text{mm}^2 \Big/ 1720\text{mm} = 4.2\text{mm}$$

$$I_{cg,bc1} = \frac{b_{c1} \cdot h_1^3}{12} = \frac{150\text{mm} \cdot (1800\text{mm})^3}{12} = 7.29 \cdot 10^{10}\,\text{mm}^4$$

$$I_{sr,bc1} = \frac{t_p \cdot h_{s1}^3}{12} = \frac{4.4\text{mm} \cdot 1720\text{mm}^3}{12} = 1.87 \cdot 10^9\,\text{mm}^4$$

$$I_{c,bc1} = I_{cg,bc1} - I_{sr,bc1} = 7.29 \cdot 10^{10}\,\text{mm}^4 - 1.87 \cdot 10^9\,\text{mm}^4 = 7.10 \cdot 10^{10}\,\text{mm}^4$$

$$\begin{aligned} EI_{eff,bc1} &= E_{sr} \cdot I_{sr,bc1} + E_c \cdot I_{c,bc1} \\ &= 200000\text{MPa} \cdot 1.87 \cdot 10^9\,\text{mm}^4 + 39262\text{MPa} \cdot 7.10 \cdot 10^{10}\,\text{mm}^4 \\ &= 3.16 \cdot 10^{15}\,\text{Nmm}^2 \end{aligned}$$

2) Section b_{c3}: $EI_{eff,bc3} = E_{sr} \cdot I_{sr,bc3} + E_c \cdot I_{c,bc3}$

To calculate $I_{sr,bc3}$, two equivalent (one top and one bottom) steel plates replace the reinforcing bars. Each plate has the same total area, and contains 1 rebar:

$$A_{sr,bc3} = 1 \cdot A_{sri} = 804.2\text{mm}^2$$

$$I_{sr,bc3} = 2 \cdot A_{sr,bc3} \cdot d_{s1y}^2 = 2 \cdot 804.2\text{mm}^2 \cdot (860\text{mm})^2 = 1.222 \cdot 10^6\,\text{mm}^4$$

$$I_{cg,bc3} = \frac{b_{c3} \cdot h_1^3}{12} = \frac{64\text{mm} \cdot (1800\text{mm})^3}{12} = 3.110 \cdot 10^{10}\,\text{mm}^4$$

$$I_{c,bc3} = I_{cg,bc3} - I_{sr,bc3} = 3.110 \cdot 10^{10}\,\text{mm}^4 - 1.222 \cdot 10^6\,\text{mm}^4 = 3.110 \cdot 10^{10}\,\text{mm}^4$$

$$\begin{aligned} EI_{eff,bc3} &= E_{sr} \cdot I_{sr,bc3} + E_c \cdot I_{c,bc3} \\ &= 200000\text{MPa} \cdot 1.222 \cdot 10^6\,\text{mm}^4 + 39262\text{MPa} \cdot 3.110 \cdot 10^{10}\,\text{mm}^4 \\ &= 1.22 \cdot 10^{15}\,\text{Nmm}^2 \end{aligned}$$

3) Section b_{s2}: $EI_{eff,bs2} = E_s \cdot I_{s,bs2} + E_{sr} \cdot I_{sr,bs2} + E_c \cdot I_{c,bs2}$

To calculate $I_{sr,bs2}$, two equivalent (one top and one bottom) steel plates replace the reinforcing bars. Each plate has the same total area, and contains 2 rebar:

$$A_{sr,bs2} = 2 \cdot A_{sri} = 1608.5\text{mm}^2$$

$$I_{sr,bs2} = 2 \cdot A_{sr,bs2} \cdot d_{s1y}{}^2 = 2 \cdot 1608.5\text{mm}^2 \cdot \left(860\text{mm}\right)^2 = 1.858 \cdot 10^9\,\text{mm}^4$$

$$I_{s,bs2} = I_y = 9.825 \cdot 10^8\,\text{mm}^4$$

$$I_{cg,bs2} = \frac{b_{s2} \cdot h_1^{\,3}}{12} = \frac{476\text{mm} \cdot \left(1800\text{mm}\right)^3}{12} = 2.304 \cdot 10^{11}\,\text{mm}^4$$

$$I_{c,bs2} = I_{cg,bs4} - I_{sr,bs2} - I_{s,bs2} = 2.304 \cdot 10^{11}\,\text{mm}^4 - 1.858 \cdot 10^9\,\text{mm}^4 - 9.825 \cdot 10^8\,\text{mm}^4 = 2.276 \cdot 10^{11}\,\text{mm}^4$$

$$\begin{aligned} EI_{eff,bs2} &= E_s \cdot I_{s,bs2} + E_{sr} \cdot I_{sr,bs2} + E_c \cdot I_{c,bs2} \\ &= 206000\text{MPa} \cdot 9.825 \cdot 10^8\,\text{mm}^4 + 200000\text{MPa} \cdot 1.858 \cdot 10^9\,\text{mm}^4 + 39262\text{MPa} \cdot 2.276 \cdot 10^{11}\,\text{mm}^4 \\ &= 9.51 \cdot 10^{15}\,\text{Nmm}^2 \end{aligned}$$

4) Section b_{s4}: $EI_{eff,bs4} = E_s \cdot I_{s,bs4} + E_{sr} \cdot I_{sr,bs4} + E_c \cdot I_{c,bs4}$

To calculate $I_{sr,bs4}$, two equivalent (one top and one bottom) steel plates replace the reinforcing bars. Each plate has the same total area, and contains 1 rebar:

$$A_{sr,bs4} = 1 \cdot A_{sri} = 804.2\text{mm}^2$$

$$I_{sr,bs4} = 2 \cdot A_{sr,bs4} \cdot d_{s1y}{}^2 = 2 \cdot 804.2\text{mm}^2 \cdot \left(860\text{mm}\right)^2 = 9.291 \cdot 10^8\,\text{mm}^4$$

$$I_{s,bs4} = 2 \cdot A_{\text{a}} \cdot d_{sy}{}^2 = 2 \cdot 80800\text{mm}^2 \cdot \left(513\text{mm}\right)^2 = 4.801 \cdot 10^{10}\,\text{mm}^4$$

$$I_{cg,bs4} = \frac{b_{s4} \cdot h_1^{\,3}}{12} = \frac{424\text{mm} \cdot \left(1800\text{mm}\right)^3}{12} = 2.061 \cdot 10^{11}\,\text{mm}^4$$

$$I_{c,bs4} = I_{cg,bs4} - I_{sr,bs4} - I_{s,bs4} = 2.061 \cdot 10^{11}\,\text{mm}^4 - 9.291 \cdot 10^8\,\text{mm}^4 - 4.801 \cdot 10^{10}\,\text{mm}^4 = 1.572 \cdot 10^{11}\,\text{mm}^4$$

$$\begin{aligned} EI_{eff,bs4} &= E_s \cdot I_{s,bs4} + E_{sr} \cdot I_{sr,bs4} + E_c \cdot I_{c,bs4} \\ &= 206000\text{MPa} \cdot 4.801 \cdot 10^{10}\,\text{mm}^4 + 200000\text{MPa} \cdot 9.291 \cdot 10^8\,\text{mm}^4 + 39262\text{MPa} \cdot 1.572 \cdot 10^{11}\,\text{mm}^4 \\ &= 1.625 \cdot 10^{16}\,\text{Nmm}^2 \end{aligned}$$

$$EI_{eff} = 2 \cdot (EI_{eff,bc1}) + 2 \cdot (EI_{eff,bs2}) + 2 \cdot (EI_{eff,bc3}) + EI_{eff,bs4} = 4.403 \cdot 10^{16}\,\text{Nmm}^2$$

The factored shear force V_{Ed} = 8000 kN for the complete section is distributed in the 5 sections (2 b_{c3}, 2 b_s and 1 b_{c4}) :

$$V_{Ed,bc1} = V_{Ed} \cdot \frac{EI_{eff,bc1}}{EI_{eff}} = 8000\text{kN} \cdot \frac{3.16 \cdot 10^{16}\,\text{Nmm}^2}{4.40 \cdot 10^{16}\,\text{Nmm}^2} = 574\text{kN}$$

$$V_{Ed,bc3} = V_{Ed} \cdot \frac{EI_{eff,bc1}}{EI_{eff}} = 8000\text{kN} \cdot \frac{1.22 \cdot 10^{15}\,\text{Nmm}^2}{4.40 \cdot 10^{16}\,\text{Nmm}^2} = 221\text{kN}$$

$$V_{Ed,bs2} = V_{Ed} \cdot \frac{EI_{eff,bs2}}{EI_{eff}} = 8000\text{kN} \cdot \frac{9.51 \cdot 10^{15}\,\text{Nmm}^2}{4.40 \cdot 10^{16}\,\text{Nmm}^2} = 1728\text{kN}$$

$$V_{Ed,bs4} = V_{Ed} \cdot \frac{EI_{eff,bs4}}{EI_{eff}} = 8000\text{kN} \cdot \frac{1.63 \cdot 10^{16}\,\text{Nmm}^2}{4.40 \cdot 10^{16}\,\text{Nmm}^2} = 2952\text{kN}$$

- **Calculation of shear in section b_{s4}:**

Section b_{s2} is a composite steel-concrete section having 2 reinforced concrete flanges, 2 steel "flanges" (the HD sections) and 1 reinforced concrete web. To establish longitudinal shear in section b_s, it is convenient to transform the composite section into a single material section or "homogenized" section. The single material can be either steel or concrete.

Choosing concrete, the moment of inertia of the homogenized concrete section I_c* is such that the stiffness $E_c\, I_c$* of the homogenized section is equal to the stiffness $EI_{eff,bs2}$:

$$I_c^* = {EI_{eff,bs4}}\Big/{E_{cm}} = 1.625 \cdot 10^{16}\,\text{Nmm}^2 \Big/ 39262\text{MPa} = 4.139 \cdot 10^{11}\,\text{mm}^4$$

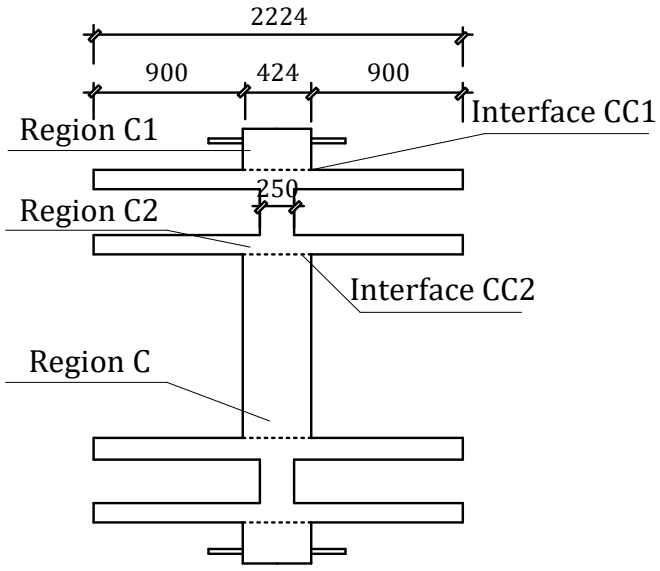

Figure 10-30 Homogenized equivalent concrete section bs – Example 2

In a homogenized concrete section (Figure 10-30), the width of the concrete equivalent to the width of the steel flanges is:

$$b_s^* = b_{s4} \cdot {E_s}/{E_{cm}} = 424\text{mm} \cdot {206000\text{MPa}}/{39262\text{MPa}} = 2224\text{mm}$$

The width of the concrete equivalent to the width of the steel web is:

$$t_w^* = t_w \cdot {E_s}/{E_{cm}} = 47.6\text{mm} \cdot {206000\text{MPa}}/{39262\text{MPa}} = 250\text{mm}$$

The resultant longitudinal shear force on interfaces like CC1 and CC2 in Figure 10-30 is:

$$V_{Ed,l} = \frac{V_{Ed,bs2} \cdot \text{S}}{I_\text{c}^*}$$

where:

S is the first moment of areas of regions C1 or C2 taken about the neutral axis of the section as illustrated in Figure 10-30.

Using S, the longitudinal shear is calculated at the steel-concrete interfaces CC1 and CC2 in order to size the force transfer mechanisms required for the member to act as a fully composite section.

- **Calculation of longitudinal shear force applied at interface CC1:**

S_{CC1} is the section modulus for the region C1 as defined in Figure 10-30:

The height of the C1 region is:

$$h_1' = \frac{h_1}{2} - \left(d_{sy} + \frac{d}{2} \right) = \frac{1800\text{mm}}{2} - \left(513\text{mm} + \frac{474\text{mm}}{2} \right) = 150\text{mm}$$

The area is:

$$A_1 = b \cdot h_1' = 424\text{mm} \cdot 150\text{mm} = 63600\text{mm}^2$$

$$S_{CC1} = A_1 \cdot \left(\frac{h_1}{2} - \frac{h_1'}{2} \right) = 63600\text{mm}^2 \cdot \left(\frac{1800\text{mm}}{2} - \frac{150\text{mm}}{2} \right) = 5.247 \cdot 10^7\,\text{mm}^3$$

The resultant longitudinal shear force on interface CC1 is:

$$V_{Ed,CC1} = \frac{V_{Ed,bs} \cdot S_{CC1}}{I_\text{c}^*} = \frac{2952\text{kN} \cdot 5.247 \cdot 10^7\,\text{mm}^3}{4.139 \cdot 10^{11}\,\text{mm}^4} = 374\frac{\text{N}}{\text{mm}}$$

On 1-meter length of column:

$$V_{Ed,CC1} = 374\frac{\text{kN}}{\text{m}}$$

- **Calculation of longitudinal shear force applied at interface CC2:**

S_{CC2} is the section modulus for the combined regions C1 and C2 (the HD profile):

The equivalent area in concrete for the HD profile is:

A_a =80800 mm^2

The equivalent are in concrete for the HD profile is:

$$A_a^* = A_a \cdot E_s / E_{cm} = 80800\text{mm}^2 \cdot 206000\text{MPa} / 39262\text{MPa} = 423942\text{mm}^2$$

The distance of HD center to the neutral axis is:

d_{sy} = 513 mm

The moment of area of the equivalent steel profile is:

$$S_{HD} = A_a^* \cdot d_{sy} = 423942\text{mm}^2 \cdot 513\text{mm} = 2.175 \cdot 10^8\,\text{mm}^3$$

Area of concrete between the flanges:

$$A_{c\_CC2}^* = b \cdot d\text{-}A_a = 424\text{mm} \cdot 474\text{mm} - 80800\text{mm}^2 = 120176\text{mm}^2$$

Moment of area of concrete between the flanges:

$$S_{c\_CC2}^* = A_{c\_CC2}^* \cdot d_{sy} = 120176\text{mm}^2 \cdot 513\text{mm} = 6.165 \cdot 10^7\,\text{mm}^3$$

The section modulus of combined regions C1 and C2, is equal to:

$$S_{CC2} = S_{c\_CC2}^* + S_{HD} + S_{CC1} = 6.165 \cdot 10^7\,\text{mm}^3 + 2.175 \cdot 10^8\,\text{mm}^3 + 5.247 \cdot 10^7\,\text{mm}^3 = 3.334 \cdot 10^8\,\text{mm}^3$$

The resultant longitudinal shear force at interface CC2 is:

$$V_{Ed,CC2} = \frac{V_{Ed,bs} \cdot S_{CC2}}{I_c^*} = \frac{2952\text{kN} \cdot 3.334 \cdot 10^8\,\text{mm}^3}{4.139 \cdot 10^{11}\,\text{mm}^4} = 2378\frac{\text{N}}{\text{mm}}$$

On 1-meter length of column:

$$V_{Ed,CC2} = 2378\frac{\text{kN}}{\text{m}}$$

- **Evaluation of necessary amount of shear studs:**

Geometrical characteristic of the shear studs correspond to State of Art – Table 3.2.2 where:

d = 25 mm – diameter of the shear stud;

f_u = 450 MPa – maximum stud tensile strength;

For a shear stud with a diameter d = 25 mm, the design shear strength is equal to:

$$P_{Rk} = \min\left(0.43 A_s \sqrt{E_c f_c}, 0.7 f_u A_s\right) = \min\left(273.3\text{kN}, 154.4\text{kN}\right) = 154.4\text{kN}$$

For a length of a column of 1 m, the necessary amount of shear studs to different interfaces is:

$$n_{studs\_CC1} = \frac{V_{Ed1\_CC1} \cdot 1\text{m}}{P_{Rk}} = \frac{374 \frac{\text{kN}}{\text{m}} \cdot 1\text{m}}{154.4\text{kN}} = 2.42 \Rightarrow 3 \text{ studs} / 1\text{m}$$

$$n_{studs\_CC2} = \frac{V_{Ed1\_CC2} \cdot 1\text{m}}{P_{Rk}} = \frac{2378 \frac{\text{kN}}{\text{m}} \cdot 1\text{m}}{154.4\text{kN}} = 15.4 \Rightarrow 18 \text{ studs} / 1\text{m}$$

Suppose the studs are installed in three rows, then the space of the studs is 167mm. The JGJ code specifies that the space should not be less than 6 times the diameter of the stud, which is 150mm in this example. The space is **OK**.

11 Conclusions

The results of the static and quasi-static tests on reinforced columns with four encased steel sections have been validated with FEM methods and compared with simplified code provisions methods.

The simplified methods provided by codes are generally valid for composite compression members with one steel encased section. However, research program results show that code provisions are valid also for mega columns with more than one encased steel section.

1) Simplified design approaches are proposed and described in this report in accordance with Chinese codes JGJ 138. The design approaches are applicable to mega columns within a 15% eccentricity ratio.

2) A new extended method based on Eurocode 4 design has been developed in order to design the composite columns with several steel profiles embedded. The method is an extension of the Plastic Distribution Method and takes into account all the assumptions that are defined in EC 4 - Clause 6.7. Two numerical models have been created in order to simulate the behavior of experimental tests. Comparing the adapted simplified method and the two simplified numerical models created in Abaqus and Safir, similar results to the experimental part are obtained. The Adapted Distribution Method N – M interaction diagram has been obtained based on a simple method presented in the European design code EC4. These expressions have been developed for the cases of composite sections with several encased steel profiles and they are presented in Chapter 9. The simplified method can be used to quickly and easily do a manual evaluation of the axial force-bending moment interaction curve.

3) The current ACI 318, AISC-LRFD, Eurocode4, and JGJ 138 are evaluated in this test program. For the test specimens, the current codes are able to provide precise predictions on the axial and flexural capacities with sufficient margins of safety.

4) The finite element analyses are conducted as a supplementary to the test research. FEA demonstrated that the interface strength and stiffness influenced the capacity of mega columns dramatically when subjected lateral loads. This implied that the shear demand on the interfaces became much larger when the steel profiles were separate from one another.

More thoughtful analyses imply that the enhancement in capacity was contributed by both the interface strength and interface stiffness, and that the efficiency of shear studs got smaller as the number of shear studs grew. In a real structure, however, the shear force between the concrete and the steel profiles is contributed by shear studs, bond stress, and friction, but the FEA results only reflect the influence of shear studs. With the existence of bond stress and friction, the influence of shear studs in a real structure may not be as significant as it is shown in the FEA.

Appendix A 1:1 Scale Column Predesign

Calculate the capacity, utilizing AISC requirements, of a 9 meter tall 1800 mm square composite column supporting gravity and seismic loadings with 60 MPa cube strength concrete, 10% 460 MPa embedded steel, and 0.1% 400 MPa longitudinal reinforcement.

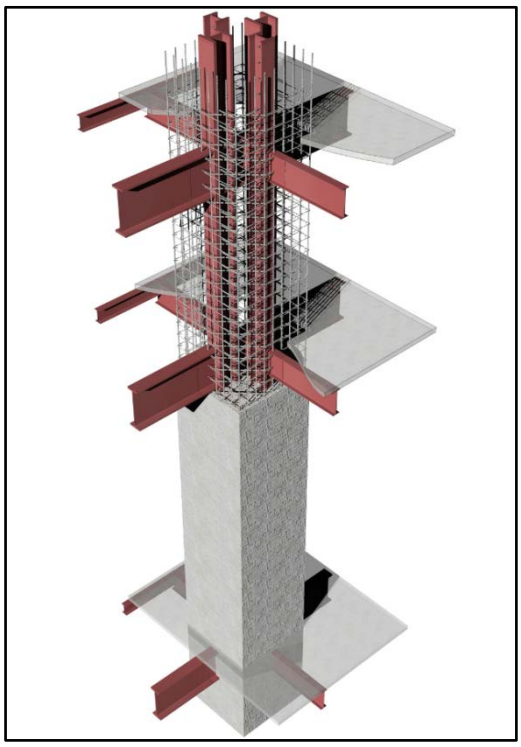

Figure A-1 3D isometric of composite building column (Information provided by MKA 2016)

A.1 Determine the material properties of the column

Table A-1 Material Properties

Material	Grade	Yield Stress (MPa)	Unit Weight (kg/m^3)	Modulus of Elasticity (E - MPa)
Concrete	C60	50[a]	1500[b]	17664[c]
Embedded Steel	HISTAR 460	460[d]	7850	200,000
Rebar	HRB400	400[d]	7850	200,000

a. 21 MPa $\leq f'_c \leq$ 70 MPa [AISC I1.3(1)]

C60 refers to 60 MPa 28 day cube strength; however, AISC requirements are with respect to 28 day cylinder strength, which is 50 MPa for C60 concrete.

b. 1442 kg/m^3 $\leq w_c \leq$ 2563 kg/m^3 [AISC I2.1.1b]

c. $E_c = 0.043 w_c^{1.5} 33\sqrt{f'_c}$ [AISC I2.1.1b]

d. $F_y \leq$ 525 Mpa [AISC I1.3(2)]

A.2 Determine column unbraced length and effective length factor

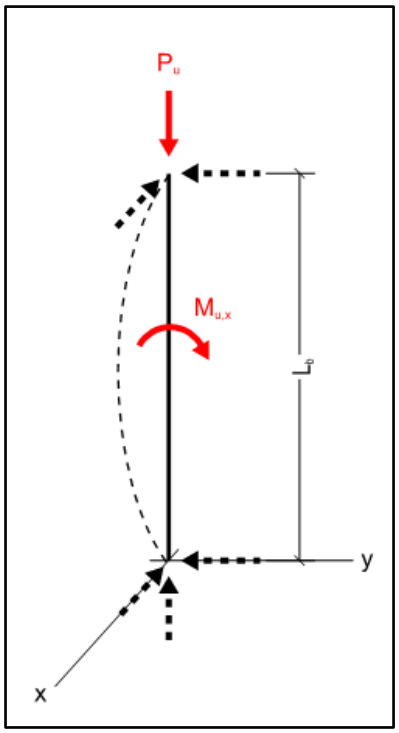

Figure A-2 Column free body diagram (Information provided by MKA 2016)

The assumed buckled shape and boundary restraints for the column are shown in Figure A.1 above. The building's floor diaphragms are assumed to restrain translational movement in the x and y directions at the top and bottom of the column as indicated by the dashed arrows. Additionally, the incoming floor framing connections are assumed to provide negligible rotational stiffness; therefore, the column is assumed to freely rotate about each axis at its top and bottom. Based on these assumed boundary conditions, the buckled shape (indicated by the dashed line) and effective length factor, K, are determined per AISC Table C-A-7.1.

Column unbraced length:

$L_b = 9$ m

Colum effective length factor:

$K_x = 1.0$

For composite columns with floor diaphragms at the top and bottom, K = 1.0 is a conservative value as there is some inherent rotational stiffness in the incoming floor framing. Taking this stiffness into account will result in lower K values as calculated per AISC Appendix 7.

A.3 Select embedded steel shapes, and longitudinal reinforcement

Use an 1800 mm X 1800 mm section with (4) HD400X634 embedded steel shapes and (32) 32mm diameter longitudinal reinforcing bars (9 bars along each face).

Gross area of column section:

$$A_g = B \times H = 1800 \text{ mm} \times 1800 \text{ mm} = 3{,}240{,}000 \text{ mm}^2$$

Area of embedded steel shapes:

$$A_s = 4 \times 80{,}800 \text{ mm}^2 = 323{,}2000 \text{ mm}^2$$

$\rho_s \geq 1\%$ [AISC I2.1.1a(1)]

$$\rho_s = \frac{A_s}{A_g} = \frac{323{,}200 \text{ mm}^2}{3{,}240{,}000 \text{ mm}^2} = 9.98\% \geq 1\% \ (OK)$$

Area of longitudinal reinforcement:

$$A_{sr} = 32 \times \pi\left(\frac{32}{2}\right)^2 = 25{,}736\ \text{mm}^2$$

$$\rho_{sr} \geq 0.4\% \qquad \text{[AISC I2.1.1a(3)]}$$

$$\rho_{sr} = \frac{A_{sr}}{A_g} = \frac{25{,}736\ \text{mm}^2}{3{,}240{,}000\ \text{mm}^2} = 0.79\% \geq 0.4\%\ (OK)$$

Area of concrete:

$$A_c = A_g - A_s - A_{sr} = 3{,}240{,}000\ \text{mm}^2 - 323{,}200\ \text{mm}^2 - 25{,}736\ \text{mm}^2$$
$$= 2{,}891{,}064\ \text{mm}^2$$

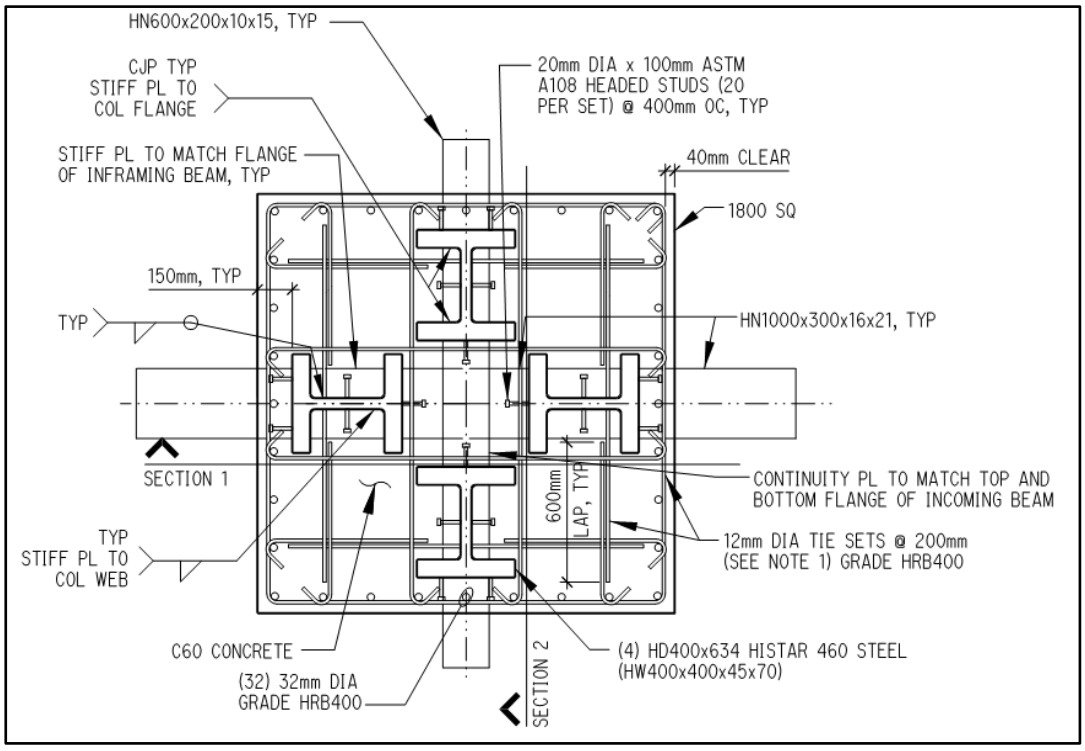

Figure A-3 Column section (Information provided by MKA 2016)

A.4 Determine the column axial capacity

Compressive strength reduction factor:

$$\Phi_c = 0.75 \qquad \text{[AISC I2.1.1b]}$$

Nominal axial compressive strength:

$$\text{If } \frac{P_{no}}{P_e} \leq 2.25: \quad P_n = P_{no}\left[0.658^{\frac{P_{no}}{P_e}}\right]$$
$$\text{If } \frac{P_{no}}{P_e} > 2.25: \quad P_n = 0.877 P_e$$

[AISC I2.1.1b (I2-2 & I2-3)]

Where:

$P_{no} = F_y A_s + F_{ysr} A_{sr} + 0.85 f'_c A_c$ [AISC I2.1.1b (I2-4)]

$= 460 \text{ MPa} \times 323{,}200 \text{ mm}^2 + 400 \text{ MPa} \times 25{,}736 \text{ mm}^2 +$
$0.85 \times 50 \text{ MPa} \times 2{,}891{,}064 \text{ mm}^2 = 281{,}836{,}594 \text{ N}$
$= 281{,}837 \text{ kN}$

$P_e = \frac{\pi^2 EI_{eff}}{(KL)^2}$ [AISC I2.1.1b (I2-5)]

$EI_{eff} = E_s I_s + 0.5 E_{sr} I_{sr} + C_1 E_c I_c$ [AISC I2.1.1b (I2-6)]

$C_1 = 0.1 + 2\left(\frac{A_s}{A_s + A_c}\right) \leq 0.3$ [AISC I2.1.1b (I2-7)]

$= 0.1 + 2\left(\frac{323{,}200 \text{ mm}^2}{323{,}200 \text{ mm}^2 + 2{,}891{,}064 \text{ mm}^2}\right) = 0.3011 > 0.3$

$= 0.3$

$I_s = 2 \times I_{X,HD400X634} + 2 \times A_{HD400X634} \times d_{HD400X634}{}^2 + 2 \times I_{Y,HD400X634}$
$= 2 \times 2.74 \times 10^9 \text{ mm}^4 + 2 \times 80{,}800 \text{ mm}^2 \times (513 \text{ mm}^2)^2 +$
$2 \times 9.89 \times 10^8 \, mm^4 = 4.99 \times 10^{10} \, mm^4$

$I_{sr} = \sum\left(I_{32\text{mm rebar}} + A_{32\text{mm rebar}} \times e_{y,\text{rebar}}{}^2\right)$
$= 1.22 \times 10^{10} \text{ mm}^4$

$I_c = \frac{BH^3}{12} = \frac{1800 \text{ mm} \times (1800 \text{ mm})^3}{12} = 8.75 \times 10^{11} \text{ mm}^4$

$EI_{eff} = 200{,}000 \text{ MPa} \times 4.99 \times 10^{10} \text{ mm}^4 +$
$0.5 \times 200{,}000 \text{ MPa} \times 1.22 \times 10^{10} \text{ mm}^4 +$
$0.3 \times 17{,}664 \text{ MPa} \times 8.75 \times 10^{11} \text{ mm}^4 = 1.58 \times 10^{16} \text{ N} - \text{mm}^2$
$= 1.58 \times 10^{13} \text{ kN} - \text{mm}^2$

$P_e = \frac{\pi^2 \times 1.58 \times 10^{13} \text{ kN} - \text{mm}^2}{(1.0 \times 1000 \times 9 \text{ m})^2} = 1{,}928{,}744 \text{ kN}$

$\frac{P_{no}}{P_e} = \frac{281{,}837 \, kN}{1{,}928{,}744 \, kN} = 0.146 \leq 2.25$

$\frac{P_{no}}{P_e} \leq 2.25$: $P_n = 281{,}837 \text{ kN} \times (0.658^{0.146}) = 265{,}116 \text{ kN}$

$\Phi P_n = 0.75 \times 265{,}116 \text{ kN} = 198{,}837 \text{ kN}$

A.5 Determine the axial reduction factor for the maximum unbraced length

When calculating the axial-flexure (P-M) interaction diagram to determine the true column capacity, an axial reduction factor (λ) is applied to the axial capacities determined from the strain-compatibility and plastic stress distribution methods. This axial reduction factor serves to account for the reduced axial capacity due to buckling of the maximum unbraced length of the column. The axial reduction factor is calculated as the ratio of the nominal axial capacity (P_n) to the plastic axial capacity (P_{no}).

$$\lambda = \frac{P_n}{P_{no}} = \frac{189{,}703\ \text{kN}}{281{,}837\ \text{kN}} = 0.897 \qquad \text{[AISC Fig. C-I5.2]}$$

A.6 Determine the P-M interaction diagram

Per AISC I1.2, it is permitted to use either the plastic stress distribution method, or the strain-compatibility method to determine the strength of the encased composite section. AISC P-M interaction capacities for bending about the x axis as determined by both the strain compatibility and full plastic stress distributions are presented below in Figure A.4.

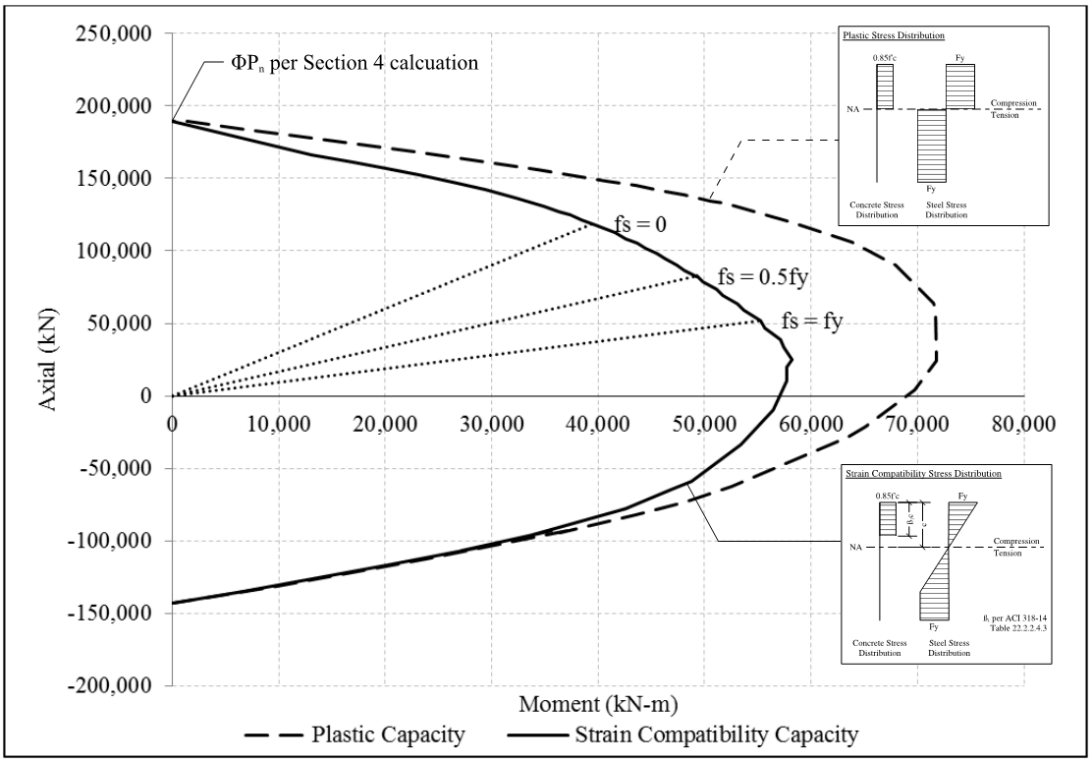

Figure A-4 P-M interaction curve for flexure about the x axis (Information provided by MKA 2016)

A.7 Select column transverse reinforcement

AISC requires that the concrete encasement of the steel core be reinforced with continuous longitudinal reinforcement and lateral ties. For composite columns in low seismic areas the tie spacing need only satisfy the limits specified in AISC.

$$s_{max} = \begin{bmatrix} 350\ mm\ (10\ to\ 12\ mm\ bars) \\ 406\ mm\ (13\ mm\ and\ larger\ bars) \\ 0.5\ \times Least\ column\ dimension \end{bmatrix} \text{[AISC I2.1a(2)]}$$

Additional tie requirements must be met in regions of moderate to high seismicity per the AISC Seismic Design Manual (AISC 341). The transverse reinforcement of the column is designed to meet the requirements of moderately ductile members.

Using 12 mm diameter tie bars for the transverse reinforcement:

Required extent of hinge-zone ties:

$$L_o = \text{Max}\begin{bmatrix} \frac{1}{6}L_b \\ \text{Max}(B, H) \\ 450\text{ mm} \end{bmatrix} = \text{Max}\begin{bmatrix} 1500\text{ mm} \\ 1800\text{ mm} \\ 450\text{ mm} \end{bmatrix} \quad \text{[AISC 341 D1.4b(1)(2)]}$$

$$= 1800\text{ mm}$$

Maximum spacing of ties:

$$s_{max} = \text{Min}\begin{bmatrix} \frac{1}{2}\text{Min}(B, H) \\ 8d_{b,Longit} \\ 24d_{b,Ties} \\ 300\text{ mm} \end{bmatrix} = \text{Min}\begin{bmatrix} 900\text{ mm} \\ 256\text{ mm} \\ 288\text{ mm} \\ 300\text{ mm} \end{bmatrix} \quad \text{[AISC 341 D1.4b(1)(1)]}$$

$$= 256\text{ mm};\quad \text{Used } 200\text{ mm} \quad (OK)$$

Note that, per AISC 341 D1.4b(1)(3), tie spacing outside of the 1800 mm hinge zones is not permitted to exceed two times the s_{max} calculated above.

The User Note in AISC I2.1.1a requires that ACI 318 sections 7.10 and 10.9.3 be satisfied in addition to AISC tie requirements (10.9.3 pertains to spiral reinforcement and does not apply to this example). Six legs of transverse reinforcement (two legs from exterior hoop and four additional cross-ties) are provided in each direction to satisfy clear spacing requirements of laterally unsupported longitudinal reinforcement.

$$s_{h,longit} \leq 152\text{ mm} \quad \text{[ACI 318-11 7.10.5.3]}$$

$$s_{h,ties} = \frac{B - 2 \times cover}{n_{legs} - 1} = \frac{1800\text{ mm} - 2 \times 40\text{ mm}}{6 - 1} = 344\text{ mm}$$

Ties are provided at no less than every other longitudinal bar.

$$s_{h,Longit} = \frac{1}{2}s_{h,ties} - d_{b,Longit} = \frac{1}{2} \times 344\text{ mm} - 32\text{ mm}$$

$$= 140\text{ mm} < 152\,mm \quad (OK)$$

A.8 Select load transfer mechanism between steel and concrete

For the test specimen design, mechanically connecting the concrete to the embedded steel shapes is ensured through 20 mm diameter nelson stud engagement. Full capacity behavior within a composite section when steel and concrete are combined is a research project goal.

For a typical design, load transfer required (V'_r) is calculated based on whether the load applying element (typically floor framing) is connected to steel:

$$V'_r = P_r\left(1 - F_y A_s / P_{no}\right) \qquad \text{[AISC I6.2a (I6-1)]}$$

Or concrete:

$$V'_r = P_r\left(F_y A_s / P_{no}\right) \qquad \text{[AISC I6.2b (I6-2)]}$$

Where P_r is the ultimate load applied at the connection point.

For example, if P_r for each embedded steel column of the test specimen is 3983 kN:

$$V'_r = 3983 \text{ kN} \times (1 - (4 \times 460 \text{ MPa} \times 80{,}800 \text{ mm}^2)/281{,}837 \text{ kN})$$
$$= 3983 \text{ kN} \times .472 = 1880 \text{ kN}$$

V'_r must then be transferred over the load introduction length (LIL), which extends above and below the connecting element by two times the minimum dimension of the column parallel to the incoming framing (see AISC Fig. C-I6.1).

Load introduction length:

$$LIL = 2 \times (2 \times B) + \text{Connection Depth} \qquad \text{[AISC Fig. C-I6.1]}$$
$$= 2 \times (2 \times 1800\ mm) + 0_{(connection\ depth\ neglected)} = 7200\ mm$$

Strength reduction factor for steel headed stud anchor in composite component:

$$\Phi_v = 0.65 \qquad \text{[AISC I8.3a]}$$

Capacity of a single 20mm diameter nelson stud:

$$Q_n = F_u A_{sa} \qquad \text{[AISC I8.3a (I8-3)]}$$
$$Q_n = 460 \text{ MPa} \times \pi \times \left(\frac{20}{2}\right)^2 = 144.4 \text{ kN}$$
$$\Phi Q_n = 0.65 \times 144.4 \text{ kN} = 94 \text{ kN}$$

Determine number of studs required to transfer load:

$$n = \frac{V'_r}{\Phi Q_n} = \frac{1880 \text{ kN}}{94 \text{ kN}} = 20 \text{ studs per embedded steel column}$$

With attaching studs to each flange and each side of the web:

$$n_{\text{column face}} = 20 \div 4 = 5 \text{ studs per face}$$

Stud spacing required:

$$s_{required} = \frac{LIL}{n_{column\ face}} = \frac{7200\ mm}{5} = 1440\ mm$$

$s_{min} = 4\emptyset = 4 \times 20\ mm = 80\ mm \quad (OK)$ [AISC I8.3e]
$s_{max} = 32\emptyset = 32 \times 20\ mm = 640\ mm\ (Controls)$ [AISC I8.3e]
$s_{provided} = 400\ mm < 640\ mm \quad (OK)$

The stud density of the test specimen, though, is potentially more than what may be required from actual conditions in practice. Unlike the limitations due to the test specimen sizes, a composite mega column will have multiple floors over which to develop the full capacity of the embedded steel section. In actual practice, the engineer needs to consider a mechanical interaction between concrete and steel to achieve the following:

- Develop the contributory load from any one floor, over the load introduction length of that floor.
- Ensure concrete confinement for the concrete within the composite section, not allowing the concrete/steel interface to be the weak link in the system.
- Ensure strain compatibility can be maintained between the concrete and steel, so full section capacities can be achieved.
- Further research and code defined guidance is encouraged around the topic of composite nelson stud minimum densities, or other forms of mechanical engagement between the concrete and steel.

12 References

1. COMPOSITE MEGA COLUMNS WITH ENCASED STEEL SECTIONS: EXPERIMENTAL CAMPAIGN. First methodological report. March – August 2014

2. COMPOSITE MEGA COLUMNS WITH ENCASED STEEL SECTIONS: EXPERIMENTAL CAMPAIGN. Peer reviewers' comments and responses of the research team. November 2014

3. COMPOSITE MEGA COLUMNS WITH ENCASED STEEL SECTIONS: EXPERIMENTAL CAMPAIGN. Third report: August 2014 – July 2015

4. COMPOSITE MEGA COLUMNS WITH ENCASED STEEL SECTIONS: EXPERIMENTAL CAMPAIGN. Final report: December 2015

5. "DESIGN OF COLUMN WITH SEVERAL ENCASED STEEL PROFILES FOR COMBINED
COMPRESSION AND BENDING", A. Plumier, T. Bogdan, H. Degèe

6. "DESIGN FOR SHEAR OF COLUMNS WITH SEVERAL ENCASED STEEL PROFILES. A PROPOSAL.", A. Plumier, T. Bogdan, H. Degèe

All references listed above can be requested via e-mail to: Dario Trabucco;
dtrabucco@ctbuh.org

13 Code References

1) Eurocode 4 (2004): *Design of composite steel and concrete structures*

2) AISC (2015): Specifications for Structural Steel Buildings – draft version

3) ACI 318-14: Building code requirements for structural concrete

4) Chinese code JGJ 138-2016: Code for Design of Composite Structures

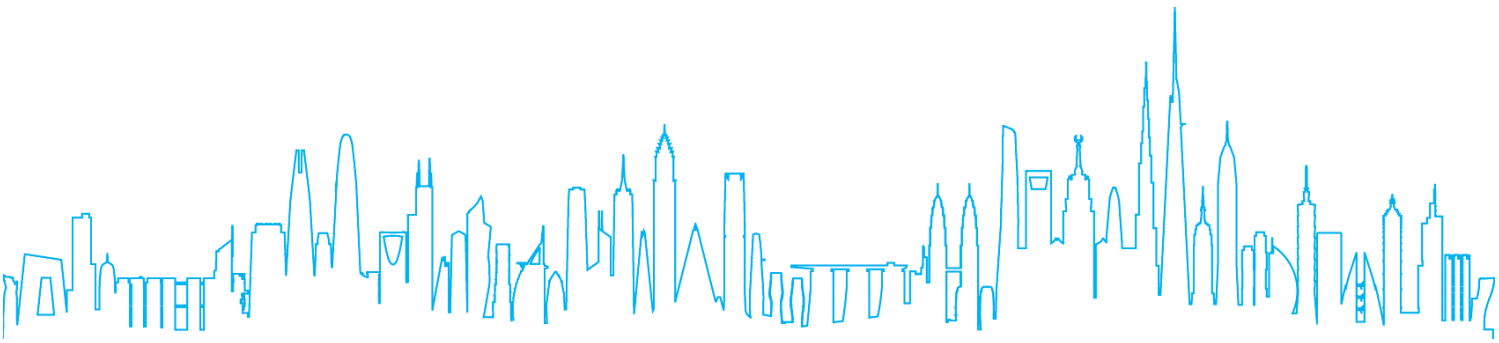

Council on **Tall Buildings** and **Urban Habitat** | www.ctbuh.org | www.skyscrapercenter.com
Global Headquarters: The Monroe Building, 104 South Michigan Avenue, Suite 620, Chicago, IL 60608, USA | 1 (312) 283-5599 | info@ctbuh.org
Research & Academic Office: Iuav University of Venice, Dorsoduro 2006, 30123, Venice, Italy | +39 041 257 1276 | research@ctbuh.org
Asia Headquarters: Wenyuan Building, Tongji University, 1239 Si Ping Rd, Yangpu District, Shanghai, China 200092 | +86 21 65982972 | china@ctbuh.org